Development of a Methodology for the Multiphysic Best-Estimate Modelling of PWR Core along Irradiation

Paolo Cattaneo

▶ **To cite this version:**

Paolo Cattaneo. Development of a Methodology for the Multiphysic Best-Estimate Modelling of PWR Core along Irradiation. Chemical and Process Engineering. Université Grenoble Alpes [2020-..], 2020. English. NNT : 2020GRALI037 . tel-03012160

HAL Id: tel-03012160

https://theses.hal.science/tel-03012160

Submitted on 18 Nov 2020

HAL is a multi-disciplinary open access archive for the deposit and dissemination of scientific research documents, whether they are published or not. The documents may come from teaching and research institutions in France or abroad, or from public or private research centers.

L'archive ouverte pluridisciplinaire **HAL**, est destinée au dépôt et à la diffusion de documents scientifiques de niveau recherche, publiés ou non, émanant des établissements d'enseignement et de recherche français ou étrangers, des laboratoires publics ou privés.

THÈSE

Pour obtenir le grade de

DOCTEUR DE L'UNIVERSITE GRENOBLE ALPES

Spécialité : MEP : Mécanique des fluides Energétique, Procédés

Arrêté ministériel : 25 mai 2016

Présentée par

Paolo CATTANEO

Thèse dirigée par **Elsa MERLE,** Professeur, Université Grenoble Alpes et codirigée par **Didier SCHNEIDER**, Ingénieur Chercheur, CEA Saclay

préparée au sein du **Laboratoire de Physique et d'Etude des Cœurs, CEA Saclay.**
dans **l'École Doctorale I-MEP2 - Ingénierie - Matériaux, Mécanique, Environnement, Energétique, Procédés, Production**

Développement d'une Méthodologie de Modélisation Multiphysique de type Best-Estimate d'un Cœur de REP en Évolution

Development of a Methodology for the Multiphysic Best-Estimate Modelling of PWR Core along Irradiation

Thèse soutenue publiquement le **28 septembre 2020**,
devant le jury composé de :

Madame Elsa MERLE
Professeur, Université Grenoble Alpes, Directeur de thèse
Monsieur Grégoire ALLAIRE
Professeur, Ecole Polytechnique, Président du jury et Rapporteur
Monsieur Jean RAGUSA
Professeur, Texas A&M University, Rapporteur
Monsieur Cheikh M'Backé DIOP
Directeur de recherche, CEA, Examinateur
Monsieur Bertrand IOOSS
Chercheur senior, EDF R&D, Examinateur
Madame Nathalie MARIE
Ingénieur-chercheur, CEA, Examinateur
Monsieur Didier SCHNEIDER
Ingénieur-chercheur, CEA, Encadrant CEA

Résumé

Cette thèse vise à améliorer la modélisation des Réacteurs à Eau Pressurisée (REPs). Les réacteurs nucléaires en général peuvent être considérés comme des systèmes multiphysiques : leur modélisation nécessite la prise en compte de la neutronique, de la thermohydraulique, de l'évolution isotopique et de la physique du combustible. Ces travaux concernent le développement d'un schéma de calcul d'évolution de type multiphysique avec maillage raffiné (échelle cellule du combustible) et son optimisation numérique. La démarche classique est basée sur l'utilisation de solveurs spécialisés sur un sous-ensemble des physiques combinée avec des modèles simplifiés pour les autres disciplines. Grâce à la disponibilité croissante de ressources de calcul et à la grande flexibilité des langages de programmation modernes, des outils de simulation s'appuyant moins sur des modèles simplifiés sont en cours de développement. Un schéma de calcul a ainsi été implementé pendant cette thèse en exploitant les outils de la plateforme SALOME et des solveurs développés au CEA. APOLLO3® est utilisé pour la neutronique, FLICA4 ou THEDI pour la thermohydraulique et la conduction de chaleur et MENDEL pour le calcul d'évolution. La neutronique est traitée avec une approche en deux étapes avec homogénéisation à l'échelle de la cellule de combustible. La thermohydraulique est traitée avec FLICA4 à l'échelle sous-canal. La conduction de chaleur est résolue, par FLICA4 également, explicitement dans tous les crayons du coeur. Un algorithme de couplage définit donc les échanges entre le modèle de neutronique cœur et ceux de thermohydraulique et conduction de chaleur. Cette approche demande moins de puissance de calcul que les schémas high-fidelity basés sur un calcul direct (i.e. sans homogénéisation sous conditions limites simplifiées) et il fait moins d'hypothèses que les schémas basés sur une technique de reconstruction de la forme de puissance fine.

Les calculs d'évolution sont modélisés comme une séquence d'états permanents. Pour cela, une partie conséquente de la thèse est dédiée à l'optimisation du schéma de calcul en permanent. Un cas d'étude simple (mini-cœur : 5x5 assemblages REPs plus réflecteur) est défini pour pouvoir exécuter un grand nombre de simulations dans un temps acceptable. Sur ce cas test, la meilleure approche pour la résolution du couplage est sélectionnée d'après une analyse de performance basée sur les écarts avec la référence et les coûts de calcul. Par rapport à l'optimisation numérique, deux des méthodes les plus utilisées, le point-fixe et Anderson, sont testées en confirmant la supériorité de cette dernière. Une généralisation du point-fixe basée sur les convergences partielles, largement utilisée dans l'industrie mais peu référencée dans la littérature, est étudiée en détails. Bien que l'efficacité de cette technique dépende des solveurs considérés, elle résout, dans notre cas, les problèmes de stabilité du point fixe et offre une meilleure efficacité que la méthode d'Anderson. Alors qu'il est difficile d'utiliser directement la méthode d'Anderson avec les convergences partielles, une version modifiée est proposée. Des tests préliminaires donnent des résultats prometteurs en termes d'efficacité.

Afin de prendre en compte l'évolution des propriétés thermomécaniques du combustible, un

modèle simplifié pour le coefficient d'échange thermique dans le jeu pastille-gaine est inclus dans le schéma. Les premiers tests confirment l'importance de ce modèle. La recherche de la concentration de bore ciblé est implémentée. Pour obtenir la compatibilité avec le point-fixe généralisé aux convergences partielles, une méthode de Newton est adaptée. Tous les éléments mentionnés jusqu'à maintenant sont combinés ensemble pour produire un schéma de calcul d'évolution multiphysique, qui est appliqué avec succès sur un scénario d'irradiation à puissance constante.

Mots clés: *Multiphysique, Maillage-Raffiné, Méthodes-Numériques, Calcul-d'Évolution, REP, Convergences-Partielles.*

Abstract

This thesis aims at improving the modelling of Pressurized Water Reactors (PWRs). Nuclear reactors in general can be considered as multiphysic systems, as their accurate representation often requires to account for neutronics, thermal-hydraulics, isotopic evolution and fuel performance. In particular, this work concerns the development of a multiphysic calculation scheme for fine mesh (pin cell resolution) depletion calculations and its numerical optimization. Conventional approaches generally employ solvers specialised on a subset of the relevant physics, while resorting to simplified models for the rest. Thanks to the increasing availability of computational resources and to the greater flexibility of modern programming languages, many research groups are working on the development of simulation tools that rely less on the use of simplified models. A general coupling scheme is developed exploiting the tools from the SALOME platform. It ensures the compatibility with a set of the CEA solvers, including APOLLO3® for the neutronics, FLICA4 or THEDI for the thermal-hydraulics and heat conduction and MENDEL for the depletion calculations. Through the coupling of an APOLLO3® core solver with FLICA4, it is possible to combine two-steps neutronic simulations based on pin-cell homogenization with subchannel thermal-hydraulics and heat conduction on every fuel rod. This approach requires less computing power than the *high-fidelity* direct calculations (i.e. with no *a priori* homogenization) and it makes fewer assumptions than the faster running schemes based on the pin-power-reconstruction technique (i.e. the combination of coarse mesh calculations with form functions for the local refining of the results).

Following a widespread approach, the depletion calculations are modelled as a sequence of steady-states. For this reason, a large part of the thesis is devoted to the optimization of the steady-state scheme. A simple case study (mini-core: 5x5 PWR fuel assemblies plus reflector) is defined in order to allow to perform a large number of simulations in an acceptable time. Based on this test, the best combination of models is selected by analysing the performance in terms of discrepancies with respect to the reference and computational cost. As regards the numerical optimization, two of the most common iterative methods found in literature, the fixed-point and the Anderson algorithms, are tested confirming the superiority of the latter both in terms of robustness and efficiency. A variant of the fixed-point method, here referred to as generalised fixed-point with partial-convergences, which is widespread in the nuclear industry, but rarely mentioned in publications, is studied in detail. Although the effectiveness of this technique depends on the considered solvers, for the cases studied in the context of the thesis, this method solves the major robustness problems of the fixed-point method and offers a higher efficiency than the Anderson method. Afterwards, a modified Anderson algorithm that adopts the core principle of the partial-convergences is proposed. Preliminary tests lead to promising results in terms of efficiency improvement.

In order to account for the evolution of the fuel thermal-mechanical properties during irradiation, a simplified fuel gap heat transfer model is included in the scheme. The first tests confirm

the importance of including this model. For the depletion scheme, the research of the target boron concentration is implemented. To do so, an approximated Newton method is developed to be compatible with the generalised fixed-point with partial-convergences. All the elements mentioned so far are combined together to produce a multiphysic depletion calculation scheme, which is successfully tested on a constant power irradiation scenario.

Keywords: *Multiphysics, Fine-Mesh, Numerics, Depletion, PWR, Partial-Convergences.*

Acknowledgments

Many people have importantly contributed to this thesis. I feel very lucky that I got to know them and that I could spend these years in their company.

I would like to start by thanking my thesis director Elsa Merle and my CEA supervisors Didier Schneider, Frédéric Damian and Anthime Farda for their availability and expert guidance. I really appreciate the time they have managed to took out of their full agendas for me. I thank Jean-Charles Le Pallec for contributing to set the basis for this PhD. I would like also to express my gratitude to the laboratory directors I have had during the thesis Fadhel Malouch and Céline Guenaut. With their availability and comprehension they ensured the best working conditions for me.

A PhD on multiphysics is somehow supposed to make the student interact with a lot of peoples from different laboratories, but I totally did not expect to receive so much support from so many people. I would like to thanks Roland Lenain and Cyril Patricot for their active and determinant contribution. Their continuous support has been decisive for the thesis. I am extremely grateful to Dominic Caron, Simone Santandrea and Daniele Sciannandrone for all the things they taught me and all the time they dedicated to help me. I sincerely thanks Benoit Normand and Karim Ammar for their expert guidance and incredible availability. I would like to express my gratitude to Florian Abeguile for all his support and patience.

I would like to thank many other people in the SERMA department for the pleasant moments I have spent with them. Indeed, many others have given an important contribution to the thesis by accompanying me through the highs and lows of life. In particular, I would like to thank Alberto, Andrea, Antonio, Gregory, Paul, Simone and Vito and all the other PhD students with whom I have spent wonderful moments.

Even if many years have passed, I still feel very grateful to many professors I had during my previous education for their inspiring lessons, careers and lives that will not stop to be an example for me.

When it comes to the acknowledgements, my family is right there on top of my mind as they have always supported me in any decision I take, even when it might push me away from home.

A special thank is for my girlfriend Claudia who has always been there despite the distance that has often physically divided us. She has supported me more than anyone else by believing in me way more than I do.

List of Publications

- P. Cattaneo, R. Lenain, E. Merle, C. Patricot, and D. Schneider, "Numerical Optimization of a Multiphysics Calculation Scheme Based on Partial Convergence," *Annals of Nuclear Energy*, vol. 151, 2020. https://doi.org/10.1016/j.anucene.2020.107892.

- P. Cattaneo, R. Lenain, E. Merle, C. Patricot, and D. Schneider, "Numerical Optimization of a Multiphysics Calculation Scheme," In *Proceedings International Conference On the Physics Of Reactor (PHYSOR)*, Cambridge, United Kingdom, 2020. https://www.physor2020.com/proceedings.

- P. Cattaneo, F. Damian, J.-C. Le Pallec, E. Merle, and D. Schneider, "Development of a Multiphysics Best-Estimate Approach for LWR Reference Calculation," In *Proceedings International Congress on Advances in Nuclear Power Plants (ICAPP)*, Juan les Pins, France, 2019. https://hal-cea.archives-ouvertes.fr/cea-02339458v2.

- D. Tomatis, I. Zmijarevic, and P. Cattaneo, "A Simple Multiphysics Coupling for High-Fidelity Neutronic Modelling in Fuel Performance Codes," In *Proceedings International Conference On Physics Of Reactor (PHYSOR)*, Cancun, Mexico, 2018. https://hal.archives-ouvertes.fr/hal-02415500/document.

Sta' senza pensier'!

Quotation from Gomorra TV series, particularly relevant for Ph.D. life and pandemics, when many problems are beyond your control.

Contents

List of Figures

List of Tables

Acronyms

API Application Programming Interface. 39, 69, 86

BC Boron Concentration. 102

BEAVRS Benchmark for Evaluation and Validation of Reactor Simulations. 41, 97, 154, 162

BOC Beginning Of Cycle. 41, 42, 74, 154

CAD Computer-Aided Design. 69

CBC Critical Boron Concentration. xxv, 35, 41, 43, 45, 47

CEA Commissariat à l'énergie atomique et aux énergies alternatives. iii, v, xxxi–xxxiv, 55, 63, 64, 66, 69, 71, 96

CFD Computational Fluid Dynamics. 25, 30, 45

CRW Control Rod Worth. xxv, 45

CTF COBRA-TF. xvi, 36–38, 43, 44

DNB Departure from Nucleate Boiling. 9, 109

DSA Diffusion Synthetic Acceleration. 60

EC Equivalence Coefficient. 60, 61

EDF Électricité de France S.A. xxxi, xxxiii, 55, 63, 66, 69

EOC End Of Cycle. 41, 42, 154

HPMC High Performance Monte Carlo Methods for Core Analysis. xxxii, 36

HZP Hot Zero Power. xxv, 45

IAEA International Atomic Energy Agency. 135

ICoCo Interface for Code Coupling. 70, 90

IRSN Institut de Radioprotection et de Sûreté Nucléaire. xxxi–xxxiii, 63

JFNK Jacobian-free Newton-Krylov. 47, 50, 52–54, 127

KAIST Korean Advanced Institute of Science and Technology. 97

LOCA Loss Of Coolant Accident. 13, 26, 36, 39, 63, 66

LWR Light Water Reactor. 31, 35, 43

MATRA Multichannel Analyzer for steady states and Transients in Rod Arrays. xxxii, 45

MED Modèle d'Echange des Données. xxxiii, 35

MOC Method Of Characteristics. xvii, 43, 56, 58, 59, 77, 80–82, 157

MOC Middle Of Cycle. 41, 42

MOX Mixed Oxide Fuel. 12

MPI Message Passing Interface. 60

NNR Numerical Nuclear Reactor. 45

P_N Spherical Harmonics. 63

PCI Pellet Cladding Interaction. 11

PWR Pressurized Water Reactor. v, xv, xvii, xviii, 1, 3–13, 17, 19, 24, 27, 30, 35–38, 41–43, 45, 46, 66, 67, 70, 71, 80, 88, 95–99, 104, 111, 112, 146, 157, 161

REA Rod Ejection Accident. 68, 70

RIA Reactivity Insertion Accident. xviii, 39, 66, 71, 98

RMS Root Mean Square. xxv, xxvi, 41–43, 45, 103, 104, 107, 108, 110, 123, 140

S_N Discrete Ordinates. 56, 58, 60, 63, 70

SERMA Service d' Études des Réacteurs et de Mathématiques Appliquées. 55, 66, 70, 98

SFR Sodium Fast Reactor. 31, 46, 63

SP_N Simplified-P_N. 60, 63, 70, 78, 79, 159

SPH SuPer-Homogenization. 60–62, 78, 79, 86, 101, 104, 158

SPRC Service de Physique des Réacteurs et du Cycle. 56

SSH Self-Shielding. xvi, 17, 18, 32, 33, 56, 57, 59, 83

VUSAT VERA-CS Uncertainty and Sensitivity Analysis Toolkit. 42

Glossary

ALCYONE Fuel performance code, CEA. xvii, 66–68, 70, 79–81, 137

APOLLO2 Deterministic multi-purpose neutronic code, CEA, EDF, FRAMATOME. 55–60, 71, 74

APOLLO3® Deterministic multi-purpose neutronic code, CEA, EDF, FRAMATOME. iii, v, xviii, 55, 56, 58–61, 63, 66, 70, 71, 74, 76, 78, 80, 85, 86, 89, 91–93, 95, 101, 137, 157

BEAVRS Benchmark for Evaluation and Validation of Reactor Simulations, Massachusetts Institute of Technology. xxv, 41, 45, 46

BISON Fuel performance code, Idaho National Laboratory. 44

CASL Consortium for Advanced Simulation of Light Water Reactors, established by the US Department of Energy and based at Oak Ridge National Laboratory. xxxiv, 42, 47, 54

CASMO Neutronic code for lattice calculations, Studsvik. xxv, 31, 40–42, 46

CAST3M Thermal-mechanic code, CEA. 66

CATHARE Thermal-hydraulic system code, joint cooperation between CEA, EDF, Framatome and IRSN. 39, 63

COBAYA Deterministic neutronic code, Universidad Politécnica de Madrid. 38

COBRA-TF Subchannel thermal-hydraulic code, North Carolina State University. 36

CORPUS Framework for multiphysic simulations with specialised solvers, CEA. 69, 70, 86, 90, 91, 137

CPU years Number of years of the computing time ideally required with one processor. 40, 43

CRONOS Deterministic neutronic code, CEA. 34, 55, 60

DARWIN Isotopic depletion code, CEA. 66

DRACCAR Fuel performance code for loss of coolant accident, developed by IRSN. 39

DYN3D Deterministic reactor dynamics code, Helmholtz-Zentrum Dresden-Rossendorf. xvi, 36–39, 47

DYNSUB DYN3D coupled with SUBCHANFLOW. 37

ECCO Deterministic neutronic code for lattice calculations, CEA. 55, 56

ERANOS Deterministic neutronic code for core calculations, CEA. 55, 56

FLICA4 Subchannel thermal-hydraulic code, CEA. iii, v, xvii, xviii, 39, 64, 65, 70, 71, 74, 80, 83, 89–91, 137, 138, 158

FRAPCON Fuel performance code, developed at Pacific Northwest National Laboratory for the U.S. Nuclear Regulatory Commission. 39, 68

GeN-Foam Generalized Nuclear Foam, multiphysic code, École polytechnique fédérale de Lausanne and Paul Scherrer Institut. 31

HEMERA Framework for multiphysic simulations with specialised solvers, CEA and IRSN. 69

HPMC High Performance Monte Carlo Methods for Core Analysis, European project (2011-2014). 36, 39

HYDRA-TH Computational fluid dynamics code, Los Alamos National Laboratory. 45

Insilico Neutronic code, gathering both a deterministic solver, Denovo, and a Monte Carlo one, SHIFT, Oak Ridge National Laboratory. 45

KENO Monte Carlo neutronic code, Oak Ridge National Laboratory. 45

MAMBA MPO Advanced Model for Boron Analysis, Los Alamos National Laboratory and Massachusetts Institute of Technology. 45

MAMMOTH Multiphysic code based on MOOSE, Idaho National Laboratory. 31

MATRA Multichannel Analyzer for steady states and Transients in Rod Arrays, Korea Atomic Energy Research Institute. 45

MCNP Monte Carlo N-Particle (neutronic) code, Los Alamos National Laboratory. 39

McSAFE High Performance Monte Carlo Methods for Safety Demonstration, European project (2017-2020). 36, 39, 71

MED Modèle d'Echange des Données, hierarchical data format based on HDF5 used in the SALOME platform. 35, 69, 70, 85, 86, 89–91, 93, 126, 137, 138

MENDEL Isotopic depletion code, CEA. v, xviii, 66, 74, 75, 86, 92, 93

MONK Monte Carlo neutronic code, UKAEA Safety and Reliability Directorate. 39

MOOSE Multiphysics Object-Oriented Simulation Environment, fuel performance code, Idaho National Laboratory. 44

MPACT Deterministic neutronic code, Oak Ridge National Laboratory and the University of Michigan. xvi, xxii, 43, 44, 149

NNR Numerical Nuclear Reactor, multiphysic code (nTRACER+ MATRA), Korea Atomic Energy Research Institute and Argonne National Laboratory. 31, 45, 46

nTRACER Neutronic code for direct calculation, Seoul National University. xxxiii, 45

NUMPS Numerical Multi-Physics project, VTT Technical Research Centre of Finland. 31

NURESAFE NUclear REactor SAFEty simulation platform, European project (2013-2015). 36

NURESIM European simulation platform for nuclear reactor safety (based on SALOME, 2005-2008). 31, 35, 36, 39

NURISP NUclear Reactor Integrated Simulation Project, European project (2009-2012). 36, 37, 39, 40

OECD/NEA Organization for Economic Co-operation and Development, Nuclear Energy Agency. 37, 38

ORIGEN Isotopic depletion code, Oak Ridge National Laboratory. 43, 44

SALOME Coupling platform for multiphysic simulations, developed by CEA, EDF and OPEN CASCADE. iii, v, 35, 69, 86–92

SCANAIR Fuel performance code for reactivity insertion transients, developed by IRSN in cooperation with EDF. 39

SERPENT Monte Carlo neutronic code, VTT Technical Research Centre of Finland. 39, 40

SHARP Multiphysic code, Argonne National Laboratory. 31

SIMULATE Neutronic code for core calculations, Studsvik. xxv, 31, 40–42, 46

SUBCHANFLOW Subchannel thermal-hydraulic code, Karlsruhe Institute of Technology. 37–39

THEDI Diphasic thermal hydraulic code, CEA. v, xvii, 63–65, 74, 80, 83, 89–92

TIAMAT VERA-CS coupled with BISON. 44, 117

TRANSURANUS Fuel performance code, European Institute for Transuranium Elements. 39, 40

TrioCFD Computational fluid dynamic code, open-source. 64

TRIPOLI Monte Carlo neutronic code, CEA. 39, 55, 66, 71, 76, 77

URANIE Uncertainty analysis platform, based on ROOT, CEA. 36

VERA-CS Virtual Environment for Reactor Applications Core Simulator, CASL. xvi, xviii, 31, 42–46, 98

VUSAT VERA-CS Uncertainty and Sensitivity Analysis Toolkit, CASL. 42

Chapter 1

Introduction

Independently from any political discussion about nuclear, Pressurized Water Reactor (PWR), as the most widespread nuclear reactor type in the world, is a crucial component of the economy, the environment and the security of France and of the entire world. Given the cost and the complexity of building experimental nuclear reactors and the increasing computational power available to researchers and industries, modelling covers a very important role in the economy and the safety of the reactors. This PhD thesis is about the multiphysic modelling of a PWR core along irradiation. Hence, its general aim is the improvement modelling capabilities and the increase in the understanding of reactor physics.

This introduction chapter is structured in three sections aiming at giving the context of the PhD studies, the definition and the nature of the target problem and a description of the adopted methodology.

1.1 Nuclear Reactor Core as a Multiphysic System

In this section, the concept of multiphysics of nuclear reactor cores is introduced from a physics-based point of view. In the first part, some general examples are provided for other multiphysic systems and for nuclear reactors in general. In the second one, a more detailed analysis is done for the PhD thesis context: a PWR core along irradiation. The fundamental elements that define this system are reported for every concerned discipline and the main interdependencies among physics are introduced.

1.1.1 Introduction to Multiphysic Issues

Multiphysic Issues in General

The most characterizing keyword of this PhD thesis is multiphysics, which in this context refers to multiphysic modelling. The general definition of such a word is quite intuitive, as it simply corresponds to any model accounting for multiple physics. However, the actual meaning in the context of reactor physic simulations is something more specific that needs several concepts to be defined beforehand, hence, a more precise definition is given later in the introduction. The majority of engineering problems could suite the wide definition of multiphyisic problem. For instance, let us consider an electric cable: the electromagnetic field and the heat transfer are largely influencing each other. Therefore, both these physical phenomena have to be addressed in order to find an accurate solution of the problem. In this example, the transport of electrons through the wire implies a certain heat generation according to the electrical resistance of the cable. On the other hand, the electrical resistance itself depends on the heat conduction, as the resistivity of the materials is determined by the local temperature. Some examples of modelling strategies for this problem are given in [15, 16]. Another typical illustration is the simulation of the wing of an aeroplane, where fluid and structural dynamics are strongly coupled. To accurately model the fluid dynamics, the temperature and the deformations fields of the wing are needed. At the same time, the structure dynamics compute these quantities using the pressure field and the heat transfer coefficient as input. Hence, in many aerospace applications these disciplines are treated together, for instance as in [17]. One further example is the multiphysic modelling of the cardiac function, like in [18, 19]. In this case, in order to reproduce the heart's behaviour under given conditions, the biomedical branches of fluid mechanics, solid mechanics and electromagnetism are combined together.

Multiphysic Issues in Nuclear Reactor

Nuclear reactors are intrinsically multiphysic systems. Indeed, in most of the power reactors, the neutron transport is exploited to generate heat, which for the majority is generated in the solid fuel, is transmitted to the coolant by conduction and is removed by the latter through forced convection. The heat generation naturally affects the temperature and density fields of the materials. In turn, the different neutron reactions probabilities depend on both these quantities. This is a crucial aspect of nuclear reactors, which has been exploited to obtain a system that is self-stabilizing in most of the scenarios. In the sense that a power excursion would reduce the probability for neutrons to undergo fission, hence, the power would receive a negative feedback intrinsically opposing to any divergent behaviour. Moreover, depending on the time scale, the effect of neutron transport can be also measured in terms of isotopic change mostly in the fuel, i.e. neutron transmutation. At the start-up of a reactor, effects can be seen already on a small time scale, in the order of minutes. This

is linked to the intrinsic nature of fission, a heavy element (like uranium-235) is split into (in most of the cases) two fission products. These fission products can be or rapidly become neutron poison, in the sense that elements like xenon-135 and and samarium-149 are characterized by extremely high capture cross-sections[1] that have a measurable impact on the reactivity (this quantity is mentioned as $\rho := \frac{k_{eff}-1}{k_{eff}}$) of the core even for small variations in their concentrations. On a longer time scale, the reduction in the content of uranium-235 due to neutron absorption (i.e. capture + fission) and the production of new fissile isotopes like plutonium-239 and 241 consequently to multiple neutron captures on uranium-238 have to be considered. Furthermore, the neutron transport and the operating conditions impact also the chemistry and the mechanics of the fuel, leading to variations in the geometry and thermal-mechanical properties. These changes in turn may affect the neutronics. Therefore, depending on the scenario to be modelled, the neutronic modelling may require to address also isotopic depletion, themal-hydraulics, heat conduction, thermal-mechanics and eventually other disciplines related to the fuel modelling.

1.1.2 Multiphysics of PWRs along Irradiation

In this sub-section, the multiphysic modelling of PWR along irradiation is introduced. To do that, some of the most fundamental elements of PWR modelling of the core are introduced from a single-physic perspective and finally an overview of their interactions focusing on the neutronics is given.

Introduction to PWRs

This PhD thesis focuses on the modelling of the nuclear reactor core of the PWR type. This reactor design is largely the most widespread one for energy production. According to [20], in 2016, 289 of the 448 operational nuclear power reactors are PWRs. Nowadays, nuclear energy represents the second-largest source of low-carbon electricity after hydroelectric [21, 22]. By producing about 10 % of the total electricity generation, corresponding to 2700 TWh (data for 2018 [21]), it is one of the main actors in the fight against climate change. However, nuclear is facing a strong decline in western countries, where the number of operational reactors is decreasing. The steep raise in renewable power has been just sufficient to replace nuclear: the low-carbon share in the total energy production has not increased in the last two decades (36 % both in 1998 and 2018[21]). In France, this is even more a crucial topic, since about 79.6 % of the energy production is from nuclear reactors [23] and all of them are PWRs [24]. Only one reactor is under construction in France, the EPR of Flamanville. Designed and developed by Framatome (ex Areva-NP) and Électricité de France (EDF), it is considered as a third generation PWR.

[1] The cross-section quantifies the probability of a given reaction (in this case radiative capture) among neutrons and the nucleus of the considered isotope.

Neutronics of PWRs

As the majority of the operating reactor designs, PWRs are thermal reactors using low-enriched uranium dioxide as fuel, which means that each uranium isotope is bounded to two oxygen-16 atoms (UO_2). By low-enrichment, it is meant that, in the fresh fuel, uranium-235 represents from 2 to 5 % of the total uranium nuclei, while the rest is mainly uranium-238. The fundamental principles, on which thermal reactors are based, are described by the simple tough very popular Fermi's four-factors formula, which is reported in Eq. (1.1). It was firstly used to predict the critical mass of the famous first atomic pile, while, in this paragraph, this formula is just used to introduce the main stages of neutron's life in a thermal reactor.

$$k_\infty = \epsilon * p * f * \eta \tag{1.1}$$

- k_∞ is the infinite multiplication factor.
- ϵ is the fast fission factor.
- p is the resonance escape probability.
- f is the thermal utilization factor.
- η is the reproduction factor.

The main principle behind thermal reactors is indeed the thermalization, which is the process of slowing the neutron down to thermal energy, which is about 0.025 eV and corresponds to the equilibrium speed of the medium, which is defined by the temperature. This slowing down is obtained through the use of a moderating material. In PWRs, this material is the water, the very low mass of hydrogen nuclei allows to absorb large portions of the neutron kinetic energy at every scattering collision. This property is one of the reasons that makes the water a good moderator even if its capture cross-section is not so small. Each fission produces on average 2.5 new neutrons which could be classified as fast, as their average kinetic energy is about 2 MeV.

In Eq. (1.1), the infinite multiplication factor (k_∞) represents the global neutron balance (defined as the ratio of the neutron population over two consecutive generations) without accounting for the neutron leakages. The fast fission factor (ϵ) is the number of neutrons slowing down below 1 MeV per each neutron produced by thermal fission. Its main role is to account for the portion of neutrons that may cause fission before slowing down to 1 MeV. The neutron slowing down needs to happen with the lowest number of collisions in order to avoid the so-called resonances. The resonances are energy intervals in which the capture probability increases sharply. For simple isotopes, the presence of these peaks of the interaction probability can be explained by the minimization of the kinetic energy of the products of the considered reaction. For this reason, they occur at slightly higher energies

than the excited levels of the target nucleus. The fission and radiative capture cross-sections of uranium-235, which is the main fissile isotope in fresh fuel, are available in Fig. 1-1. Since the resonances constitute a major filter in neutron slowing down, their presence is accounted by p, the probability to escape the resonances.

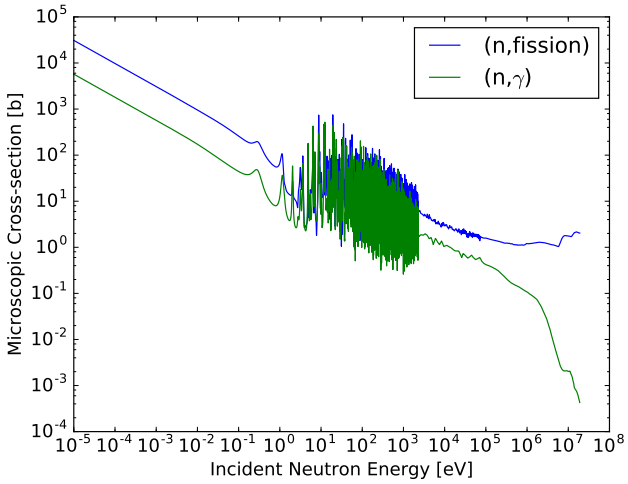

Figure 1-1: Radiative capture (n,γ) and fission (n,fission) cross-sections of uranium-235, source [1]. The purpose is to show the competing reactions in the main fissile isotope of the fresh fuel and to underline the presence of the resonances. Above few keV resonances do not disappear, they just become too close to each other for the resolution, for this reason they are called unresolved resonances.

Once the neutrons are thermalized, the main turning point is whether they are absorbed in the fuel or in other materials, this is represented by f, the thermal utilization factor. The reproduction factor (η) is the average number of fission neutrons produced per neutron absorbed in the fuel. With η the neutron's life-cycle in an infinite thermal reactor is closed. To account for the finiteness of the reactor's size, the escape probability should be added for fast and thermal neutrons.

A confirmation that this formula captures the essential physics of PWRs is given by the typical neutron spectrum found in this reactor type, this quantity is available in Fig. 1-2. Indeed, it is possible to observe two peaks in neutron population at thermal and fast energies. Moreover, the neutron populations around these peaks rather accurately reproduce the Maxwell distributions respectively centred in 0.1 eV and 1.3 MeV.

Basic Design Elements of PWR Cores

Before introducing the multiphysic nature of PWRs, some fundamental design elements have to be illustrated. First of all, the fuel rods of a PWR are composed of hundreds of fuel pellets axially piled up and immobilized by a spring. The spring has also the role of keeping a free volume to accommodate the gas produced in the fuel (mainly gaseous fission products and helium), which is

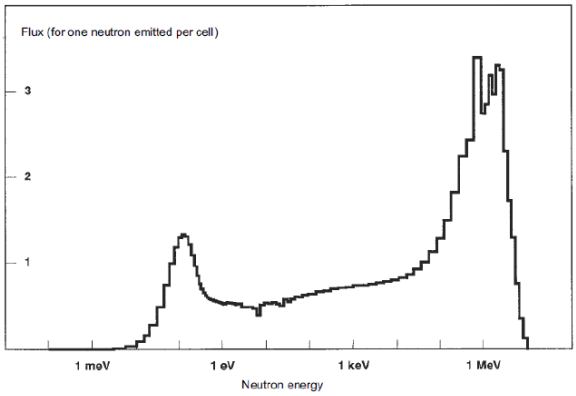

Figure 1-2: Typical PWR neutron energy spectrum [2]. Attention is posed on the peaks at thermal and fast energies.

partially released within the fuel rod during operation. A fuel rod's representation is given in Fig. 1-3.

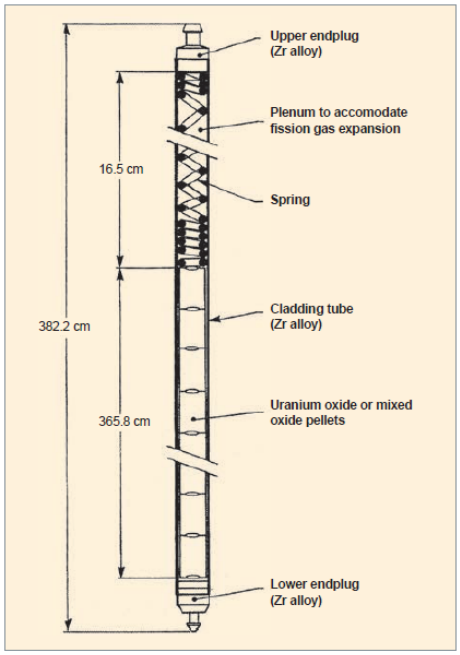

Figure 1-3: Description of the typical fuel rod design for PWRs, courtesy of [3], page 10.

Each pellet has a diameter roughly of 1 cm and a similar height, so the fuel rod is very thin and tall (approximately 1 cm of diameter and 4 m of height). The fuel is contained in a cladding often made of zirconium alloys, this material is chosen for its low capture cross-section and good thermal-mechanical properties. In Fig. 1-3, it is also possible to notice that the fresh fuel pellets are not exactly cylindrical after their fabrication. To avoid the contact among them, which may be caused by their expansion, some material is removed from the pellet extremities, obtaining their typical diabolo shape. Furthermore, fresh fuel rods are charged with helium at 2.5 MPa, with the aim of

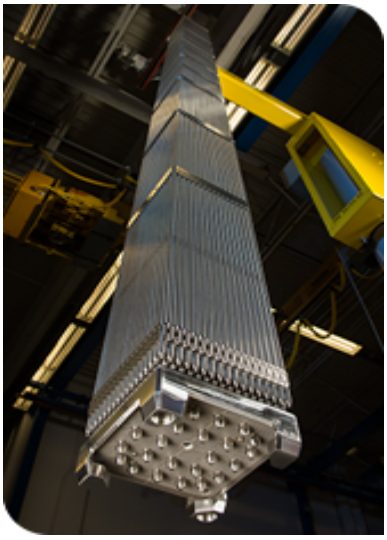

(a) PWR fuel assembly [25].

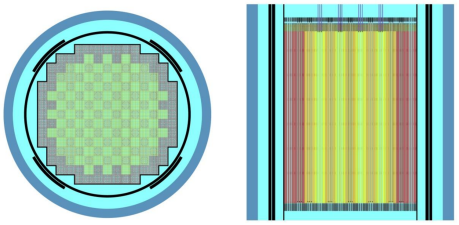

(b) Radial and axial sections of a PWR [26].

(c) Fuel pellets, courtesy of Framatome [27].

Figure 1-4: Hierarchical overview of the core. The core radius is about 2 m, the axial height is roughly 4 m. Depending on the design, core is made of 200 fuel assemblies, each of them is about the same height of the core and is around 20 cm large. Every assembly is made of 265 fuel rods and 24 guide tubes. Every fuel rod is made of cylindrical fuel pellets with both diameter and height in the order of 1 cm.

partially compensating the pressure outside the cladding and of improving the heat conduction in the gap between the fuel and the cladding [3], pages 9 and 10.

The fuel rods are kept together in square fuel assemblies, with a size of about 20 cm, which usually contain 265 of them and 24 thimble tubes, which are vacant tubes mostly used to insert the control rods within the reactor. The core is composed of roughly 200 fuel assemblies approximating a cylindrical shape with a diameter between 3 and 4 meters and slightly larger height. This description can be visualized in Fig. 1-4.

In this figure, it is also possible to visualize that the core is contained in the reactor pressure vessel, which is generally considered as the second barrier between the radioactive materials and the biosphere. All the material that is in between the core and the vessel, both radially and axially, is referred to as reflector, as from the neutronic point of view it aims at reflecting the escaping neutrons again into the core. In reality, some of the materials composing the reflector have also other functions like reinforcing structural integrity or shielding the reactor pressure vessel from neutrons. Generally, an important part of the reflector is constituted by water for both its shielding, reflecting and cooling capabilities.

Thermal-Hydraulics of PWRs

In PWRs, the water plays both the role of moderator and coolant. These reactors, for how advanced they could be, just convert the heat generated by fissions into electricity through a Rankine cycle.

However, the heat generating system of the Rankine loop is not the reactor itself. In fact, the Rankine loop constitutes a secondary circuit, while the core power of the reactor is extracted by a primary loop that transfer it to the secondary one through the steam generator. In this way, eventual radioactive leakages from the fuel rods would be kept in the primary circuit, resulting in several design simplifications for the secondary loop. The core power is removed by a mostly vertical water flow through the fuel rods, directly cooling the cladding outer surface. As anticipated by the name of the reactor type, this water flow is highly pressurized, at about 15.5 MPa and 300 °C. The water mass flow rate through the core is very large, several millions of kilograms per hour in standard operation. Such a flow rate at this high pressure requires pumps consuming few Megawatts of electricity, but it allows the extraction of few thousands of Megawatts of heat. In this way, all the power can be removed with a small temperature increase of the water across the core, about 30 K. Such a low temperature increase contributes to making the reactor more homogeneous and maximize the thermodynamical efficiency.

Under nominal conditions, the water of the primary circuit stays close to saturating conditions but always below. Just some subcooled boiling may locally happen due to the temperature gradient caused by the heat flux. This phenomenon affects just a small portion of the water, where the steam may reach few per mille in volume, while the channel average temperature is well below saturation. Nevertheless, as stated in [28], it is important to model this void formation also during normal operation as it heavily affects the heat transfer coefficient. Indeed, the subcooled boiling is a very effective heat transfer mechanism, but pushing the thermal-hydraulic conditions too far, boiling crisis may occur. When this happen, the heat transfer rapidly and strongly deteriorates and the cladding temperature may overcome the one imposed by safety limits. This problem is quite typical of nuclear power plant as the heat removal mechanism is power dominated, in the sense that the heat source is controlled and the cladding temperature depends on the cooling capability. In combustion plants instead, the maximum temperature is controlled, as it is determined by the flue gas and the heat removed depends on the efficiency of the process.

A simple model to interpret this phenomenon is given for the pool boiling by the famous experiment of Nukiyama [29]. Pool boiling occurs when the fluid is globally at rest, even if natural convection may induce some local movements. In PWRs, the mechanism is rather flow or forced-convective boiling, in the sense that the boiling happens with the fluid circulating through the core. However, this experiment has been central in the qualitative description of the boiling crisis in general, the main plot is reported in Fig. 1-5.

The main outcome of this study is that, when controlling the heat flux as in the figure, a sudden temperature increase of the cladding outer surface is expected above a certain power level. The quantity on the x-axis is the wall superheat temperature, which corresponds to the difference between the wall temperature and the saturation temperature of the water. The wall temperature

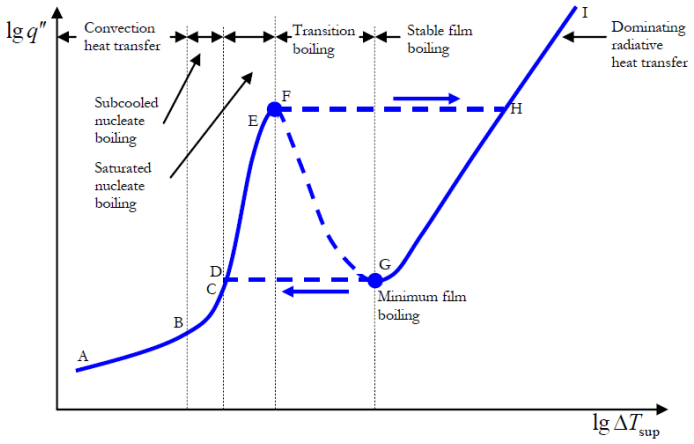

Figure 1-5: Nukiyama curve describing the boiling crisis as a transition from different heat transfer mode. It should be noticed that PWRs heat removal mechanism is power controlled (instead of temperature controlled as in most of the conventional plants). The boiling crisis happens when moving from the F to the H point: for a given heat flux, the wall superheat temperature suddenly increases. Source [4].

is the temperature at the interface between the water and the solid material, which in PWRs corresponds to the temperature of the cladding outer surface. In this plot, this sudden increase happens when moving from the F point to the H one and the temperature increase is very large even on a logarithmic scale. Although this curve describes a boiling crisis happening while leaving the saturated boiling condition (i.e. when the average water temperature is above saturation), such a crisis may happen also during subcooled nucleate boiling under PWR's operating thermal-hydraulic conditions. In PWRs this phenomenon is called Departure from Nucleate Boiling (DNB), as it happens when leaving the nucleate boiling.

Fuel Performance of PWRs

The integrity of the cladding of the fuel rods is very important for the safety and the economy of reactors. The age of fuel rods is generally measured with the burnup. This quantity is also called fuel utilization as it quantifies the energy that is extracted per unit mass of heavy metal, which in case of uranium dioxide, is the mass of uranium. The typical burnup range found in reactors is from 0 to 60 MWd/kg. Below 30 MWd/kg, the fuel pellets are capable of preventing the release of the majority of the radioactive fission products. The main leakage mechanism for low exposures is the "knockout", which corresponds to the release of gaseous fission products close to the outer fuel surfaces as a consequence of collisions with other elements. The expelled elements reach the allocated free space, called plenum. Beyond 30 MWd/kg other mechanisms become predominant and cause releases up to the 5 % of the total fission products, as described in [3], pages 17 to 19. The radioactive elements accumulated in the plenum are kept within the fuel rod by the cladding, which can consequently be considered as the first barrier between the radioactivity and the biosphere. Even

if several other barriers are present, like the reactor pressure vessel and the containment building, cladding failure may imply the sharp increase of the radioactivity level in the primary circuit and the reactor shutdown, which entails considerable economic losses.

Fuel rods mechanical integrity is a limiting factor in terms of plant's power uprate, speed in reactor start-up and maximum achievable burnup. Therefore, a lot of attention is put into its modelling, which is often referred to as fuel performance or fuel behaviour. The fuel performance is a multiphysic problem in itself, because ideally it requires the full solution of neutronics, thermal-hydraulics, heat conduction, fuel chemistry, fuel mechanics and fuel transmutation. Fortunately, not every single aspect of fuel performance has an important influence on neutronics. What matters the most is the estimation of the temperature distribution, which may be strongly affected by the change of fuel thermodynamic properties. Hence, to improve the prediction of neutronic quantities it is important to model the behaviour of the fuel-cladding heat transfer coefficient along exposure. Even if the fuel and the cladding are separated just by a thin layer (a maximum of 80 μm) of helium, which has a relatively high conductivity for a gas, this layer accounts for a big portion of the total thermal resistance, hence, it has a big influence on the fuel temperature. A typical radial temperature profile in a fuel rod at 200 W/cm is reported in Fig. 1-6.

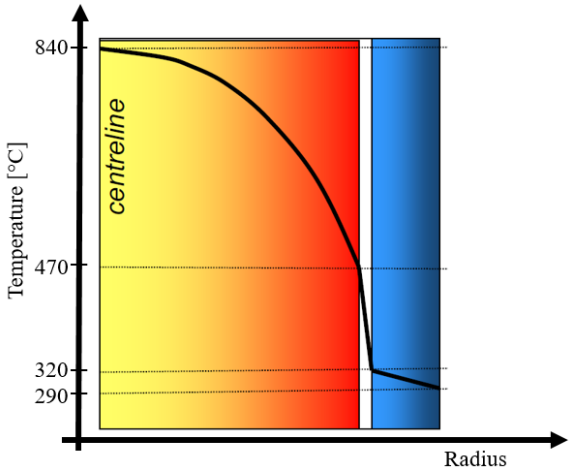

Figure 1-6: Typical temperature profile assuming 280 °C of water bulk temperature, 200 W/cm of linear power and typical PWR thermodynamic properties. Courtesy of [5].

During a fuel rod lifetime, the fuel-clad heat transfer coefficient may vary from 5'000 W/m^2/K to 200'000 W/m^2/K, as confirmed by [10], pages 7 and 8. The peak value corresponds to the moment when the fuel and the cladding begin the mechanical contact. The main phenomena driving the gap size are described in [30]. Basically, at the very beginning of the power ramp, the fuel expands due to instantaneous thermal expansion. The same mechanism summed to the increase in the rod pressure, which derives from the raising temperature, make the cladding displace outwards. In early irradiation, the fuel volume decreases due to the densification: the higher temperature reduces

the concentration of fuel structural defects. After this short phase, which lasts few MWd/kg, the cladding starts to creep inward (it reduces its radius at constant load due to stressful environment) and the fuel volume increase due to swelling. This latter consists in the accumulation of fission products which occupy a larger volume than the fissile elements and it is largely due to the noble gaseous fission products that may even cluster in bubbles. A contribution to swelling is also given by the α-decay of transuranic elements, that similarly forms helium clusters (called helium bubbles). Due to these two phenomena, the gap width constantly decreases until mechanical contact is reached. For this reason the gap heat transfer coefficient consistently increases until about 30 MWd/kg. The only opposed process is the release of gaseous fission products with lower conductivity like xenon and krypton.

Once the gap is closed, the heat conduction is dominated by the fuel conductivity which degrades significantly due to the increase of structural defects. This process that begins when the fuel and the cladding enter in contact is called Pellet Cladding Interaction (PCI). It is an important safety concern as it endangers the cladding integrity and it is an important limiting factor to the speed of power ramps and to plants uprate. In France, many nuclear reactors perform the load following, which consists in slowly changing the power level to adapt to the grid needs. For this reason, in this country, the study of PCI is a key research topic.

PWRs along Irradiation

Modelling PWR along irradiation means to reproduce the reactor's behaviour under normal operating conditions over long time intervals that require to account for the isotopic transmutation. This type of simulations is also called depletion calculations as they also address the consumption of fissile material. Under the typical operating conditions, the reactor power ramp is sufficiently slow to allow to model the scenario as a sequence of steady-states characterized by evolving isotopic concentrations and power levels. Therefore, the fundamental mode of the neutron flux is researched, i.e. the flux that perfectly satisfies the steady-state equation. In respect of the thermal-hydraulics and of the heat conduction, the steady-state conditions define a state in which the energy is not accumulated in any material, hence, all the power generated in the core is removed by the coolant. In PWRs, this balance is obtained by keeping the reactor almost always under critical conditions (effective multiplication factor equal one, $k_{eff} = 1$) by adjusting the boron concentration or the control rod insertion for the fuel depletion, for the different operating conditions (e.g. power level) and for the varying thermal-mechanical properties (e.g. fuel temperature). Boron-10 is a thermal neutron poison and its presence in the water is regulated by changing the boric acid concentration. Adjusting the boron concentration allows to change the core reactivity in a rather homogeneous way, as its concentration is almost constant over the core, but it is a slow process. For quicker reactivity changes, the control rods are deployed. They are commonly assembled into blocks of rods

activated together, each block has a specific purpose. The safety blocks are devoted to the core rapid shutdown. The shim blocks are used for large reactivity changes. The regulating rods are used to perform fine manoeuvres and reactivity control. The neutron absorber is generally boron or cadmium. Due to the fact that they are inserted into the core through the guide tubes, generally from above, and to their strong absorption cross-section they heterogeneously affect the neutron flux distribution in the core.

Multiphysics of PWRs

Depending on the phenomena to be modelled, the variables to be predicted and the considered scenario, different subsets of physics may be considered. In this paragraph, without descending into the modelling details, a coupling scheme for the modelling of PWRs along irradiation is introduced with the aim of showing the main interdependencies among the selected physics. The scheme is depicted in Fig. 1-7. Several schemes exchanging more variables could be conceived, but they would go beyond this introductory purpose, further analyses of additional variables to be exchanged are reported in Chapter 4.

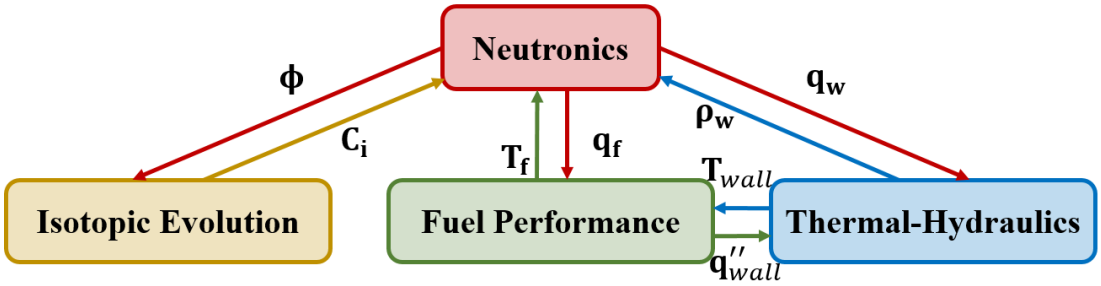

Figure 1-7: Introductory multiphysic coupling scheme aiming at underlining the main variables that are shared among physics. $\boldsymbol{\phi}$ is the neutron flux, $\boldsymbol{C_i}$ is the concentration of the i-isotope, T_f is the fuel temperature, q_f is heat generated in the fuel, q_w is heat generated in the water, ρ_w is the water density, T_{wall} is the wall temperature (clad outer surface) and q''_{wall} the wall heat flux.

The neutronics and the isotopic evolution are naturally coupled as the isotopic evolution is mainly caused by the neutron interactions with the matter and the isotopic composition is a key factor for the neutron transport. However, making abstraction, even with no neutron flux the isotopic composition of the reactor would still change due to radioactive decays, especially if Mixed Oxide Fuel (MOX) fuel is considered. By MOX, it is meant that also several plutonium isotopes are included before irradiation. Hence, they might be formalized as two different physics.

In the case of thermal-hydraulics, even if the water flow rate is very high, the heat flux deriving from the conduction through the fuel pellet and the power directly generated in the water have a significant effect on the density profiles along the channels. The water direct heating is caused by the neutrons slowing down that releases a non-negligible amount of energy. Other particles like electrons of the beta decays and photons may contribute as well as their energy may not be entirely

deposited in the fuel.

In respect to neutronics, the moderator density impacts mainly two of the four factors. A density increase would imply a larger probability to escape the resonances as on average neutrons would undergo more scattering collisions before reaching again the fuel, but at the same time it would lower the fuel thermal utilization factor as more neutrons would be captured in water. Moreover, a density increase would also raise the non-leakage probability as all the collisions would become more likely. In Fig. 1-8, the two factors are reported as a function of the moderator to fuel ratio, which corresponds to the fraction of the atomic number densities (i.e. the number of atoms per unit volume) of the moderator over the fuel isotopes. These curves can be drawn asymptotically for any reactor, considering that with no moderator the probability to escape the resonances would be virtually zero, while with only moderator it would be one. The same for the fuel thermal utilization factor, which with no water it is one, while with no fuel it is zero. A maximum reactivity is found for a given moderator to fuel ratio. This point would move to higher moderator quantities if the leakage probability is included. An other perturbation is introduced if considering a varying boron concentration in the moderator, as the fuel thermal utilization factor would decrease more rapidly moving the maximum to lower ratios. Reactors with moderator to fuel ratio higher than the one that maximizes the reactivity are called over-moderated, if the contrary is true they are under-moderated. PWRs are under-moderated by design, for several reasons, mainly the following two. Under-moderation contributes to a negative power feedback, as a power increase implies a moderator density reduction that reduces the multiplication factor with a stabilizing effect opposed to power excursions. The under-moderation helps also to face Loss Of Coolant Accident (LOCA), as for the same principle the reduction in moderator density has a negative impact on reactivity. It should be noticed that, as boron concentration increases, the reactor could become over-moderated, hence, limits are imposed on the maximum levels.

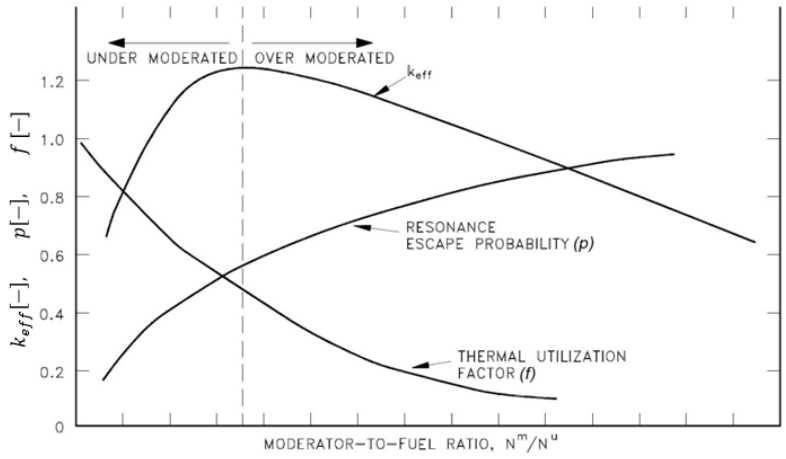

Figure 1-8: Impact of density variations on the neutronics interpreted with the four-factors formula. This plot, source [6], is also used to introduce the concept of under vs over-moderation.

The power generated in the fuel, about 97 % of the total, which is mostly coming from the kinetic energy of the fission fragments, is transferred to the cladding and finally removed by heat convection of the coolant. The remaining 3 % directly heats up the moderator as it is carried by neutral particles (a more detailed analysis is given in sub-section 4.2.1). Considering the geometry of the fuel rods, the heat is conducted to the cladding outer surface predominantly through the radial direction. As in steady state conditions all the power reaches the moderator, the cladding outer surface temperature, called wall temperature, can be determined independently from the fuel temperature profile. The direct water heating, therefore, is just affecting the heat conduction as lesser power is generated in the fuel and the wall heat flux is lower. In this context, the fuel performance has the role of modelling the evolution of the fuel geometry. In particular, it is important to forecast when there is contact between the fuel and the cladding as this has a major impact on the heat conduction.

Every cross-sections depends on the temperature. In fact, if in Fig. 1-7, the thermal-hydraulics shares only the water density with the neutronics, it is because under nominal conditions, the water pressure is constant enough to approximately associate every density to a temperature value. The reason for this simplification will become clearer when speaking about the modelling approach. Anyway, it should be considered that, for the moderator, a relative density variation has a larger impact on the neutronics than the equivalent temperature one. For the fuel, the opposite is true, because it is a solid material, hence, under normal operating conditions, density variations happen on a lower scale, but also because of the Doppler effect. This phenomenon is another negative feedback, like the moderator one, and it is of crucial importance for safety concerns. In many scenarios the fuel warms-up more rapidly than the moderator, hence, the Doppler feedback intervenes faster than the one linked to the moderator. The Doppler effect is strongly connected to the resonances, which are not so important in water cross-sections, while they are abundant in the heavy isotopes of the fuel. The global outcome of this phenomenon is that, as temperature raises, the resonant isotopes absorb more neutrons and since uranium-238 is way more abundant than uranium-235 the number of radiative captures increases much more than the one of fission events. Similarly to the famous Doppler effect of wave physics, in nuclear reactors it is driven by particles relative speed. At 0 K, the resonances appear as very sharp peaks of the absorption cross-section, few eV thick, that, as mentioned before, correspond to the small intervals of velocities that would lead the target nucleus to one of its excited levels while minimizing the kinetic energy of the products. The temperature increase flattens these peaks out, reducing the maximum values whilst preserving the integral below the curve. This flattening corresponds to an enlargement of the range of speeds that implies resonant absorptions. In theory, if the neutron flux were constant in energy within a resonance, the absorption rate would stay rigorously constant. On the contrary, the probability to be absorbed for neutrons interacting at energies close to the resonance peaks is so high that the neutron flux is strongly perturbed spatially and energetically. The sharp decrease of the neutron flux within the resonance

energy intervals within the resonant media is what makes the Doppler broadening increase the absorption probability. In fact, the broadening increases the cross-section's value where the neutron flux is higher and reduces it where it is lower. Therefore, the global outcome is a lower probability to escape the resonances, which is equivalent to a reactivity decrease. It should be noticed that the lower the kinetic energy of the incoming neutron, the more important is the nucleus speed on the relative velocity, hence the greater is the Doppler broadening. For this reason, a very important role is played by two resonances of uranium-238, which are respectively centred at 20.87 and 6.67 eV.

All this analysis is based on a sort of global approach, however, most of these quantities are in reality multidimensional fields. Therefore, the actual problem is more complex, but these elements can still help to make a simplified analysis and understand local flux variations linked to changes in other variables.

1.2 Main Issues of Multiphysic Modelling of a PWR along Irradiation

In this section, the focus is on the main issues of the multiphysic modelling of the considered type of scenario. In the first part, this is done focusing on the individual physics, while introducing the fundamental governing equations and the complexities they may hide. In the second one, the specific meaning of multiphysic modelling is given and some general issues of such an approach are introduced. Since the modelling choices are not presented yet at this stage, this part is intended to be very introductory.

1.2.1 Single-physic Problems

Deterministic Neutronics

The deterministic approach for neutronic modelling is to solve the neutron transport equation, also called Boltzmann equation through the discretization of the phase space. On the contrary, Monte Carlo methods solve the same equation but following a probabilistic approach. While for steady state calculations at fixed conditions the Monte Carlo methods are considered the reference in terms of accuracy of the results, their application to depletion simulations and to multiphysic modelling is still under exploration. Monte Carlo methods are generally more computationally expensive than the deterministic alternative and their coupling with other solvers entails a certain number of additional complexities.

The integro-differential formalism is available in Eq. (1.2) and (1.3). The first term represents the neutron density variation per unit time, in steady-state it is null. The second one accounts for the streaming of neutrons outside the considered volume. The third is the total reaction rate, that

basically is composed of the scattering to another energy and any type of absorption. The variables are defined as it follows: ψ is the angular flux, V_n the neutron velocity module, the phase-space is composed by $(\boldsymbol{r}, E, \boldsymbol{\Omega}, t)$, respectively the location, neutron's kinetic energy, the unitary vector representing the direction of the neutron and the time, Σ is the total macroscopic cross-section (i.e. the sum of the number densities of each isotope multiplied by their microscopic cross-section) and Q is the neutron source, the terms that gathers every positive contribution to the neutron balance for that energy, that place and that time: the fission rate, the scattering from other energies to the considered one and eventually an external neutron source.

$$1/V_n \frac{\partial \psi(\boldsymbol{r}, E, \boldsymbol{\Omega}, t)}{\partial t} + \boldsymbol{\Omega} \nabla \psi(\boldsymbol{r}, E, \boldsymbol{\Omega}, t) + \Sigma(\boldsymbol{r}, E, t)\psi(\boldsymbol{r}, E, \boldsymbol{\Omega}, t) = Q(\boldsymbol{r}, E, \boldsymbol{\Omega}, t) \tag{1.2}$$

$$\begin{aligned} Q(\boldsymbol{r}, E, \boldsymbol{\Omega}, t) = \int_0^\infty dE' \int_{4\pi} d^2\Omega' \psi(\boldsymbol{r}, E', \boldsymbol{\Omega}', t)\Sigma_s(\boldsymbol{r}, E' \to E, \boldsymbol{\Omega}' \to \boldsymbol{\Omega}, t) + \\ + \frac{\chi_i}{4\pi} \int_0^\infty dE' \int_{4\pi} d^2\Omega' \psi(\boldsymbol{r}, E', \boldsymbol{\Omega}', t)\Sigma_f(\boldsymbol{r}, E', t)\upsilon(E') + S(\boldsymbol{r}, E, \boldsymbol{\Omega}, t) \end{aligned} \tag{1.3}$$

The neutron transport equation is in reality a specific case of the Boltzmann equation for a given gas (neutrons) moving within another one (nuclides). The hypotheses behind this model are widely explained in [31], pages 43 to 47 and they are listed here:

- The neutron mean free path (i.e. the average distance before the following collision, order of millimetre to centimetre) is much larger than the distance at which the particles may begin to interact (order of femtometres).
- As in most of the applications about 10^8 n/cm^3 are measured, the number of neutrons is sufficiently high to justify a statistical treatment, hence to define a neutron density function.
- Since the density of nuclei of the underlying medium is about 10^{15} times larger than the neutrons one, the neutron-neutron interaction is neglected. Which is important for making the neutron transport a linear partial differential equation.
- Gravity impact is neglected because of the speed and the lifetime, 10 m/s^2 against speed of larger than 2000 m/s and lifetime comprised between 10^{-5} and 10^{-3} seconds.
- Neutron decay is neglected due to the large doubling time (11 minutes) as compared to the neutron lifetime.
- Relativistic effects are neglected as the maximum kinetic energy 20 MeV is only 2 % of the rest mass.
- As classical neutral particles, neutrons travel in straight lines and are fully described by their position and their velocity vectors.

If the heterogeneity of a problem is generally what dictates the mesh refinement, from the point of view of neutrons, nuclear reactors are very heterogeneous systems. Considering the variables of the phase space it is possible to obtain an order of magnitude of the problem's dimension. As already introduced, the cross-sections of the heavy isotopes are characterized by a stiff energy dependency. For instance, above all, it is important to account for the uranium-238 as the most abundant uranium isotope in the fuel of PWRs. Its cross-section is given in Fig. 1-9, in order to address its resonances, hundreds of energy meshes are required. The typical size of the material heterogeneity in a PWR is given by the thickness of the cladding, which is in the order of the millimetres. This is also about the mesh dimension required to adequately capture the stiff gradients of the neutron flux in the fuel. Therefore, considering that commercial reactors size is typically in the order of meters, about a thousand meshes per Cartesian coordinate are required ($(10^3)^3 = 10^9$ spatial regions are needed). So for the purely neutronic problem, considering that few hundreds of angular directions have to be used, the global problem is a linear system with about 10^{13} ($10^9 * 10^2 * 10^2$) degrees of freedom per time step. Similar back-of-the-envelope calculations can be found in [31], pages 61 to 63.

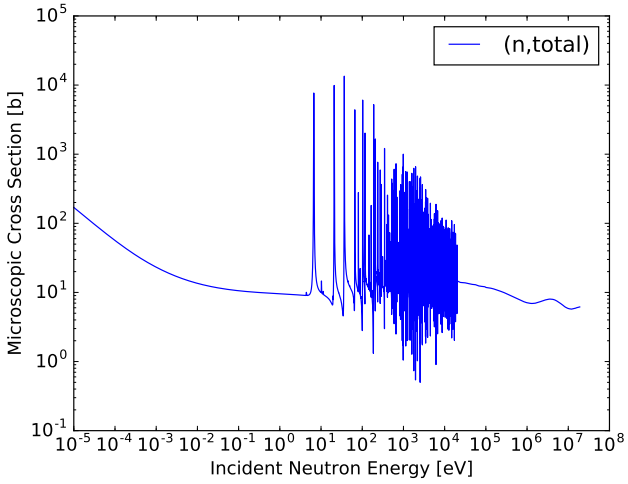

Figure 1-9: Total cross section of uranium-238, it is used to justify the need of a fine energy mesh to capture the stiff energy dependency of the most abundant isotope of uranium; source [1].

A further reason for the mesh refinement is the Self-Shielding (SSH), a physical phenomenon that needs to be addressed with a special treatment. It deals with the fact that in some energy and space meshes the neutron flux variation is extremely abrupt. The not entirely thermalized neutrons going back from the moderator to the fuel, with an energy close to the resonances, encounter a very large absorption cross-section. The absorption probability is so large that it significantly affects this portion of the neutron flux. While crossing a small region of several tens of micrometers in the outermost ring of the fuel pellet, the neutron flux in these energy intervals decreases of several orders of magnitude. This happens also in the cladding due to its interface position and the resonances of

zirconium-90. It is useful to reason in terms of reaction rate, which is defined as the product of the scalar flux (see Eq. 1.4) and the macroscopic cross-section ($\Sigma(\boldsymbol{r}, E, t)$).

$$\phi(\boldsymbol{r}, E, t) := \int_{4\pi} d^2\Omega \; \psi(\boldsymbol{r}, E, \boldsymbol{\Omega}, t) \tag{1.4}$$

The name Self-Shielding derives from the fact that the neutron flux ends up to decrease so much in those regions (like if the outermost region is shielding the interior of the pellet) that the absorption reaction rate is not as stiff as the cross-sections or the flux. The consequence of this are largely impacting the fuel performance. This outermost ring, called rim region, becomes richer in plutonium (due to capture on uranium-238 and following isotopes), it achieves higher burnup, UO_2 grains are strongly restructured and dispersed micrometer-size porosity is formed [32].

Thermal-Hydraulics

The derivation of the fundamental equations of thermal-hydraulics is rather straightforward, as they correspond to the physical principles of mass, momentum and energy conservation. However, the so formulated problem can be extremely complicated or even impossible to solve. In Eq. (1.5), the general formulation, called Cauchy formulation, of the momentum conservation is given. Where $\boldsymbol{u}$ is the flow velocity, ρ is the density, t is the time, $\boldsymbol{g}$ is the body acceleration (e.g. gravity), $\bar{\bar{\sigma}}$ is the Cauchy stress tensor defined as the sum of the pressure and the viscosity terms ($\bar{\bar{\sigma}} = -p\bar{\bar{I}} + \bar{\bar{\tau}}$) and $\otimes$ is the outer product. By making the hypotheses that the stress linearly depends only on the gradient of the velocity and that the fluid is assumed to be isotropic, the famous Navier-Stokes equation may be derived from Eq. (1.5). It is reported in Eq. (1.6), where μ is the dynamic viscosity, $\tilde{p} := p - \zeta\nabla\cdot(\boldsymbol{u})$ and ζ is the volume viscosity. Together with the classical mass and energy balance equation, Eq. (1.6) form the Navier-Stokes equations, which belong to class of nonlinear differential equations. Even if they are widely used in many engineering problems, they hide significant complexities. The demonstration of whether solutions always exist and whether they would be infinitely differentiable in the entire domain is considered as one of the seven most important open problems in mathematics and 1 million dollar prize is available for any demonstration or counterexample [33].

$$\frac{\partial}{\partial t}(\rho\boldsymbol{u}) + \nabla\cdot(\rho\boldsymbol{u}\otimes\boldsymbol{u}) = \nabla\bar{\bar{\sigma}} + \rho\boldsymbol{g} \tag{1.5}$$

$$\frac{\partial}{\partial t}(\rho\boldsymbol{u}) + \nabla\cdot(\rho\boldsymbol{u}\otimes\boldsymbol{u}) = -\nabla\tilde{p} + \mu\nabla^2\boldsymbol{u} + \frac{1}{3}\mu\nabla(\nabla\cdot\boldsymbol{u}) + \rho\boldsymbol{g} \tag{1.6}$$

By neglecting the viscous term ($\bar{\bar{\sigma}} = -p\bar{\bar{I}}$), it is possible to obtain the simpler Euler form of the momentum conservation, reported in Eq. (1.7).

$$\frac{\partial}{\partial t}(\rho \boldsymbol{u}) + \nabla \cdot (\rho \boldsymbol{u} \otimes \boldsymbol{u}) = -\nabla p + \rho \boldsymbol{g} \tag{1.7}$$

Another complexity derives from the fact that these equations account for one single flow field, while multiple may be required in case of multi-component or multiphase flows. As stated before in the introduction, in PWRs multiple biphasic flow might occur locally. The most rigorous approach would be to solve the previously mentioned balance equations for each phase, or even dividing each phase in multiple fields characterized by similar properties. In addition, new conservation equations should be formulated for the fields interfaces, the jump conditions.

Under the interpenetrating continua hypothesis, the generic local and instantaneous conservation for the phase k field is given in (1.8). The continuum approximation is at the base of the vast majority of engineering models and deals with the treatment of a discrete and eventually heterogeneous field as it was point-wise defined over the entire domain. This approximation is accurate for almost any thermal-hydraulic problem as the modelling scale is much larger than the one where molecular motion become significant. This equation ensures that the generic quantity Ψ_k is conserved as net balance of the efflux term $\boldsymbol{J}_k$ and the body source term ϕ_k. Conveniently substituting the quantities of Table 1.1, the mass, momentum and energy conservation are written for each phase, in complete analogy with the Cauchy formulation. In the energy conservation, e_k is the internal energy, $\boldsymbol{q}_k''$ is the heat flux vector field and q_k''' is the body source of energy, for instance due to neutron scattering.

$$\frac{\partial}{\partial t}(\rho_k \Psi_k) + \nabla \cdot (\rho_k \boldsymbol{u}_k \Psi_k) = -\nabla \cdot \boldsymbol{J}_k + \rho_k \phi_k \tag{1.8}$$

Table 1.1: Different meanings of the generic local and instantaneous conservation law.

Conservation Law	Ψ_k	$\boldsymbol{J}_k$	ϕ_k
Mass	1	0	0
Momentum	$\boldsymbol{u}_k$	$p_k \bar{\bar{I}} - \bar{\bar{\tau}}_k$	$\boldsymbol{g}$
Energy	$e_k + u_k^2/2$	$\boldsymbol{q}_k'' + (p_k \bar{\bar{I}} - \bar{\bar{\tau}}_k)\boldsymbol{u}_k$	$\boldsymbol{u}_k \boldsymbol{g} + q_k'''$

The jump conditions can be derived imposing the mass, momentum and energy conservation through the phases interfaces, by performing volume and ensemble averaging and eventually neglecting the surface tension as done for the Eq. (1.9), (1.10) and (1.11). Where, a_i represents the interfacial area, V is the volume and $p_{k,i}$, $\bar{\bar{\tau}}_{k,i}$ are respectively the interfacial pressure and the shear stress tensor.

$$\sum_k \Gamma_k = \sum_k \frac{1}{V} \int_{a_i} \rho_k \boldsymbol{n}_k \cdot (\boldsymbol{u}_k - \boldsymbol{u}_i) dS = 0 \tag{1.9}$$

$$\sum_k \boldsymbol{M}_k = \sum_k \frac{1}{V} \int_{a_i} \boldsymbol{n}_k [\rho_k (\boldsymbol{u}_k - \boldsymbol{u}_i)\boldsymbol{u}_k + p_{k,i} \bar{\bar{I}} - \bar{\bar{\tau}}_{k,i}] dS = 0 \tag{1.10}$$

$$\sum_k E_k = \sum_k \frac{1}{V} \int_{a_i} \boldsymbol{n}_k [\rho_k (\boldsymbol{u}_k - \boldsymbol{u}_i)(e_k + u_k^2/2) + \boldsymbol{q}_k'' + (p_{k,i} \bar{\bar{I}} - \bar{\bar{\tau}}_{k,i}) \boldsymbol{u}_k] dS = 0 \tag{1.11}$$

Fuel Performance

As specified in the introduction, the complexity in the fuel performance modelling stems from the fact that it deals with a multiphysic problem, as it requires the coupled resolution of neutronics, thermal-hydraulics, heat conduction, fuel chemistry, fuel mechanics and fuel transmutation. The stability of the global algorithm often requires the use of advanced numerical methods, as in the case of [34]. The focus of this paragraph is on the heat conduction problem as it is what affects the most the neutronics.

As the fuel and the cladding are solid, the heat is transferred through them by conduction. This is true under good approximation also for the fuel-clad gap. This simply derives from geometrical reasons that make convective movements negligible. On the other hand, mostly in accidental scenarios where the temperature raises significantly, the radiation heat transfer may be accounted for accurate calculations as it depends on $(T_{fo}^4 - T_{ci}^4)$, respectively being the temperature of the fuel outer surface and the cladding inner surface. The heat conduction is based on the heat equation, which is available in Eq. (1.12). Where $\boldsymbol{r}$ is the location, t is the time, ρ is the density, T is the temperature, c_p is the specific heat capacity at constant pressure, $k(\boldsymbol{r}, T, t)$ is the conductivity and q''' is the volumetric heat generation term. The latter being the consequence of fission reaction rate and other radiation interaction rates. Basically, this equation has to be solved using the clad wall temperature as boundary condition, the heat generation term from the neutronics, the geometry as computed by the other physics and the conductivity and the specific heat capacity at constant pressure corresponding to the chemical evolution of the materials. It should be noticed that every term depends on the time as the burnup affects all these quantities and the power generation may follow a precise ramp. However, under normal operation, the time scale of the power variations and of the burnup effects is generally large enough to decouple these problems from the heat conduction. $-k(\boldsymbol{r}, T, t)\nabla T(\boldsymbol{r}, t))$ is the conduction term describing how the heat flows through the media. It derives from the Fourier law, which available in Eq. (1.13).

$$\rho(\boldsymbol{r}, t) c_p(\boldsymbol{r}, T, t) \frac{\partial T(\boldsymbol{r}, t)}{\partial t} - \nabla \cdot (k(\boldsymbol{r}, T, t) \nabla T(\boldsymbol{r}, t)) = q'''(\boldsymbol{r}, t) \tag{1.12}$$

$$\boldsymbol{q}'' = -k(\boldsymbol{r}, T, t) \nabla T(\boldsymbol{r}, t)) \tag{1.13}$$

Isotopic Evolution

The isotopic evolution models the variation of the nuclide concentrations following radioactive decays and the particles reaction rates. In this context, as previously specified, only neutron-nuclei

interactions are considered and neutron radioactive decays are totally neglected. The set of ordinary differential equations describing this phenomenon is called Bateman equations in honour of the mathematician who firstly derived them [35]. The generalised version that includes the effects of neutron transport is reported in Eq. (1.14). Where $N_i(\boldsymbol{r},t)$ is the concentration of the nuclide i, $\varsigma(\boldsymbol{r},t)$ is the microscopic reaction rate and λ is the total decay constant accounting for all the radioactive decays. On the left-hand side of the equation, there is the variation of the concentration of the nucleus i per unit of time. On the right of the equation, there are four terms. The first one is the production of the considered isotope through reaction rate of neutrons on other nuclei (e.g. radiative capture or fission). The second one is the production rate consequent through the decays of other nuclei yielding the considered isotope. The third one accounts for the removals by any radioactive decay changing the nucleus composition of the considered isotope. The fourth term is the disappearance of the nuclei i through any neutron interaction.

$$\frac{\partial N_i(\boldsymbol{r},t)}{\partial t} = \sum_{m\neq i} \varsigma_{i\leftarrow m}(\boldsymbol{r},t)N_m(\boldsymbol{r},t) + \sum_{m\neq i}(\lambda_{i\leftarrow m}N_m(\boldsymbol{r},t)) - \lambda_i N_i(\boldsymbol{r},t) - \varsigma_i(\boldsymbol{r},t)N_i(\boldsymbol{r},t) \tag{1.14}$$

- $\frac{\partial N_i(\boldsymbol{r},t)}{\partial t}$ is the variation in time of the i-nuclide's number density field.
- $\sum_{m\neq i}\varsigma_{i\leftarrow m}(\boldsymbol{r},t)N_m(\boldsymbol{r},t)$ is the production of $N_i(\boldsymbol{r},t)$ through nuclear reactions on other isotopes.
- $\sum_{m\neq i}(\lambda_{i\leftarrow m}N_m(\boldsymbol{r},t))$ is the production of $N_i(\boldsymbol{r},t)$ due to the radioactive decays of other isotopes.
- $\lambda_i N_i(\boldsymbol{r},t)$ is the removal of $N_i(\boldsymbol{r},t)$ caused by its radioactive decay (which may lead to different nuclides).
- $\varsigma_i(\boldsymbol{r},t)N_i(\boldsymbol{r},t)$ is the disappearance of $N_i(\boldsymbol{r},t)$ following nuclear reactions on this type of isotope.

1.2.2 Coupled Problem

Specific Definition of Multiphysics Modelling in Reactor Physics

Since the beginning of reactor physics modelling, unless for zero power experimental reactors or for the monitoring of zero power configurations of commercial reactors, realistic neutronic simulations have always included the coupling with a thermal-hydraulic module. However, reactor physicists focusing on neutronics have often treated the thermal-hydraulics as a secondary physics in service of the neutronics. Generally, a coarse meshing has been adopted, discretizing the core in radial meshes

representing one fuel assembly or a quarter of it for both neutronics and thermal-hydraulics. Moreover, frequently, the thermal-hydraulic simulations have been modelled with a 1D-axial approach, which neglects the exchanges of mass, momentum and energy among the fuel assemblies. Thanks to this coarse spatial discretization, such a simplified approach has often lead to sufficiently accurate results. However, the analysis of some safety and design parameters, like for instance the maximum linear power, may require a higher resolution. The conventional approach has been to derive them through the use of conservative assumptions.

In the last decade, thanks to the increasing computing power and to the bigger role played by the simulations in reactor design and safety assessment, many research groups have started to target higher-fidelity simulations that allow to directly retrieve variables at a finer scale, typically at the fuel pin cell level. In this way, more physical insight can be achieved and the safety and design phases can be supported with more accurate data. On the other hand, this intrinsically means to solve problems of bigger dimension and, most of the times, it requires the deployment of more advanced models in every physics. The enhancement of the modelling accuracy by replacing the simplified modules and assumptions by a more complete treatment of the coupled problem is the essence of multiphysic modelling.

Intrinsic Complexities of the Coupled Problem

In general, the coupling problems are both theoretical and very practical. For instance for the neutronics, since the cross-sections depend on the temperature and the density of the media, as shown in Eq. (1.15) (which is the steady-state version of Eq. (1.2)) and Eq. (1.16) (which simply derives from the definitions of macroscopic cross-section and number density), in coupled simulations, they are not fixed parameters. In fact, they depend on the thermal-hydraulic results, which are determined by the heat generation, which in turn is mainly function of the neutron flux. For this reason, in this kind of multiphysic problems, the neutronics is not linear anymore ($\Sigma_j(T,\rho) = \Sigma_j(T(\psi),\rho(\psi))$. Like in this example, in many applications, the interdependencies may change the nature of the problem, hence, it is important to treat the problem accordingly.

$$\boldsymbol{\Omega}\nabla\psi + \Sigma(T,\rho)\psi = \int_0^\infty dE' \int_{4\pi} d^2\Omega'\psi\Sigma_s(T,\rho) + \frac{\chi_i}{4\pi}\int_0^\infty dE' \int_{4\pi} d^2\Omega'\psi\Sigma_f(T,\rho)\upsilon + S \tag{1.15}$$

$$\Sigma_j(T,\rho) = \sum_i N_i * \sigma_{i,j}(T) = \sum_i \frac{\rho_i * N_{AV}}{M_i} * \sigma_{i,j}(T) \tag{1.16}$$

Very often, some physical phenomena may require different modelling scales. For this reason, strategies for the condensation of quantities computed on a finer scale and for the reconstruction of the missing information have to be developed. Moreover, the domains of each physics may completely

or partially overlap or even just communicate through an interface, hence, the compatibility among different models should be studied case by case.

Many questions rise about the structure of a multiphysic simulation tool, it may be composed of a set of single-physics solvers or be built monolithically since the beginning, accounting for all the physics of interest. In the first case, a great advantage is the possibility of using pre-existing codes that would also facilitate the modularity of the calculation scheme. The most frequent problems may be linked to the data exchanges, to the compatibility among solvers potentially written in different programming languages, to the supervision strategy and to the numerical problems. By numerical problems, it is meant that stability, accuracy and robustness are endangered by the use of pre-existing solvers with different internal precisions and discretization techniques. For this reason, especially in this case, the numerical optimization of the multiphysic coupling scheme is a crucial step of multiphysic modelling. The second approach would require very large efforts in order to achieve the capability of treating realistic full-scale problems. Furthermore, it would suffer the risk of being too application dependent.

Finally, while developing a coupling scheme it is important to have an idea of the sensitivity of each physics to another specifically for the particular modelling scenario. Given a set of targeted variables, it would be beneficial to have an idea about the order of magnitude of the cost and the benefits of adding a new model or removing simplifying hypotheses. Therefore, another issue of multiphysic modelling is that it often requires multi-disciplinary competences and a broad vision of the problem.

1.3 Strategies for the Multiphysic Modelling of a PWR along Irradiation

In this section, the fundamental modelling strategies adopted in the thesis are described. Firstly, the general approach behind the single-physics resolution is introduced to provide the main concepts and nomenclatures. In the second part, a general outline of the thesis is given.

1.3.1 Fundamental Elements on Single-Physics Modelling

Deterministic Neutronics

In respect of deterministic neutronic modelling, in order to handle a problem with so many degrees of freedom, mainly two different strategies are found in literature: dimensionality reduction and massive parallelism.

The first one is the classic and most widespread approach. It consists of two steps, a homogenization process, dealing with space homogenization and energy condensation, and the actual resolution

of the problem in its integrity, for this reason it takes the name of two-steps calculations. Given the general design of PWR cores, the main idea behind the homogenization is to exploit the fact that the reactor core may be considered as composed by the repetition of few fundamental domains, the characteristic assembly types. For this reason, during the first step, called lattice calculations (or spectra calculations), several 2D fuel assemblies are finely computed under simplified boundary conditions and for a set of possible core parameters. In this way, homogenized cross-sections are computed preserving the reaction rates so that an equivalent problem is defined on coarser energy and spatial meshes. In most of the cases, the parameters used in depletion calculations are burnup, fuel temperature, boron concentration and moderator density. Via this parametrization it is possible to synthesize, under simplifying hypotheses, how the neutronic cross-sections are influenced by the other physics. Most often, this homogenization is carried out independently from the coupling scheme and it could be seen as a preparation phase. The second step of the neutronic calculations, referred to as core calculations, deals with the computation of the entire domain defined by the homogenized cross-sections.

With respect to the massive parallelism, in the last decade some direct calculation schemes have been conceived relying on the use of very large computing power and thanks to efficient acceleration techniques. By direct simulations it is meant the resolution of the heterogeneous problem in its integrity without the homogenization under simplified boundary conditions. Many examples of both two-steps and direct calculations are given in the Chapter 2. For instance, [36, 37] belong to the first kind and [38, 39] follow the second one.

Thermal-Hydraulics

In a very similar way, the thermal-hydraulic modelling also deals with a necessary averaging in space and time of the equations, which, to some extent, is essential for the mathematical treatment of the governing equations. While for the neutronics the link between the low-dimensions problem and the reference one is done by the homogenization, for the thermal-hydraulics the information loss is resupplied under the form of closure laws. These equations are needed to bring information from the microscopic scale to the coarser one, in other words, to sum up the global effect of the neglected microscopic phenomena. For example, while modelling molecular motion, thanks to the averaging, it is possible to model the effects related to the global speed of the molecules, their macroscopic motion, i.e. the convection mechanism. However, in order to account for the diffusive component, which consists of the fluctuations of the speed around the average value, a closure law is needed. For the species mass flux it is the Fick's law and, while, in an extremely similar way, for the heat transfer, the conduction is represented by the Fourier's law.

As previously described in the introduction, some subcooled boiling may occur in PWRs, locally creating a biphasic flow. This type of flow may be modelled by considering a single field, which

corresponds to considering the flow as an undistinguished mixture of steam and liquid water. More advanced techniques use the multifield approach, which consists in the decomposition of the flow into portions characterized by a similar thermal-hydraulic behaviour. In the case of subcooled boiling, the flow regime is called bubbly flow, because it is characterized by steam bubbles created on the cladding wall and eventually detaching and disappearing in the main liquid bulk. Therefore, it might be worth consideration to consider two fields, one for the liquid bulk and the other for the steam bubbles.

Coming back to the closure laws, they are in general needed for inter-field or boundary interactions or, like in the single-field approach, to synthesize the lack of a multifield treatment. In most of the practical applications, on top of the closure laws, empirical or semi-empirical correlation may be included to simplify the treatment of complex terms. One simple example is the friction law for single-phase flow in a channel given by Darcy and Weisbach [40]. It reintegrates the microscopic effect of the pressure loss that occurs in pipes due to the fluid's viscosity along the surface of the pipe. The modelling of the momentum exchange between the wall and the fluid due to viscosity is substituted by a semi-empirical relation. Macroscopic variables like section's average velocity and the pipe's diameter are combined with an empirical friction factor based on the roughness of the surface and a dimensionless number characterizing the fluid motion in terms of its inertial force over the viscous one, the Reynold's number. Indeed, when it comes to hydraulic modelling, engineers often resort to dimensionless numbers in order to generalise the validity of correlations and properties found for specific experiments to wide class of problems.

Another key issue in fluid dynamics is the turbulence modelling. In fact, in most of the practical applications the flow is in the turbulent regime, which means that its motion is characterized by chaotic changes in pressure and speed. The opposite flow regime is the laminar one, which is characterized by a smooth behaviour. The motion type radically influences the modelling choices and the correlations to be used. A practical way to establish whether a flow is turbulent is to compare the Reynold's number to the reference value relative to the considered application (the higher this number the more turbulent is the flow). A common modelling approach is to average the Navier-Stokes equations in time in order to obtain a formulation in which most of the time-fluctuating components of the velocity disappear. However, one term describing the convective acceleration cannot be rigorously eliminated. In the context of Computational Fluid Dynamics (CFD), this term may substituted by a closure law (specifically called turbulence model) like for instance the famous $k - \epsilon$ model [41].

Fuel Performance

For the reasons introduced before, the fuel performance is clearly an example of modelling strategy for complex multiphysic systems. Depending on the importance of each physics on the key target

variables, simplified models may be used. For instance, the neutron transport may be reproduced by a model based on one group diffusion and the thermal-hydraulics, may be addressed using the 1D-axial Euler equation. Many models rely on empirical and semi-empirical models, often specifically working for some fuel rod types. Another important simplification that is often made is to have separate models depending on the scenario to be treated. A typical example are the twin fuel performance codes FRAPCON [42] and FRAPTRAN [43]. FRAPCON deals with steady-state fuel behaviour at high burnup (normal operating conditions). FRAPTRAN treats reactivity and Loss Of Coolant Accident. Both codes have been developed for the U.S. Nuclear Regulatory Commission by the Pacific Northwest National Laboratory, but because of the different targeted scenarios, two separated tools have been created.

Given the different sensitivities and interdependencies among physics, complex numerical algorithms are often involved. Nested iteration loops are frequently deployed in order to divide the convergence in subsets of the global problem. In many cases nonlinear solvers are implemented to face robustness and stability issues.

Isotopic Evolution

The strategy for the depletion simulations depends on the neutronic approach, direct versus two-steps, few examples are reported in Section 2.1. A crucial parameter in depletion calculations is the number of nuclides contained in the libraries. In case of industrial depletion calculations, few tens of isotopes may be considered [44], for referential calculations generally several hundreds of them are included, whilst in extreme cases two thousands different nuclides have been tested [38]. The associated memory cost depending on the resolution strategies may increase more than linearly and become a significant part of the total memory requirement.

Within a neutronic two-steps approach, the depletion calculations are performed at both stages. During the first step generally a large number of nuclides is considered, but generally, to reduce the memory footprint, the homogenized cross-sections are stored assembling a certain number of isotopes together into a fictitious one. Under this approach, the concentration of the fictitious isotope has no physical meaning, the macroscopic cross-section ($\Sigma = N\sigma$) condenses the contribution of all the isotopes for every combination of burnup and core parameters. Hence, in the second step, the Bateman equations are actually solved just for the isotopes that have not been assembled in the fictitious one, the particularized ones. In the second step, the depletion calculations compute only the concentration of the particularized nuclides, while the burnup dependence of their microscopic cross-sections is just pre-tabulated during the lattice calculations.

Generally, the Bateman equations are solved combining an iterative method, like Runge-Kutta, and a variant of the predictor-corrector approach. For instance, in [45], a polynomial extrapolation of the neutron flux and of the reaction rates within the time step are combined with a predictor-

corrector method. The order of the polynomial is arbitrary and just limited by the number of previously computed time steps. In this case, the predictor calculation consists of three points. Using the extrapolated neutron flux and reaction rates together with the isotopic concentrations at the beginning of the time step, the Bateman equations are solved to obtain the number densities at the end of the time step. In the second point, a flux calculation is performed with these number densities in order to obtain the new neutron flux and reaction rates. Finally, these quantities are compared to the extrapolated values and if the discrepancy is lower than a criterion the calculations proceeds to the next time step. On the contrary, if the test fails the corrector step has to be carried out. This procedure corresponds to repeating the predictor calculations using the last flux and reaction rates for the time interpolation. In case of failure the corrector step is iteratively repeated using the last computed flux.

1.3.2 Layout of the Thesis

The thesis is divided into nine chapters (introduction included). The second chapter deals with a review of the state of the art of the multiphysic coupling schemes. This survey addresses both the modelling choices and implementation details and the numerical methods adopted in the most relevant simulation tools. The third chapter introduces the codes available for this work and some examples of previously realized coupling schemes. An overview on the development of the general structure of the coupling scheme realized in the thesis is given in the fourth chapter. Starting from the formalization of the problem, the main modelling choices are discussed and, finally, some details are given about the implementation details. In the fifth chapter, the multiphysic coupling scheme is applied on a steady-state case study, a simple numerical algorithm is implemented and the best combination of models is selected from a set of suitable solutions. A major role of the thesis is to test the deployment of advanced models that allow to estimate a set of variables at the fuel pin scale. Given the problems of robustness and efficiency of this initial numerical method, in chapter six, a range of alternative solutions is explored and a customization of a widespread algorithm is proposed. The generalization of the coupling scheme for the modelling of PWRs along irradiation is described in chapter seven. In particular, models accounting for the evolution of thermodynamic properties of the fuel during the exposure and an algorithm for the research of a target boron concentration are included in the coupling scheme. Afterwards, a simple method for depletion calculations is implemented. In the last part of this chapter, the global scheme including all the previously mentioned features and exploiting the optimized numerical algorithm is tested on a constant power irradiation scenario. Finally, the discussion and the conclusions are respectively given in chapters eight and nine.

Chapter 2

State of the Art

The multiphysic modelling has increasingly attracted the interest of the nuclear reactor physicists world wide. Recently, a large number of projects has started. Most of them approach the problem combining pre-existing specialised solvers that treat only a subset of the physics. In particular, if it is chosen to avoid intrusive modifications of the solvers, the technique takes the name of black-box coupling [46]. The advantages in terms of simplicity and modularity are clear. Whilst, the main inherent disadvantage is that, in this way, it is possible to access only to a limited set of variables. Hence, some advanced algorithms conceived specifically for a given multiphysic coupling scheme may not be viable because of the need for unavailable internal quantities (an example is given in [47]). This could constitute a limit in terms of stability and robustness for very strongly coupled problems, but many successful works of this type have been published. As a matter of fact, in literature there are few examples of solver directly dealing with the multiphysic problem in its integrity, hence, using the so-called monolithic approach. Most of the fuel performance codes are in some sense using a monolithic approach, but as stated in the introduction they extensively rely on strongly simplified models for neutronics and thermal-hydraulics. One example of solver simultaneously dealing with neutron diffusion and thermal-mechanics is given in [48].

Once the adopted models are identified and it is defined how the data is exchanged among them, it still needs to be defined the numerical method to be used to ensure the convergence. The coupled neutronic, isotopic depletion, thermal-hydraulic and fuel performance problem falls under the class of large nonlinear system of equations. Given the increase in both the problem size and the complexity of the models, the numerical algorithm is very important to ensure a stable and efficient resolution of the problem. In literature, a wide range of solutions specific to this kind of problems is available. The state of the art is divided in two parts: the first focuses on the modelling choices and the data exchange, while the second deals with the most common numerical solutions.

2.1 Modelling Choices and Data Exchange

In this section, a variety of coupling schemes is considered. All of them rely on the use of specialised solvers. Only coupling schemes including at least neutronics, thermal-hydraulics and heat conduction for the modelling of PWRs are considered. Applications referring to steady-state and depletion simulations are preferred, but also few examples of coupling schemes conceived for the modelling of fast transient scenarios are reported, as some of the techniques they adopt could be implemented in this work. The coupling schemes are divided into three groups following the conventional, the *best-estimate* or the *high-fidelity* approach. *High-fidelity* being the most accurate level of modelling, while the *best-estimate* one generally refers to simulation schemes that aim at approaching such a precision, while reducing the computing cost. For a more detailed description of some specific single-solver methods please refer to Chapter 3.

As explained in the introduction, the level of homogenization is a crucial factor as it determines the problem dimension, its complexity and also the scale at which variables are exchanged. For this reason, the level of fidelity is often directly associated to the homogenization level. For the conventional approach, coarse mesh homogenization is considered together with low order transport approximation. The reported *best-estimate* deal either with a hybrid approach, coarse mesh homogenization plus pin power reconstruction, or with pin-cell homogenization. Clearly, especially, when choosing to have the different physics on different scales also condensation techniques have to be considered, as for example in the case of sub-pin temperature radial distribution and coarse mesh neutronic homogenization. In respect of the *high-fidelity* approach direct heterogeneous calculations are reported. Few examples of Monte Carlo are reported as the problematic encountered may be quite different.

A similar classification applies for the thermal-hydraulics. For the conventional approach, quantities are averaged at the assembly level. In this case, the flow can be assumed as prevalently axial, hence, unless the radial power distribution is very heterogeneous, 1D models are sufficient and each channel is considered as completely isolated from the others. The intermediate level of refinement deals with radial meshes of the subchannel type (i.e. the space included at the centre of four fuel rods). At this scale 3D models are required, especially considering the intrinsic heterogeneities of fuel assemblies (guide tube, fuel with burnable poison, etc.). Both *best-estimate* and *high-fidelity* schemes often include subchannel thermal-hydraulics, but eventually the *high-fidelity* ones may use multi-field modelling. Beyond this discretization level, CFD is required, but it is still too expensive for full core calculations. Its application is generally limited to a small portions of the domain.

With respect to the fuel performance, it is generally included just in the most advanced schemes. In the case of conventional ones, a simple heat conduction may be performed by the thermal-hydraulic solver using fuel properties averaged over the irradiation cycle and therefore, burnup independent geometry, conductivity laws and chemical compositions. In alternative, in some cases,

simplified correlations to include the burnup dependency of the conductivity and the fuel-clad heat transfer coefficient may be used. For the *best-estimate* approach, empirical laws accounting for the burnup effects may be used. Metamodels and pre-calculated lookup tables are often found in both *best-estimate* and *high-fidelity* coupling schemes. Finally, for the most referential calculations the specialised fuel performance solver may be included.

For the depletion calculations, attention is given to the number of tracked nuclides. Innovative strategies are reported for the *high-fidelity* schemes, as the computing cost of solving each steady-state becomes prohibitive.

For the conventional schemes, a sort of generic approach is described, the considered sources are reactor physics manuals, in particular [31], but also some publications of industrial calculation schemes are reported. In the other sub-sections, the attention is centred on two among the largest projects worldwide. The first one is NURESIM European Platform and following projects [49] as rich in *best-estimate* applications. The second one is VERA-CS [38, 50] which is a reference for *high-fidelity* modelling. Another example is added for each group, due to its remarkable performance, respectively CASMO/SIMULATE[36] and NNR [51]. Confirming the large interest in multiphysics, many other projects are found in literature. Among the most famous ones that are missing, there are GeN-Foam [52], MAMMOTH [53], NUMPS [54] and SHARP [55] (mostly for Sodium Fast Reactor (SFR)).

2.1.1 Conventional Approach

In this section, the industrial approach for multiphysic depletion calculation schemes is globally described without entering into details that may be specific to a given company. As mentioned before, such an approach naturally gives more attention to the neutronics. For industrial calculations, almost in any case, the neutronics is performed following the two-steps calculations; a description of this process can be found in [31], pages 196 to 199. The raw input is a set of referential multi-group neutron cross-section, characterized by about three hundred energy groups. These cross-sections have been previously computed directly from experimental data using reference calculations made once and for all and they are valid for almost any deterministic modelling of Light Water Reactor (LWR). The multigroup cross-sections depend on the isotope, the reaction, the energy group and the temperature. As specified in the introduction of this section, the first step aims at creating an equivalent problem of lower dimension. Ideally, a set of cross-sections depending on few energy groups and describing the average response of a coarse mesh, should aim at preserving the reaction rates of the reference problem. However, to do so the multi-group neutron flux should be known, since different neutron flux would lead to different homogenized cross-sections. On the other hand, the real neutron flux is the ultimate unknown of the problem, hence, an approximated one is used in the homogenization phase. Exploiting the fact that the core is made out of the repetition of several

type of fuel assembly, each different type of assembly is used for the homogenization. The reactor under nominal conditions is almost always critical, therefore every assembly in it is critical too. For this reason, the assembly is considered under reflective conditions and a homogeneous leakage term is iteratively researched until the critical state is found. In order to cope with the abrupt variation of the flux due to the resonances, before that the flux and leakage calculations are performed, the SSH calculations have to be done for the main resonant isotopes. Exploiting the fact that most of the heterogeneity is in the radial plane, in order to reduce the computing time, just 2D transport calculations are done.

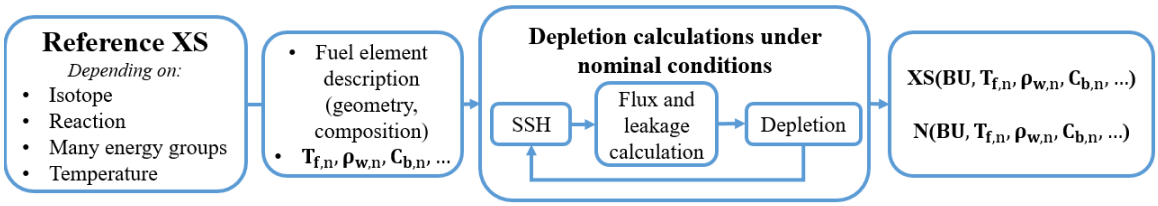

Figure 2-1: Depletion calculations (within lattice calculations) scheme under nominal conditions used to produce homogenized cross-sections (**XS**) for the nominal conditions and the isotopic composition of the assembly at every burnup step. SSH stands for Self-Shielding calculations. The nomenclature of the variables is the same used in sub-section 1.1.2. The subscript n stands for nominal value, while **N** represents the number density fields that are produced for each burnup step and can be used for the perturbation calculations.

The few-groups homogenized cross-sections should also contain how the cross-sections of each medium vary for a combination of independent parameters. These parameters are normally the burnup, the fuel temperature, the moderator density and temperature, the boron concentration and eventually the presence of a control rod. In order to reduce the number of calculations to be performed to compute the associated homogenized cross-sections, a depletion calculation is done for each assembly type under the guessed nominal conditions, as described in Fig. 2-1. Afterwards, for a subset of the evolution steps, using the stored isotopic number densities, each assembly problem is solved for every possible combination of the other parameters, as synthesized in Fig. 2-2. In this way, few groups cross-sections are stored for every possible combination of the parameters, depending on the specific medium, the considered reaction and for few energy groups. Therefore, even if this process is performed in a fully decoupled way, it produces cross-sections capable of modelling how a medium behave under a range of possible multiphysic states.

It should be noticed that for every medium the homogenized cross-sections include the contribution of all the isotopes contained in it. However, the distinction between microscopic cross-sections and isotopic concentration is kept just for few isotopes, while a fictitious isotope assembles the contribution of all the others. This distinction is made just to reduce the memory footprint. For this fictitious isotope the burnup becomes just a parameter that affects the homogenized macroscopic cross-section. While, for the isotopes that are tracked separately, the actual isotopic concentrations

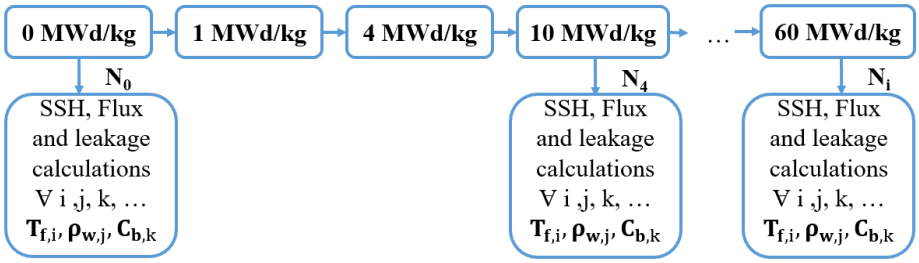

Figure 2-2: Scheme of branch calculations. This step of the lattice calculations is needed to compute the homogenized cross-sections for a subset of the burnup steps and for core conditions different from the nominal ones. SSH stands for Self-Shielding calculations.

are available and can be used for depletion calculations and their microscopic cross-sections are parametrized in burnup. Generally, at least the most important fission products (the ones that have directly or through their descendants the biggest impact on the reactivity) are kept separately because of their rapidly changing concentrations. A global scheme of the homogenization is reported in Fig. 2-3.

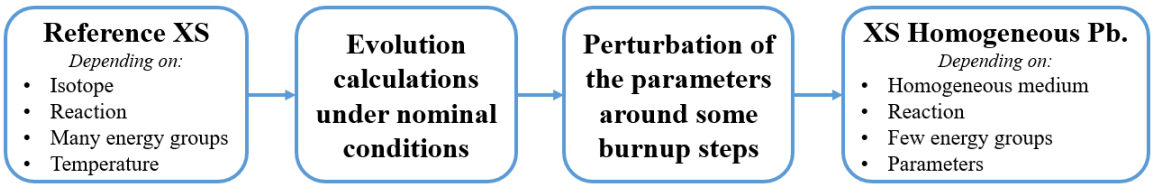

Figure 2-3: Global scheme of the cross-section (**XS**) homogenization process. The general purpose is to underline that the target is to produce equivalent homogeneous cross-sections for few energy groups.

A different treatment is needed for the homogenization of the reflector. Since no fissile material is contained in the reflector structures, the neutron flux spectrum is mostly dictated by the neighbouring fuel assemblies. One of the simplest approach, commonly used in the french industry, is the 1D traverses homogenization technique [56]. This method consists in performing source calculations through the reflector on one characteristic neutrons direction, considering a system that includes also a set of adjacent assemblies. In this way, the homogenised cross-section are computed so that the proportion of neutrons reflected back to the core along the considered direction is kept equal to the heterogeneous case. In most of the cases, zero flux on the outer surface of the reflector is used as boundary condition. Also in this case, the calculations may be performed for a combination of parameters, which normally are the boron concentration, the burnup of the neighbouring fuel assembly, its temperature, the density and the temperature of the coolant that passes through the reflector and temperature of the structures. Nevertheless, the dependence on these parameter is milder.

The last step before the core calculations is the equivalence problem, a description is given in

[31], pages 53 and 54. The cross-sections were produced imposing the conservation of quantities between a heterogeneous and a homogeneous calculations performed by a lattice solver. The equivalence is needed to account for the fact that the core solver is different from the lattice one. A similar equivalence process is also performed when replacing the heterogeneous problem with the homogeneous one. Multiple strategies exist, a different approach is used for the fuel and for the reflector assemblies. A further differentiation is made depending on the chosen spatial discretization technique: nodal expansion against finite element or finite difference methods. These methods are a crucial step in the resolution of the problem since they transform the differential equations into a system of algebraic equations, some insight is given in [57, 58].

After the equivalence process, the focus finally returns to the entire domain. As mentioned in the introduction of this sub-section, the reactor is modelled by the coupling of the core solver to a thermal-hydraulic model. In industrial applications this is often a module integrated in the neutronic core, like in the case of CRONOS [59, 60], but coupling schemes with a specialised solver are becoming more and more common. An example of how these schemes are realized can be found in [31], pages 215 to 217. The core solver often relies on 3D nodal diffusion methods with few energy groups and coarse radial meshing (assembly-wise). This approximation has demonstrated great robustness and time efficiency. This scale of modelling matches very well also the needs of a simplified thermal-hydraulic module. Indeed, as mentioned in the introduction, under nominal conditions the effects of the transversal flow are quite negligible in case of coarse mesh. Moreover, the prediction of the power distribution is simplified by two elements. The first is that the mean free path of the particles is sufficiently small as compared to the assembly size that it is quite accurate to assume that all the energy produced by fission is released within the mesh. While, on finer scales, the photons transport and the neutron scattering might significantly change the balance. The second consideration is that with this meshing, it is easier to estimate the heat generation directly in water, because at the subchannel scale the fuel to moderator ratio varies among channels. A global repartition constant might be effectively used to reproduce the average heat generation in water. For steady-state conditions, all the power produced in the fuel is removed by the coolant, therefore, the direct water heating is only needed to compute the cladding wall heat flux and for the heat conduction in general. In fact, the heat conduction is performed using one average fuel rod per fuel assembly. In some cases, the evolution of the conductivity and of the gap width are taken into account via parametric tables. Local variables like the maximum fuel centreline temperature are obtained through post-processing by the use of conservative factors that overestimate the local peaking factor. The radial discretization for the three physics is represented Fig. 2-4. Further in this sub-section and in Chapter 4, it is possible to appreciate some of the challenges associated to a further radial mesh refinement.

The depletion calculations are normally treated as a sequence of steady-state calculation. Every

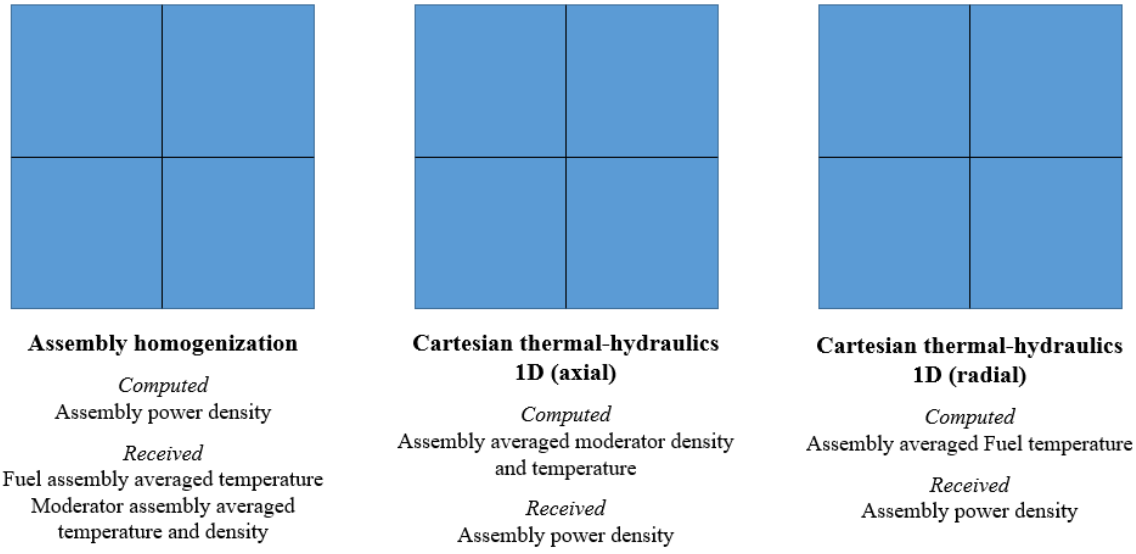

Figure 2-4: Typical radial discretizations according to the conventional multiphysic modelling, a system of 2x2 assemblies is reported in this example. For the heat conduction, an equivalent fuel rod is considered for each fuel assembly. The reported heat conduction mesh describes the resolution of the results (assembly-wise), while the sub-pin radial discretization used for the simulation of each equivalent fuel rod is not displayed. Assembly homogenized variables are exchanged among the three physics.

steady-state simulation includes the resolution of the coupled neutronics and thermal-hydraulics problem plus the research of the boron concentration and of the control rods that make the reactor critical. Different time step management strategies are adopted, one of the most widespread is the predictor-corrector. Finally, the easiest way of validating such a scheme is to compare the predicted Critical Boron Concentration (CBC) to the measured one in actual reactor, when this data is available. An example is given by the code ARTEMIS produced by Framatome [61], which has demonstrated to be able to predict the CBC over five cycle of a commercial PWR within a maximum error of 40 ppm.

2.1.2 *Best-Estimate*

NURESIM Platform

NURESIM is the European platform for best-estimate simulations in support to the safety and the design of LWRs. In past years, a lot of effort has been put into multiphysic modelling. A set of neutronic, thermal-hydraulic and fuel performance codes produced by several European organizations have been integrated in an environment derived by the open-source software SALOME [62]. SALOME provides tools for data manipulation, exchange and storage. The fields and the meshes of the variables of every physics are exchanged under the MED (Modèle d'Echange des Données) format, which is a specification of the HDF5 format [63]. In the last fifteen years, this platform has

been continuously extended thanks to the European projects NURESIM, NURISP, NURESAFE [49] and more recently to HPMC and McSAFE [64, 65]. The first three projects have focused on design basis accidents. In particular, in terms of PWR multiphysic modelling, some of the transients that have been treated are the boron dilution accident, the rod ejection accident, the main steam line break and the Loss Of Coolant Accident. The most recent projects, High Performance Monte Carlo Methods for Core Analysis (HPMC) and McSAFE focus also on the pin-by-pin multiphysic depletion calculations. However, as the acronym says, Monte Carlo codes are deployed in this project. NURESIM includes the open-source software for uncertainty quantifications URANIE [66]. Overall, none of these projects exactly matches the simulation type that is targeted in this PhD thesis. Nevertheless, the works published in this context are rich of interesting techniques that may be transposed to the multiphysic pin-by-pin modelling along irradiation.

In NURESIM several fast running calculation schemes able to locally predict the pin power distribution are implemented. These methods are based on the pin-power-reconstruction method [67, 68]. This technique deals with the combination of a coarse mesh calculation of the entire domain, generally assembly homogenized and with two energy groups, and a local heterogeneous form function to access approximated local safety variables. Two neutronic codes implemented in NURESIM are able to perform the pin power reconstruction. Both of them have given the flexibility to the user to arbitrary choose in which meshes perform the pin-power-reconstruction, thanks to a non-conform definition of the geometry. In [69], the implementation of the pin power reconstruction in the reactor dynamics code DYN3D [70] is described. In this case, assembly homogenization is done and the heterogeneities within the node are taken into account through the combination of a semi-analytical and form functions. The semi-analytical one is derived from the homogeneous cross-sections, through the resolution of the two groups diffusion with the boundary conditions given by the core solver and under the hypothesis of exponential variation in time. The form function derives from the necessity to account for the heterogeneities that are always present within a fuel assembly (guide tubes, control rods, poisoned fuels). It is computed as the normalized fission rates per pin cell, which are computed by a lattice solver in a decoupled way for a set of burnup states [69].

An application of this method within a multiphysic coupling scheme for transient calculations is available in [37]. In this application, DYN3D is coupled to the thermal-hydraulic code COBRA-TF [71], which is shortly described in the following section. Also CTF allows to use non-conform meshes, hence, it is possible to obtain a consistently hybrid approach with local refinement only where necessary. The radial discretization is depicted in Fig. 2-5. In this example, the thermal-hydraulic channels are defined rod centred, instead of the classic coolant centred approach. A limitation of this pin power reconstruction is that, while the refined power distribution is used by CTF, DYN3D only receives the thermal-hydraulic variables averaged over the coarse mesh (assembly-wise). Indeed, the thermal-hydraulic feedback is integrated via the semi-analytical function, which only deals with the

assembly homogenized cross-sections. However, it should be noticed that this function also accounts for the variation of the parameters in the neighbouring assemblies via the boundary conditions. The results obtained with this technique are compared to the standard assembly-wise approach on a 3x3 PWR MOX/UO_2 mini-core with radial reflector derived by the transient OECD/NEA benchmark [72]. During the peak, the hybrid approach allows to predict a 0.7 % higher total power and 35 K (+3.1 %) higher maximum fuel temperature. At the end of the transient, the assembly-wise model stabilizes at a power 6.7 % higher and an average fuel temperature 10 K larger (+1.5 %). As stated by the authors, due to the lack of local thermal-hydraulic feedback, the prediction of the pin-wise quantities during the peak of the transient can be considered as systematically overestimated. Overall, the hybrid model is giving an inexpensive and conservative estimate of local quantities, more representative than just applying a form factor based post-processing.

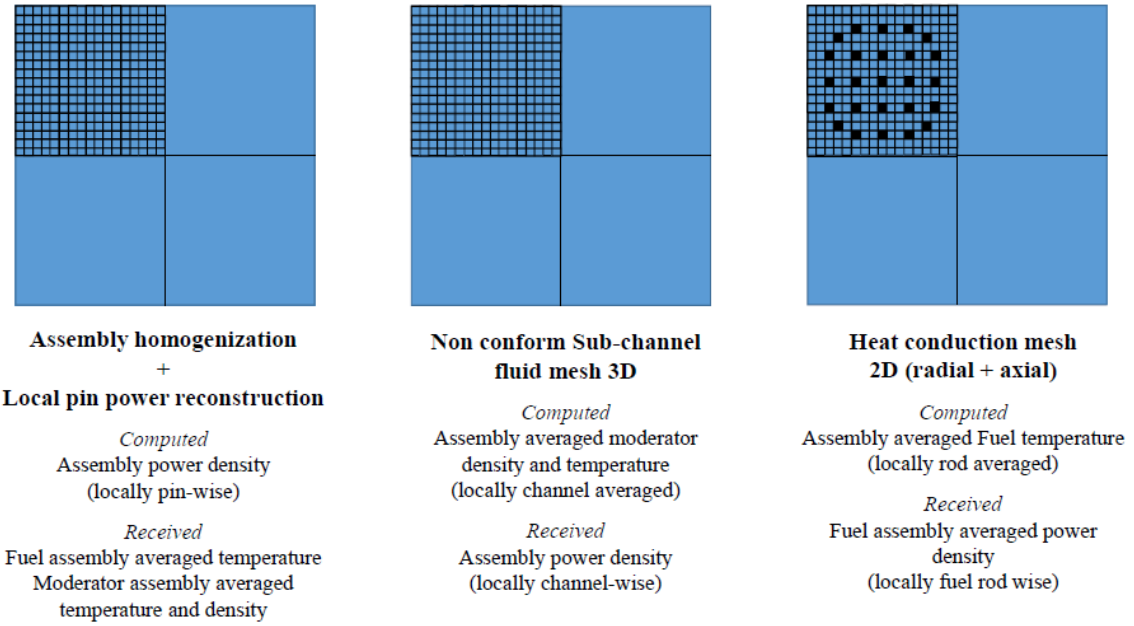

Figure 2-5: Hybrid approach used in some DYN3D/CTF coupling schemes to predict variables at the pin-cell scale only in a subset of the assemblies. In this example, the meshes are reported for a 2x2 assemblies system. For the heat conduction, in case of coarse discretization, an equivalent fuel rod is considered for each fuel assembly. The reported heat conduction mesh describes the resolution of the results (assembly-wise or pin-wise), while the sub-pin radial discretization used for the simulation of each equivalent fuel rod is not displayed. The thermal-hydraulic feedback is always integrated on the coarse mesh.

DYNSUB [73], another coupling scheme based on DYN3D and SUBCHANFLOW has been realized outside the perimeter of the European project. It has been successfully applied for a full core rod ejection accident with one eight symmetry [73, 74] and good results emerged from a validation process [75] against experimental results on the Special Power Excursion Reactor Test III [76, 77]. The main difference with what has been done in NURISP is that DYNSUB performs full-

core pin-cell homogenized calculations using the simplified spherical harmonics of order three (SP_3). Therefore, the computing cost is much higher, but the accuracy is significantly improved thanks to the avoidance of reconstruction techniques and the integration of a pin-by-pin thermal-hydraulic feedback.

The other neutronic code that allows to perform the pin power reconstruction is COBAYA3 [78, 79]. In this case, the pin power reconstruction is obtained through an iterative process between ANDES (Analytic Nodal Diffusion Equation Solver) [80] and COBAYA3-PBP, the pin-by-pin solver of COBAYA3. ANDES is used for the 3D resolution of the whole domain with a quarter of assembly homogenization. From its results, the boundary conditions are updated for the sub-domains to be more accurately calculated by COBAYA3-PBP. This lattice solver computes the fine power distribution, update the nodal cross-sections and set the new boundary conditions for ANDES. This process is iteratively repeated until local convergence criteria are satisfied both for the nodal and the pin-by-pin solutions. This pin power reconstruction technique requires more computing power than the one presented for DYN3D/CTF since several lattice and core calculations have to be performed before convergence. On the other hand, the subchannel feedback can be accurately integrated at the local scale and even the quality of the homogenized cross-sections is improved thanks to the integration of the more accurate boundary conditions.

This power reconstruction technique has been applied in [81]. For this application, COBAYA3 is coupled to the thermal-hydraulic code SUBCHANFLOW [82, 83] in a hybrid approach similar to the one just mentioned for DYN3D/CTF [37]. A coupling scheme COBAYA3/SUBCHANFLOW was already realized in [84]. SUBCHANFLOW is based on a two phase, single field, three-equations model. The three conservation equations are the mass, momentum and energy balance for the mixture. The main simplifying hypothesis of the model is zero convective transport of lateral momentum due to the dominant friction term. In the last section of [81], a code-to-code validation of this hybrid scheme against the reference COBAYA3-PBP/CTF whole core pin-by-pin and the standard nodal approach coupled to CTF is presented. The selected case study corresponds to the steady-state conditions obtained at the end of the rod ejection accident described in the OECD/NEA PWR MOX/UO2 benchmark [72] (the same benchmark used by CTF/DYN3D). The considered core configuration is very asymmetrical and permits to fully test the capabilities of the hybrid scheme. Nevertheless, the power level is 16.2 % of the nominal power, hence the global thermal-hydraulic coupling is expected to be weak, at least outside the assembly where the control rod has been ejected. The main result is that the hybrid scheme allows to access to local safety parameters of the targeted assembly with a computing time eight times lower than the reference(4.8 h vs 37.3 h) and using only one processor, instead of the 113 CPUs exploited for the reference simulation. The obtained power distributions on the coarse nodes are axially integrated to be compared over a 2D plane. The maximum observed relative discrepancy is in the refined assembly, the hybrid approach under-predicts the power of

the 4.24 %. The hottest fuel centreline temperature predicted by the hybrid model is 1441.2K, to be compared to 1238.4 K as computed by the reference and 1090.2 K according to the standard approach (without power reconstruction). It should be considered that the standard approach can only calculate an average value for the quarter of assembly, hence, it is necessarily underestimating the pick temperature. As suggested by the authors, probably a big part of the discrepancies is deriving from the different thermal-hydraulic solver and the different treatment of the transversal flows. Nevertheless, the results cannot be judged as totally satisfactory.

In respect of the fuel performance modelling, the codes SCANAIR [85] and DRACCAR [86, 87] have been implemented in NURISP [49]. Both of them mainly target accidental scenarios. SCANAIR treats Reactivity Insertion Accidents (RIAs), its validation is based on the Cabri International Program [88], the NSRR [89] and other experiments. In order to better reproduce this type of transient, its thermal-hydraulic module may be substituted by the coupling with the thermal-hydraulic subchannel code FLICA4 [90] (its description is given in sub-section 3.2.1), as specified in [49]. DRACCAR aims at reproducing Loss Of Coolant Accidents, for this purpose, it is coupled to the thermal-hydraulic system code CATHARE [91]. Both SCANAIR and DRACCAR need to perform fuel performance calculations in order to provide the initial conditions for the transient. This task is handled by FRAPCON [42], as explained in [92] and [93] for SCANAIR and the same approach is planned in [94] for DRACCAR [1]. FRAPCON is one of the reference codes for the fuel behaviour modelling of the type considered in the thesis. Indeed, it is specialised in the simulation of the fuel rods under steady-state conditions along one or more irradiation cycles. Its application in NURESIM has only the role of preparing the initial conditions for the transient calculations of the other two fuel performance codes. In a similar way, TRANSURANUS [96] is coupled to DYN3D in [97], but this is done outside the NURESIM platform. Anyway, also in this case, even if TRANSURANUS is capable of modelling fuel under normal operation, it is used only to model accidental scenario like boron dilution [98].

In the context of HPMC and McSAFE the selected neutronic Monte Carlo codes are : MCNP [99], MONK [100], SERPENT [101] and TRIPOLI [102]. These solvers are coupled to SUBCHANFLOW or FLICA4 and it is planned to include also TRANSURANUS in the scheme in order to account for the evolution of the fuel thermal properties. Many interesting neutronics-thermal-hydraulics coupling schemes have been realized. Some of them were already built during the NURISP project and have been compared on a single pin benchmark [103]. SERPENT/SUBCHANFLOW has been tested on a single fuel assembly benchmark [104] and its capability to scale to a full VVER (water-water energetic reactor) core is shown in [105]. At the LPEC laboratory a PhD thesis has been done, within McSAFE cooperation, on the coupling of Tripoli-4® and SUBCHANFLOW for the modelling of a RIA [106]. Nevertheless, all these works mostly focus on the problems specific to the coupling

[1] It is unclear whether these applications are part of the NURISP platform: in [95] it is specified that the APIs will be based on what has been done in NURESIM, but [92, 93, 94] do not mention anything about it.

of Monte Carlo codes.

A very interesting coupling scheme, SERPENT/TRANSURANUS, is implemented in [107]. This is among the first coupled burnup calculation schemes for normal operation in NURISP. The modelling capability is demonstrated on a case derived from the burnable absorber rod benchmark [108]. The domain is a 3x3 rods lattice, the central one contains Gd_2O_3 doped UO_2 and it is surrounded by others made out of fresh UO_2. The rods containing burnable poisons, especially gadolinium, are the most difficult to be computed by simplified neutronic modules like the one present in TRANSURANUS. For this reason, this benchmark offers the possibility to measure the need for a more accurate neutronic model by comparing the results produced by the stand-alone TRANSURANUS and those computed by the coupling scheme. To simplify the comparison, the thermal-hydraulic conditions are pre-calculated and imposed in a decoupled way to both the calculations schemes. SERPENT computes the radial power distribution at the sub-pin level, under the hypothesis that it is entirely deposited where the fission events occur. Since TRANSURANUS uses an even finer radial mesh, a piecewise linear fit that conserves the total power of the axial slice is used in order to convert the power distribution to the fuel performance mesh. For the exchange of the fuel temperature profile, values per node are provided to SERPENT and in this case a simple volume averaging is needed. Both these data exchanges are not done in memory, they require creations and manipulations of files. The isotopic depletion is done using 14th order Chebyshev Rational Approximation Method (CRAM) [109] and the linear extrapolation time integration method with 10 sub-steps. CRAM can be considered as a less expensive alternative to the classic predictor-corrector scheme. The results show that the neutronic module of TRANSURANUS may predict a local power up to -60% or $+80\%$ different from the coupled model at 0.21 MWd/kgU. The discrepancies decrease significantly with the exposure. At 12.6 MWd/kgU the error is still comprised between -28% and $+18\%$. Nevertheless, as found in [110] and in previous studies of the PhD student [111], this large difference in the local power has a mild effect on the fuel performance. The maximum local temperature difference is 56 °C at 0.21 MWd/kgU and 23 °C at 12.6 MWd/kgU. Hence, as stated also by the author, there is not a big impact on the prediction of safety parameters. For the coupled simulation, the total simulation time is 24.5 days with 144 processor, hence 9.7 CPU years [2]. In respect to the small domain and the relatively high computing time, it should be considered that SERPENT is a Monte Carlo code and that the power distribution is computed on a extremely fine scale.

CASMO/SIMULATE

CASMO and SIMULATE are two deterministic neutronic codes developed by Studsvik AB Swedish company. CASMO is the component for lattice calculations, while SIMULATE targets core simu-

[2]The machine utilized consists of one high-memory node consisting of four Intel Xeon E7-8890 v3 processors with 72 physical cores sharing 2 TB of RAM.

lation, for this reason, they are often mentioned together (CASMO/SIMULATE), referring to the two-steps scheme they are combined in. CASMO/SIMULATE has been used in LWR analysis for more than thirty years. Essentially, it exploits coarse mesh nodal calculation combined to a pin power reconstruction technique [67]. Already in 2009, this code has shown excellent multiphysic modelling capabilities while coupled to COBRA IIIC for thermal-hydraulic 3D simulations. The robustness and the quality of this simulation tool has been proven on international benchmarks and experiments [36, 67, 112]. Moreover, sensitivity and uncertainty analysis capabilities have been implemented and verified on the UAM benchmark [113].

In particular, in [112], CASMO-5/SIMULATE-5 and its new thermal-hydraulic module and its newly implemented hybrid depletion strategy are tested on the Benchmark for Evaluation and Validation of Reactor Simulations (BEAVRS) [26]. This benchmark may be considered as a world wide reference, also because it is very difficult to access to operational data during normal operation for an entire PWR core. Moreover, the measurements are highly detailed and permit to asses the capability of predicting local variables. The considered thermal-hydraulic module has a 1D model and is used with an assembly-wise radial discretization. The hybrid depletion strategy is very similar to the one described in the previous sub-section. The actual number densities of some isotopes are computed during the core calculations, while for the others the number densities predicted by the lattice simulations are used. The results reported in [112] show a reduction in the prediction capability of this calculation scheme (CASMO-5/SIMULATE-5) as compared to the measured data and the previous version CASMO-4/SIMULATE-3. At the beginning of the first cycle, the CBC is over-predicted of a maximum of about 150 ppm by both the calculation schemes. During the rest of the cycle, it is within a range of 50 ppm for both the simulation schemes. In the second cycle the discrepancy is steadily decreasing with burnup, starting from a value of -115 ppm that becomes about -75 ppm at the end of the cycle. A similar trend is observed for CASMO-4/SIMULATE-3, starting from about -80 ppm and ending at about -20 ppm. These results are summed up in Table 2.1.

Table 2.1: The difference between the CBC as predicted by the CASMO/SIMULATE calculation schemes and the measured values provided by the BEAVRS benchmark for the first two cycles.

ΔCBC [ppm]	1st Cycle	2nd Cycle
CASMO-5/SIMULATE-5	+150	-115
CASMO-4/SIMULATE-3	+150	-85

Further comparisons have been performed on the power distribution as measured by the fission chambers and as predicted by the virtual fission chamber detectors modelled by CASMO-5/SIMULATE-5 (assembly-wise). The results are available for three burnup states Beginning Of Cycle (BOC), Middle Of Cycle (MOC) and End Of Cycle (EOC), respectively corresponding to 0, 6.112 and 12.519 MWd/kg, they are reported in Table 2.2 in terms of Root Mean Square (RMS)

and maximum absolute value (MAX(ABS())).

Table 2.2: The relative difference between the assembly-wise and axially collapsed power distributions as predicted by CASMO-5/SIMULATE-5 and the measured values for three burnup steps.

$\Delta_{rel}q$ [%]	BOC	MOC	EOC
RMS()	6.89	2.62	3.52
MAX(ABS())	+16.5	+6.1	-6.5

2.1.3 *High-Fidelity* and Massive Parallelization

CASL-VERA

The Consortium for Advanced Simulation of Light Water Reactors (CASL) [114] has developed VERA-CS, the Virtual Environment for Reactor Applications Core Simulator [38, 50, 115]. The aim of VERA-CS is to perform high-fidelity simulations of PWRs following the standards required by the U.S. Department of Energy Nuclear Reactor Simulation Hub. VERA-CS is a real reference for this PhD thesis, since it contains several coupling schemes dedicated to the modelling of the same type of scenario. The key target variables are local parameters like the pin-resolved power distributions, moderator density and fuel temperature and global ones like the boron letdown along irradiation. However, this project gathers among the most advanced calculation schemes and often the most high-fidelity models are deployed. The capability of performing full core depletion calculations at very fine scale has been demonstrated on multiple applications and validated on international benchmarks and against published data of commercial reactors. Neutronic codes among the most advanced have been coupled to referential thermal-hydraulic subchannel and fuel performance ones, creating a state of the art modelling environment. Also VERA-CS has included a dedicated toolkit for uncertainty and sensitivity analysis: VERA-CS Uncertainty and Sensitivity Analysis Toolkit (VUSAT)[116].

One key feature of VERA-CS, which exceeds the perimeter of this PhD thesis, is the fully coupled modelling capability of some phenomena related to the Chalk River Unidentified Deposit (CRUD)[117, 118]. The CRUD is a porous material accumulating on the outer surface of the cladding, which can trap the water in the proximity of the cladding. It can be an important safety concern in both nominal and accidental conditions. In nominal conditions it may cause power shifts due to the boron accumulation, it can enhance the localized corrosion due to the degradation of the heat transfer coefficient and it can increase the radioactivity of the fuel rods as the trapped elements may be activated by neutron capture.

With respect to the trade-off precision versus computing cost, referential simulations are provided, but the required computing power is enormous. Reasonable calculation times are achieved mainly thanks to the massive parallelization. Normally the simulations are performed on platforms with a prohibitive number of cores, up to more than 300'000. Practical example of their performance are

available in many publications. For instance, the depletion calculation of the first cycle of Watt Bar Unit 1, which is presented in [115], is performed on a powerful cluster [3], using 4088 processors and obtaining a total computing time of 22 hours and 45 minutes, corresponding to 254.8 CPU years. In terms of precision, they have showed to be able to predict along the cycle the CBC within 16 ppm and the 3D neutron pin cell flux with a RMS inferior to 4.6 %.

In VERA-CS, one of the most famous coupling scheme is based on MPACT [119], which is coupled to CTF for the thermal-hydraulics and to ORIGEN [120] for the isotopic transmutation. The characteristic radial discretization of this coupling scheme is depicted in Fig. 2-6. The main whole-core calculation methodology of MPACT is based on the 2D/1D fusion technique [121], which was previously explored by [122] and [123]. In MPACT, the homogenization under simplified boundary conditions is not performed at all and there is no energy condensation, the number of groups present in the library is kept through the entire simulation. This number is at least 23, most often 51 energy groups are used. The only homogenization is a dynamic one performed for the Coarse Mesh Finite Difference (CMFD). This technique is used to accelerate the convergence and stabilize the 2D/1D coupling. Within this approach, the 2D and the 1D problems are coupled by the transversal leakage terms. The SP_N solver is used for the axial direction where the anisotropy is generally lower, except in the proximity of the control rods, of the reflector or of the mixing grids. The Method Of Characteristics (MOC) is used for the 2D calculations in order to access the power distribution at the sub-pin level. Even if this method does not converge to the 3D MOC calculations, as it introduces approximations, it often offers very accurate radial calculations at a significantly lower cost.

With respect to the thermal-hydraulics, CTF uses a two fluids, three fields model. Two fluids refers to liquid water and vapour. Three fields refers to the individual treatments of the fluid film, the fluid drops and the vapour. The choice of modelling the three fields is rather advanced for LWR applications. Its full potential is expressed for the flow regimes in which these three phases have very different speeds. For PWR in nominal conditions, where the vapour is present in very small volumes, such an approach should not add much in terms of precision. The model consists of nine equations, the phasic mass, momentum and energy conservations for each of the fields. CTF offers both the 3D Cartesian and the sub-channel models, within VERA-CS, most of the applications are at the sub-channel level.

The depletion scheme used by ORIGEN is described in [12]. In ORIGEN, the same space discretization of MPACT may be used, but the calculation is done over regions that, within the pin, are only radially dependent. During the cycle calculation, xenon equilibrium is assumed. The flux is assumed constant within each time step, but the predictor-corrector and the sub-step methods are used. The sub-step method consists of making multiple depletion calculations within two consecutive

[3] SGI® ICETM X cluster with 684 physical nodes, where each node contains two 12-core 2.5-GHz Intel Xeon E5-2680 processors with available hyperthreading and 128 GB of RAM

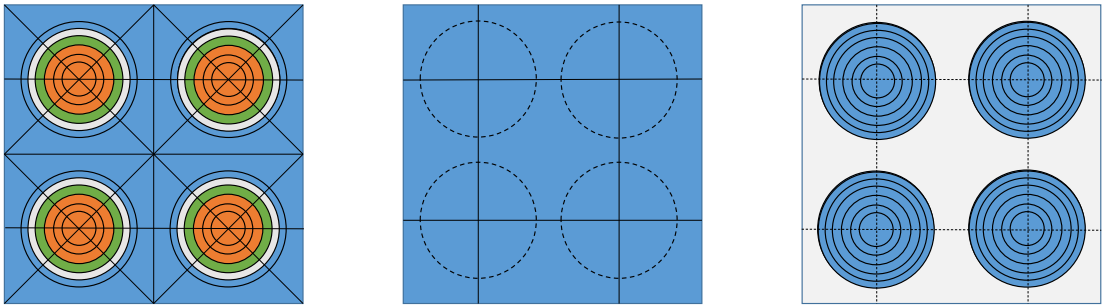

2D MOC transport mesh (coupled to axial SP_3)

Computed
Sub-pin power density

Received
Fuel rod averaged temperature
Clad averaged temperature
Moderator temperature and density

Sub-channel fluid mesh 3D

Computed
Channel moderator density and temperature

Received
Channel averaged power density (4 quarters of fuel rods)

Heat conduction mesh 2D (radial + axial)

Computed
Fuel temperature (4 quadrants)
Clad temperature (4 quadrants)

Received
Fuel rod averaged power density

Figure 2-6: Typical modelling scale for the depletion calculations performed by VERA-CS. In this example, a 2x2 fuel rods system is represented. The neutronics is computed by MPACT, the thermal-hydraulics and the heat conduction are performed by CTF.

transport resolutions. This is done by renormalizing the flux to account for the variation of the particle number densities in order to keep the same total power. The depletion can be done using the latest release of MPACT multi-group library which contains 295 isotopes, in alternative the full ORIGEN chain containing about 2300 isotopes can be used. However, the authors themselves state that the full chain is typically not needed for most of the applications [38].

Two ways of accounting for the evolution of the fuel thermal properties have been implemented. The most accurate one deals with a direct coupling with BISON [30, 124], the fuel performance code built on the Multiphysics Object-Oriented Simulation Environment MOOSE [34], in this case the coupling environment takes the name of TIAMAT [125]. The second approach deals with the generation of fuel temperature tables parametrized on local linear power and burnup [115]. BISON offers the possibility to model UO_2 fuel with zirconium based cladding both along irradiation and in accidental scenarios. It offers the possibility of performing both 2D (radial and axial or radial and azimuthal) and 3D (xyz) unstructured mesh calculations using finite-elements. In some cases, fuel performance calculations may be substituted by the simple heat conduction at constant fuel thermal properties performed by CTF.

More than the use of the state of the art solvers, the solidity of the coupling schemes implemented in VERA-CS is built on its validation process. A series of ten benchmarks ranging from pin scale under steady-state conditions to full commercial reactor refuelling [8] has been published. The data of these benchmarks are publicly available as well as the referential results produced with

continuous energy Monte Carlo methods like KENO [126]. The Watts Bar Nuclear Plant unit 1 is a PWR designed by Westinghouse, which was completed in 1996. Most of the experimental data is coming from this reactor. Furthermore, VERA-CS has been also tested over the first depletion cycle of the BEAVRS benchmark [127].

Among the other neutronic solvers that have been implemented in VERA-CS, there is also Insilico [128], which gathers a deterministic and a Monte Carlo solvers. The deterministic one is Denovo [129], it allows for S_N and SP_N core simulations. While the Monte Carlo solver for neutron and photon transport is SHIFT [130]. Two other peculiar solvers that have been implemented in VERA-CS are HYDRA-TH [131] and MAMBA [117, 132]. HYDRA-TH is a CFD code using a hybrid finite-element/finite-volume incompressible/low-Mach flow Navier-Stokes equation solver. MAMBA (MPO Advanced Model for Boron Analysis) contains BMD (Boron Deposition Model), which is essential to reproduce the main CRUD related phenomena.

NNR

NNR (Numerical Nuclear Reactor) is a joint Korean and American project for multiphysic referential calculations. It deals with coupled calculation schemes with direct core neutronic calculations (1 step approach) using nTRACER [39] and subchannel thermal-hydraulics simulated by MATRA (Multichannel Analyzer for steady states and Transients in Rod Arrays) [133]. The NNR has been tested on the BEAVRS benchmark both for Hot Zero Power (HZP) conditions against measurements and a Monte Carlo reference and along a simplified depletion cycle only against the measured data [134]. The maximum discrepancies found for several core configurations in HZP conditions are reported in Table 2.3 in terms of effective multiplication factor and Control Rod Worth (CRW). In terms of predicted CBC along the cycle, the maximum difference is of 25 ppm.

Table 2.3: Maximum discrepancies in term of effective multiplication factor and CRW over a set of core configurations for HZP conditions. Values expressed in pcm. The standard deviation for the Monte Carlo calculations is 5pcm.

HZP	max(Δk_eff)	max(Δ CRW)
Measured	180	59
Monte Carlo	95	33

A further comparison has been done on the prediction of the 2D assembly-wise detector signals at HZP conditions. The RMS over the quarter of core is 4.3 % and the maximum discrepancy is +12.2 % in an assembly next to the reflector.

2.1.4 Main Conclusions

A large number of research groups has shown its interest in the multiphysic modelling of PWRs. The vast majority of the coupling schemes are realized through the combination of specialised solvers,

apart from the case of fuel performance codes that are often not included in the coupling scheme or substituted by simplified models. Furthermore, while, for instance, for the Sodium Fast Reactors it is important to account for fuel geometrical deformations [135], for PWRs, at least in normal operating conditions, they are always neglected.

CASMO/SIMULATE[36], NNR [51] and VERA-CS [38, 50] have shown the capability of performing simulations exactly matching the objective of this PhD thesis. All of them have used the BEAVRS as reference benchmark [127] to test the quality of their modelling. While CASMO/SIMULATE utilizes assembly-wise radial discretization plus pin-power-reconstruction, NNR and VERA-CS do not use any *a priori* homogenization. With respect to the thermal-hydraulics, a subchannel code is selected in the vast majority of the *best-estimate* and *high-fidelity* calculation schemes. Of these three examples, only VERA-CS has been directly coupled with a fuel performance code.

For these reasons, it seems attractive to implement a coupling scheme for multiphysic depletion calculations of PWRs that relies on pin-cell homogenization, subchannel thermal-hydraulics and addressing the fuel performance with simplified models. The pin-cell homogenization combined with subchannel thermal-hydraulics may lead to a more accurate prediction of local variables than the coarse mesh approach and it should ask for significantly lower computing resources than the direct calculations. Finally, as described in [10] and [30], an accurate prediction of the width of the fuel-cladding gap along irradiation could lead to an important improvement in the prediction of local quantities. A simplified approach might be sufficient to capture the essential of this behaviour as it is reported in [115].

2.2 Numerical Methods

The general approach for multiphysic depletion simulations is to solve the problem as a series of steady-state calculations linked by the depletion iterations algorithm. Hence, it is often possible to treat the iteration scheme for the resolution of the steady-states independently from the depletion algorithm. For this reason, in this section most of the focus is given to the numerical methods used in reactor physics for the resolution of the steady-state problem, which carries a big part of the numerical complexity and is getting the attention of a large number of research groups. Nevertheless, these methods might be generalised to solve the depletion calculations or simply integrated in standard nested depletion iteration schemes.

As stated in the introduction, the multiphysic problem can be seen as a large nonlinear system of equations. The solution is characterized by a state, in which, all the physics are coherent to each others. For instance, the power distribution as computed by the neutronic solver corresponds to a given field of moderator density, hence, the density calculated by the thermal-hydraulic solver using this power profile should be close enough to the one used to compute the power. This should be true

for the entire list of considered variables, which normally may include also the fuel temperature, cladding heat flux, cladding outer temperature, the nuclide concentrations, the multi-group neutron scalar flux, the CBC and the control rod insertion. Since most of the solvers has been conceived for solving just a subset of the physics, normally they only compute the previously mentioned variables and not their partial derivatives with respect to each others. Moreover, these function evaluations rely on iterative processes, hence, these variables contain different levels of numerical noise. For these reasons, the implementation of methods requiring an accurate estimation of the derivatives do not appear competitive. There is therefore a rich literature in terms of numerical methods that only require function evaluations, for example [136].

In this framework, the fixed-point with relaxation (or damped fixed-point) has been widely used in reactor physics simulations, for instance in [137, 138]. Also many coupling schemes using DYN3D are based on the fixed-point: [74, 97, 37].

Given the high cost needed for the evaluation of the multiphysic function, it is important to try to exploit to the greatest extent the information produced during iterations. For this reason, many works focus on more advanced methods that often fall in the class of quasi-Newton methods; the most widespread are Anderson acceleration [139] and Jacobian-free Newton-Krylov (JFNK) [140]. CASL has published an analysis on the application of the Anderson method to a simplified neutronic/thermal-hydraulic system, which reveals promising results [141]. Moreover, the same research group has also published a comparison of Anderson and JFNK to the damped fixed-point iterations [142]. In this context, the neutronics is modelled with Denovo using a SP_3 solver coupled to the Advanced Multi-Physics (AMP) package [143] for subchannel thermal-hydraulics and fuel performance. The problem deals with the steady-state multiphysic solving of a single fuel assembly. These tests have been done for a rather special coupling scheme in which the lattice calculations are not decoupled from the rest of the scheme. The results show that in this particular scheme, using these more advanced methods lead just to modest efficiency gains. The preconditioning is a technique used to transform the treated problem into another one easier to solve from the numerical point of view, it is very often used in methods like the JFNK. An interesting comparison between preconditioning strategies for JFNK in multiphysic modelling of transient simulations is given in [47]. Another famous acceleration algorithm for the fixed-point iterations is the Aitken technique [144]. This method has been also successfully applied to a similar multiphysics problem by [145], but, currently, in reactor physics, it is just not as popular as the other two considered techniques.

This section is divided in four parts, the first three aiming at introducing the damped fixed-point, Anderson's acceleration and the JFNK and the last one giving the conclusions for this section. These methods are intentionally treated from a slightly more general perspective than the one of multiphysic simulations.

2.2.1 Damped Fixed-Point

The fixed-point algorithm is one of the simplest and most common methods and it is used for a wide range of applications. In fact, it is sufficient to formalize the problem in the form $\boldsymbol{G}(\boldsymbol{x}) = \boldsymbol{x}$, under which it often naturally falls, to create a sequence of the type of Eq. (2.1). Nevertheless, multiple ways exist to define $\boldsymbol{G}$, corresponding to different numerical methods. In the multiphysic context, $\boldsymbol{x}$ is the vector of all the variables, for instance any sub-set of multi-groups neutron scalar flux, heat sources, water density, fuel temperature and nuclide number densities. The solution of the problem is $\boldsymbol{x}^*$, respecting $\boldsymbol{G}(\boldsymbol{x}^*) = \boldsymbol{x}^*$.

$$\boldsymbol{x}^{k+1} = \boldsymbol{G}(\boldsymbol{x}^k) \tag{2.1}$$

A sufficient condition for local convergence of the fixed-point method is given by the following statement. This notation is adopted for the Jacobian matrix of $\boldsymbol{G}$, $\mathbf{J}_{\boldsymbol{G}} = \frac{\partial \boldsymbol{G}}{\partial \boldsymbol{x}}$ and for its spectral radius (i.e. the maximum in module of the eigenvalues of the matrix), $\rho(\mathbf{J}_{\boldsymbol{G}}(\boldsymbol{x}))$. If $\boldsymbol{G}$ has a fixed-point, $\boldsymbol{G} \in C^1$ in its proximity and $\rho(\mathbf{J}_{\boldsymbol{G}}(\boldsymbol{x}^*)) < 1$ then there exists a neighbourhood of the solution in which any initial guess makes the sequence converge [146], page 297. Moreover, all the values of the sequence stay within this interval. In respect of the speed of convergence, it could be demonstrated (e.g. [146], page 262 for the scalar case) that, except in case of null spectral radius, the fixed point converges linearly [4] and its rate of convergence is equal to the spectral radius, following Eq. (2.2). Such a variable is almost never computed in practical applications, because to derive it, the solution of the problem should be known and even to compute the Jacobian in a given point is generally prohibitive. However, this analysis is important to better understand the fixed-point method and the relaxation (or dumping) technique.

$$\lim_{k\to\infty} \frac{\|\boldsymbol{x}^{k+1} - \boldsymbol{x}^*\|}{\|\boldsymbol{x}^k - \boldsymbol{x}^*\|} = \rho(\mathbf{J}_{\boldsymbol{G}}(\boldsymbol{x}^*)) \tag{2.2}$$

As stated before there is not a unique way of writing $\boldsymbol{G}$. Starting from the problem in the residual form ($\boldsymbol{F}(\boldsymbol{x}) = \mathbf{0}$), any formulation of the type of Eq. (2.3) would be valid under the condition that $\boldsymbol{H}$ is a homogeneous and continuous operator. Homogeneous meaning that $\boldsymbol{H}$ respects $\boldsymbol{H}(t * x, t * y) = t^n * \boldsymbol{H}(x, y)$ for a constant n.

$$\boldsymbol{G}_{\boldsymbol{H}}(\boldsymbol{x}) = \boldsymbol{x} - \boldsymbol{H}(\boldsymbol{F}(\boldsymbol{x})) \tag{2.3}$$

For this reason, a simple choice of $\boldsymbol{H}$ would be a multiplicative constant, which is referred to as the relaxation factor (α). In this way, a new sequence $\boldsymbol{G}_\alpha$ is built, whose relation with $\boldsymbol{G}$ ($\boldsymbol{G} \equiv \boldsymbol{G}_{\mathbf{I}}$)

[4] The order of converge is defined as the value q respecting the following relation $\lim_{k\to\infty} \frac{\|\boldsymbol{x}^{k+1} - \boldsymbol{x}^*\|}{\|\boldsymbol{x}^k - \boldsymbol{x}^*\|^q} < M$. Linear convergence means $q = 1$, while quadratic $q = 2$.

is specified in Eq. (2.4).

$$\boldsymbol{x}^{k+1} = \boldsymbol{G}_\alpha(\boldsymbol{x}^k) = \boldsymbol{x}^k - \alpha * \boldsymbol{F}(\boldsymbol{x}^k) = \alpha * \boldsymbol{G}_\mathbf{I}(\boldsymbol{x}^k) + (1-\alpha) * \boldsymbol{x}^k \tag{2.4}$$

It is easy to demonstrate that the eigenvalues of $\boldsymbol{G}_\alpha$ are linearly related to those of $\boldsymbol{G}$, as written in Eq. (2.5).

$$\lambda_i(\alpha) = \alpha * (\lambda_i - 1) + 1 \tag{2.5}$$

Hence, such a simple approach can transform a non convergent sequence into a convergent one, as shown by Eq. (2.6).

$$max(\lambda_i) < 1 \Rightarrow \exists\ \alpha > 0 : |\lambda_i(\alpha)| < 1, \forall i \tag{2.6}$$

Moreover, it can also accelerate its convergence by reducing the spectral radius, as suggested by Eq. (2.2). The relaxation does not impact all the eigenvalues in the same way. Considering non-relaxed eigenvalues smaller than one, in order to nullify a positive eigenvalue, α should be greater than the unity, while for any negative eigenvalue α should be comprised between zero and one. The more the maximum and the minimum eigenvalues are distant, which can be expressed by the dominance ratio, the less room for optimization there is. In particular, to minimize the spectral radius, it appears that the optimal α is where $|\lambda_M(\alpha)| = |\lambda_m(\alpha)|$, respectively being the minimum and the maximum, which brings to Eq. (2.7). The entire derivation of these equations and a wider analysis of numerical methods for multiphysic coupling can be found in [147].

$$\alpha_{opt} = \frac{1}{1 - \frac{\lambda_M + \lambda_m}{2}} \tag{2.7}$$

In Fig. 2-7, it is possible to visualize an example of this optimization process for arbitrary eigenvalues.

The fixed-point method can be justified by the zeroth order Taylor expansion of the residual problem, the following methods belong to the quasi-Newton class. Hence, they could be seen as a fixed-point plus a correction term accounting for some estimations of the Jacobian matrix.

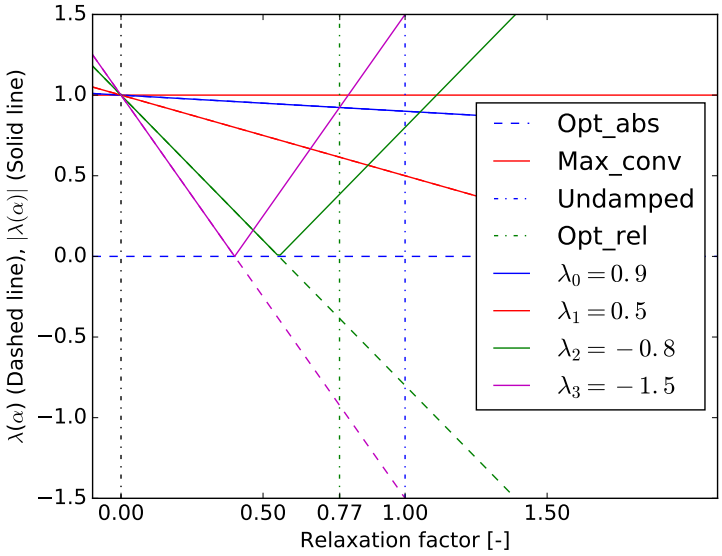

Figure 2-7: Effect of the relaxation factor over the modules of the eigenvalues $|\lambda_i|$. $|\lambda(\alpha)| > 1$ means divergent behaviour, the limit is underlined by the horizontal solid red line (Max_conv). The original eigenvalues correspond to relaxation factor equals to one, put in evidence by the dash-dot blue line (Undamped). λ tending to zero means optimal rate of convergence, signalled by the horizontal dashed blue line (Opt_abs), but, it is not possible to reach this value for all the eigenvalues if the undamped ones have different values. In order to minimize the spectral radius the optimum relaxation factor is where the maximum and minimum eigenvalues are equal in modules. In the example it is 0.77 and it is indicated by the green dash-dot line (Opt_rel).

2.2.2 Anderson Acceleration

The Anderson algorithm [139] is a low-degree generalised secant method, which could also be seen as an acceleration technique for the fixed-point. Indeed, it aims at exploiting to a greater extent the results obtained during the previous iterations in order to create a faster converging sequence. More in details, this acceleration is based on the linear combination of the latest M (arbitrary parameter) iterations, using weights obtained from the minimization of a quadratic residual. As demonstrated by [148], this process actually corresponds to the formation of a rank-M approximation of the inverse Jacobian of residual function $\boldsymbol{F}(\boldsymbol{x})$. There are multiple good reasons to prefer, among the quasi-Newton methods, a low order one. Since the evaluation of $\boldsymbol{F}(\boldsymbol{x})$ is very expensive and its solution has a precision limited by the internal solvers iterative processes, all the finite differences schemes, like JFNK, may appear less competitive because of their lower tolerance to the numerical noise. A more detailed analysis is available in [149]. In the works presented by [139] and [148], it is argued that, approaching convergence, linear dependencies arise among the iterates, implying an increasing ill-conditioning of the matrix that has to be solved to obtain the M weights. This can be seen as another pros for the low-order methods, since they suffer less of this ill-conditioning.

In place of the vector of unknowns $\boldsymbol{x}$ appearing previously in the text, in the Anderson algorithm

$\hat{\boldsymbol{x}}$ is used. This notation change is motivated by the willing to have an unknown vector containing homogeneous quantities with the same order of magnitude in order to avoid a decoupling of the algorithm. In his original paper [139], Anderson suggested to normalize the residual by "some measure of the local "size" of the solution vector". For the same reason, also $\boldsymbol{F}$ is modified into $\hat{\boldsymbol{F}}$ in order to accept and return normalized quantities. The weights θ_j^k are determined from the minimization of the residual as defined in Eq. (2.10). This minimization constitutes a linear system of dimension M, hence generally trivial to solve. Adapting the formalism given by [148], Algorithm 1 is built. The intermediate variables $\hat{\tilde{\boldsymbol{x}}}^k$ and $\hat{\tilde{\boldsymbol{F}}}^k$ are defined in Eqs. (2.8) and (2.9). In the algorithm appear again α which is the relaxation factor in analogy to the one of the damped fixed-point. In fact, even in the original paper it is suggested not to apply the relaxation unless empirical experience is available. Several convergence tests may be selected, for instance, the absolute or relative step size ($\Delta\hat{\boldsymbol{x}}^k := \hat{\boldsymbol{x}}^{k+1} - \hat{\boldsymbol{x}}^k$), or the residual at the current iteration may be checked ($\hat{\boldsymbol{F}}(\hat{\boldsymbol{x}}^{k+1})$), in absolute or relative value. Even a combination of them is allowed.

$$\hat{\tilde{\boldsymbol{x}}}^k := \hat{\boldsymbol{x}}^k + \sum_{j=1}^{M_k} \theta_j^k * (\hat{\boldsymbol{x}}^{k-j} - \hat{\boldsymbol{x}}^k) \tag{2.8}$$

$$\hat{\tilde{\boldsymbol{F}}}^k := \hat{\boldsymbol{F}}(\hat{\boldsymbol{x}}^k) + \sum_{j=1}^{M_k} \theta_j^k * (\hat{\boldsymbol{F}}(\hat{\boldsymbol{x}}^{k-j}) - \hat{\boldsymbol{F}}(\hat{\boldsymbol{x}}^k)) \tag{2.9}$$

$$R^k = \frac{1}{2}(\hat{\tilde{\boldsymbol{F}}}^k)^T \cdot \hat{\tilde{\boldsymbol{F}}}^k \tag{2.10}$$

Algorithm 1 Anderson acceleration.

$\hat{\boldsymbol{x}}^1 = \hat{\boldsymbol{G}}(\hat{\boldsymbol{x}}^0)$
$k = 1$
while $\|\Delta\hat{\boldsymbol{x}}^k\| > \Delta_{conv}$ **do**
  $M_k = min(M, k)$
  minimize R^k for θ_j^k:
    $\sum_{j=1}^{M_k}(\hat{\boldsymbol{F}}(\hat{\boldsymbol{x}})^k - \hat{\boldsymbol{F}}(\hat{\boldsymbol{x}})^{k-l})^T \cdot (\hat{\boldsymbol{F}}(\hat{\boldsymbol{x}})^k - \hat{\boldsymbol{F}}(\hat{\boldsymbol{x}})^{k-j})\theta_j^k$
      $= (\hat{\boldsymbol{F}}(\hat{\boldsymbol{x}})^k - \hat{\boldsymbol{F}}(\hat{\boldsymbol{x}})^{k-l})^T \cdot (\hat{\boldsymbol{F}}(\hat{\boldsymbol{x}})^k) \quad \forall_{l=1,\dots,M_k}$
  $\hat{\boldsymbol{x}}^{k+1} = \hat{\tilde{\boldsymbol{x}}}^k + \alpha * \hat{\tilde{\boldsymbol{F}}}^k$
  $k = k + 1$
end while

2.2.3 Jacobian-free Newton-Krylov

The Jacobian-free Newton-Krylov method has recently become very popular in many scientific research areas [150] and many innovative multiphysic coupling schemes are based on it (e.g. [151, 152, 153]). The Newton iterations, Eq. (2.12), are derived approximating $\boldsymbol{F}$ at the first order, as in Eq. (2.11), and searching its zero.

$$\boldsymbol{F}(\boldsymbol{x}^{k+1}) = \boldsymbol{F}(\boldsymbol{x}^k) + \boldsymbol{F}'(\boldsymbol{x}^k) \cdot (\boldsymbol{x}^{k+1} - \boldsymbol{x}^k) + o(\|(\boldsymbol{x}^{k+1} - \boldsymbol{x}^k\|) \tag{2.11}$$

$$\mathbf{J}(\boldsymbol{x}^k) \cdot \delta\boldsymbol{x}^k = -\boldsymbol{F}(\boldsymbol{x}^k), \qquad \boldsymbol{x}^{k+1} = \boldsymbol{x}^k + \delta\boldsymbol{x}^k \tag{2.12}$$

Even if the Newton iterations may lead to quadratic convergence, their applicability to engineering problems is severely limited by the cost of computing the Jacobian matrix. The main idea behind JFNK is to perform Newton iterations without computing nor storing the Jacobian matrix. This is possible combining the Newton iterations with a Krylov subspace method. Indeed, this type of methods allows to solve the linear problem of Eq. (2.12) without ever computing the Jacobian. The only information required by Krylov subspace methods is the repeated product of the considered matrix, which in this case is the Jacobian one, and the guess vector, which in this case is the residual. In this way the Krylov subspace is formed as in Eq. (2.14), using the initial guess of the residual $\boldsymbol{r}_0$ as defined in Eq. (2.13).

$$\boldsymbol{r}_0 = -\boldsymbol{F}(\boldsymbol{x}^k) - \mathbf{J}(\boldsymbol{x}^k) \cdot \delta\boldsymbol{x}^k \tag{2.13}$$

$$K_j = span(\boldsymbol{r}_0, (\mathbf{J}(\boldsymbol{x}^k) \cdot \boldsymbol{r}_0), (\mathbf{J}(\boldsymbol{x}^k) \cdot (\mathbf{J}(\boldsymbol{x}^k) \cdot \boldsymbol{r}_0)), ..., ((\mathbf{J}(\boldsymbol{x}^k))^{j-1} \cdot \boldsymbol{r}_0)) \tag{2.14}$$

Finally, this series of products is carried out using the first order approximation of the product of the Jacobian times a vector as in Eq. (2.15), hence avoiding any direct computation of the Jacobian matrix.

$$\mathbf{J}(\boldsymbol{x}) \cdot \boldsymbol{v} \approx [\boldsymbol{F}(\boldsymbol{x} + \varepsilon * \boldsymbol{v}) - \boldsymbol{F}(\boldsymbol{x})]/\varepsilon \tag{2.15}$$

The choice of the perturbation parameter (ε) is based on the expected level of precision on each component of the vector. This parameter should be as low as possible in order to have a good approximation of the Taylor expansion, whose error is proportional to ε. But at the same time, too small values have to be avoided due to the numerical noise. Various strategies to select ε are reported in [150]. One of the most advanced technique is given in the article where the JFNK was firstly introduced [140]. It is reported in Eq. (2.16), where $b := \sqrt{\varepsilon_{rel}}$ and $\boldsymbol{x}\_size$ is a user given typical size of $\boldsymbol{x}$. ε_{rel} refers to the machine epsilon, but often it is substituted by the maximum reachable precision in the evaluation of $\boldsymbol{F}$.

$$\varepsilon = \frac{b}{\|\boldsymbol{v}\|_2} * max(|\boldsymbol{x}^T \cdot \boldsymbol{v}|, \boldsymbol{x}\_size * |\boldsymbol{v}|) * sign(\boldsymbol{x}^T \cdot \boldsymbol{v}) \tag{2.16}$$

Some of the best known Krylov methods used in this context are the Generalized Minimal RESidual (GMRES) [154], the Bi-Conjugate Gradient STABilized (BiCGSTAB) [155] and the Transpose-

free Quasi Minimal Residual (TFQMR) [156]. In Algorithm 2, the GMRES based JFNK is described.

Algorithm 2 Jacobian-free Newton-Krylov based on GMRES.

given $\boldsymbol{x}^0$
$k = 0$
while $\|\delta\boldsymbol{x}^k\| > \Delta_{conv,N}$ **do**
  $\mathbf{J}(\boldsymbol{x}^k) \cdot \delta\boldsymbol{x}^k = -\boldsymbol{F}(\boldsymbol{x}^k) \rightarrow \boldsymbol{x}^{k+1} = \boldsymbol{x}^k + \delta\boldsymbol{x}^k$
  $j = 0$
  while $\|\mathbf{J}(\boldsymbol{x}^k) \cdot \delta\boldsymbol{x}_j + \boldsymbol{F}(\boldsymbol{x}^k)\|_2 > \Delta_{conv,K}$ **do**
    $\boldsymbol{r}_0 = -\boldsymbol{F}(\boldsymbol{x}^k) - \mathbf{J}(\boldsymbol{x}^k) \cdot \delta\boldsymbol{x}^k$
    $\delta\boldsymbol{x}_j = \delta\boldsymbol{x}_0 + \sum_{i=0}^{j-1} \beta_i * (\mathbf{J}(\boldsymbol{x}^k))^i \cdot \boldsymbol{r}_0$
    $j = j + 1$
  end while
  $k = k + 1$
end while

The β_i coefficient are derived by the minimization of the euclidean norm of the residual over a space of dimension much smaller than the real problem. To be coherent with the notation adopted previously, the superscript k corresponds to the outer iterations (the Newton ones), the subscript j relates to the GMRES iterations. In particular, the Newton update ($\delta\boldsymbol{x}^k$) is the converged $\delta\boldsymbol{x}_j$ from the GMRES iterations (the full notation would be $\delta\boldsymbol{x}^k_{j=\infty}$). It should be notice that the superscript i in $(\mathbf{J}(\boldsymbol{x}^k))^i$ is the power to which the Jacobian matrix is raised. The initial guess for the GMRES iteration, is to set $\delta\boldsymbol{x}_0$ to zero, as this is the value that should be reached when approaching the convergence of the Newton iterations. The convergence test of the Newton iterations can be performed on the norm of the Newton update ($\|\delta\boldsymbol{x}^k\|$), on its relative value ($\frac{\|\delta\boldsymbol{x}^k\|}{\|\boldsymbol{x}^k\|}$), on the norm of the residual ($\|\boldsymbol{F}(\boldsymbol{x}^k)\|$), on its relative drop ($\frac{\|\boldsymbol{F}(\boldsymbol{x}^k)\|}{\|\boldsymbol{F}(\boldsymbol{x}^0)\|}$) or in any combination of them.

Very often the simple JFNK algorithm, as presented here, is extended by a globalization method for the Newton iterations and by the introduction of a preconditioner for the linear iterations. The preconditioner is a key element for the global efficiency of the method, in practice it can drastically reduce the number of GMRES iterations. In fact, it has been demonstrated that GMRES may offer a slow convergence at the beginning of the iterative process.

2.2.4 Main Conclusions

Given the development of increasingly complex multiphysic calculation schemes, many research groups have shown a lot of interest in the deployment of advanced numerical methods. In fact, the numerical optimization of the global calculation scheme is crucial to increase its robustness and to enhance its efficiency.

Three methods have been considered, the damped fixed-point iterations, the Anderson acceleration and the Jacobian-free Newton-Krylov (JFNK). It has been found that the vast majority of the *best-estimate* calculation schemes just relies on the damped fixed-point iterations, while the reported *high-fidelity* examples often focus on the JFNK. In respect of the fixed-point algorithm, although,

often, the damping technique accelerates and stabilizes the iterations in a very simple and effective way, optimal values of this parameter are case dependent and difficult to determine, most of the times they are derived empirically. The strong dependency on the relaxation factor is one of the major problems of the fixed-point method. Moreover, part of the interest to the Anderson method and the JFNK stems from the objective of further exploiting the results expensively obtained in the previous iterations.

CASL has shown that, on a simplified case, the Anderson method has revealed greater robustness and faster convergence than the damped fixed-point iterations, without adding much complexity [141]. Even if the JFNK is attracting most of the attention, as described in [149] and [157], lower order methods (like Anderson) might be preferable in many contexts due to their higher tolerance to the numerical noise. Furthermore, the implementation of an efficient JFNK is complexified by the necessity of studying its preconditioning. For these reasons, it seems particularly interesting to apply the Anderson acceleration on a *best-estimate* multiphysic calculation scheme.

Chapter 3

Available Tools

In this chapter, a brief overview is given about some of the specialised solvers available during the PhD thesis. After that, the essential tools in support of the development of a coupling scheme are described. Finally, examples of multiphysic coupling schemes previously realized within the CORPUS project are reported.

3.1 Neutronic Models

Most of the codes for neutronic simulations developed at Commissariat à l'énergie atomique et aux énergies alternatives (CEA) have been conceived, maintained and expanded at the Service d' Études des Réacteurs et de Mathématiques Appliquées (SERMA), the department where the PhD thesis is held. The first CEA neutron transport code is APOLLO [158]. Currently it is used in its newer versions APOLLO2 [159, 160] and APOLLO3® [161]. APOLLO2 is a deterministic code used for lattice calculations of thermal reactors, it has been realized also with the financial support of EDF and Framatome. It is still deployed in various two-steps calculation schemes for industrial applications. At CEA, it is most often combined with CRONOS2 [59] for the 3D core calculations. APOLLO3® is a common project of CEA with Framatome and EDF and it includes both lattice and core solvers.

The same companies have also developed the TRIPOLI-4® [102] Monte Carlo code for the transport of both neutron and photons. TRIPOLI-4® is capable of performing both criticality and source calculations. As discussed in the state of the art, this code is also involved in projects aiming at performing multiphysic simulations [162, 64, 106]. Its capability of performing depletion calculations has been verified against the results of APOLLO2 and the measured data of an experimental reactor [163, 164].

Another example of neutronic two-steps calculation scheme is given by ECCO [165]/ERANOS

[166][1]. ECCO is the lattice code and ERANOS the core one, both of them are specialised on the modelling of fast reactors.

In this section, APOLLO2 and APOLLO3® are described, as they are the neutronic codes used in the PhD thesis.

3.1.1 APOLLO2

The most important components of APOLLO2 are the Self-Shielding (SSH) module and the flux solvers. The SSH technique is a crucial step needed to adjust the reference many groups cross-sections to address the SSH phenomenon. It should be noticed that this process is required for both homogeneous and heterogeneous calculations and it is highly influenced by the temperature of the media. The cross-sections produced through this process are commonly called self-shielded cross-sections.

The flux solvers are based on three methods for the resolution of the transport equation. Two of them deal with the integral form of the transport equation: the Collision Probabilities and the Method Of Characteristics (MOC). The other one solves the integro-differential form combining the Discrete Ordinates (S_N) for the angular discretization and a nodal method for the spatial one. The Collision Probabilities and the MOC share many similarities. Their main advantage is the capability of using unstructured meshes to describe the exact core geometry. This is not possible with the nodal methods and is extremely important for practical applications. For the 2D resolution, the main difference among them stems from the treatment of the angular variable. The Collision Probabilities uses special functions for the integration of the dependency on the polar angle, while the MOC relies on a S_N based numerical integration [31], page 84. Even if these special functions allow to very accurately integrate over the polar angle, the Collision Probabilities method is strictly valid only in case of isotropic scattering, while the MOC is capable of treating an arbitrary order of anisotropy. Although transport corrections are available, they imply an overall approximation which is difficult to control. For this reason and more practical ones, the MOC is the main flux solver of APOLLO2 [160]. In this sub-section, a brief description of the Self-Shielding Technique, the Discrete Ordinates and the MOC is given.

Self-Shielding Technique

The following description has been realized mainly thanks to [167]. Both APOLLO2 and 3 include a Self-Shielding module based on the Livolant-Jeanpierre model [168]. This model is based on the slowing-down equation for an infinite and homogeneous mixture reported in Eq. 3.1. It should be noticed that under the approximation of infinite and homogeneous mixture the angular dependency

[1]These codes have been developed and are maintained and expanded by Service de Physique des Réacteurs et du Cycle (SPRC).

is completely removed.

$$[\Sigma^{abs}(E) + \Sigma^{mod}(E)]\psi(E) = R_{abs}\psi(E) + R_{mod}\psi(E) \tag{3.1}$$

In Eq. 3.1, the homogeneous medium is decomposed in moderating and absorbing materials. The cross-sections are identified by their superscripts, while the slowing-down operators by their subscripts: $R_i = \int_E^{E/\alpha_i} dE' \Sigma_s^i(E' \rightarrow E)\psi(E')$. The essence of the Livolant-Jeanpierre model is the factorization of the flux ($\psi = \Phi * \phi$), which is represented as the product of a slowly varying function (Φ) representing the macroscopic slowing-down of the neutrons and another one (ϕ), whose value is one outside the resonances, while it quickly decreases approaching the peaks in order to capture the local behaviour. The first term is called asymptotic flux and it is defined as the solution of the slowing-down equation inside the moderator. The second one is referred to as the self-shielded factor or the fine-structure flux and is obtained through the fine-structure equation. This equation is reached in few steps. The first one is substituting the definition of Φ ($\Sigma^{mod}(E)\Phi(E) = R_{mod}\psi(E)$) in Eq. 3.1. The second step derives from the hypothesis that the asymptotic flux varies slowly enough to be considered constant in the slowing-down operator of the absorbing medium in the resonance interval ($R_{abs}\Phi(E)\phi(E) \cong \Phi(E)R_{abs}\phi(E)$). Finally, dividing all the terms for the number density of the absorbing material the Eq. (3.2) is obtained. Where $r_{abs}\phi = \frac{R_{abs}\phi}{N_{abs}} = \int_E^{E/\alpha_i} dE' \sigma_s^i(E' \rightarrow E)\phi(E')$ is the new slowing-down operator and $\sigma_d = \frac{\Sigma_s^{mod}}{N_{abs}}$ is the dilution cross section. This equation can be obtained

$$(\sigma^{abs} + \sigma_d)\phi = r_{abs}\phi + \sigma_d \tag{3.2}$$

The fine-structure equation could be solved numerically for each resonance of each isotope and tabulated as a function of the dilution cross-section and temperature once and for all.

Having this model in mind, the heterogeneous flux needed to compute the self-shielded heterogeneous cross-sections is obtained through a double equivalence process for space and energy. The space equivalence is done using pre-tabulated reference reaction rates for the infinite and homogeneous media and solving the heterogeneous version of the fine-structure equation. To solve this equation the Collision Probability is often the preferred method. Once the heterogeneous reaction rates are found, the multi-group fine-structure equation is iteratively solved to find the self-shielded cross-sections that preserve the reaction rates.

A particularly valuable aspect of the SSH module of APOLLO2 and 3 is the capability to simultaneously perform the SSH calculation for an ensemble of resonant isotopes (called the resonant mixture) [169]. The possibility to address the overlapping of the resonance of the different values has shown to strongly contribute to the accuracy of the simulations [31], page 65 to 72.

Discrete Ordinates

The Discrete Ordinates (S_N) method deals only with the angular discretization, the main idea is to transform an integro-differential equation into a set of differential ones by substituting the integral term with a quadrature formula. Such a formula, in the case of 3D angular integration, assumes the form reported in Eq. (3.3), f being a generic function depending on the direction Ω and w_n the weight associated to each direction $\mathbf{\Omega}_n$. Many valid choices for the set of directions and their weights are present in literature, for instance in APOLLO2 the product and the level-symmetric angular quadrature formulas are deployed [45, 170].

$$\int_{4\pi} d^2\Omega f(\mathbf{\Omega}) = \sum_{n=1}^{N} w_n f(\mathbf{\Omega}_n) \tag{3.3}$$

The accuracy of the method is affected by the choice and the number of the directions. In the acronym S_N, the index N represents the order of the method. This parameter is not strictly equal to the number of the directions (appearing as N in Eq. (3.3)). However, the more it increases, depending on the considered quadrature formula, the higher is the number of associated directions. In case of strongly anisotropic sources or little diffusive media, the set of directions might not be sufficient to capture phenomena happening on small angular portions and eventually lead to nearly zero fluxes, the so called ray effect.

Method Of Characteristics

This description is mostly based on [31], pages 82 to 86. The Method Of Characteristics (MOC) is one of the most widespread technique for industrial calculations. The reason for such a wide utilization relies on its capacity of treating complex geometry, arbitrarily high scattering anisotropy orders and general boundary conditions with a high level of accuracy. A part of its advantage over other methods stems from the possibility to effectively use unstructured meshes. This type of mesh is particularly needed for the typical reactor geometries in order to accurately model it with a relatively low number of meshes.

In principle, the MOC could be used for any hyperbolic partial differential equation, but it is typically applied to the first order ones. Its name derives from the resolution of a partial differential equation over the characteristic curves, on which the problem can be expressed as an ordinary differential equation. This is particularly simple to visualize for the neutron transport, in fact in this case, the characteristic curves are just straight lines parallel to the considered neutron velocity. This is due to the fact that before a collision, the neutrons are supposed to travel in straight lines, as opposed, for instance, to the charged particles that continuously interact with the medium.

In APOLLO2 the MOC is essentially used for 2D (radial) flux calculations, while in APOLLO3®, even if 2D calculations are still central, the extension to 3D ones is under development [171]. The

following brief description is pertinent for 2D calculations assuming constant cross-sections and source in each region.

Considering the neutron transport equation, as introduced in Eq. (1.2), it is possible to derive the steady-state and multi-group equivalent. Within a given group this equation can be expressed as in Eq. (3.4), where the group index is dropped to simplify the notation.

$$\boldsymbol{\Omega}\nabla\psi(\boldsymbol{r},\boldsymbol{\Omega}) + \Sigma(\boldsymbol{r})\psi(\boldsymbol{r},\boldsymbol{\Omega}) = Q(\boldsymbol{r},\boldsymbol{\Omega}) \tag{3.4}$$

In this optic, the neutron position can be expressed as $\boldsymbol{r} = s*\boldsymbol{\Omega}+s_\perp*\boldsymbol{\Omega}_\perp$, where $\boldsymbol{\Omega}$ is the neutron direction, $\boldsymbol{\Omega}_\perp$ is the perpendicular direction and s_i are the modules of the components as projected on these two directions. By applying this change of notation into Eq. (3.4) and considering the equation over a line defined by a constant $s_\perp$ and constant direction $\boldsymbol{\Omega}$ (i.e. a characteristic line), it is possible to obtain Eq. (3.5). From this equation, it is clear that over this line the phase-space is reduced to s, hence, the problem becomes an ordinary differential equation.

$$\frac{d\psi(s_{\perp,k}*\boldsymbol{\Omega}_\perp + s*\boldsymbol{\Omega},\boldsymbol{\Omega})}{ds} + \Sigma(s_{\perp,k}*\boldsymbol{\Omega}_\perp+s*\boldsymbol{\Omega})\psi(s_{\perp,k}*\boldsymbol{\Omega}_\perp+s*\boldsymbol{\Omega},\boldsymbol{\Omega}) = Q(s_{\perp,k}*\boldsymbol{\Omega}_\perp+s*\boldsymbol{\Omega},\boldsymbol{\Omega}) \tag{3.5}$$

Basing on this equation, it is possible to derive the transmission and the balance equations. The transmission equation describes the relation between the flux entering in a portion of the domain (D_i) and the flux exiting D_i through a characteristic line. The balance equation, instead, provides insight of the averaged value of the flux over the piece of characteristic line contained in D_i, while guaranteeing the conservation of the exact number of neutrons.

In order to reconstruct the 2D-averaged flux, it is needed to integrate orthogonally to $\boldsymbol{\Omega}$ (i.e. over $\boldsymbol{\Omega}_\perp$). In this way, the contributions of the 1D-averaged value corresponding to a set of characteristic lines is gathered in each volume V_i corresponding to the previously mentioned region D_i.

3.1.2 APOLLO3®

APOLLO3® is a multi-purpose deterministic neutronic code capable of performing both lattice and core calculations and applicable for both thermal and fast reactors. The core of the code is mainly written in C++ and FORTRAN 90 with the aim of enhancing the flexibility of the software architecture and of reaching high computation performances.

The Self-Shielding module for thermal reactors derives from the one of APOLLO2. One of the main extensions that have been implemented deals with the capability to account for the up-scattering phenomenon [172]. The flux solvers for lattice or direct calculations are based on the Collision Probabilities, short and long Method Of Characteristics, respectively IDT [173, 174] and TDT [175, 176]. These solvers are the result of the incorporation and the extension of the corre-

sponding solvers of APOLLO2. In APOLLO3®, both IDT and TDT have been further developed to perform also 3D calculations [173, 177, 178, 171].

APOLLO3® provides an equivalence module for the SuPer-Homogenization (SPH) technique [179]. This module can be seen as an intermediate step between lattice and core calculations, which mainly aims at improving the capacity of a specific core model to reproduce the reference results set by the lattice solver during the production of homogenized cross-sections.

Two core solvers for the computation of thermal reactors are available in APOLLO3®: MINOS [180] and MINARET [181, 182]. Both of them offer the possibility of performing steady-state, kinetics or perturbation calculations. Within MINOS, which is the descendant of CRONOS2, the flux may be computed under the diffusion approximation or by using the Simplified-P_N (SP_N) method. With respect to the spatial discretization, the Raviart-Thomas-Nédélec finite elements [183, 184, 185] are used, which belong to the class of the mixed dual finite elements. MINOS is applicable on both cartesian and hexagonal 3D geometries. In respect of MINARET, this solver computes the flux using the Simplified-P_N (SP_N) and Discrete Ordinates (S_N) methods. Both 2D and 3D calculations are possible respectively with unstructured and semi-unstructured (cylindrical) meshes. The spatial discretization relies on the discontinuous Galerkin finite element method. For the S_N computations, parallelism is obtained using Message Passing Interface (MPI) to distribute the S_N directions over the available processors. Finally, the simulations are accelerated using the Diffusion Synthetic Acceleration (DSA) [186] adjusted according to [187].

As the main concepts underlying the S_N method have been described in the the previous subsection, here, the focus is given to the SPH equivalence technique, the diffusion approximation and the SP_N method.

SuPer-Homogenization Equivalence Technique

The SuPer-Homogenization (SPH) deals with the research of a set of factors that applied to the homogenized cross-sections make the core solver reproduce the average reaction rates obtained in the lattice calculations. By reaction rates, it is meant the homogenized ones, hence defined over macro-regions (for instance pin-cell or quarter of assembly) and for few energy groups. This sort of calibration is performed under the same simplified boundary condition used during the homogenization phase. These factors are called SPH factors or Equivalence Coefficients (ECs), in Eq. (3.6) they appear as $\mu_{m,g,s}$, where m is the macro-region index, g is the energy group and s is the state-point defined by the combination of assembly parameters (for instance fuel temperature, moderator density, burnup and boron concentration). The term $\Sigma^{lattice}_{m,g,s}$ represents the homogenized cross-sections as produced by the lattice solver, prior to the application of the ECs, while, $\Sigma^{core}_{m,g,s}$ is the unknown of the problem as it depends on $\mu_{m,g,s}$. It should be noticed that the EC is only applied to the total cross-section, no difference is made for the reaction types.

$$\Sigma^{core}_{m,g,s} = \Sigma^{lattice}_{m,g,s} * \mu_{m,g,s} \tag{3.6}$$

The reaction rate balance is defined in Eq. (3.7).

$$\Sigma^{core}_{m,g,s} * \phi^{core}_{m,g,s} = \Sigma^{lattice}_{m,g,s} * \phi^{lattice}_{m,g,s} \tag{3.7}$$

Manipulating this equation it is possible to form Eq. (3.8), which underlines the non-linearity of the problem.

$$\mu_{m,g,s} = \frac{\phi^{lattice}_{m,g,s}}{\phi^{core}_{m,g,s}(\mu_{m,g,s})} \tag{3.8}$$

Furthermore, this problem does not impose any constraint on the norm of the solution. For a given solution field of ECs, any multiplication by a constant would lead to another valid solution, as at convergence it cancels out as shown in Eq. (3.9).

$$\Sigma^{core}_{m,g,s} * \phi^{core}_{m,g,s} = \Sigma^{lattice}_{m,g,s} * \mu_{m,g,s} * \phi^{lattice}_{m,g,s} * \frac{1}{\mu_{m,g,s}} = \Sigma^{lattice}_{m,g,s} * \phi^{lattice}_{m,g,s} \tag{3.9}$$

For this reason several normalization techniques have been developed. In APOLLO3®, the flux-volume [188] and the Selengut [189] ones are available. The flux-volume simply consists of normalizing the factors to the assembly volume integrated flux as computed by the lattice solver. The Selengut one is more advanced, but requires also informations about the neutron currents. Unfortunately, in APOLLO3®, the Selengut normalization is not available for pin-by-pin homogenization.

In APOLLO3®, the SPH problem with flux-volume normalization is solved using the fixed-point iterations as presented in Algorithm 3. Where, $q(\Sigma, \phi)$ is the function that computes Q, the neutron source as defined in the neutron transport equation, and $f(Q)$ is the function that computes the flux associated to the neutron source according to the specific core solver. It should be noticed that this process could be carried out independently for each state-point (s). $\bar{\phi}^{solv_i}_{g,s}$ represents the neutron scalar flux integrated over all the m macro-regions of the assembly. $\Sigma^{core,k+1}_{s}$ and $\phi^{core,k}_{s}$ correspond to the entire fields for that state-point (including all the regions and energy groups).

Diffusion Approximation

The diffusion equation can be derived from any of the following hypotheses: the angular flux is linearly dependent on the angle, the scalar flux is linearly dependent on the space variable or considering the absorption term much smaller than the leakage one and the latter much smaller than the scattering one. All these hypothesis bring to the same result, all of them in fact imply the same thing, the prevailing scattering term makes smoother the dependency of the angular flux on the angle and space variables. The coarser the spatial and energy meshes are, the higher the average

Algorithm 3 Fixed-point resolution of the SPH equivalence problem.

for Every state-point s **do**
  $\mu^0 = 1$
  while $\forall m, g : \frac{|\mu^{k+1}_{m,g,s} - \mu^k_{m,g,s}|}{\mu^k_{m,g,s}} < \epsilon$ **do**
    $\forall m, g : \Sigma^{core,k+1}_{m,g,s} = \Sigma^{core,k}_{m,g,s} * \mu^k_{m,g,s}$
    $Q^{k+1} = q(\Sigma^{core,k+1}_s, \phi^{core,k}_s)$
    $\phi^{core,k+1}_s = f(Q^{k+1})$
    $\forall m, g : \mu^{k+1}_{m,g,s} = \frac{\phi^{lattice}_{m,g,s}}{\phi^{core,k+1}_{m,g,s}}$
    $\forall m, g : \mu^{k+1}_{m,g,s} = \mu^{k+1}_{m,g,s} * \frac{\bar{\phi}^{core}_{g,s}}{\bar{\phi}^{lattice}_{g,s}}$
    $k = k + 1$
  end while
end for

number of scattering collisions the neutrons undergo within a given mesh. Hence, the fundamental hypotheses are generally easier to be fulfilled in case of coarse homogenization. This is one of the reasons that have contributed to make the diffusion approximation so popular in industrial calculation. Other reasons may be found in the fact that it generally brings to extremely low computing time and memory footprint and because that, from the mathematical point of view, it is a robust approximation. Nevertheless, for the same observations, it is clear that the accuracy of this approach is degraded in case of highly absorbing media (for instance control rods or burnable poisons), heterogeneous systems (different assembly types), close to the boundary layers or to strong localized neutron sources.

Integrating every term over Ω under the hypothesis of linear dependency of the angular flux on this variable, it is possible to obtain the Fick's law for neutrons. This law associates the neutron current (definition recalled in Eq. (3.10)) to the scalar flux; it is reported in Eq. (3.11).

$$\boldsymbol{J}(\boldsymbol{r}, E, t) := \int_{4\pi} d^2\Omega \; \boldsymbol{\Omega}\psi(\boldsymbol{r}, E, \boldsymbol{\Omega}, t) \tag{3.10}$$

$$\boldsymbol{J}(\boldsymbol{r}, E, t) \approx -D\nabla\phi(\boldsymbol{r}, E, t) \tag{3.11}$$

Integrating the transport equation (given in Eq. (1.2)) over Ω and substituting the current with the diffusion term of the fix law it is possible to obtain the diffusion equation, available in Eq. (3.12).

$$1/V_n \frac{\partial\phi(\boldsymbol{r}, E, t)}{\partial t} - \nabla \cdot D\nabla\phi(\boldsymbol{r}, E, t) + \Sigma(\boldsymbol{r}, E, t)\phi(\boldsymbol{r}, E, t) = Q(\boldsymbol{r}, E, t) \tag{3.12}$$

The diffusion equation allows to reduce the problem's dimension by removing the angular variable and from the numerical point of view is much simpler to treat. As mentioned in the introduction, in MINOS the diffusion equation is solved with the Raviart-Thomas-Nédélec finite elements.

Simplified-P_N

As anticipated by the name, this method is a simplified version of the Spherical Harmonics (P_N). The P_N-method is based on the decomposition of the angular flux in a series of orthogonal functions called, spherical harmonics. This method has been deployed in many fields of physics, as for instance for the modelling of electron orbitals and for the gravitational field. A generic definition of the spherical harmonics is given in Eq. (3.13). Where $Y_m^l(\boldsymbol{\Omega})$ are the real spherical harmonics satisfying the Laplace equation and $\varphi_m^l(\boldsymbol{r})$ are the coefficients that become the unknowns of the equation.

$$\psi(\boldsymbol{r}, \boldsymbol{\Omega}) = \sum_{m=0}^{\infty} \sum_{l=-m}^{+m} \varphi_m^l(\boldsymbol{r}) Y_m^l(\boldsymbol{\Omega}) \tag{3.13}$$

As for the S_N, this method does not introduce any approximation but the truncation to a finite order N. While the Spherical Harmonics method does not suffer of the ray effect, it is rather complex and computationally expensive to use this decomposition for the 3D resolution. For this reason such a method is hardly ever used in industrial calculation schemes. In APOLLO3®, one solver using the P_N-method has been implemented especially for the simulations of SFRs: PASTIS [161, 190].

As reported in [31], pages 74 and 75, the Simplified-P_N were firstly introduced by E. M. Gelbard [191]. His aim was to generalise and improve the diffusion operator. His main intuition was that, locally, the transport solution could be simplified assuming an infinite plane geometry, hence, requiring only the 1D Spherical Harmonics. At that time, the required computing power was still prohibitive and the justification of this approach was mainly based on empirical results. For these reasons, this method became popular only after that several theoretical justifications were published [192, 193, 194] demonstrating its asymptotic validity. Two variants of the SP_N-method are implemented in APOLLO3®, one in MINOS [180] and the other in MINARET [195].

3.2 Thermal-Hydraulic Models

As stated in the introduction, the thermal-hydraulic codes may be classified by their targeted modelling scale and if they focus on the reactor core only or they model also other reactor components (thermal-hydraulic system codes). System codes are typically needed to model transient scenarios like Loss Of Coolant Accidents, for this purpose, CEA has developed CATHARE3 [196] together with EDF and with the financial support of Framatome and IRSN. This code enjoys a wide range of applications ranging from various reactor types (with all sort of coolant: water, sodium, helium and others) to rocket cryogenic engines [91].

Several simplified thermal-hydraulic models have been integrated in CEA neutronic codes. The most recent one is THEDI [197] (THErmohydraulique DIphasique, which in English translates to diphasic thermal-hydraulics), which is implemented in APOLLO3®. Contrary to most of the sim-

plified codes, it offers also the possibility to perform system calculations, but it is limited to a 1D resolution. For the 3D subchannel modelling, CEA has created FLICA4. For even more refined modelling scales, CEA relies on the TrioCFD [198], which became open-source in 2015. This section focuses on FLICA4 and THEDI.

3.2.1 FLICA4

FLICA4 [90, 199] is based on a 3D, biphasic flow code allowing to perform subchannel simulations. The adopted spatial discretization method is based on the finite volumes. The two phases are dealt with a single field model using the mixture mass (Eq. (3.15)), momentum (Eq. (3.16)) and balance conservation (Eq. (3.17)) equations together with the steam mass balance (Eq. (3.18)). In these equations, variables with no index refer to the mixture field and they are obtained following Eq. (3.14), where χ is a generic variable.

$$\chi = (\sum_{k=l,v} \alpha_k \rho_k \chi_k)/\rho \tag{3.14}$$

The index k represents the phase index (l for the liquid water and v for the steam). α_v is the void fraction, the volume fraction of the vapour phase within the mixture ($\alpha_l + \alpha_v = 1$). With respect to the equations presented in the introduction, the other new variables are $\bar{\bar{\Pi}}$ the viscous stress tensor, $\boldsymbol{\tau}$ the wall drag force, $\boldsymbol{q}$ heat flux accounting for molecular and turbulent conductivity, E is the total energy (kinetic plus internal energy), M_v is the steam mass diffusion term accounting for mixture turbulence and Γ represents the mass exchanges between phases. This last term is modelled as the sum of Γ_w, which is the steam generation on the wall (cladding outer surface) and $\Gamma_{l,v}$, which is the evaporation/condensation rate in the bulk of the mixture.

$$\frac{\partial}{\partial t}(\rho) + \nabla \cdot (\rho \boldsymbol{u}) = 0 \tag{3.15}$$

$$\frac{\partial}{\partial t}(\rho \boldsymbol{u}) + \nabla \cdot (\sum_{k=l,v} \rho_k \alpha_k \boldsymbol{u}_k \otimes \boldsymbol{u}_k + \alpha_k \bar{\bar{\Pi}}_k) = \rho \boldsymbol{g} + \boldsymbol{\tau} \tag{3.16}$$

$$\frac{\partial}{\partial t}(\rho E) + \nabla \cdot (\sum_{k=l,v} (\rho_k \alpha_k \boldsymbol{u}_k E_k + \alpha_k \bar{\bar{\Pi}}_k \cdot \boldsymbol{u}_k) - \boldsymbol{q}) = \rho \boldsymbol{u} \cdot \boldsymbol{g} + q''' \tag{3.17}$$

$$\frac{\partial}{\partial t}(\rho_v \alpha_v) + \nabla \cdot (\alpha_v \rho_v \boldsymbol{u}_v + \alpha_v M_v) = \Gamma \tag{3.18}$$

Both the Zuber and Findlay [200] (1965) and the Ishii [201] (1977) drift-flux models can be used to estimate the relative velocity between phases. These models can be seen as semi-empirical closure laws used to replace a multi-field treatment. Nevertheless, these relations have shown to

simplify the problem while being very accurate when the motions of the two phases are strongly coupled. The generic form of this closure equation is given in Eq. (3.19). In this equation, $\boldsymbol{J}$ is the volumetric velocity defined by $\boldsymbol{J} = \alpha_v * \boldsymbol{u}_v + \alpha_l * \boldsymbol{u}_l$. C_0 is the drift flux distribution parameter, which accounts for the local velocity distribution before the averaging process and its computation is based on correlations. $\boldsymbol{u}_{v,lim}$ is also given by semi-empirical correlations, its physical meaning corresponds to the speed the steam would have in case of static bulk.

$$\boldsymbol{u}_v = C_0 \boldsymbol{J} + \boldsymbol{u}_{v,lim} \tag{3.19}$$

FLICA4 is also able to perform 1D radial heat conduction in the fuel. For transients calculation, given the interdependencies among the wall heat flux and wall temperature, these variables are solved implicitly.

3.2.2 THEDI

THEDI has been conceived as C++ dynamic library in order to enhance its flexibility and facilitate its integration in neutronic codes. Even if it could be considered as a simplified thermal-hydraulic code, it enjoys a wide range of applications as it is capable of biphasic flow modelling of steady-state and transients and it allows to perform system thermal-hydraulic simulations. Indeed, it treats the combination of multiple reactor components modelled as channels connected to each other, either in series or in parallel. The fundamental physical model is based on four equations, similar to the ones presented for FLICA4. One small difference is in the energy balance, which does not treat the conservation of the total energy but only of the internal one. This does not constitute any physical approximation, it is just a reformulation of the same system of equations. The correlations used to close the systems are also mainly derived from the ones used in FLICA4, the drift-flux model is chosen also in this case.

The main simplification of this code is the 1D (axial) thermal-hydraulic modelling. This assumption is found to be very accurate when assuming typical radial meshes as big as one fuel assembly or a quarter of it. On the other hand, at the subchannel scale, the radial heat gradient generally necessitates a 3D modelling. In fact, the radial motion of the water and the heat transfer among channels can effectively improve the heat removal. This is especially true, when considering that the heat source for a given channel may significantly differ from the heat generated in the adjacent one. Like in the case of guide tubes or fuel rods with burnable poison next to fresh fuel. The 1D treatment is also crucial for parallel computing, as parallel channels may be effectively distributed over different processors.

THEDI also computes the heat conduction in the solid, which in this case may be the fuel or another reactor component, like a heat exchanger. Due to these different applications, the solid

object may be coupled to other channels dealing with different fluids and flow directions.

3.3 Isotopic Evolution Model

The isotopic evolution codes produced at the CEA are mainly two, DARWIN-2 [202] and its successor MENDEL [203]. In this section, a description of the latter is given as it is the current depletion solver for APOLLO3® and TRIPOLI-4®.

3.3.1 MENDEL

The main goal of this code is to compute the time-evolution of a set of interest isotopes. Generally, it is used to follow the fuel isotopic concentrations, along the entire fuel cycle, both inside and outside the reactor. Other quantities related to the radioactive decay may be computed as the mass content of each isotope, the residual power, the energy spectrum of emitted radiations, the neutron source and the radiotoxicity. The main targeted isotopes are heavy nuclei, fission products, activation products. Outside commercial nuclear fission reactors, another important application is represented by the accelerators, in particular to track spallation products, but it targets also fusion reactors and nuclear medicine.

As described in the introduction, the isotopic depletion is modelled by the Bateman equations. In MENDEL, these equations are solved using Runge-Kutta time step method.

3.4 Fuel Performance Models

The main CEA fuel performance code for PWRs is ALCYONE [204] and it has been developed in cooperation with Framatome and EDF. Its thermal-mechanic module is directly derived by the CEA code CAST3M [205, 206]. In particular ALCYONE has been integrated in the PLEIADES [207, 208] platform for fuel performance codes. This integration aims at exploiting synergies among the integrated solvers and at sharing a set of pre and post-processing tools, as well as a database containing the physical properties, experimental results and validation tests.

In this section, a simplified modelling for the gap heat transfer coefficient along irradiation is also briefly described. This model has been realized during an internship held at CEA-SERMA under the direction of Dr. K. Ammar and Ing. N.-G. Castaing.

3.4.1 ALCYONE

ALCYONE is able to model the fuel behaviour under normal operating conditions, power ramps and accidental scenarios (RIA and LOCA). Like in most of the fuel performance codes, ALCYONE treats each fuel rod separately, as its simplified models do not account for the environment. In

other words, the thermal hydraulic channel is considered isolated from the rest of the core and the neutronics simplified models are derived by full reflection boundary conditions. For this reason, many multiphysic coupling schemes have been realized to asses the interest of integrating the environment effect on the fuel behaviour. In the typical fuel performance modelling of ALCYONE, the fuel rod is divided in about 30 axial slices, which interact with each other mainly through global quantities like the pressure in the fuel-cladding gap. An exemplification of the multi-1D modelling is given in Fig. 3-1.

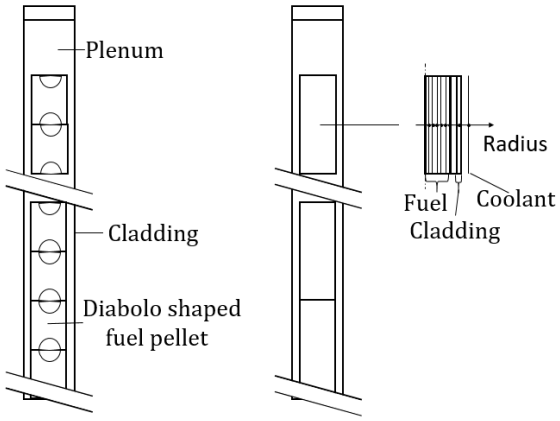

Figure 3-1: Typical discretization used in ALCYONE simulations of fuel performance under normal operating conditions. A typical PWR fuel rod is constituted of about 200 fuel pellets, while in this meshing the fuel rod is divided in around 30 axial slices. In the multi-1D modelling, each slice is only radially discretized in about 40 volumes.

As introduced in sub-section 1.1.2, the fuel performance is a multiphysic problem in itself. For this reason the resolution scheme of the global problem may become rather complex. In ALCYONE, for each time step, a three-level nested fixed-point iteration scheme is solved. The outermost loop deals with the computation of variables for the entire fuel rod, while, in the intermediate one, the convergence is researched for each axial slice. The innermost loop deals with most of the multiphysic problem, as the treated physics are particularly strongly coupled to each other. A simplified version of the iteration scheme is reported in Fig. 3-2, the convergence is tested at each iteration of the multiphysic and the rod integral loops.

It should be noticed that the neutronics is outside the multiphysic iteration loop because the considered simplified model uses one group cross-sections only tabulated in burnup. This is due to the fact that the temperature dependency is not directly addressed by this simplified model. However, it has been found that the exact radial sub-pin shape of the neutron flux may not have a strong impact on the other physics [110, 111].

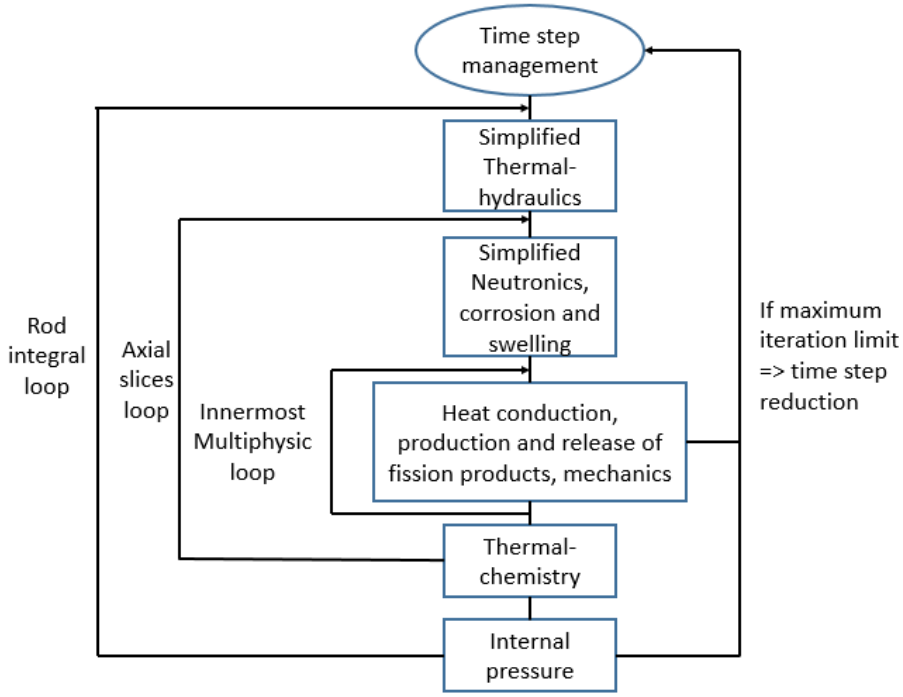

Figure 3-2: Simplified iteration loop used in ALCYONE. For each time step, a three level nested fixed-point iteration scheme has to be solved. Convergence criteria have to be met for both the multiphysic and the rod integral loops.

3.4.2 Simplified Gap Heat Transfer Coefficient Model

Referring to what has been introduced in sub-section 1.1.2, the gap thickness strongly affects the heat conduction in the fuel rods. Since fuel performance simulations of many fuel rods generally require a lot of computing power, simplified models approximating the evolution of the gap heat transfer coefficient are becoming more and more frequent (e.g. [115]). In particular in [209], a methodology to calibrate a simplified model for the Rod Ejection Accident (REA) and to quantify its uncertainty is presented. This is especially true for complex multiphysic schemes aiming at computing variables at the pin-cell scale, as they require a higher number of fuel rods to be modelled and they benefit more from an increase in accuracy on the local temperature field.

The specific model produced in the context of this internship deals with the calibration of an analytical function that approximates a database of fuel irradiation scenarios under a set of different operating conditions, which has been produced with ALCYONE. From experimental data and from FRAPCON simulations [10], pages 7 and 8, it has been observed that the gap heat transfer coefficient exhibit an abrupt variation at the moment of contact between fuel and cladding. For this reason, in this simplified model, two separate calibrations are effectuated: one for the burnup interval before the beginning of the contact and the one after this moment. The variables used for the calibration refer to average quantities of the considered slice: burnup, linear power and water bulk temperature.

This model implicitly neglects the dependency on the irradiation history: whether the burnup value has been reached with a high power level for long time or the opposite, whether the power has been constant or many or significant variations occurred. Moreover, integral quantities like the pressure inside the cladding are also not included in the calibration procedure. However, this model has shown good agreement with the database and has demonstrated the importance of passing from a constant value to more accurate models. The structure of this analytical representation of the gap heat transfer coefficient is given in Eq. (3.20), where $\boldsymbol{p}_i$ is the vector of calibrated parameter for that burnup interval and $BU_{closure}$ is an estimated burnup at which the fuel-cladding contact starts.

$$\begin{cases} H = h(BU, q', T_{bulk}, \boldsymbol{p}_1) & if BU < BU_{closure} \\ H = h(BU, q', T_{bulk}, \boldsymbol{p}_2) & else \end{cases} \tag{3.20}$$

3.5 Coupling Tools

This section is about the informatic tools that have been created to facilitate the realization of multiphysic coupling schemes. For what concerns CEA, a central role is played by the SALOME platform [62], which has been jointly developed by CEA, EDF and Open Cascade. SALOME platform is a generic tool for a wide list of applications, which is particularly useful when communications among solvers and manipulation of large fields of data are required. With respect to the multiphysic coupling scheme for the reactor core simulations using specialised solvers, more specific projects have been carried out at CEA. The most recent one is CORPUS [210], the successor of HEMERA[211, 212]. In this section, SALOME and CORPUS are shortly outlined.

3.5.1 SALOME Coupling Platform

One of the most important functions of SALOME is to offer a standardised solution for field representation. This apparently simple task hides many complexities and plays an essential role in the development of a multiphysic coupling scheme. Since each solver involved in a coupling scheme represents variables from its own perspective and in its own programming language, SALOME gives one standard definition of field that has to be respected by every solver interface. This constraint helps to increase the modularity and the generality of the coupling schemes. The fields are represented under the MED format, a specification of the HDF5 format [63]. The MED library is written in C and C++, while its Application Programming Interface is available in C, FORTRAN and Python.

Conforming to this standard means to access to a long list of tools for the field manipulation that simplifies and makes more efficient the calculation scheme in all of its phases. For instance, for the pre-processing, the mesh creation is optionally helped by a Computer-Aided Design (CAD) interface. Inside the calculation scheme, several modules contribute to efficiently and easily perform

data manipulation and field interpolations. Moreover, even if the MED format does not require file creations, as it allows direct data exchanges in memory, it also provides efficient solutions for permanent data storage. In respect of the post-processing, many tools are provided for the visualization and elaboration of the results, which may be crucial in case of complex variables. Finally, several modules are available to foster the statistical data analysis and the evaluation of uncertainties.

3.5.2 CORPUS

CORPUS has been developed with the aim of creating and maintaining a set of multiphysic calculation schemes. A broad range of scenarios is treated and the simulations are generally realized through the combination of existing specialised codes. Each of this code has to be initially integrated in the CORPUS platform as a component. This process is based on the Interface for Code Coupling (ICoCo). Basically, all the codes are supervised under the format of shared library, which has been previously created by the compiling of the given solver wrapped within the standardized ICoCo interface. This process is mainly required to supervise solvers eventually written in different programming languages and to make uniform the solvers interfaces.

Some of the coupling schemes realized within this framework are reported in the next section.

3.6 Pre-Existing Coupling Schemes

Specifically at SERMA department, several coupling schemes for the multiphysic modelling of PWRs have been carried out within the CORPUS project. During the PhD thesis of A. Targa [7], coupled simulations of the Rod Ejection Accident (REA) have been realized. In [210], this accident scenario is modelled with a coupling scheme based on APOLLO3® for performing two-groups diffusion calculations and ALCYONE for the fuel performance. For the thermal-hydraulics, ALCYONE's simplified module is used. The diffusion solver is used with a quarter of assembly radial discretization and one equivalent fuel rod is modelled for each of these radial meshes. The results found for a 3x3 mini-core plus reflector are satisfactorily compared to the ones obtained with an adiabatic model. In [213], the same transient is modelled and the impact of replacing the simplified thermal-hydraulic module by FLICA4 is assessed. Another development studied during this PhD thesis deals with a pin-power-reconstruction obtained from the combination of MINARET-S_N and MINOS-SP_N [214], but the results have been judged only partially satisfactory.

In the PhD thesis of G.-K. Delipei [209], the uncertainty quantification associated to multiphysic calculation schemes like the just mentioned ones is studied [215, 216]. In the post-doc of D. Caron, the quasi-static method has been used to perform multiphysic transient calculations [217]. This technique allows to exploit the different characteristic time scales of the intervening phenomena to improve the efficiency of the coupling scheme. During her PhD thesis, M. Faucher [106] studied the

integration of TRIPOLI-4® in a multiphysic coupling scheme for RIAs [2]. Finally, a wide list of numerical methods for multiphysic coupling schemes has been reviewed during the PhD thesis of C. Patricot [147].

3.7 Conclusion

CEA provides a large set of specialised solvers and coupling tools that could be used for the realization of a multiphysic coupling scheme for the modelling of PWR cores along irradiation. In particular, with these tools it is in theory possible to achieve the target fixed in sub-section 2.1.4. Both APOLLO2 and APOLLO3® can produce pin-cell homogenized cross-sections and APOLLO3® provides multiple solvers that could effectively use them for core calculations. Even if, for industrial calculations, FLICA4 has been mainly deployed with coarse radial mesh discretizations and eventually only local refining in one assembly, it is also capable of performing full 3D subchannel simulations over larger domains. With respect to fuel performance, both a specialised solver and a simplified model are available.

Even if many works have been carried out on the development of multiphysic calculation schemes, almost none of them has been centred on fine scale resolution of the coupled system (pin-cell neutronics and subchannel thermal-hydraulics). Moreover, most of the studies have been centred on accidental scenarios, whilst most of the time the depletion calculations have been treated with a more conventional approach. For these reasons, the multiphysic fine-scale depletion calculations are rather unexplored and the literature review suggests that it could be an interesting topic to focus on. Finally, the flexibility of the codes may allow to effectively test some of the numerical methods found in sub-section 2.2.4.

[2] This PhD work has been carried out within the McSAFE project.

Chapter 4

Development of the Multiphysic Coupling Scheme for Steady-State Calculations

This chapter deals with the realization of a first version of the multiphysic coupling scheme aiming at the resolution of steady-state problems. As specified in paragraph 1.1.2, the steady-state problem constitutes an essential part of the depletion calculations. The very first step of this chapter deals with the interpretation and formalization of the problem and its decomposition in a set of sub-problems. In the second section, the physical models are implemented using specialised solvers. In the third section, the structure for data exchanges among the solvers is implemented.

4.1 Problem Formalization

For this initial step, the fuel performance is neglected. Under this simplification, the problem can be modelled using just a power generation, a thermal-hydraulic and a depletion models, as exemplified in Fig. 4-1 or equivalently represented by the system of equations (4.1). The resolution of the problem consists of the research of a set of variables that is simultaneously satisfying all the models. At this stage, the variables are still rather abstract, in the sense that their exact definition depends on the choice of the models and on the modelling scales. The nomenclature used is the same as for Fig. 1-7.

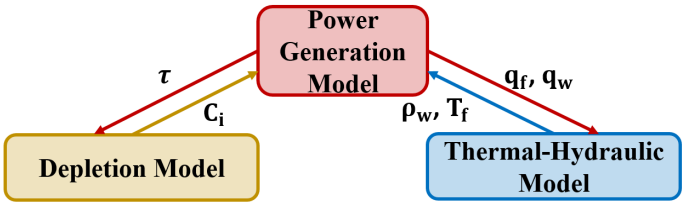

Figure 4-1: Multiphysic coupling scheme for steady-state calculations without a fuel performance solver.

$$\begin{cases} (\boldsymbol{\rho_w}, \boldsymbol{T_f}) = TH(\boldsymbol{q_w}, \boldsymbol{q_f}) \\ (\boldsymbol{\tau}, \boldsymbol{q_w}, \boldsymbol{q_f}) = N(\boldsymbol{\rho_w}, \boldsymbol{T_f}, \boldsymbol{C_i}) \\ \boldsymbol{C_{FP}} = FP(\boldsymbol{\tau}) \end{cases} \tag{4.1}$$

In this context, the TH operator solves both the thermal-hydraulics and the heat conduction in the fuel. For this reason it needs to receive two separates power distributions, one for the direct heat generation in the water and one for the power deposited in the fuel. The considered thermal-hydraulic solvers to be deployed in this model are FLICA4 and THEDI. They both consider a user-given constant fuel-gap heat transfer coefficient. Even if the steady state problem is chosen, this simplifying hypothesis may lead to strong approximations as this coefficient also depends on parameters others than the burnup (for instance instantaneous thermal expansion due to temperature gradient) and a heterogeneous burnup distribution might be considered. For instance, even at Beginning Of Cycle, the reactor core could be loaded with assemblies at different burnup. However, for simplicity this problem will not be addressed until Chapter 7. The output of this operator is the volume averaged density in each thermal-hydraulic mesh and the temperature profile in every axial slice of fuel.

The N function aims at calculating the power distribution corresponding to the density, temperature and isotopic concentrations fields. The choice of the name for this operator derives from neutronics, as it is the main source of heat generation. However, neutrons are not the only particles depositing energy in the reactor; this point is briefly described in the following section. Both APOLLO2-APOLLO3® and APOLLO3®-APOLLO3® two-steps schemes are suitable choices for the modelling of heat generation consequent to the neutron transport. Instead of the multigroup scalar flux $\boldsymbol{\phi}$, in this scheme, the reaction rates $\boldsymbol{\tau}$ are transferred to the depletion model, because they are required by MENDEL. There is no substantial difference between these two quantities as the macroscopic cross-sections can be regarded as a parameter within a given neutronic calculation ($\boldsymbol{\tau} = \boldsymbol{\phi\Sigma}$). The dependency of macroscopic cross-sections on temperature, density and isotopic number densities has to be addressed in both lattice and core calculations. Nevertheless, as described in Section 2.1, at least for coarse radial discretization, it is a current practice to account for these parameters during two-step neutronic simulations.

The FP operator calculates the equilibrium concentration of fission products. It is considered also for these steady-state calculations because the fission products concentrations may evolve on a time scale much lower than that of the fuel depletion and isotopes like xenon-135 and samarium-149 have a strong influence over the power distribution and the total reactivity balance. The chosen solver for this model is MENDEL.

In the following section, the implementation choices for each operator are described, whilst Section 4.3 focuses on the data exchanges among each model. The coupling scheme is implemented to deal with both coarse (quarter of assembly) and fine (pin-cell scale) radial discretizations.

4.2 Modelling Choices

4.2.1 Power Generation Model

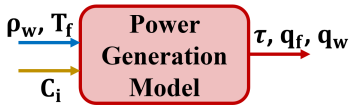

Figure 4-2: Generic power generation model.

As introduced in the previous section, the power generation model, whose scheme is reported in Fig. 4-2, may require more than just solving the neutron transport. In fissile media, the approximation that the heat generation is just proportional to the fission rate is commonly accepted. However, even if during normal operation the vast majority of the power generation derives from the fission events, a small part of this energy is not deposited "locally". Considering about 202.7 MeV of energy produced by a fission event on uranium-235, about 82 % is kinetic energy of the fission fragments, but the rest is carried by photons, neutrons, betas (electrons and positrons) and antineutrinos [218]. Since the fission fragments are heavy and charged particles, they strongly interact with the matter and release all their energy within few microns, which compared to the typical mesh characteristic length (>1 mm) means "locally". In respect of the beta particles, they account for about the 3.5 % of the fission energy and, as charged particles, they also release most of their energy within the fuel. The kinetic energy of antineutrinos is around the 4.7 % of the total and under good approximation it is totally released outside the reactor (cross-section inferior to 10^{-19} b for proton rich material). For what concerns neutrons, they carry 2.4 % of the total kinetic energy and they release a big portion of it via the scattering in the water. Finally, the photons are responsible for the 7.5 % of the energy and they may deposit a significant part of it outside of the given fuel pin. Their interaction with a nucleus depends on their energy and it is proportional to the atomic number squared, cubic or even to the power of four depending on the reaction. For this reason, the heat generation due to photon interactions may require the photon transport to be modelled.

Following this analysis, it is clear that having just the fission rate means to have only a part of the total information. In fact, part of the power consequent to the fission rate in a given mesh might be shared with neighbouring meshes and even within a given mesh, distinction should be made between the power deposited directly in the water and that generated in the fuel. As briefly discussed in the introduction, in steady-state conditions and neglecting axial heat conduction, all the power generated in the fuel is transferred to the coolant. However, it is important to distinguish how much is directly heating the water as this portion of energy does not contribute to the heat conduction. For this reason, accounting for direct heating means reducing the wall heat flux and often the fuel centreline temperature.

With respect to quarter of assembly radial discretization, as described in sub-section 2.1.1, the conventional method is just to assume all the power to be distributed within the mesh and distribute the heat generation between the fuel ad the water with a simple constant factor. Basically, the power profile corresponds to the fission rate multiplied by the average fission energy of the medium and normalized to the total power. After that, the heat generation in a medium (water or fuel) is obtained scaling by the constant factor. The value of the repartition constant is often set around 2.6 % in the water and 97.4 % in the fuel. The mesh size contributes to the problem simplification also in terms of computation of the heat generation. Indeed, the size of the fuel assembly is about 20 cm, which is greater than the average range of photons in the reactor. Hence, accounting for the power deposition in meshes others than the one where the fission event occurs does not contribute much to the shape of the heat generation distribution. Furthermore, the coarse mesh simplifies also the fuel-water power repartition as local heterogeneities (as thimble tubes, control rods or burnable poison) are less important at this scale. Nevertheless, for some specific applications, like simulation of the reflector heating and measurement on irradiation devices in experimental reactors, industrial calculation schemes may include photon transport as in [219].

A different analysis has to be made for pin-cell homogenization. Two calculation schemes that could be used to account for photon transport are described in [220]. Rigorously, neutron-photon transport should be treated as a coupled problem as also photons interaction with nuclei may be a neutron source. Anyway, even a decoupled treatment, in which, from the neutron transport a photon source is defined, could significantly increase the computing time. Moreover, some developments may be required to effectively include photon transport in APOLLO3® core calculations.

In [220], the impact of neglecting the photon contribution to the heat generation is assessed on several benchmarks and against TRIPOLI-4® (which can provide a reference solution for the steady-state problem). It is found that photons can significantly change, up to the 30 %, the power in the fuel rods with gadolinium as burnable poison, while in normal fuel rods the impact is assessed to be about 1 %. As expected, in non-fissile media, like the structures and the moderator, the impact is even larger.

Since the effect of photons on power distribution seems to be rather important at the pin-cell scale, several options to include it are considered during this PhD thesis. The basic one is to keep the repartition constant used for the coarse discretization. The conventional alternative would be to create an energy deposition cross-section during the lattice calculations by performing coupled neutron-photon transport. This option may more than double the calculation time and require several developments. A third, innovative approach was also considered. It deals with the calibration of a sort of pin-by-pin assembly power repartition map based on 2D TRIPOLI-4® calculations. The dependency of this repartition map on the core parameters would define the number of maps to be computed, hence, the efficiency of the method. Even if these developments were judged interesting, as they may require an important portion of the PhD thesis, they have been left for future improvements. The power generation model under this simplification can be seen as the combination of a neutronic model and a repartition module as in Fig. 4-3. Anyhow, even the state of the art deterministic multiphysic core depletion coupling schemes generally do not account for photon transport [51, 115].

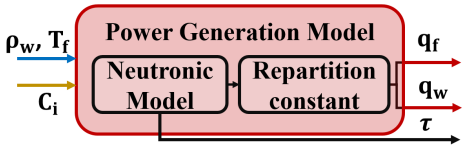

Figure 4-3: Power generation model based on a neutronic model and a repartition module (simple constant).

Neutronic Model

As described in sub-section 2.1.4, the pin-cell homogenization constitutes an interesting trade-off between time and accuracy, as compared to the referential direct calculations and the fast-running coarse homogenization plus pin-power-reconstruction. In the context of multiphysic simulations, two-steps calculations offer several advantages. Once the lattice calculations are performed, the parametrized homogenized cross-sections contain already the information of how the neutronics responds to other physics. Therefore, solving neutronics for different thermal-hydraulic conditions just means to interpolate cross-sections for a new combination of parameters.

Apart from what concerns the pin-cell homogenization, the rest of the lattice calculations for the fuel assemblies are chosen to be performed with a conventional MOC calculation scheme. The chosen parameters are fuel temperature, moderator density, boron concentration and burnup. In order to simplify the task, control rods are not taken into account during this PhD thesis as their treatment would make the problem significantly more complex and it is not a central topic in multiphysic simulations. The moderator temperature is treated as a dependent parameter of moderator density. In fact, in nominal conditions, the relative variation of pressure is rather small, hence, assuming a

constant pressure it is possible to use the water tables to approximate the temperature corresponding to a given density. This is done also because the neutronics depends much more on the water density than on the water temperature (non-resonant medium).

Even in the definition of the parameters of lattice calculations, refining the homogenization scale may lead to a certain number of complications. With respect to assembly or quarter of assembly homogenization, the homogeneous cross-section for a given fuel temperature is computed from its corresponding heterogeneous eight of assembly (due to general symmetry and simplified boundary conditions) in which all the fuel regions are at this given temperature. A similar approach is followed for the moderator density (and temperature). While considering a pin-cell homogenization, the same heterogeneous calculations are used, but in the moment of core calculations, different temperature or density values may be imposed on every pin cell. For instance in the case of fuel temperature, this implicitly means that the cross-section used for a given pin cell corresponds to a heterogeneous calculation in which all the fuel contained in the assembly is at the same temperature, irrespectively of the considered temperature field. For what concerns the boron, its concentration is assumed to be homogeneous throughout all the core, hence, no difference is made in this case. The burnup is the parameter hiding the greatest complexity. During the depletion lattice calculations under nominal conditions, the cross-sections are stored for a set of target burnup values, which correspond to the assembly average burnup, also called global burnup. For each global value, every pin cell achieves a given local burnup depending on the integrated local fission reaction rate multiplied by the average fission energy of the medium as computed by the lattice solver. During core calculations, a new depletion history is constructed, but also in this case each pin cell cross-section actually corresponds to a flux calculation with the local burnup distribution as computed during the lattice calculations. For this reason, the local burnup distribution "seen" from each pin cell may actually significantly differ from the one found in core calculations. Even if a potential alternative to this approach has been discussed, the homogenization process as described is kept and its limitations are the object of further studies. The alternative approach is described in the following sub-section.

In respect of the reflector homogenization, this is not considered as a central topic of the PhD thesis, as its dependency on other physics is much weaker than in the rest of the core. Therefore, a simplified modelling based on 1D traverses is used in a similar manner to what presented in sub-section 2.1.1. The choice of the core solver is not made at this stage, as it might be interesting to compare different core models for the pin-cell homogenization and on a multiphysic case study. For what concerns the SPH technique, its effectiveness on the pin-by-pin homogenization has been widely tested and it is found to be particularly effective [188, 221]. In particular, in [221] it has been tested for the SP_N method and an improvement to better preserve the referential reaction rates are proposed. Whilst, in APOLLO3® the SPH treatment of a diffusion solver corresponds to the state of the art, for the SP_N, this procedure could be further improved according to the last cited source.

However, the tests on this method have shown already high accuracy level against the reference results, hence, the hypothesis of using the SPH for a SP_N model is not discarded.

Alternative Multiphysic Homogenization Procedure

In this sub-section, an alternative homogenization procedure is presented. This method is the result of discussions with several colleagues; even if judged promising, it has not been implemented due to the amount of developments that would be required. The main idea behind this method is the willing to introduce a simplified multiphyisic model within the cross-section homogenization phase to improve the modelling accuracy. In this way, homogenized cross-sections, as simple as the one obtained with the standard approach might intrinsically include complex informations like fuel density and geometry variations or radial temperature profile corresponding to given wall temperature and burnup. A key difference lies in the parameters choice.

The first step of this procedure is the production of a table of thermal-mechanic variables as fuel geometry, density and temperature profiles as function of linear power, water bulk temperature and burnup. This table is obtained from a set of independent fuel performance simulations performed over a standard irradiation period at constant power (just as the lattice calculations) for a set of linear powers and bulk temperatures. Basically, a theoretical axial slice is simulated by a fuel performance code (e.g. ALCYONE) assuming an average environment. This should eventually be repeated for every fuel rod type.

As in the conventional approach a depletion lattice calculation could be performed under nominal conditions ($q'_{nom}, T_{bulk,nom}, C_{boron,nom}, ...$) and at each burnup step the fuel geometry, density and temperature profiles could be updated from the thermal-mechanic table (using the local q' and $T_{bulk,nom}$). While the assembly average linear power is q'_{nom}, iterations should be done to find consistency between the computed rod average linear power and the thermal-mechanic conditions. From what is found in [110], this coupling is expected to be weak, hence only few iterations should be required. After that, for a subset of burnup steps, the other combinations of parameters might be used to compute the rest of the cross-sections and also in this case an iterative process may be required to converge on the local power distribution. During core calculations, a similar iterative process should be done including also a thermal-hydraulic model. Similarly to what is experienced with the local burnup in the conventional scheme, also in this case, the inconsistencies between the assembly local power distribution used for the homogenization and that found during core calculations.

The number of parameters would be the same as in the conventional calculations, but the number of assembly averaged linear power values to be considered has to be investigated. Moreover, the cost of multiphysic iterations with the lattice solver may be prohibitive and preliminary tests show that neglecting the power history when producing the thermal-mechanic tables may become a

strong approximation for high exposures. Finally, exploratory neutronic simulations with different density profiles compatible to the burnup effect of PWRs have shown a weak dependency on this phenomenon. Several aspects of this scheme should be further analysed and eventually it could be considered for future studies.

4.2.2 Thermal-Hydraulic Model

For what concerns the thermal-hydraulic model, solvers like FLICA4 or THEDI can perform the full task, i.e. thermal-hydraulics and heat conduction in the fuel as shown in Fig. 4-4.

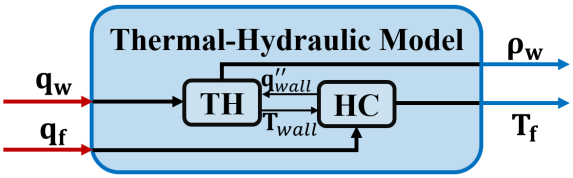

Figure 4-4: Thermal-hydraulic model including 1D heat-conduction in the fuel.

On the other hand, the heat conduction is solved on a scale different from the others. Indeed, for each axial slice, the 1D radial heat conduction problem is solved using the wall temperature as boundary condition and the sub-pin radial temperature profile is computed. In principle, a sub-pin radial power profile could be used. Since the power generation model provides just the cell averaged power deposited in the fuel (quarter of assembly or pin-cell), the radial power profile has to be reconstructed. In the case of quarter of assembly, the average linear power is computed using the number of fuel rods and their geometry. Once the equivalent pin-cell power is obtained, only the integral of the sub-pin radial power profile is available, no information is known on its shape.

The simplest solution is to assume a flat sub-pin heat generation profile equal to the average value which is deducted from the cell integrated power. In [111], a work of the currently PhD students and his former supervisors during a previous internship, a similar problem is faced. In a fine coupling of a lattice solver (APOLLO3®-MOC) and a fuel performance code (ALCYONE), even if a sub-pin power profile is produced by the MOC model, its resolution is too low as compared to the one required by the fuel performance code. In that particular example, for simplicity, an equal radial mesh is used for both the models. Nevertheless, this is not be an efficient solution, hence during the internship few power reconstruction techniques have been explored. Before describing them, it should be considered that ALCYONE includes two simplified models for estimating the sub-pin radial profile. The most recent one, PRODHEL [204], does much more than simply computing the sub-pin radial neutron flux and heat generation profiles, but let us focus on the this part. The prediction of the heat generation profile is based on the fission reaction rate multiplied by the average fission energy. One energy group cross-sections are used and the flux is obtained as a combination of Bessel functions [222]. Those functions are the solution of the flux under the diffusion approximation

in a cylindrical homogeneous medium of infinite height. Therefore, this method could be seen as an empirically adjusted diffusion equation. An example of these shape functions is reported in Fig. 4-5 for a set of axial slice average burnup values. A set of similar shape functions could be stored for each burnup value and it could be used to improve the power reconstruction. The additional cost of this reconstruction technique would be almost negligible. The function would simply be normalised to the pin-cell integral value provided by the neutronics.

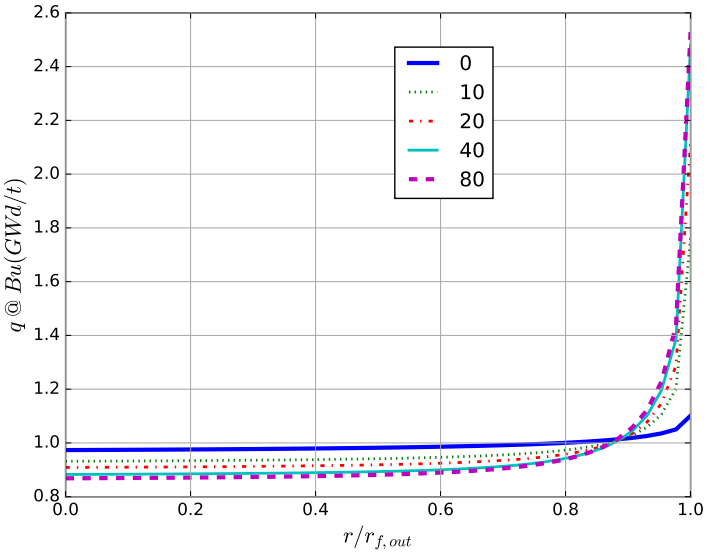

Figure 4-5: Sub-pin power profile as predicted by ALCYONE's simplified neutronic model for a set of average burnup of an axial slice. On the x-axis, the radius normalised to the fuel dimension, on the y-axis the heat generation normalised to one.

Coming back to the sub-pin power reconstruction strategies studied during the internship, it should be noticed that they have a slightly different task, as they are used to reconstruct a sub-pin coarse power profile. For instance, it is considered a 12 meshes power profile computed by a MOC calculation. However, it could be interesting to compare PRODHEL's solution to what obtained from the MOC model. One of the reconstruction techniques is based on the Palmer's function [223], which is reported in Eq. (4.2). Where r_{ext} is the outer fuel radius and c_1 and c_2 are two parameters bounded into a given interval. The two parameters could be used to fit the continuous function over the node averaged values that are produced by a specialised neutronic model.

$$f(r) = 1 + 3\ exp(-c_1(r_{ext} - r)^{c_2}) \tag{4.2}$$

The comparison of PRODHEL with the MOC predicted power and its reconstructions is presented in Fig. 4-6. The prediction of PRODHEL is simply normalised to the MOC value (which appears in the legend as "AP3"). "Linear projection" represents one of the tests to extend with a

piece-wise linear function, under the constraint that the derivative at the centre is null (due to the symmetry and continuity of the derivative); other linear interpolations may be tested to preserve different quantities. "Palmer projection" is just a least squares fitting of the two parameters of the Palmer's function.

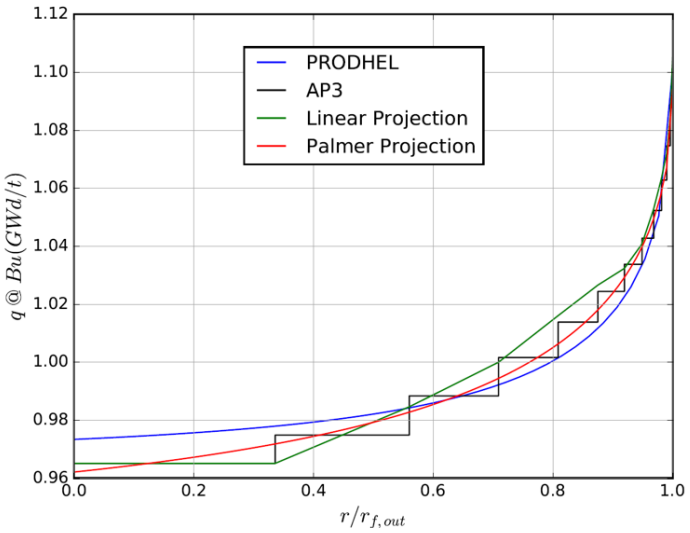

Figure 4-6: Comparison of the power profile as predicted by PRODHEL and the referential one computed by a MOC based model using 12 nodes radial discretization. Exploratory trials of reconstruction techniques of the MOC power profile are also displayed.

It is observed that for the considered application, PRODHEL has predicted the power profile within an error bound lower than 2 %. Hence, storing this shape function for a given fuel rod and for a set of burnup steps seems a promising alternative. Another strategy could be to store the sub-pin radial power profile as computed by the lattice calculations or eventually just the fitted parameters of the Palmer's function for a set of burnup steps. This method could also be expanded to include more parameters like the ones used for the storage of cross-sections. Even if the premises are good, both these methods should be further investigated. Nevertheless, as introduced in Section 2.1 and as found by [110, 111], the fuel performance and the heat conduction are not so strongly affected by the exact sub-pin radial power distribution. Therefore, the considered methods and more advanced ones are supposed to have a minor impact on the estimated temperature profile. Since the heat conduction is already strongly simplified due to the absence of a fuel performance model, for simplicity the flat sub-pin power profile is chosen.

Although the sub-pin temperature profile could be one of the targeted variables, the neutronic model requires just a scalar value for each pin-cell that corresponds to an isotherm profile. The first formula associating a uniform temperature distribution to a non-uniform one in order to preserve the neutron absorptions in a resonant medium is found in [224]. This is called Rowland effective temperature and it is reported in Eq. (4.3). Its derivation is based on a cylindrical geometry (infinite

height is considered), a medium only made of uranium-238, a parabolic temperature profile and no scattering. A generalization of this formula for a non-parabolic temperature profile is given by [225], it is referred to as Santamarina effective temperature and it appears in Eq. (4.4). In this equation, $T_{vol.avg}$ is the volume average of the temperature, T_{centre} is the fuel centreline temperature and $T_{f,out}$ is the fuel outer surface temperature.

$$T_{uniform} = \frac{4}{9}T_{centre} + \frac{5}{9}T_{f,out} \tag{4.3}$$

$$T_{uniform} = T_{vol.avg} - \frac{1}{18}(T_{centre} - T_{f,out}) \tag{4.4}$$

These formulae can be seen as a correction of the fuel average temperature aiming at giving more weight to the outer surface temperature. The outermost layer of the fuel is where most of the resonant captures occurs, due to the phenomenon introduced as Self-Shielding. In general, these formulae should be contextualized with the weak dependency of the neutronics on the fuel temperature profile. To give an order of magnitude, the Doppler coefficient for uranium dioxide fuel is about -2.5 pcm/K, which means that an increase of one degree of the fuel temperature of the entire system generally corresponds to a reduction of 2.5 pcm and, under normal operating conditions, the two formulae differs of only few K. For simplicity often the Rowland formula is used.

After the sub-pin power reconstruction and the effective temperature have been set, only the classical thermal-hydraulic modelling choices have to be made. Three thermal-hydraulic models are chosen, they are represented in Fig. 4-7. One based on THEDI for 1D calculations with quarter of assembly. The other two use FLICA4 solvers for 3D quarter of assembly and subchannel simulations.

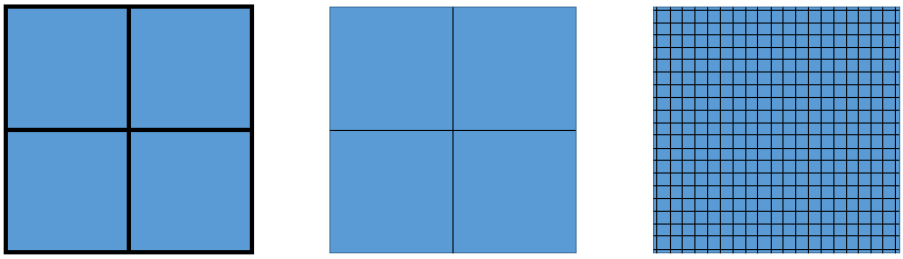

Figure 4-7: Different thermal-hydraulic models, from the left to the right: 1D quarter of assembly using THEDI, 3D quarter of assembly and 3D subchannel using FLICA4. The 1D modelling is represented by the thick solid lines that means no mass, energy and momentum is radially transferred.

It should be noticed that in all these thermal-hydraulic models the fuel is modelled under the porous media approach. The solid fuel is homogeneously spread within each thermal-hydraulic mesh defining the so-called volume porosity, representing the ratio of the fluid volume over the total. Regardless of the mesh dimensions, an equivalent heating surface is defined and for each direction the flow area and the hydraulic diameter are attributed. Hence, thermal-hydraulic variables are

computed as volume averaged or lumped quantities. Under this approach, every thermal-hydraulic mesh may contain an arbitrary number of fuel rods to which it is coupled by the heat conduction calculation. At the subchannel level, a small difference arises, one fuel rod may be shared by multiple thermal-hydraulic meshes (it is very often the case). For this reason, it is important to define to which thermal-hydraulic channels a fuel rod is connected with. This result also in a small complexity increase due to the power contribution to thermal-hydraulic channels that may derive from multiple fuel rods and the heat conduction that has to consider several (generally four) different wall temperatures. The resulting overall scheme is summed up in Fig. 4-8.

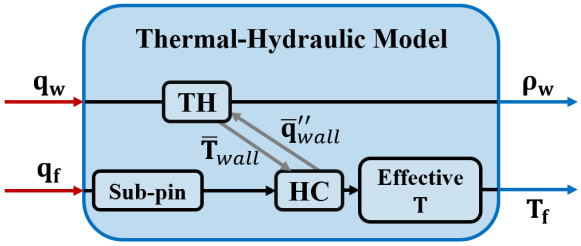

Figure 4-8: Detailed thermal-hydraulic model including 1D heat-conduction in the fuel. A sub-pin radial power reconstruction module is required as the fuel power distribution is pin-cell integrated. An effective temperature is used in order to comply with the neutronic cross-sections parametrization. A line appears over wall temperature and heat flux as they may be the result of the averaging of multiple values as one fuel rod might be associated to multiple thermal-hydraulic channels and vice-versa.

4.2.3 Depletion Model

Since neutronic calculations are very often coupled to a depletion solver, its integration in the coupling scheme is straightforward. The calculation mesh coincides with the one used for neutronic core simulations and the field of number densities and cross-section are generally under a format compatible for both the solvers. In this coupling scheme, the general depletion model, which is available in Fig. 4-9, is only used to find the equilibrium concentrations of the fission products.

Figure 4-9: General depletion model.

During the cross-sections homogenization, the isotopes that are chosen to be particularized are the xenon-135 with its precursor iodine-135 and the samarium-149 with its precursors neodymium-147, promethium-147, 148, 148m[1] and 149. While xenon-135 and samarium-149 appear in almost every manual of neutronics due to their strong radiative capture cross-section and their consequent

[1] m stands for metastable, i.e. its nucleons stay excited for a relatively long time as compared to nuclear processes, around 10^{-9} s.

effect on reactor dynamics, it is worth noticing that also promethium-147 and 148m have a considerable weight on the reactivity. Another important point is that xenon-135 is unstable, its half-life is about 9.2 hours and it takes 40 to 50 hours for its concentration to stabilize, whilst samarium is stable and its equilibrium concentration is reached after about 20 days. For this reason, the research of their asymptotic concentrations is a rather theoretic simulation as in the meantime, also the fuel isotopic concentration would be significantly changed as well as the core conditions. Anyhow, on the contrary, the choice of the evolution time step would be completely arbitrary and the initial concentrations of the fission products would influence the result. Therefore, the research of the equilibrium concentrations of fission products should be seen as a preparation for the depletion calculations and a way to increase the complexity of the numerical problem.

4.3 Implementation Details

At the highest level the supervision of the different models is effectuated in Python. Each of the presented fields of variables transits in the supervisor under the MED format. Macroscopic operators like the ones introduced in the system of equations 4.1 are defined. Each of them is a Python function that prompts its model's interface. Within the interfaces, it is present a generic interpolator which needs to be initialized before the beginning of the multiphysic calculations: the interpolation matrices are created once and after that they are just applied on the fields. This approach allows to launch simulations at different scales and with different models by simply changing the options of the main supervisor script. The operators are briefly described in the following sub-sections.

4.3.1 Neutronic Operator

The global scheme of the neutronic operator is available in Fig. 4-10.

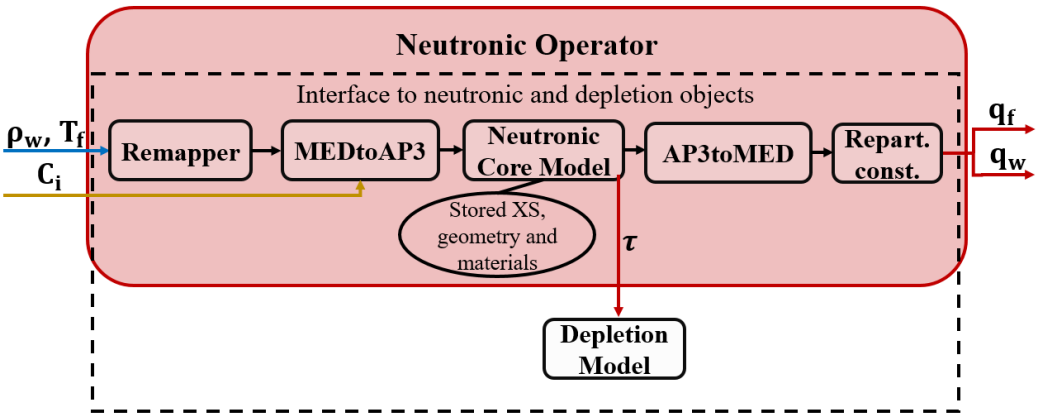

Figure 4-10: Representation of the global implementation of the neutronic operator. The considered neutronic core model is based on APOLLO3®. Several cross-sections databases might be prepared for different core models.

This operator includes a generic neutronic core model, which requires a specific set of homogenized cross-sections and the definition of the geometry and the material distribution of the case study. While the cross-sections are solver dependent, due to the SPH technique that works for a given neutronic core model, the geometry and the material distribution do not. For this reason, in addition to the lattice calculations, a preparation script relative to the case study has to be launched once and for all to create and store its description. The interface to neutronic objects has been written during this work, it is coded in Python and it is solver independent. For simplicity and due to their inherent compatibility, the neutronic and the depletion models share the same interface. In fact, APOLLO3® and MENDEL are just imported as shared libraries (equivalent to shared objects) and they are managed through their Python APIs. Basically, to increase the flexibility with the aim of performing a large range of tests, within this PhD thesis, APOLLO3® is not built-in as a CORPUS component, but just imported without modifications as shared object. Anyway, also the way of including components in CORPUS is changing towards more flexible solutions.

The interface provides methods to convert fields from the APOLLO3® to the MED format that exploits efficient renumbering functions available in the MED library. As already introduced, the isotopic concentration fields are defined on a mesh compatible with that of neutronic quantities, hence, interpolations are not required and they can directly be converted to the APOLLO3® format. On the contrary, the fuel effective temperature and the moderator density fields need a remapper. The remapping operations and in general most of the fields manipulations are done on MED variables to take advantage of the tools provided by SALOME. In particular, the available remapper can perform this operation on a wide spectrum of applications: different field natures (e.g. intensive or extensive), 1D, 2D lines, 2D surfaces, 3D surfaces and 3D volumes and different spatial discretizations (constant, linear or parabolic). Within this work, only conservative interpolations of 3D volumes with constant values within the cells are considered. Conservative refers to the preservation of physical quantities between the source and the target mesh. For instance, a mesh integrated power of the source field may be divided into multiple volumes, but regardless of the new meshing, the total integrated power within the volume contained in the original mesh should be exactly conserved.

During a field interpolation from a source mesh (S) to a target one (T), it is important to distinguish whether S and T are overlapping or not. Overlapping just means that both the meshes are fully and exactly covering the same portion of domain so that both Eq. (4.5) and (4.6) are verified. In these equations, the index identifies each cell of the target or source mesh and $Vol(C)$ is a function associating the volume to a given cell.

$$\sum_{S_j} Vol(T_i \cap S_j) = Vol(T_i) \tag{4.5}$$

$$\sum_{T_i} Vol(S_j \cap T_i) = Vol(S_j) \tag{4.6}$$

In case of non-overlapping meshes, the nature of the field needs to be further specified. In fact, within this situation, it is impossible to ensure that the two main principles of the interpolations are respected at the same time. These principles are conservativity and maximum principle. The first one implies that the volume integral of the given quantity is preserved during the interpolation, assuming that the source field is zero were not defined. In this way, the interpolation matrix is formed using Eq. (4.7).

$$M_{i,j} = \frac{Vol(T_i \cap S_j)}{Vol(T_i)} \tag{4.7}$$

The maximum principle requires that the values of the target field are bounded by the maximum and minimum values of the corresponding source meshes. This leads to an interpolation matrix built as a weighted average of the field over all the intersections of the source and the target meshes, as written in Eq. (4.8).

$$M_{i,j} = \frac{Vol(T_i \cap S_j)}{\sum_{S_j} Vol(T_i \cap S_j)} \tag{4.8}$$

Intensive variables for which the conservativity is more important than the maximum principle are called "reverse integral", whilst if the maximum principle has to prevail they are classified as "conservative volumic". More information about SALOME remappers is publicly available in [226].

Interpolation of the Moderator Density Field

For what concerns the moderator density, its interpolation is needed to pass from the thermal-hydraulic to the neutronic representation. This variable is an example of intensive field as its value does not depend on the size of the considered volume, but rather on the local conditions. Under the porous medium approximation, which is made by both the considered thermal-hydraulic solvers, all the materials are mixed within each mesh, so that the entire volume of the core is represented without discontinuities. Analogously, after the homogenization process at the pin-cell or quarter of assembly scale, all the materials are blended in each mesh. Under both representations, the moderator density is defined without discontinuities over the entire core domain, hence, the meshes are overlapping. For this reason, there is no need to further specify the field's nature. Anyway, the moderator density would be classified as "reverse integral", as the total mass is often the quantity to be preserved during this remapping.

Under the conventional approach, described in sub-section 2.1.1, both thermal-hydraulics and neutronics are simulated with a quarter of assembly radial meshing. In this way, if the same axial

mesh is used, there is no need for interpolations, otherwise, this could be straightforwardly done with SALOME's remapper. With respect to pin-cell homogenized neutronics and subchannel thermal-hydraulics or any hybrid combination with the coarse radial mesh, in these situations, the remapping becomes more complicated. As specified before, consequently to the porous media approach and to the neutronic homogenization process, the moderator density is defined all over the core. In both the field representations (thermal-hydraulic and neutronic), every mesh contains water and a mix of other materials. For this reason, the meshes used as support of the moderator density field are very often composed of cells that account also for the total volume, which encloses also the other materials. This does not cause any problem under the conventional discretization, as in this case the proportion of water is constant in every mesh. On the contrary, for what concerns pin-cell homogenized neutronics and subchannel thermal-hydraulics, this assumption is not strictly valid anymore. Concerning neutronics, pin-cells in the assembly periphery contain an extra layer of water and thimble tubes occupy a different volume from fuel rods, these different pin-cells are represented in Fig. 4-11. In respect of thermal-hydraulics, the typical subchannel discretization is coolant centred (instead of fuel centred), for this reason multiple channel types are defined and each of them may enclose a different number of fuel rod or guide tube portions. Therefore, using the pin-cell volumes (instead of the moderator ones) for the interpolation would not exactly conserve the total mass of water.

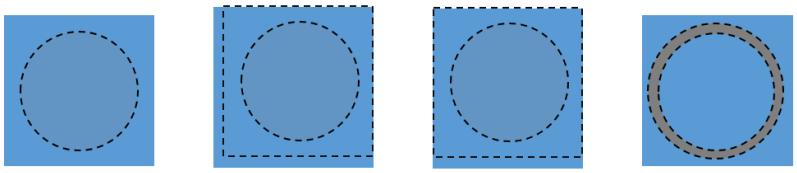

Figure 4-11: Characteristic type of cells that are used in the neutronic pin-cell homogenization for a PWR fuel assembly. Each cell type has a different moderator to total volume ratio. From the left to the right, the pin cell is rod centred away from assembly boundaries, at the corner of the assembly, at the assembly boundary and thimble tube centred. It should be noticed that water is present in all the configurations.

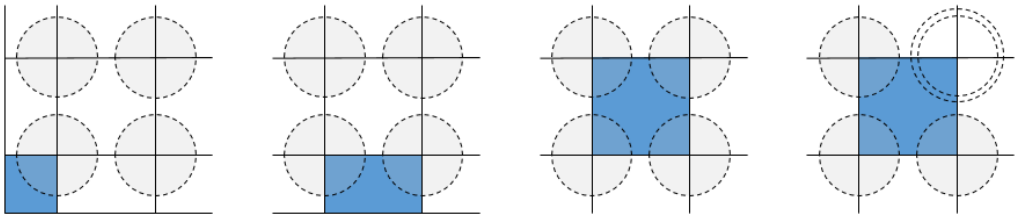

Figure 4-12: Typical cell types of subchannel thermal-hydraulic modelling (coolant centred instead of rod centred). Each cell type has a different moderator to total volume ratio, depending on the channel dimension and the number of portions of fuel rod and thimble tube.

A solution that has been identified to use the moderator volume for the construction of the interpolation matrix, hence, with the aim of preserving the total mass of water, is to use intermediate support meshes that represent the actual moderator volume in each pin-cell for both the original source and the target meshes. This technique would not be particularly complicated to implement, but the moderator volume within a neutronic mesh is not currently accessible during the core calculations as only the homogeneous geometry is defined during this phase. However, since under normal operating conditions the radial density gradient is supposed to be rather mild, the approximation of using the cell volumes instead of the moderator ones should not bring to large errors. Therefore, the interpolations are carried out with the fields as defined by the solvers and the use of the exact moderator volume is left for future improvements.

Interpolation of the Fuel Effective Temperature Field

The fuel effective temperature has to be interpolated from the heat-conduction mesh to the neutronic one. Also this variable is intensive, but in this case the "conservative volumic" nature is more appropriate as its volume integral is not necessarily what should be preserved. The conceptual problems presented for the moderator density interpolation are not similar to the ones to be faced for the fuel effective temperature. The neutronic and the heat conduction meshes are both rod centred.

Different representations are used by the heat conduction models of THEDI and FLICA4, therefore separate discussions are given. First of all, THEDI can also be supervised trough its APOLLO3® interface (unofficially called here THEDI-AP3), which would allow exchanges and interpolations with the neutronic model without resorting to the MED library. However, to keep the calculation scheme general, THEDI-AP3 is used as and independent object that communicates with APOLLO3® only via MED fields just as FLICA4. As anticipated, in this work, THEDI is used only with a quarter of assembly discretization, however, independently from the thermal-hydraulics the heat conduction could be performed on every fuel rods. In every case, both when one equivalent fuel rod is considered per each quarter of assembly and when every fuel rod is explicitly modelled, the fuel effective temperature is produced on a mesh compatible to the one of APOLLO3®. Therefore, interpolations may be required only in case of hybrid schemes, in which the neutronics and the fuel effective temperature are on different scales (e.g. quarter of assembly neutronics and every fuel rod explicitly modelled for the heat conduction). These interpolations are carried out by the SALOME's remapper considering the "conservative volumic" nature.

The representation of the fuel effective temperature of FLICA4 is rather different. The support mesh does not cover the entire cell volume but only the fuel one. For this reason, empty spaces are left at the periphery of the pin-cell (or equivalently of the quarter of assembly cell). Moreover, the thimble tubes are not modelled at all, an empty space is left at their place. FLICA4 representation

of the fuel effective temperature is reported in Fig. 4-13.

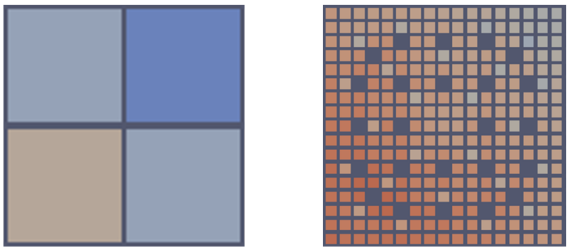

Figure 4-13: Fuel effective temperature of a typical fuel assembly as represented by FLICA4. On the left, heat conduction is performed for an equivalent fuel rod for each quarter of assembly, while on the right every fuel rod is explicitly modelled.

Even if such a mesh might appear as complicated to handle, it is not. If the fuel effective temperature and the neutronic mesh are at the same scale, the required transformation is simpler than an interpolation: every fuel effective temperature value is univocally associated to a pin-cell, hence, only a cell renumbering is required. This operation is needed to ensure that each effective temperature is associated to the correct pin-cell and SALOME provides a function that can efficiently perform this task. If the fuel effective temperature and the neutronic mesh are not at the same scale a simple interpolation is required. Since SALOME's remapper intrinsically does the renumbering and it is rather efficient, it is used for both the operations, considering the "conservative volumic" nature.

4.3.2 Thermal-Hydraulic Operator

The global scheme of the thermal-hydraulic operator is represented in Fig. 4-14.

The interfaces of the two considered thermal-hydraulic solvers are implemented so that they are interchangeable. In the main options it is possible to select whether the operator is based on FLICA4 or THEDI-AP3, but this does not affect at all the definition of the operator. It is still untested, but with small adjustments even a combination of the two solvers is theoretically possible. From the implementation point of view, FLICA4 is used as a CORPUS component, for this reason, here it is unofficially referred to as FLICA4-CORPUS. This choice derives from mainly practical reasons. Originally FLICA4 is supervised with the Gibiane programming language, while its CORPUS interface allows to prompt the solver in Python using the ICoCo interface. This interface is convenient also because it already contains the vast majority of the functionalities that are needed in a coupling scheme and it is already compatible with the MED fields. Nevertheless, for simplicity, in order to make every function exactly match the signature of the other interfaces, FLICA4-CORPUS is further encapsulated in a Python interface created ad hoc for the purpose of the thesis. Ideally the most rigorous approach would be to directly modify the ICoCo interface according to the needs, but in some cases, it might become significantly more complex than adding this extra

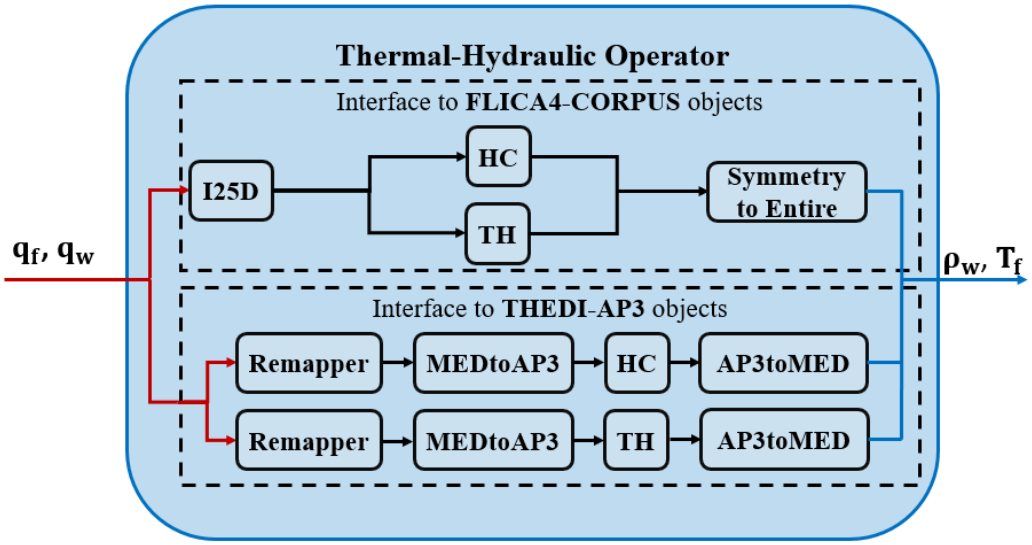

Figure 4-14: Representation of the global implementation of the thermal-hydraulic operator. Attention is drawn on the possibility to define a scheme in which this operator is used independently from the chosen thermal-hydraulic model.

layer on top of it. For what concerns THEDI-AP3, a Python interface has been implemented in the PhD thesis in order to convert the MED fields into APOLLO3® representation and vice-versa and to assemble a set of macro functions that facilitates the construction of the coupling scheme.

Another implementation detail deals with the symmetry management. As specified before, the operators only produce variables over the entire domain, even if the calculations may be performed on a portion of it thanks to the exploiting of the problem's symmetry. While for APOLLO3® simulations, the entire geometry is defined and then specific symmetry simplifications may be applied afterwards, for FLICA4 only the symmetry simplified geometry is given by the user. In other words, for FLICA4 simulations, the geometry contains only the channels that have to be simulated and, in each of them, symmetrical boundary conditions can be specified. This type of modelling requires an additional step to reconstruct the entire fields from the symmetrical ones. This function has been implemented during this work out of a combination of the available SALOME tools. For what concerns THEDI-AP3, the coarse geometry definition used for the APOLLO3® core calculations is imported and it is used without exploiting the symmetries. In fact, this model is anyway significantly faster-running than the others, hence, the time saving due to the symmetry would have an almost negligible impact on the total calculation time.

Interpolation of the Power Field in FLICA4

In respect of the interpolation of the power field from the neutronic to the FLICA4 representation, a specific interpolator is used, I25D. This remapper does not belong to SALOME, it is one of the extra-tools provided by CORPUS. It is designed to perform the specific task of interpolating

the total integrated power (deposited in both fuel and moderator) over the thermal-hydraulic and the heat-conduction meshes. The integrated power is specifically required as the interpolation of extensive fields is considered. In order to address the possibly varying fuel volume proportion in each thermal-hydraulic cell, more information than the neutronic, thermal-hydraulic and heat conduction meshes are required. The fuel mass and localization (whether it is present or not within a cell) and the porosity (water to total volume ratio) of the thermal-hydraulic mesh have to be provided to the interpolator. The use of this remapper is particularly convenient to correctly interpolate in case of subchannel discretization.

Interpolation of the Power Field in THEDI

For what concerns the power interpolation from the neutronic to the heat conduction mesh, the interpolation is needed only in case of pin-cell neutronics and quarter of assembly heat conduction or the opposite, neutronics over the quarter of assembly and heat conduction performed for every fuel cell. The second combination is never considered in this work, but it would be an interesting solution if a subchannel code performs the thermal-hydraulics. Also in this case, to keep the scheme general, the interpolator is used in any case. In any case, the meshes are overlapping and the integrated power is transferred as an extensive quantity using the SALOME's remapper. The interpolation matrix is built using one of the forms presented in Eq. (4.9), which are both valid as the meshes are fully overlapping.

$$M_{i,j} = \frac{Vol(T_i \cap S_j)}{\sum_{T_i} Vol(S_j \cap T_i)} = \frac{Vol(T_i \cap S_j)}{Vol(S_j)} \tag{4.9}$$

With respect to the power interpolation from the neutronic to the thermal-hydraulic mesh, it should be considered that only a quarter of assembly discretization is chosen for the THEDI based model. Therefore, if the same meshing is used for the neutronics, just a renumbering of the cells might be required, otherwise, a simple interpolation should be used to account for the contribution of all the pin-cells contained in each quarter of assembly. This operation is not as trivial as it might appear, because in the 17x17 fuel assemblies design, a set of fuel rods is shared between two or even four quarters of assembly. Nevertheless, also this interpolation might be carried out with the SALOME's remapper, considering the integrated power as an extensive field.

4.3.3 Depletion Operator

The global scheme of the depletion operator is available in Fig. 4-15. This operator is based on MENDEL. In this calculation scheme, this solver has only to interact with the neutronic operator based on APOLLO3® with which it is fully compatible. Therefore, the fields could potentially be exchanged directly under the APOLLO3® format. As specified before in this chapter, the main input

to this operator is the neutronic multigroup reaction rates. Among all the exchanged variables, these reaction rates are the only fields that are not converted to the MED format and are not transiting through the supervisor's environment. This implementation limits the flexibility and the generality of the calculation scheme as it can work only with APOLLO3® and MENDEL. Moreover, if the numerical algorithm requires manipulations of the reaction rates, they have to be performed at the APOLLO3® level. The main reasons for this approach are informatic ones, mainly the following two. MENDEL solver is integrated in APOLLO3® with a limited and optimized programming interface that do not make this exchange as straightforward as the others. The second one is that the structure of the MED fields does not include the energy variable. Another justification lies in the fact that the number of fields to be eventually converted to the MED format would be equal to the number of energy groups times the number of considered reactions multiplied by the number of particularized isotopes. For these reasons, the improvement of this part of the coupling scheme is left for future works.

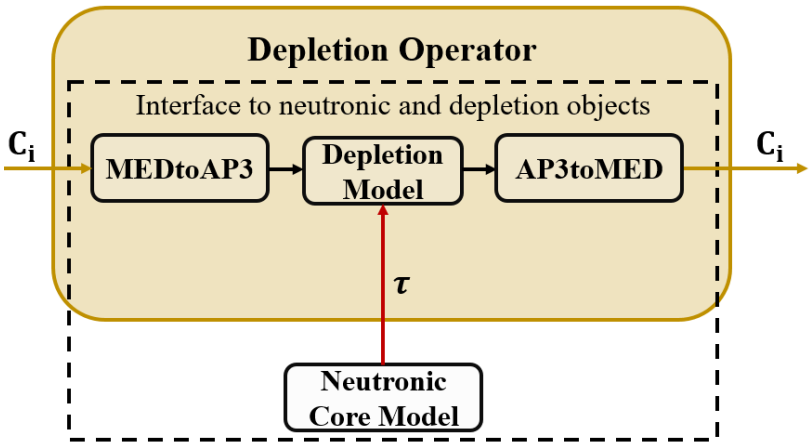

Figure 4-15: Representation of the global implementation of the depletion operator, based on MENDEL solver library, which in this context is used for the research of the equilibrium concentration of the fission products.

For what concerns the isotopic concentrations, they can be extracted and set as MED fields. However, when the equilibrium concentrations of the fission products are researched, like in this application, the result is not affected by the initial number densities. Finally, due to the compatibility with APOLLO3®, no interpolations are required.

4.4 Chapter Conclusion

In this chapter, the development of the multiphysic coupling scheme for steady-state problems realized during the PhD thesis is described. specialised solvers for neutronics, thermal-hydraulics and isotopic evolution are combined to find the steady-state solution for given operating conditions.

The fission products equilibrium concentrations are also researched. The main modelling choices are reported and discussed as well as the decisions regarding the practical implementation. In the following chapter, this coupling scheme is tested on an applicative case study with the aim of selecting the best models out of the available ones and assessing its capabilities.

Chapter 5

Analysis of the Application to a Steady-State Case Study

In the previous chapter, the coupling scheme realized during the PhD work is described. This simulation tool allows to select different neutronic and thermal-hydraulic models. In this chapter, a case study is defined and a simple fixed-point algorithm is implemented to solve the coupled problem. After that, a neutronic model for core calculations is chosen by comparing the relative performance of a set of candidates implemented using the solvers of APOLLO3®. These models are initially tested under fixed isothermal conditions and then in a simple coupling scheme composed of neutronics, thermal-hydraulics and heat conduction in order to verify whether in this context their relative performances are affected. Afterwards, the subchannel modelling coupled to the resolution of the heat conduction for every fuel rod is implemented. The importance of such a model refining is questioned comparing it to a hybrid approach with coarse mesh thermal-hydraulics and heat conduction. Finally, the impact on the power axial profile of the thermal-hydraulics, the heat conduction and the research of the equilibrium concentrations of the fission products is analysed.

5.1 Definition of the Case Study

The definition of the case study is a pivotal part of the thesis, as it affects the type of analysis that can be performed. A key element to set is the complexity of the case. A trade-off should be found between the computing time approximately required, sufficiently low to allow a systematic study (large number of computations), and the representativeness of the case as compared to a commercial PWR. As a rule of thumb, the time constraint is equivalent to the imposition of a computing time not larger than few hours for the most advanced neutronic model. The number of processors considered is limited to twenty in order to be able to run simulations on the assigned

computer. For what concerns the representativeness of the case study, it is not trivial to define and quantify this variable. This aspect has to be addressed in order to define a problem of similar numerical complexity and comparable physical behaviour.

A set of the key variables to take into account into the case study definition is discussed in the first sub-section. After that, an analysis of the case studies found in literature or in previous works at CEA is reported. Finally, the identified case study that is used for the rest of the thesis is described.

5.1.1 Definition of the Characterizing Variables

The size of the reactor core to be studied is one of the most important variables. Initially, cores ranging from clusters of few assemblies (experimental reactors or benchmarks for code-to-code comparisons) to small commercial PWRs are under consideration. Benchmarks with assembly designs too different from standard PWRs are excluded for practical reasons. Therefore, the core height only varies within a relatively small range of values among the examined reactors. For this reason, more than considering a reactor's average size, the number of fuel assemblies is taken into account. Most of the clusters has a squared plan, while commercial PWRs are characterized by an approximately circular one, hence, the number of assemblies is directly linked to the radial size of the core. The radial dimension is important because the computational effort required for the neutronic simulation increases at least linearly with this quantity. An important role is played by symmetries, which can divide the reactor radial size by a factor 2, 4 or 8.

The radial size of the reactor and its loading pattern strongly affects the power shape. To get a qualitative idea, the shape of the flux can be computed under the hypothesis of diffusion over a homogeneous cylindrical reactor of infinite height. In this case, the flux curvature is constant over the entire domain and it is represented by the geometric buckling. This quantity is inversely proportional to the corrected radius ($\tilde{R}$), as reported in Eq. (5.1), where j_0 is around 2.405. $\tilde{R}$ corresponds to the geometric radius plus a small extrapolated length which is characteristic of neutron transport.

$$B^2_{g,rad} = \frac{j_0}{\tilde{R}} \tag{5.1}$$

To remove the infinite height hypothesis it would be sufficient to account also for the axial buckling, but since this analysis concerns only the radial size this is not necessary. Since the reactor is assumed to be critical, the material and the geometric buckling are equal. Hence, the diffusion equation takes the form of the Helmholtz one, as expressed in Eq. (5.2).

$$\nabla^2\phi + B^2\phi = 0 \tag{5.2}$$

Within this approach, it is possible to understand how the qualitative flux shape is affected by the

radial size. Under the assumption of homogeneous medium this is also the power shape, therefore the radial power peaking factor (f_{xy}, ratio of maximum to average axially integrated power) is directly linked to the reactor's radial size. In a similar way, it is possible to assume that if the reactor's height is roughly constant, also the axial peaking factor (f_z, ratio of maximum to average radially integrated power) is not supposed to significantly change.

The total power peaking factor ($f_q = f_{xy} f_z$), as well as the operating conditions play a major role over the strength of the coupling, which directly impacts the numerical complexity. To justify this affirmation, the asymptotic impact of these variables is reported. At power levels much smaller than the nominal one, the thermal-hydraulics is completely decoupled from the neutronics. On the contrary, for higher power rates, any small perturbation on the power distribution may strongly impact the thermal-hydraulics. Considering the same average power, a higher f_q implies a higher maximum power and a larger power gradient. Both these augmentations may have a significant impact on the stability of the coupling scheme. Similar observations can be made for the water mass flux and the gap heat transfer coefficient: the higher these values the more the thermal-hydraulics and the heat conduction are decoupled from the neutronics. The water inlet temperature and the pressure boundary conditions also strongly affect the coupling degree, but in most of the considered study cases, they vary within a small range of values.

For what concerns the assemblies composition, since the focus is on multiphysics rather than on neutronics, particularly heterogeneous cores are excluded. The assessment of the impact of strong heterogeneities of the core on the multiphysics is left for future works. The reactor's size combined with the assembly initial composition and the operating conditions should ensure the possibility of completing an irradiation cycle of about hundred days without exiting from the allowed ranges of boron concentration fixed to 0 to 2000 ppm.

5.1.2 Analysis of the Available Case Studies

The definition of the domain and of the considered scenario for the case study might be independently carried out, unless an international benchmark that matches the requisites for both them is found. For what reported in Section 2.1, it is clear that the BEAVRS benchmark is a strong candidate. It is recognised worldwide, it allows code-to-code comparison with many referential solutions and it even provides experimental data. Unfortunately, the computing time for such a commercial reactor would be excessive and a lot of effort should be put in the preparation of this specific modelling. For the same reasons also the Kšrko start-up benchmark [227] has to be excluded.

An interesting reactor core is given by the KAIST 1A benchmark [228] published by the Korean Advanced Institute of Science and Technology (KAIST). The interest in this core derives from the core's dimension, as a low-size PWR is considered, from the international interest and from the easily accessible data. However, it has been conceived for 2D steady-state calculations, only a radial

description is given, hence, a 3D core should be reconstructed from it. For this reason and for the lack of multiphysic simulations performed on customized versions of this core, this benchmark is not kept. Unfortunately, no other benchmarks are found for small PWRs that are suitable for multiphysic depletion calculations. For this reason the choice is limited to a set of clusters. The geometries of the three most pertinent study cases are described in Fig. 5-1. The first one has been described in Section 3.6. It is the study case used in the PhD thesis A. Targa at SERMA. It has been used for the multiphysic modelling of RIA [213]. One assembly type is defined, but a loading plan including several burnup values is chosen. Vacuum boundary conditions are adopted for the radial boundaries. The second one is the problem 4 of the previously mentioned series of benchmark from the validation of VERA-CS. A characteristic feature of this case study is the presence, in certain assemblies, of twenty guide tubes with Pyrex burnable poison (borosilicate glass, B_2O_3-SiO_2). Moreover, the assemblies containing the burnable poison have a slightly higher enrichment than the others (2.6 % against 2.1 %). Reflective boundary conditions are applied radially. The third case study is derived from [9] and it has been used for the PhD thesis of A. S. Bielen [10]. This reactor is made of one assembly type with three possible enrichment values as described by Fig. 5-1 on the right, in which 1.9 % is denoted by light blue, 2.6 % is associated to green and 3.1 % corresponds to red. Contrary to the normal disposition in PWRs, few highly enriched assemblies are placed next to the core boundaries. In commercial reactors, this is not done in order to protect the vessel and to increase the reactivity by reducing the leakages, while for this application, this choice is justified by the willing to reduce the radial peaking factor, to match standard values of this quantity. In addition to the loading plan, reflective boundary conditions are also applied around the core. In this work, the core is used to perform sensitivity and uncertainty analysis of multiphysic depletion calculations.

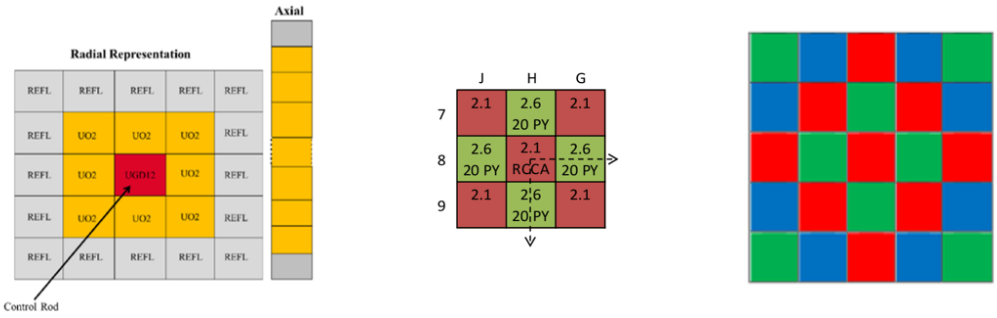

Figure 5-1: Cluster cores used for multiphysic simulations. From the left to the right, defined during A. Targa PhD thesis for RIA [7], problem 4 of the VERA-CS progression benchmarks [8] and case study derived from [9] and used in the PhD thesis of A. S. Bielen [10].

Since the core description (cross-sections, geometry, materials, etc.) is readily available for the first case study, a simple depletion calculation is performed to asses the cycle length that is possible to reach under standard operating conditions. Unfortunately, the boron concentration becomes too

low before to achieve the pre-fixed minimum constraint of about hundred days. For this reason the same test is repeated for a a 5x5 mini-core plus reflector created adding an extra layer of fuel assemblies to the radial plan. In this case, the cycle length is judged satisfactory. The main distinction between this newly created case study and the other two ([8] and [10]) is in the boundary conditions. The radial reflective boundary conditions strongly flatten the power distribution leading to radial peaking factors similar to those of PWRs or even lower. On the contrary, the vacuum radial boundary conditions cause large radial peaking factors. The additional layer of fuel assemblies allows to achieve a pin-by-pin radial peaking factor of about 1.9 while standard values for commercial PWRs range from 1.4 to 1.7 [229, 230]. A slightly higher radial peaking factor could be desirable in order to potentially increase the numerical complexity of the case study. Therefore, this 5x5 mini-core is kept as applicative case for the coupling scheme. In addition, two different reflector's compositions are tested to further modulate the radial peaking factor.

5.1.3 Description of the Chosen Case Study

The chosen 5x5 PWR assemblies mini-core with radial and axial reflectors is briefly described. Two radial reflector compositions are considered, one with equal portions of stainless steel and water (standard), the other with 95% of stainless steel and 5% of water (higher stainless steel concentration, hence referred to as heavy). The radial reflector is modelled as a homogeneous assembly with average properties and with the same dimensions of the fuel assemblies (roughly 21 cm). Only one composition is considered for each axial reflector, 25 stainless steel and 75 water for the top and 45-55 for the bottom. The top reflector is about 26 cm tall, while the bottom one around 18. All the fuel assemblies are loaded with 4% enriched urania, their 2D burnup distribution is given in Fig. 5-2.

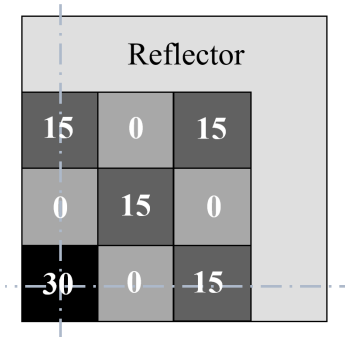

Figure 5-2: North-east quarter of the loading plan, burnup values relative to the fuel assembly are expressed in MWd/kg.

The operating conditions are similar to the nominal values of PWRs: the average linear power is 160 W/cm and the mass flux is about 3900 kg/m^2/s. Therefore, it has been chosen to keep the average linear power, which is directly linked to the total one, instead of the maximum value, which

may vary from model to model. In this way, a maximum linear power higher than standard values is expected. For this reason, the water mass flux is slightly higher too. The fuel-cladding gap heat transfer coefficient is set constant in all the core to the value of 5000 W/m^2/K, corresponding to a value typical of the beginning of cycle and standard correlations are used for the conductivities and the water heat transfer coefficient.

5.2 Implementation of the Damped Fixed-Point Coupling Scheme

For the sake of the resolution of the coupled problem, a simple fixed-point algorithm is implemented, its description is given in Algorithm 4. The theoretical background is reported in sub-section 2.2.1 and the same notation of Section 4.1 is adopted. In this way, the multiphysic iterations, which follow the index k, are defined as the sequential solution of each physics using the most update available information.

Algorithm 4 Damped fixed-point.

Flat power distribution
while $\|\Delta \boldsymbol{x}_i^k\|_2 > \Delta_i * \alpha$, for any i **do**
  $(\boldsymbol{\rho_w}^{k+1}, \boldsymbol{T_f}^{k+1}) = TH(\boldsymbol{q_w}^k, \boldsymbol{q_f}^k)$
  $(\boldsymbol{\tau}^{k+1}, \boldsymbol{q_w}^{k+1}, \boldsymbol{q_f}^{k+1}) = \alpha * N(\boldsymbol{\rho_w}^{k+1}, \boldsymbol{T_f}^{k+1}, \boldsymbol{C_{FP}}^k) + (1-\alpha) * (\boldsymbol{\tau}^k, \boldsymbol{q_w}^k, \boldsymbol{q_f}^k)$
  $\boldsymbol{C_{FP}}^{k+1} = FP(\boldsymbol{\tau}^{k+1})$
end while

The convergence is separately tested on the L2-norm[1] of the absolute residual for each variable vector $\boldsymbol{x}_i$ ($\|\Delta \boldsymbol{x}_i^k\|_2 := \|\boldsymbol{x}_i^k - \boldsymbol{x}_i^{k-1}\|_2$), where $\boldsymbol{x}$ is the linear concatenation of all the $\boldsymbol{x}_i$. Each $\boldsymbol{x}_i$ is the vectorial representation of one of the fields ($\boldsymbol{\rho_w}, \boldsymbol{T_f}, \boldsymbol{q_w}, \boldsymbol{q_f}, \boldsymbol{C_{FP}}$), apart from $\boldsymbol{\tau}$ that is not included as it is not transiting in the supervisor. A specific convergence criterion is defined for each variable once and for all from the result obtained after a very large number of converging iterations that allows to reach the maximum numerical precision relative to the scheme. Very strict convergence criteria are set, in order to ensure the reproducibility of the results. For simplicity, the damping factor (α) is applied only to the neutronic operator as all the other physics are directly linked to it. In literature this factor is found to be applied in this way, to another operator [142] or even to all of them as traditionally done in numerical mathematics [146].

The flowchart corresponding to this damped fixed-point algorithm is given in Fig. 5-3.

In order to converge to a given precision independently from the relaxation factor, if damping is applied, the convergence criteria are multiplied by α. The explanation for this is given by Eqs. (5.3) and (5.4) that show the relation between the relaxation factor and the convergence criterion.

[1] $\|y\|_2 := \sqrt{y_1^2 + y_2^2 + ... + y_n^2}$

It should be noticed that otherwise lower values of α would lead to less strict convergence tests.

$$\|x^{k+1} - x^k\|_2 = \|f(x^k) - x^k\|_2 < \Delta \tag{5.3}$$

$$\|x^{k+1} - x^k\|_2 = \|(\alpha f(x^k) + (1-\alpha)x^k) - x^k\|_2 = \alpha\|(f(x^k) - x^k)\|_2 < \Delta\alpha \tag{5.4}$$

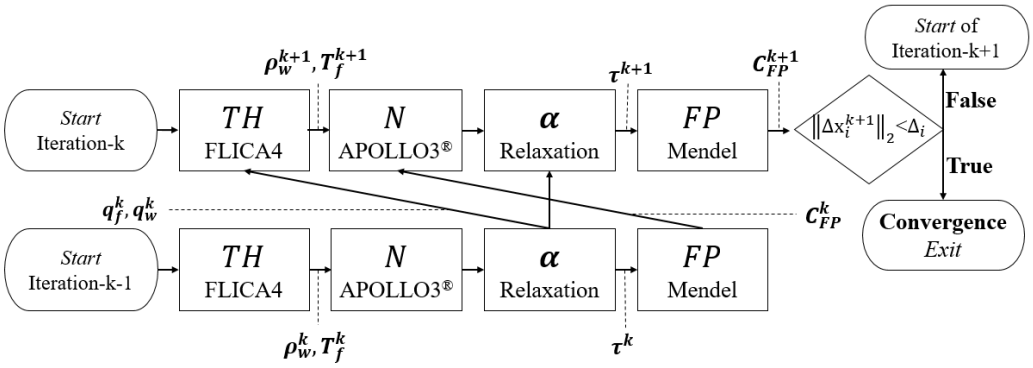

Figure 5-3: Flowchart of the main variables exchanged in the considered damped fixed-point algorithm.

5.3 Selection of the Neutronic Model for Core Calculations

To fully define the neutronic operator, the model for core calculations has to be defined starting from the core solvers available in APOLLO3®. In this section, the results provided by several neutronic solvers are compared to each other in a decoupled way, under constant isothermal conditions, to find the best precision-time trade-off. This analysis is repeated for both the standard and the heavy reflector to asses the sensitivity of the neutronic models to the different reflector's isotopic composition. After that, the same analyses are repeated using a coupling scheme that includes also the thermal-hydraulics and the heat conduction to check whether this could impact the choice of the model.

5.3.1 Decoupled Analysis of the Models

The considered neutronic models are four, all of them are combined to pin-cell homogenization and SPH equivalence. They are listed in order of increasing complexity:

- MINOS, diffusion two energy groups (*Diff.-2g*).
- MINOS, SP3 eight energy groups(*SP3-8g*).
- MINARET, S8 twenty energy groups (*S8-20g*).

- MINARET, S8 thirty energy groups (*S8-30g*).

In addition, another model using two-group diffusion over a quarter of assembly discretization is used as comparison term representing the conventional method. The *S8* models use the Discontinuous Galerkin discretization of order two both radially and axially, while for the *SP3-8g* and for the diffusion, the mixed dual finite element method with Raviart-Thomas basis functions of order two are chosen, both radially and axially. A multi-parametrized cross-sections database is created for each core neutronic model following the procedures indicated in the sub-section 4.2.1. The databases include also the cross-sections for the reflector issued by the 1D traverses procedure for nominal conditions for each energy mesh. For what concerns the axial mesh, the core and the radial reflector are divided into 30 meshes of about 14 cm, while the axial reflectors are divided into two meshes each. Homogeneous conditions over the entire core are considered in terms of fuel effective temperature, moderator density and Boron Concentration (BC), values are reported in Table 5.1.

Table 5.1: Homogeneous conditions imposed over the entire core for the decoupled analysis.

T_f [°C]	ρ_w [g/cm^3]	BC [ppm]
655.8	0.701012	600

All the solvers are compared to *S8-30g*, which is used as reference. To have a real reference, the problem should be simulated with a Monte Carlo code. However, this comparison should be seen as a sort of convergence analysis as the angular and energy meshes are increasingly refined. Moreover, this analysis has the objective of qualitatively classifying the different models more than assessing the exact magnitude of the approximation they introduce.

Comparison of the Neutronic Models for Core Calculations

The results reported here are obtained considering the heavy reflector, the analysis corresponding to the standard one is discussed afterwards. The comparison on the 3D power distribution within the core is reported for the *Diff.-2g* (quarter of assembly) in Fig. 5-4a and for the *SP3-8g* in Fig. 5-4b. In the first case, the reference power is integrated over the quarter of assembly mesh to measure the discrepancies at this scale. In both cases, the highest differences are located next to the reflector boundaries. An explanation for that is found in the simplified reflector modelling, which, apart from the models based on *Diff.-2g*, has been carried out without an equivalence process. Another possible source of error may stem from the strong flux gradient that is present in this region, which might require an axial mesh refinement.

A more detailed comparison is reported in Table 5.2 for all the models. It should be noticed that in this case $\Delta\rho$ is the reactivity difference. The performance of the *SP3-8g* is remarkable as the results produced in about 4 % of the reference time and with only one processor (instead of twenty) are in rather good agreement with the reference ones. Table 5.2 shows also the importance of

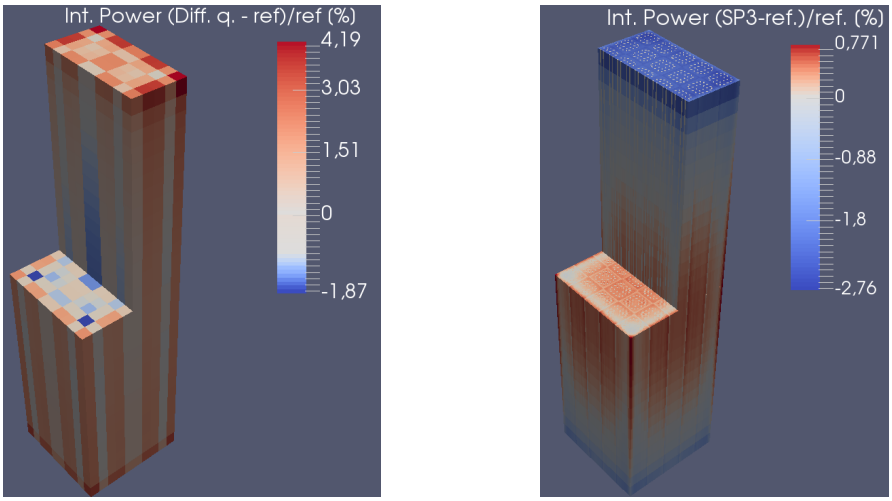

(a) *Diff.-2g (quarter)* Vs *S8-30g*. (b) *SP3-8g* Vs *S8-30g*.

Figure 5-4: Comparisons of the power distributions on the reactor core (reflector excluded) as predicted by the different neutronic models at fixed isothermal conditions. Presented in [11].

defining which are the target variables. Often in multiphysic simulations, it is especially important to accurately predict the power where it is the highest, as in this region the physics are more coupled. Anyhow, even in the core periphery the *SP3-8g* is in rather good agreement with the reference, therefore for the scope of this thesis it is kept as potential *best-estimate* model for the rest of the work.

Table 5.2: Performance assessment under isothermal conditions of the neutronic models in terms of multiplication factor, reactivity difference, maximum absolute value and RMS of the relative discrepancy on the power, radial power peaking factor and computing times ratio. The values in parentheses result from a comparison on the quarter of assembly. Both *S8* calculations are performed with twenty processors, whilst the others with only one. Presented in [11].

	S8-30g	*S8-20g*	*SP3-8g*	*Diff.-2g*	*Diff.-2g (quarter)*
k_{eff} [-]	1.19746	1.19668	1.19670	1.19445	1.19415
$\Delta\rho$ [pcm]	-	-54	-53	-210	-231
$[\max(\mathrm{abs}(\Delta \boldsymbol{q_{tot}}/\boldsymbol{q_{tot}}))]_{\mathrm{core}}$ [%]	-	0.93	2.76	8.17 (3.54)	(4.19)
$[\mathrm{RMS}(\Delta \boldsymbol{q_{tot}}/\boldsymbol{q_{tot}}))]_{\mathrm{core}}$ [%]	-	0.16	0.63	1.26 (1.07)	(1.18)
f_{xy} [-]	1.984	1.986	1.984	1.964 (1.618)	(1.622)
q'_{max} [W/cm]	431.06	431.53	432.34	427.72 (391.28)	(390.53)
t_i/t_{ref} [%]	100	63	3.7	0.1	0.001

In Table 5.2, it is also interesting to compare the *Diff.-2g* computed over the pin-cell discretization and then integrated over the quarter of assembly to the one directly calculated over the coarse mesh. As discussed in sub-section 3.1.2, in case of diffusion approximation, the coarse mesh should in principle contribute to the quality of the results as the fundamental hypotheses are easier to be fulfilled. From this comparison the opposite emerges, the power distribution predicted by the pin-by-pin diffusion integrated over the quarter of assembly matches better the integrated reference

one. The explanation for that stems from the fact that these models use cross-sections adjusted by the SPH technique that in case of pin-by-pin homogenization is more effective due to the larger number of free parameters.

Assessment of the Sensitivity of the Neutronic Models to the Reflector Composition

The same analysis is repeated for the standard reflector. The results are stored in Table A.1, available in the appendix. The relative performance of both the diffusion models becomes worse, but the rest of the models approximately shares the same consistency and relative computational cost as for the heavy reflector. It should be noticed that the purpose of this section is not to asses the physics of the two reflectors, whose description is very simplified, but rather how they affect the relative performance of each model. Anyway, to analyse the variation of the power distribution may help to better understand the reasons behind a change in relative performance. As a rule of thumb, when the gradient of the neutron flux is lower, the different models should produce more consistent results. For this scope, the same set of parameters (apart from the computing time, which is almost the same) is compared for the two reflector types, a synthesis is given in Table 5.3.

Table 5.3: Comparison of the main neutronic parameters between the two reflector types at isothermal conditions as predicted by the referential neutronic models. ρ_{heavy} and ρ_{std} respectively represent the reactivity of the cores with heavy and standard reflector. Presented in [11].

	Heavy Reflector	Standard Reflector
k_{eff} [-]	1.19746	1.18672
$\rho_{heavy} - \rho_{std}$ [pcm]	756	
f_{xy} [-]	1.984	2.126
q'_{max} [W/cm]	431.06	461.88
$[\max(\text{abs}((\boldsymbol{q_{heavy}} - \boldsymbol{q_{std}})/\boldsymbol{q_{std}}))]_{\text{core}}$ [%]	34.72	
$[\text{RMS}(\Delta \boldsymbol{q}/\boldsymbol{q_{std}}))]_{\text{core}}$ [%]	8.97	

The results show that the reflector's isotopic composition has a strong impact on neutronics. The heavy reflector allows to obtain a more reactive core at constant conditions and it flattens significantly the power distribution as confirmed by Fig. 5-5. As expected, the axial shape of the power does not change significantly and the hot-spot is at the same elevations for both the configurations. For this reason the comparison of the power radial distribution is done at the hot-spot plane. The higher power gradient found for the standard reflector, as predicted by the simple rule, comes with slightly higher discrepancies among the models.

The flattening of the power is a key target in reactor design, as it allows to extract more power with similar safety margins. In the context of this work, the lower radial peaking factor is also desirable as it comes closer to the range of values commonly found in commercial PWRs. Moreover, the larger reactivity is also beneficial, as it increase the maximum reachable cycle length. One more interesting thing that appears in Fig. 5-5 is that, when considering the heavy reflector, while most of the power is shifted from the centre to the periphery, the very outermost line of pin cells

follows the opposite trend. This is due to the fact that the standard reflector reflects more thermal neutrons thanks to the higher water content and they give an important contribution to the cells at the boundaries, while the heavy reflector kickbacks more fast neutrons, which contribute over a larger area.

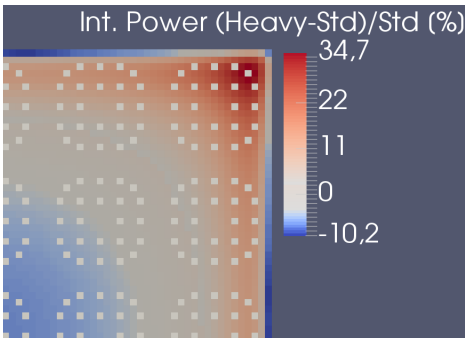

Figure 5-5: Relative difference of the power distributions in the core (reflector excluded), between the two reflector compositions. Northeast quarter of the radial section at the hot-spot plane. Presented in [11].

5.3.2 Selection of the Models Based on the Coupled Analysis

In this section, an analysis similar to the one presented in sub-section 5.3.1 is performed, but this time the models are compared within a coupled environment. At this stage, a coupling scheme of neutronics, thermal-hydraulics and heat conduction is considered. In particular, the neutronic model presented before are coupled to a thermal-hydraulic and heat conduction ones respectively using quarter of assembly radial discretization and one equivalent fuel rod per quarter of assembly as depicted in Fig. 5-6.

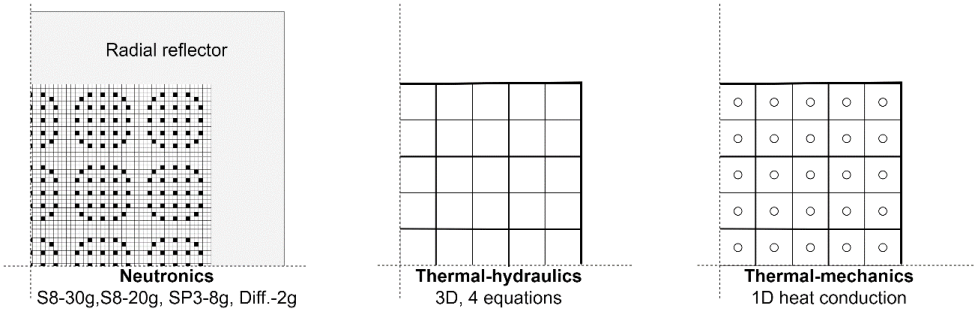

Figure 5-6: Refinement level of each physics. For the heat conduction, one average fuel pin per quarter of assembly is represented. Presented in [11].

Comparison of the Neutronic Models for Core Calculations

The comparisons of the integrated power distribution are reported in Fig. 5-7a and 5-7b. The highest discrepancies are still in the proximity of the reflectors, where the power is the lowest and this indicates once more that they could be reduced by improving the reflector modelling. Overall, the shape and the global magnitude of the differences on the power distribution are comparable to the ones obtained at fixed isothermal conditions.

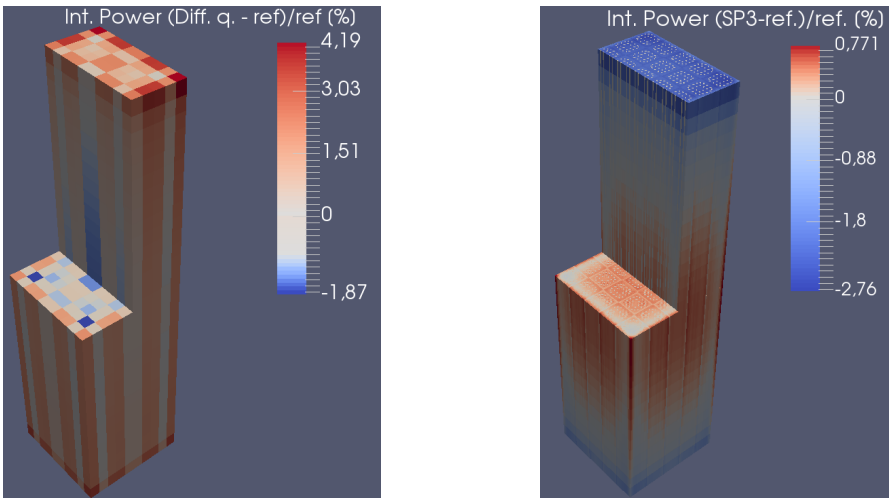

(a) *Diff.-2g (quarter)* Vs *S8-30g.* (b) *SP3-8g* Vs *S8-30g.*

Figure 5-7: Comparisons of the power distributions on the reactor core (reflector excluded) as predicted by the coupling scheme with different neutronic models. Presented in [11].

The analysis of the main neutronic variables is reported in Table 5.4. Similar conclusions to those drawn in Section 5.3.1 apply here. The relative performance of the neutronic models stays more or less constant. The inclusion of thermal-hydraulics and the heat conduction leads to a flatter radial power profile as indicated by the lower radial peaking factor. However, taking into account these physics brings to a more peaked power distribution as suggested by the maximum linear power. Indeed, even if both the moderator and the Doppler feedback are negative (i.e. they oppose to power escalations) the total power peaking factor increases. The reason for that is linked with the fact that, roughly speaking, the water bulk temperature is proportional to the integral of the linear power along the channel length, hence it is not a local feedback. The thermal-hydraulics causes a shift of the maximum power towards the bottom of the reactor where the water is denser and colder. Since, these calculations are done at fixed total power, such a shape deformation may lead to a more peaked distribution. On the contrary, with such a low value for the gap heat transfer coefficient, the fuel temperature depends a lot on the local linear power. In fact, in these conditions, the increase in bulk temperature along the entire channel is often lower than the average temperature jump in the fuel cladding gap.

Table 5.4: Performance assessment of the neutronic models coupled to thermal-hydraulics and heat conduction. The considered variables are the multiplication factor, the reactivity difference, the maximum absolute value and RMS of the relative discrepancy on the power, the radial power peaking factor and the computing times ratio. The values in parentheses result from a comparison on the quarter of assembly. Both *S8* calculations are performed with twenty processors, whilst the others with only one. Presented in [11].

	S8-30g	*S8-20g*	*SP3-8g*	*Diff.-2g*	*Diff.-2g (quarter)*
k_{eff} [-]	1.19073	1.18996	1.19001	1.18785	1.18753
$\Delta\rho$ [pcm]	-	-54	-51	-204	-226
$[\max(\text{abs}(\Delta \boldsymbol{q_{tot}}/\boldsymbol{q_{tot}}))]_{\text{core}}$ [%]	-	1.07	2.34	8.38 (3.80)	(4.64)
$[\text{RMS}(\Delta \boldsymbol{q_{tot}}/\boldsymbol{q_{tot}}))]_{\text{core}}$ [%]	-	0.26	0.45	1.31 (1.13)	(1.29)
f_{xy} [-]	1.878	1.880	1.877	1.863 (1.541)	(1.544)
q'_{max} [W/cm]	445.39	445.80	445.70	442.13 (405.06)	(404.83)
t_i/t_{ref} [%]	100	40	1.65	1.32	0.06

For what concerns the time factor, it should be considered that in this case it refers to the total time including also the thermal-hydraulics and the heat conduction. The stand-alone resolution of the thermal-hydraulics and the heat conduction needs approximately as much time as the one required by *Diff.-2g* at the pin-cell scale. These numbers can be used just to deduce the order of magnitudes, in fact, the quota of time spent for the thermal-hydraulics in the resolution of the coupling scheme may vary significantly. The convergence rate of thermal-hydraulics and heat conduction is affected by the considered power distribution. A similar topic is discussed into details in the following chapter.

Overall, the relative performance of the *SP3-8g* is almost unaffected by the coupling scheme both in terms of discrepancies and computing time. One factor that does not emerge from this analysis is the memory consumption. The *SP3-8g* has a much larger memory footprint than the other models (including also the thermal-hydraulic and heat conduction ones). However, for the considered computer this does not constitute a major problem. Hence, this model consolidates its position of good trade-off between discrepancy to the reference and computational cost.

Assessment of the Sensitivity of the Coupling Scheme to the Reflector Composition

The same analysis is repeated for the standard reflector and the main results are stored in Table A.2, available in the Appendix. Also in this case the relative performance of the models based on the diffusion approximation seems to slightly degrade, while the others stay almost unaffected. The results from the reference coupling scheme, the one using the *S8-30g* as neutronic model, for both the reflectors are compared in Table 5.5. The impact of the reflector composition on the reactivity is even larger than the one observed for the fixed isothermal conditions.

In respect of the power distribution, the maximum relative discrepancies are not at the hot-spot plane, but rather in the top of the core. In fact, in this region the thermal-hydraulic conditions differ the most, as they depend on the integral along the entire channel. Nevertheless, since the maximum

Table 5.5: Comparison of the main neutronic parameters between the two reflector types as predicted by the referential coupling scheme. Presented in [11].

	Heavy Reflector	Standard Reflector
k_{eff} [-]	1.19073	1.17768
$\rho_{heavy} - \rho_{std}$ [pcm]	931	
f_{xy} [-]	1.878	1.990
q'_{max} [W/cm]	445.39	487.36
$[\max(\text{abs}((\boldsymbol{q_{heavy}} - \boldsymbol{q_{std}})/\boldsymbol{q_{std}}))]_{\text{core}}$ [%]	41.99	
$[\text{RMS}(\Delta\boldsymbol{q}/\boldsymbol{q_{std}}))]_{\text{core}}$ [%]	9.99	

absolute discrepancies are in the radial plane including the hot-spot, the comparison on the radial power in Fig. 5-8 refers to its elevation. In fact, in this case, the hot-spot plane for the standard reflector is not exactly at the same height, it is one axial mesh below.

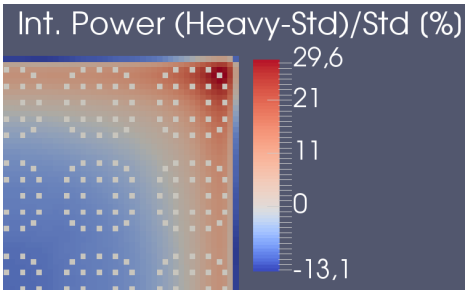

Figure 5-8: Relative difference of the power distributions in the core (reflector excluded), between the two reflector compositions as computed by the reference coupling scheme. Northeast quarter of the radial section at the hot-spot plane obtained using the heavy reflector. Presented in [11].

Overall, the coupling scheme and the reflector composition do not have a strong impact on the outstanding relative performance of the *SP3-8g*, which is judged as a good compromise and it is kept for the rest of the PhD work. The conclusions might change for more heterogeneous case studies or different homogenization levels.

5.4 Application of the Complete Coupling Scheme on the Case Study

In this section, the subchannel thermal-hydraulic modelling coupled to the heat conduction in every fuel rod is implemented. The need for such a refinement is tested on the study case using the hybrid scheme presented in the previous section as comparison term. Finally, the impact of the coupling scheme on the axial power profile is analysed.

5.4.1 Implementation of More Advanced Models

The implementation of a coupling scheme deploying advanced models is depicted as the progression from the standard ones, represented in Fig. 5-9, to the more advanced ones, reported in Fig. 5-10. To facilitate the description of the geometry for the subchannel thermal-hydraulics and heat-conduction and the coupling of these two meshes (link between thermal-hydraulic channels and fuel rods) a Python script has been implemented during the PhD work. Using such a coupling scheme with this level of refinement in every physics allows to improve the prediction of local quantities in each of the physics. For instance, to deepen the study of strongly coupled local phenomena like the DNB, which is a major safety concern and depends on both the local wall heat flux and the thermodynamic equilibrium quality ($x_e := \frac{h-h_f}{h_{fg}}$, where h is the mixture enthalpy, h_f is the liquid phase saturation enthalpy and h_{fg} is the latent heat).

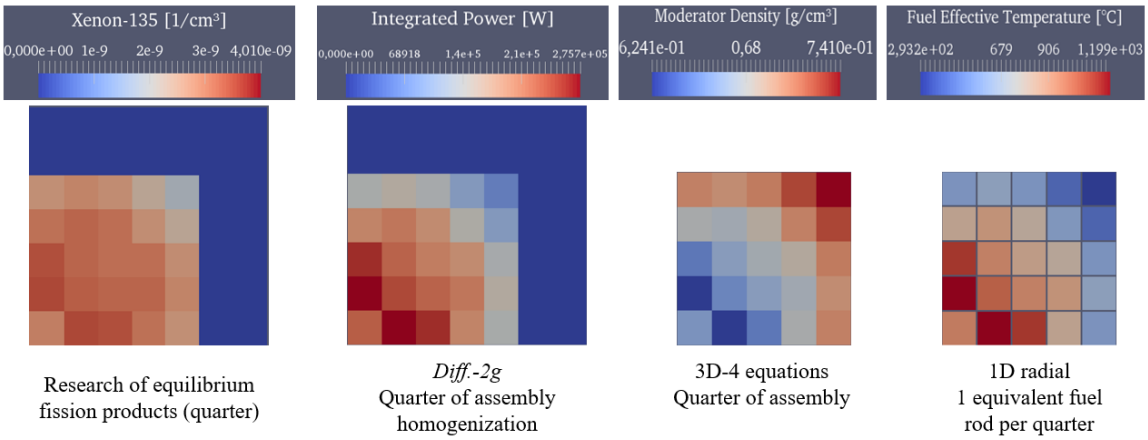

Figure 5-9: Standard coupling scheme realized with conventional models. One variable for each physics is reported in order to show every radial mesh. From left to right: xenon-135 equilibrium concentration, power integrated in the fuel, channel average moderator density and quarter of assembly effective temperature.

5.4.2 Assessment of the importance of the Thermal-Hydraulic and Heat Conduction Refinement

In this sub-section, it is assessed the importance of using a subchannel thermal-hydraulic model and solving the heat conduction for all the fuel rods. In the literature review reported in Section 2.1, the vast majority of the coupling scheme includes such a level of refinement for these two physics. In Table 5.6, the hybrid solution (pin-cell neutronics, quarter of assembly thermal-hydraulics and heat conduction) is compared to the main standard alternatives, which are based on a coupling scheme with pin-cell neutronics, subchannel thermal-hydraulics and heat conduction for all the fuel rods. Using the standard coupling scheme based on the *S8-30g* model as a reference, it is possible to observe that the hybrid scheme requires higher computing time and suffers higher discrepancies

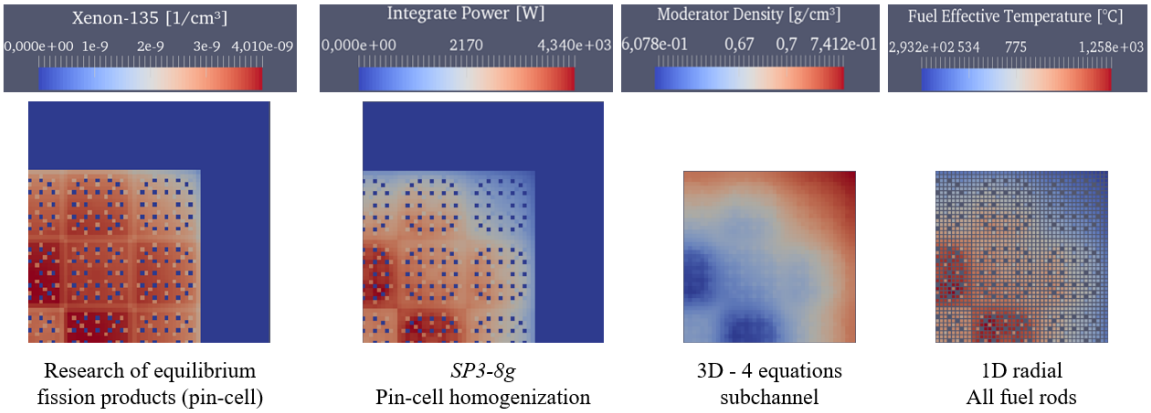

Figure 5-10: Current coupling scheme implemented for the rest of the thesis. One variable for each physics is reported in order to show every radial mesh. From left to right: xenon-135 equilibrium concentration, power integrated in the fuel, channel average moderator density and rod slice effective temperature.

than the standard one based on the *SP3-8g*. Therefore, the refinement of thermal-hydraulics and heat conduction modelling is considered more effective than improving the neutronic modelling. For this reason the standard approach is confirmed.

Table 5.6: Hybrid coupling scheme (pin-cell neutronics, quarter of assembly thermal-hydraulics and heat conduction) compared to the reference ones using subchannel thermal-hydraulics and modelling the heat conduction in every fuel rod. The main neutronic variables are reported.

	SP3-8g	*S8-30g*	*S8-30g* (hybrid)
k_{eff} [-], ($\Delta\rho$ [pcm])	1.18849 , (-51)	1.18921	1.19073 , (+107)
RMS($\Delta \boldsymbol{q_{tot}}/\boldsymbol{q_{tot}}$) [%], (max ($\Delta \boldsymbol{q_{tot}}/\boldsymbol{q_{tot}}$) [%])	0.56 , (-2.6)	0	1.36 , (-8)
t_i/t_{ref} [%]	6	100	≈97.5

5.4.3 Analysis of the impact of the Coupling Scheme on the Axial Power Profile

The power axial profile at isothermal conditions is almost symmetric (apart from the small differences due to the reflector's axial dimensions), but the other physics have a strong impact on it, so in this paragraph a brief overview of these deformations is given. For a given water mass flow rate, the higher the power level the more the thermal-hydraulics tends to bend the power distribution towards the bottom, where the water is denser and colder. As stated before, the impact of the heat conduction also depends on the value of the fuel cladding gap heat transfer coefficient, but, in most of the cases, it has a flattening effect as the average temperature increase in the fuel is predominant on the one characteristic of the moderator. To understand more the relation between the fuel temperature and the power profile, it is important to consider that the more the fuel temperature increases, the less effective the Doppler feedback becomes. To better define this point it is important to introduce the

effective resonance integral. Its definition is given in Eq. (5.5), where ΔE_{res} is the energy interval containing a resonance and ϕ is the self-shielding factor presented in sub-section 3.1.1. The effective resonance integral is a sort of effective absorption cross-section relative to a resonance energy interval that accounts for the strong flux depression in this energy range. In particular, I_{eff} is proportional to the square root of the fuel temperature. Therefore, the impact of the Doppler effect on the reactivity becomes weaker at higher temperatures.

$$I_{eff} := \int_{\Delta E_{res}} \frac{dE'}{E'} \sigma_a^{abs}(E')\phi(E') \tag{5.5}$$

At first sight, the impact of the research of the equilibrium concentrations of the fission products has also an effect similar to the heat conduction feedback. From the Bateman equations, it is possible to analytically derive the xenon-135 equilibrium concentration. Using one energy group cross-sections and considering only iodine-135 as precursor Eq. (5.6) is obtained. From this equation it is clear that the xenon concentration is asymptotically independent on the neutron flux. Even if the neutron flux in PWRs is about 10^{14} n/cm^2/s [231], the xenon is not completely saturated, as it is possible to see in Fig. 5-10, where a shape similar to the neutron flux may be recognised.

$$\boldsymbol{C}_{Xe,eq} = \frac{(\gamma_{Xe} + \gamma_I)\boldsymbol{\Sigma_f}\boldsymbol{\phi}}{\lambda_{Xe} + \sigma_{Xe}\boldsymbol{\phi}} \tag{5.6}$$

For what concerns the samarium-149, following a similar approach, assuming promethium-149 as the only precursor, it is possible to demonstrate that the equilibrium concentration of the samarium-149 is independent from the flux, as reported in Eq. (5.7).

$$\boldsymbol{C}_{Sm,eq} = \frac{\gamma_{Pm}\boldsymbol{\Sigma_f}}{\sigma_{Sm}} \tag{5.7}$$

The impact on the axial power profile of progressively adding physics to the coupling scheme is represented in Fig. 5-11. The converged power profile obtained for neutronics and thermal-hydraulics is compared to the one calculated including also the heat conduction and to the one that accounts also for the equilibrium concentration of fission products. The fission products and the heat conduction strongly contribute to the power flattening.

Even if the fission products have a stabilizing effect on the power profile, their integration in the coupling scheme may add complexity from the numerical point of view. In fact, they affect so much the neutronics that they may cause large oscillations of the solution during the convergence process. Depending on the power level, they may even compromise the stability of the scheme. In fact, for this case study, the coupling scheme including all the mentioned physics really challenges the efficiency and the stability of the fixed-point algorithm, which depending on the relaxation factor may not converge.

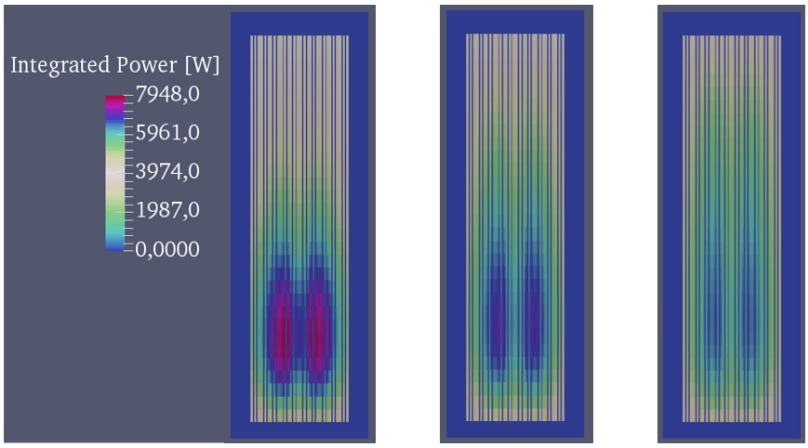

Figure 5-11: Deformation of the power profile due to the progressive inclusion of the other physics in the coupling scheme. An axial section of the mini-core is considered. From left to right: neutronics/thermal-hydraulics, plus heat conduction and plus both heat conduction and equilibrium concentration of the fission products.

5.5 Chapter Conclusion

In this chapter, a mini-core made of 5x5 PWR fuel assemblies plus reflector is selected as case study. A simple damped fixed-point algorithm is defined with the purpose of solving the coupled problem. The case study is used to compare the relative performance of four suitable neutronic models for core calculations. The assessment is performed both at fixed isothermal conditions and in a simple coupled scheme of neutronics, thermal-hydraulics and heat conduction. The simplified P_N method of order three used with eight energy groups is found to be the best compromise. The impact of two different reflector isotopic compositions and of the coupling scheme on the relative performance of this model is very small. For this reason, it is kept for the rest of the PhD studies. A subchannel thermal-hydraulic model coupled to heat conduction modelling of all the fuel rods is implemented. The need for the refinement of these two physics is demonstrated by comparison to a hybrid coupling scheme with pin-cell neutronics and quarter of assembly thermal-hydraulics and heat conduction. Finally, a brief analysis of the impact on the power axial profile of the full coupling scheme (including also the research of the equilibrium concentration of fission products) is given to facilitate the comprehension of the interdependencies among these physics. The limits of the damped fixed-point algorithm especially emerge for the coupling scheme containing all the physics, both in terms of efficiency and robustness. Depending on the relaxation factor, the convergence, may be not achievable. The problems of this algorithm are presented in detail in the following chapter and several solutions are proposed.

Chapter 6

Numerical Optimization of the Steady-State Coupling Scheme

In the previous chapter, a case study is specified and the single-physics models are selected. A simple damped fixed-point algorithm is implemented to solve the coupled problem. Especially when dealing with the multiphysic problem in its integrity, some numerical problems arise in terms of robustness and efficiency. In this chapter, those problems are analysed more in details. A generalization of the fixed-point, rather widespread in the industry but not so famous in literature, is implemented and deeply analysed. Afterwards, its performance is compared to the widely known Anderson algorithm. Finally, the customization of the Anderson algorithm following the principle of partial-convergences is explored.

6.1 Analysis of the limitation of the Damped Fixed-Point Algorithm

Before to discuss about multiphysic algorithms, which are one of the key topic of this thesis, it should be repeated that every specialised solver considered here contains in itself a numerical process, which is not modified in this PhD studies. For what concerns the role of the neutronic model that has been constituted, it solves an eigenvalue problem and, like the vast majority of the solvers, it uses the power iteration method. In particular, this algorithm iteratively researches the largest eigenvalue and its description can be found in [146], pages 192 to 198. In this type of solvers, the power iterations are just the outermost loop of a nested iterative process that may include multiple levels. In Algorithm 4, each multiphysic iteration corresponds to a neutronic solver call, which requires a variable number of power iterations that are needed to meet a set of internal precision criteria. In a similar way, the thermal-hydraulic and heat conduction model also uses an iterative process to solve

the steady-state problem. Similarly to many other solvers, it simulates a pseudo-transient until the asymptotic steady-state is reached. For this reason, also in this case, each solver call corresponds to a variable number of time steps required to meet a set of internal precision criteria. For simplicity, since in this coupling scheme the thermal-hydraulics and the heat conduction are part of the same iterative process (managed by the subchannel solver of FLICA), when talking about the thermal-hydraulic time steps, they refer also to the heat conduction. Both the power iterations and the time steps of the pseudo-transient are referred to as single-solver iterations.

In order to evaluate the performance of a given algorithm, a common estimator of the type of Eq. (6.1) is defined. This estimator defines an equivalent calculation time (t_{eqv}) based on the number of single-solver iterations multiplied by their respective average computing time, estimated once for all the applications. This choice is based on the fact that, at least for nominal conditions steady-states, both the thermal-hydraulic and the neutronic iterations respectively have an almost constant time cost and they carry most of the computing time. Moreover, with this estimator it is possible to compare calculations performed on machines with different characteristics. I_N is the number of neutronic power iterations, I_{TH} the number of thermal-hydraulic time steps and I_{FP} the number of depletion calculation. I_{FP} is also equivalent to the number of multiphysic iterations as the iterative process for the research of the equilibrium concentrations of the fission products is not subdivided into a number of iterations. For this reason, it is multiplied by an average time for the full depletion calculation (t_{FP}) summed to an estimation of the fixed time cost for data exchanges and manipulations ($t_{ex.}$).

$$t_{eqv} := I_N * t_{1N} + I_{TH} * t_{1TH} + I_{FP} * (t_{FP} + t_{ex.}) \tag{6.1}$$

In all the paper, this estimator is normalized to the best performing algorithm, as shown in Eq. (6.2) for this reason it is called relative equivalent calculation time ($t_{eqv,r}$).

$$t_{eqv,r} := \frac{t_{eqv,i}}{t_{eqv,min}} \tag{6.2}$$

The damped fixed-point algorithm defined in Section 5.2 is tested for a typical range of relaxation factors. The plot of the performance versus the relaxation factor is available in Fig. 6-1. When the algorithm converges, the associated equivalent calculation time is reported. Otherwise, if the L2-norms of the residuals do not decrease enough over the iterations, “NC” is marked on top of the relaxation factor, whereas, if the L2-norms of the residuals increase, “DIV” is used.

Without damping, divergent axial oscillations are found for the neutron scalar flux and consequently for the concentration of fission products. Due to the low value of the total heat transfer coefficient for the extraction of the heat from the fuel, also the fuel temperature follows similar oscillations. With respect to the density, the variations are prevalently axial. The axial position of

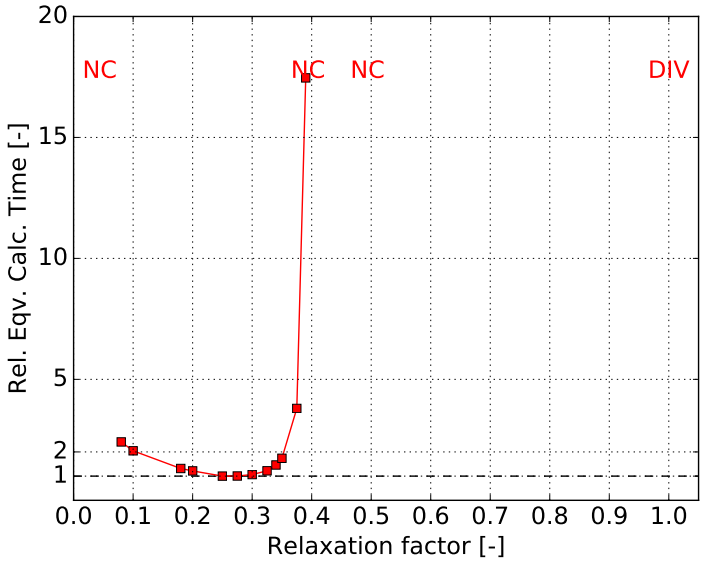

Figure 6-1: Performance of the Damped fixed-point algorithm for a range of relaxation factors. "NC" stands for Non-Convergent behaviour and "DIV" for DIVergent.

the peak of heat flux significantly impacts the density axial profile and the convergence speed. The oscillations of these quantities are reported in the appendix for the first three iterations in Fig. from B-1 to B-4. Similar oscillations have been observed also in [141]. The divergent behaviour makes the solution exit the range of validity of the parameters, hence the iterations stop. When the oscillations are observed, the eigenvalues of the Jacobian matrix of the damped fixed-point iteration function (introduced in sub-section 2.2.1) are expected to be negative and, due to the divergent behaviour, some of them are supposed to be inferior to minus one. Hence, the optimal relaxation factor is expected to be between zero and one.

Considering Fig. 6-1, the curve respects the convex shape predicted by the theory presented in sub-section 2.2.1, which consolidates the pertinence of the estimator $t_{eqv,r}$. To link the current damped fixed-point iteration function to the general theory presented in sub-section 2.2.1, it is possible to think of the global functional as composition of the operators using the neutronic variables as the only unknown. Therefore, the exact iteration function associated to the fixed-point considered here and defined by Algorithm 4 is the one defined in Eq. (6.3). Where $\boldsymbol{x}^k := [\boldsymbol{\tau}^k, \boldsymbol{q}_{\boldsymbol{w}}^k, \boldsymbol{q}_{\boldsymbol{f}}^k]$ (recall: these fields respectively represent the vector of reaction rates [1/cm^3/s] and the integrated power [W] in the water and in the fuel). $FP(\boldsymbol{x}^0)$ is the concentration of fission products as stored in the cross-sections.

$$\boldsymbol{x}^{k+1} = \boldsymbol{G}_\alpha(\boldsymbol{x}^k) := \alpha * N([TH(\boldsymbol{x}^k)]_{\boldsymbol{\rho_w}}, [TH(\boldsymbol{x}^k)]_{\boldsymbol{T_f}}, FP(\boldsymbol{x}^{k-1})) + (1-\alpha) * \boldsymbol{x}^k \tag{6.3}$$

From this point of view, the convergence criteria on all the variables not contained in $\boldsymbol{x}^k$ become

additional checks on internal variables of interest.

In particular, in Fig. 6-1, a range of relaxation factors that makes the scheme converge is found, it contains the values between 0.08 and 0.39. From a theoretical standpoint, values comprised in $\alpha \in]0, 0.08[$ should bring to convergence in a decreasingly effective way approaching zero. Obviously $\alpha = 0$ is not considered, because it means no update of the solution. Nevertheless, small values of α might bring to convergence criteria too small compared to the internal precision of the solvers. Indeed, for $\alpha = 0.05$, a plateau is observed just before reaching the convergence for some physics. So even if this case is classified as "NC", the scheme is actually converging to a result, but with a precision lower than the imposed one. An increase in the solvers internal precisions would be required to allow lower values of the relaxation factor. On the contrary, for $\alpha \geq 0.4$, an interval of non-convergence is observed, in the sense that the solution is trapped in periodic oscillations within a set of values. More insight on this behaviour is given in the next section. For even larger relaxation factors, the module of the residuals increases with the iterations. Given the small range of acceptable relaxation factors, the damped fixed-point appears as difficult to apply on case studies similar to the considered one. For such a strongly coupled problem, tighter algorithms should be used. Moreover, the performance is very dependent on the value of the relaxation factor, which is very inconvenient, because optimal values are generally not available or empirically determined. For instance, by choosing a relaxation parameter about 0.3 leads to a rather efficient convergence, while selecting 0.39 makes the algorithm more than fifteen times slower and with 0.4 or larger no convergence would be obtained.

6.2 Generalised Fixed-Point with Partial-Convergences

Given the difficulties encountered when using the damped fixed-point algorithm, in this section, a variant of this method based on the partial-convergences is introduced. This technique is already rather widespread in the industry but very few systematic studies are found in the nuclear reactor physics literature. In particular, the sensitivity of its performance to the numerical parameters is analysed. Afterwards, the evolution of the key variables along the multiphysic iterations in case of non-converging algorithm is examined.

6.2.1 Introduction

The generalised fixed-point with partial-convergences technique is based on the idea of chasing a progressive convergence of some of the single-physics models. Within this approach, the internal convergence of the neutronic and thermal-hydraulic operators is not asked at every multiphysic iteration, but it becomes just a necessary criterion for the global convergence of the scheme. The convergence of the neutronic inner iterative process can be controlled either by imposing a maximum limit on

the number of power iterations per solver call or simply by controlling the internal precision criteria. These two options are not equivalent at all, depending on the initialization of the solver, a widely varying number of iterations would be needed to obtain a given precision. There exist, since long time, industrial calculation schemes using the fixed-point with partial-convergences by controlling the number of the neutronic power iterations. However, [125] is the only reference of this practice found in literature. On the contrary, schemes based on the fixed-point with partial-convergences that control the internal precision criteria are not so frequent. The numerical justification for the use of an inexact operator is given by [232]. In this reference, it is also analysed the variation of the multiphysic convergence of TIAMAT for a set of fixed degradation of the internal convergence criteria of each of the single-physics solver (neutronics, thermal-hydraulics and fuel performance). The considered case study for this analysis is the steady-state modelling of a fuel rod at nominal conditions. Other detailed mathematical analyses of inexact methods can be found in the works of [233].

For what concerns the considered thermal-hydraulic model, the internal convergence can be controlled in an analogous way through the number of time steps of the pseudo-transient or through the modulation of the internal convergence criteria. Also in this case, it is more common in industrial calculations to impose the partial-convergences via a maximum number of time steps per solver call than by controlling the internal precision criteria, but both these techniques are even less frequently observed in literature. For instance, in [125], only the neutronic power iterations are controlled, whilst the full convergence of thermal-hydraulics is asked at each call. The explanation for that is partly linked to the specific solver structures that may not allow such flexibility and to the numerical algorithm, which may simply be not suitable for partial-convergences.

For the generalised fixed-point with partial-convergences considered in this work, the limitations are only imposed on the maximum number of single-physics iterations per solver call of neutronics and thermal-hydraulics. For the thermal-hydraulics, a constant time step of 0.01 s is considered. Since the fission products equilibrium research takes a much lower computing time than the one required for the complete resolution of the other physics and the concentration of the xenon-135 evolves in a rather stiff and not monotonous way, full convergence is always asked to this operator. The time-evolution of the concentrations of xenon-135 and samarium-149 after a power change are respectively given in Fig. B-5a and B-5b, available in the Appendix. It should be noticed that those plots refer to the variation of the total reactor power, while for these calculations, this is a fixed constraint, but a similar reasoning can be adapted to the local variations of the neutron flux.

Within this approach, a key role is played by the solver initialization at each call. Each solver restarts from the results computed at the last call. In this way, in case of stable algorithm, the number of solver specific iterations needed to meet the convergence criteria decreases along the multiphysic convergence. Therefore, after a certain point, the internal convergence of each solver

becomes reachable within a number of single-physics iterations lower than the imposed limits. The main idea behind this technique is to avoid the extra single-solver iterations needed to very precisely compute every physics while away from the global solution. Instead, a progressive convergence of all the variables is targeted. Another justification to the use of this technique could be found in its similarities with the under-relaxation ($\alpha < 1$). When the convergence of the internal solvers is approximately monotonous, the not fully converged solution is contained "in between" the solution at the previous iteration and the fully converged new guess. For this reason, when the under-relaxation is desirable, the partial convergence allows to achieve similar savings in terms of multiphysic iterations, but also to reduce the number of single-solver iterations, by avoiding the unnecessary iterations to full convergence when far from the solution.

To understand the need of the word "generalised" before "fixed-point", it is important to underline the difference introduced by this algorithm customization. For this scope, the concept of consistency of a numerical method needs to be introduced. A detailed explanation is given in [146], pages 37 and 38. For this analysis let us consider the whole multiphysic problem in the residual form ($\boldsymbol{F}(\boldsymbol{x}) = \boldsymbol{0}$) associated to the fixed-point defined in Eq. (6.3). The numerical method that solves this problem would produce a sequence of approximate problems that in a general form can be expressed as in Eq. (6.4). Where $\boldsymbol{d}$ is the exact set of data on which the solution depends and k is a certain parameter for which the unknown tends to the solution of the problem ($\lim_{k\to\infty} \boldsymbol{x}^k = \boldsymbol{x}^*$). Under the assumption of well posed problem, this is possible only if $\boldsymbol{F}^k$ approximates the real problem $\boldsymbol{F}$ for $k \to \infty$ and the same for the datum ($d^k \to d$ for $k \to \infty$).

$$\boldsymbol{F}^k(\boldsymbol{x}^k, \boldsymbol{d}^k) = \boldsymbol{0} \tag{6.4}$$

Considering a datum $\boldsymbol{d}$ admissible for $\boldsymbol{F}^k$, the method is consistent if Eq. (6.5) is respected. Moreover, such a method is said strongly consistent if the equation is valid for every k.

$$\lim_{k\to\infty} \boldsymbol{F}^k(\boldsymbol{x}^*, \boldsymbol{d}) = \lim_{k\to\infty} \boldsymbol{F}^k(\boldsymbol{x}^*, \boldsymbol{d}) - \boldsymbol{F}(\boldsymbol{x}^*, \boldsymbol{d}) = \boldsymbol{0} \tag{6.5}$$

In the context of this work, k is the index of multiphysic iterations and the datum can be considered as the case study specification, which is constant along the process. While the simple fixed-point (damped or undamped) is a strongly consistent method by definition ($\boldsymbol{F}(\boldsymbol{x}^*) = \boldsymbol{F}^k(\boldsymbol{x}^*) = 0\ \forall k$), the generalised fixed-point with partial-convergences is only consistent. In other words, the fixed-point function $\boldsymbol{G}_\alpha^k$ varies along the multiphysic iterations and nothing guarantees that, for a given k, $\boldsymbol{G}_\alpha^k(\boldsymbol{x}^*) = \boldsymbol{x}^*$. First of all, the exact neutronic operator N is substituted by a truncated one $N_{n_{int.}}$, whose maximum number of power iteration per solver call is limited to "$n_{int.}$". For this reason, the internal convergence is met only if this limit is sufficiently high that the iteration process would have stopped before reaching it anyway. Secondly, since the internal convergence

is not guaranteed, the solver initialization at the beginning of the call affects the final result. In general, the considered neutronic model restarts from the status computed at the end of the previous call, while the flat flux is used at the first iteration. Therefore, due to the initialization technique, the operator is in reality dependent on the history of previous calls. To indicate this evolution of the neutronic operator, it is indicated with $N^k_{n_{int.}}$, where k is the number of solver calls, which in this case is equivalent to the number of multiphysic iterations. Completely analogous observations apply to the thermal-hydraulics ($TH^k_{m_{int.}}$), where "$m_{int.}$" is used for the limit on the time steps), hence also for the global operator. As stated before, in case of converging algorithm, the solver initialization approaches the solution of the problem and this allows, from a certain point on, to ensure the internal convergence. In fact, the initialization becomes close enough to the solution that the number of single-physics iteration required for the convergence is inferior to the imposed limit. For this reason, as stated before, the internal convergence becomes a necessary condition for the global convergence of the scheme.

The generalised fixed-point with partial-convergences is represented by Algorithm 5 (recall of the following fields nomenclatures: $\boldsymbol{\rho_w}$ is the moderator density [g/cm^3], $\boldsymbol{T_f}$ is the fuel effective temperature [°C] and $\boldsymbol{C_{FP}}$ is the fission products concentrations [1/cm^3]). The convergence check is the same as in Algorithm 4.

Algorithm 5 Damped fixed-point with partial convergences.

Flat power distribution
while $\|\Delta \boldsymbol{x}_i^k\|_2 > \Delta_i * \alpha$, for any i **do**
  $(\boldsymbol{\rho_w}^{k+1}, \boldsymbol{T_f}^{k+1}) = TH^k_{m_{int.}}(\boldsymbol{q_w}^k, \boldsymbol{q_f}^k)$
  $(\boldsymbol{\tau}^{k+1}, \boldsymbol{q_w}^{k+1}, \boldsymbol{q_f}^{k+1}) = \alpha * N^k_{n_{int.}}(\boldsymbol{\rho_w}^{k+1}, \boldsymbol{T_f}^{k+1}, \boldsymbol{C_{FP}}^k) + (1-\alpha) * (\boldsymbol{\tau}^k, \boldsymbol{q_w}^k, \boldsymbol{q_f}^k)$
  $\boldsymbol{C_{FP}}^{k+1} = FP(\boldsymbol{\tau}^{k+1})$
end while

The associated flowchart is not drawn as it is very similar to that given in Fig. 5-3. The only difference is that, in the current algorithm, also the operators N and TH depends on the multiphysic iteration for the reasons just explained.

6.2.2 Parametric Performance study

In order to have an insight of the performance of Algorithm 5, it is applied to the case study for different tuples of maximum single-solver iterations (N_N-N_{TH}) and for a wide range of relaxation factors. In fact, for each setting, larger damping factors are tested until the divergence of the algorithm is observed.

The first test concerns a symmetrical reduction of both the neutronic and the thermal-hydraulic iterations limits. The starting values are defined from the total number of iterations required to solve the case under isothermal conditions for the neutronics and for a flat power distribution for

the thermal-hydraulics. The results are available in Fig. 6-2, "inf-inf" corresponds to no limits on the iterations, so to the same curve of Fig. 6-1. However, it is renormalized to the current lowest equivalent calculation time, which is different. The reduction of the single-physics iteration limits seems to significantly improve the performance of the algorithm: the number of equivalent iterations can be up to 15 times smaller than the best result obtained with the standard algorithm. Another important advantage of such a technique is the reduction of sensitivity on the relaxation factor. For instance, in the "1-1" case, the performance is almost constant over the entire interval of considered relaxation factors, and the divergence is not obtained for α lower than 1.8. Even if it might seem that the problem is only moved from the choice of a relaxation factor to that of the tuple of maximum single-solver iterations, the dependency on such a parameter is much smaller for any choice within few tens of iterations. The comparison between "1-1","10-10" and "20-40" shows that alternating the resolution of the two physics at each iteration is a suitable choice. However, the fixed time cost per multiphysic iteration favours the choice of few tens of single-physics iterations. Moreover, imposing "1-1" is not compatible with testing the internal convergence on more than one iterate and the dedicated internal acceleration techniques, which are usually very effective, are not applicable. For instance, in the resolution of neutronic power iterations, Chebyshev acceleration (see [234]) might be desirable, but the internal solver would have access to only one iterate, hence no acceleration technique would be available in this case.

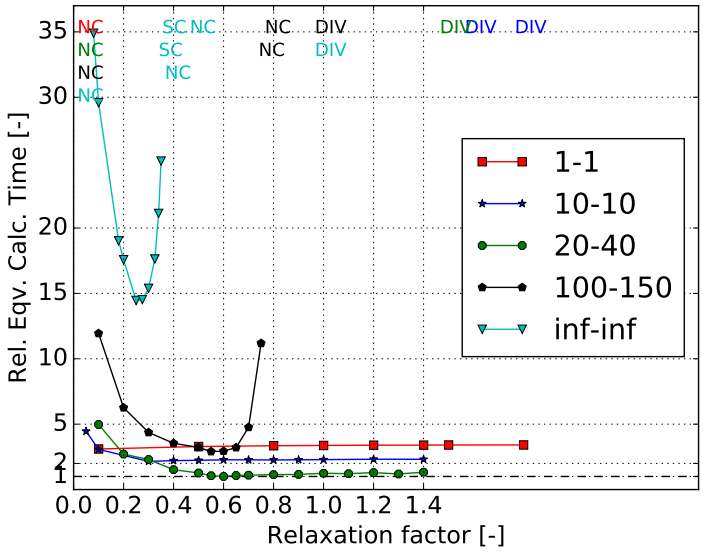

Figure 6-2: Symmetrical reduction of the limits on single-physics iterations, appearing in the tuples format: "N_N-N_{TH}". The partial convergence significantly improves the performance of the algorithm and drastically reduces the dependency on the relaxation factor. Instead of the marker, "SC" (meaning Slow-Convergence) appears in the top part of the plot if $(t_{eqv,r}) > 50$. "NC" represents non-convergence and "DIV" divergence.

The second test deals with the asymmetrical reduction of the limits on the number of single-physics iterations. The results are available in Fig. 6-3. It appears that limiting the number of neutronic iterations is more stabilizing than imposing a lower maximum of thermal-hydraulic iterations. In fact, the abrupt loss of performance and stability, observed for relaxation factors slightly higher than the optimum value, only appears when the limit on neutronic iterations is equal or greater than one hundred. In most of the cases, limiting the neutronic iterations brings to larger α_{opt}. This could be explained with the reduction in module of the most negative eigenvalues. The extreme cases "1-inf" and "inf-1" fully confirm this trend. "inf-1" diverges for almost the entire range of standard relaxation factors. "1-inf" on the contrary converges always for $\alpha \in [0.1, 1.4]$, nevertheless, it is totally not competitive in terms of computing time.

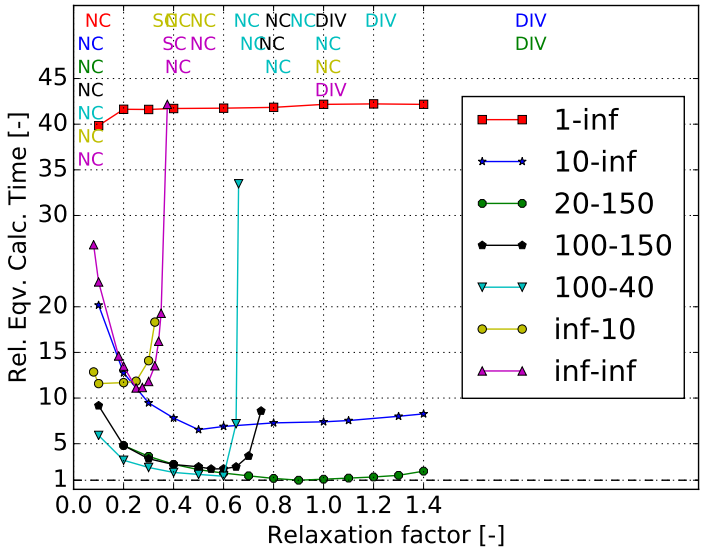

Figure 6-3: Asymmetrical reduction of the limits on single-physics iterations, appearing in the tuples format: "N_N-N_{TH}". The stability of the algorithm improves more when limiting N_N. The same notation of Fig. 6-2 is adopted.

The results reported so far are obtained assuming that the data exchange and manipulation is in the order of 2 s. In order to test their sensitivity to the manipulation time, the curves are plotted again in Fig. 6-4 for a data exchange and manipulation time of 200 s. Except for few cases, neither the shape of the curves nor their relative positions change much. This confirms that reducing the limits on the tuples not only permits savings in terms of single-physics iterations, but it also strongly affects the number of multiphysic iterations. Moreover, this low dependency on the data exchange and manipulation time helps to make the study slightly more general as implementation details and informatic optimization are kind of separated from the analysis. Nevertheless, it should be noticed that this optimization becomes essential when the limits on the single-physics iterations is very small. In particular, with respect to "1-1" setting, it is no longer competitive in terms of equivalent

calculation time.

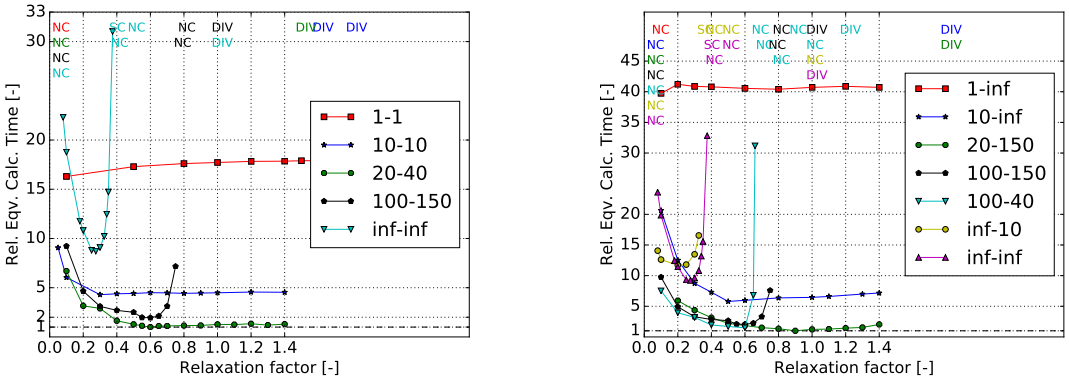

(a) Symmetrical reduction.

(b) Asymmetrical reduction.

Figure 6-4: Performance analysis of different limits on the maximum number of single-physics iterations per multiphysic call. The same analysis of Fig. 6-2 and Fig. 6-3, but assuming a data exchange and manipulation time of 200 s, instead of 2 s. The same notation of Fig. 6-2 is adopted.

Analysing the number of neutronic and thermal-hydraulic iterations separately, it is possible to have more insight on the efficiency of limiting the maximum number of iterations. It should be noticed, that in this kind of analysis, the time for the data manipulation and exchange does not have any influence. In Fig. 6-5a and 6-5c, the ratio of the total number of neutronic iterations to a reference number is reported. This reference corresponds to the amount of iterations needed to fully solve the neutronics considering the fission products concentrations as stored in the cross-sections and a given temperature and density profiles, which correspond to a flat power distribution. It appears that the total number of neutronic and thermal-hydraulic iterations to solve the coupled system with partial convergences can be comparable or, only for the outstanding "20-40", even lower than corresponding reference number. In case of asymmetrical reductions, it is found that savings on the total number of neutronic iterations are often associated to large number of total thermal-hydraulic iterations and vice-versa.

A similar observation can be made for the thermal-hydraulics, see Fig. 6-5b and 6-5d, using as reference number the number of time steps required to fully resolve for the flat power distribution. It should be noticed that the internal convergence of the thermal-hydraulics is tested on five consecutive iterations, in every case but for "1-1". For this setting, the convergence is only tested on one iteration, therefore, this method has an unjustly looser convergence criterion, which partially explains its outstanding performance. The fact that solving the whole coupled system could cost less iterations than solving the corresponding decoupled problem for the initial conditions is a rather unexpected result. It could be explained by the fact that the fission products and the thermal-hydraulics tend to flatten the power distribution, making the neutronics easier to be solved. Similarly, the thermal-hydraulics requires less iterations for lower radial power peaking factors. Hence, for similar cases

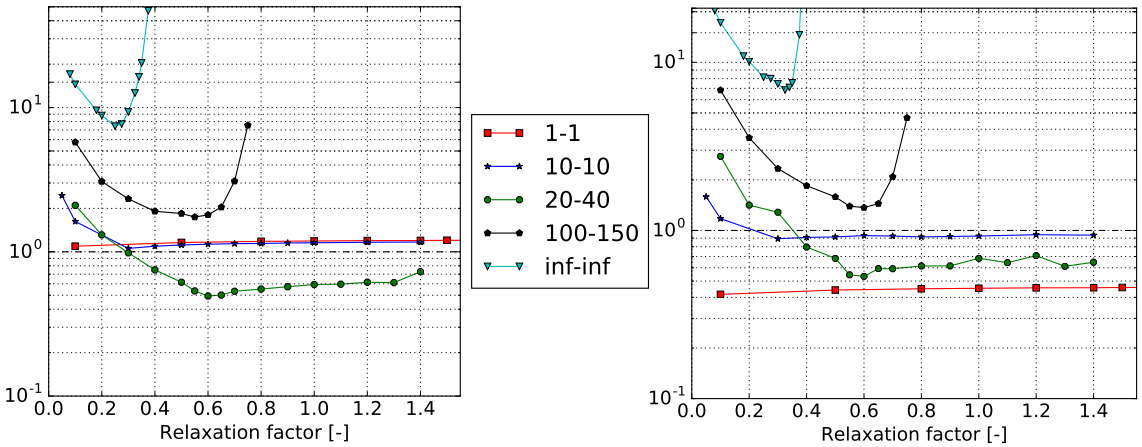

(a) $NIt.s_i/NIt.s_{ref}$ (b) $THIt.s_i/THIt.s_{ref}$

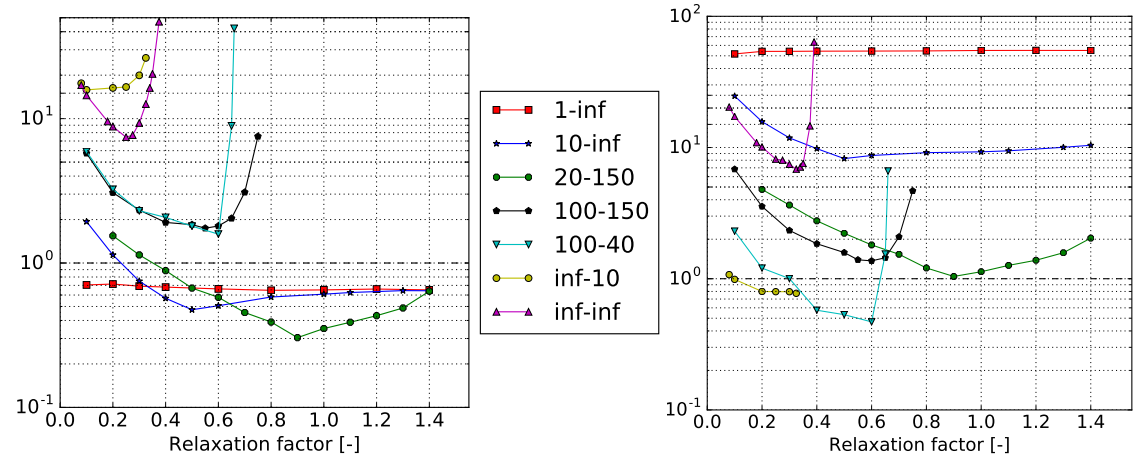

(c) $NIt.s_i/NIt.s_{ref}$ (d) $THIt.s_i/THIt.s_{ref}$

Figure 6-5: Ratio of the total number of single-physics iterations needed to fully solve the coupled problem and a reference iteration number. For the neutronics, this is the number of power iterations to completely solve the neutronics for a temperature and density profile corresponding to flat power. For the thermal-hydraulics, this is the number of iterations necessary to entirely solve the thermal-hydraulics for a flat power profile.

and initialisations, the partial-convergences methods appears as very competitive. In order to verify that all the schemes converge to the same solution, the discrepancies among the main variables are measured. The RMS and the maximum of the absolute relative discrepancy are computed for all the converging settings using "inf-inf" with a relaxation factor of 0.3 as reference. This process is repeated for the integrated power in the fuel, the moderator density, the fuel effective temperature and the xenon-135 equilibrium concentration. The histograms relative to frequency of each discrepancy are reported for these four variables in Fig. 6-6.

The results show that all the convergent settings lead to the same solution in all the observed variables within the 8 pcm of maximum absolute relative discrepancy on the pin-cells, which are

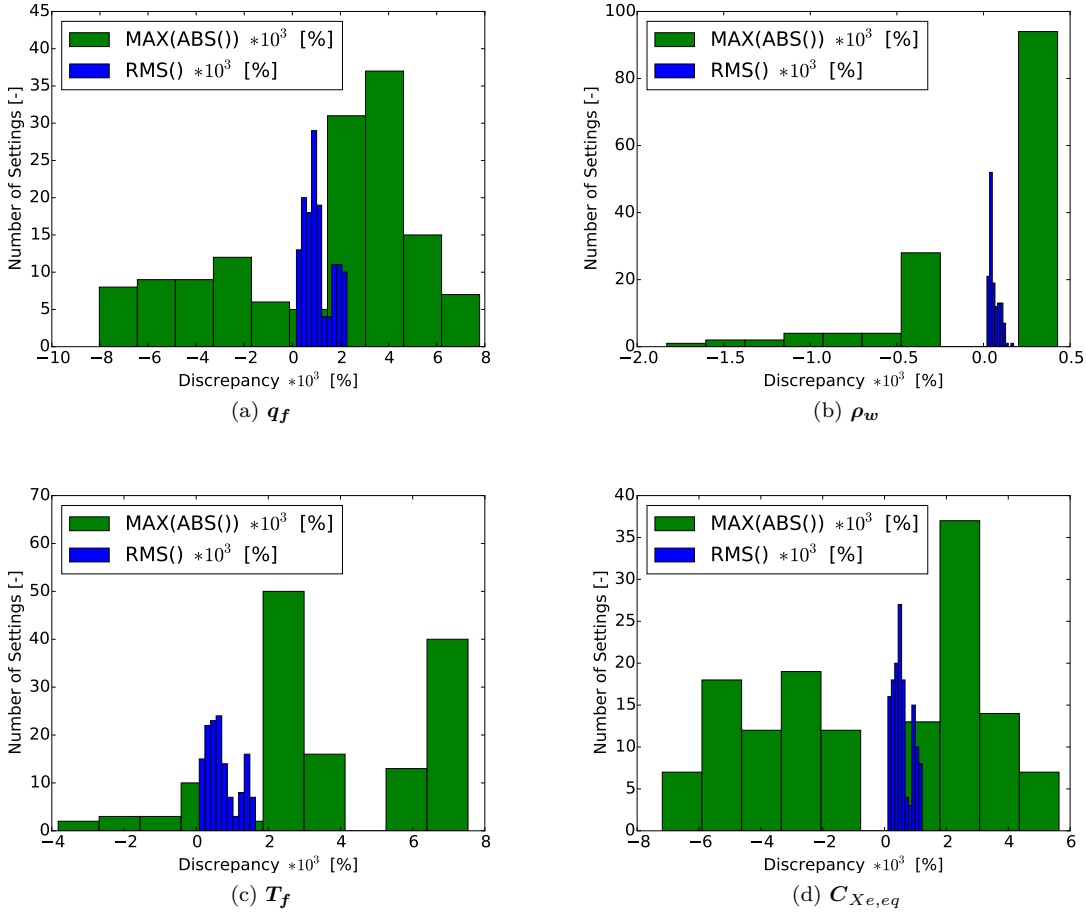

(a) $\boldsymbol{q_f}$ (b) $\boldsymbol{\rho_w}$

(c) $\boldsymbol{T_f}$ (d) $\boldsymbol{C}_{Xe,eq}$

Figure 6-6: Convergence proof based on the analysis of the relative discrepancy of each converging setting to the reference values (produced with "inf-inf" with relaxation factor 0.3). The examined variables are the integrated power in the fuel, the moderator density, the fuel effective temperature and the xenon-135 equilibrium concentration.

directly linked to the convergence criteria.

6.2.3 Analysis of the Fixed-Point Bifurcations

For both the standard damped fixed-point and the generalised one with partial-convergences, an interval of relaxation factors is found in which the algorithm does not converge, but does not diverge either. This range is generally included between the largest damping factor that ensures the convergence and the smallest one that leads to the divergence of the solution. In case of non-convergence, the solution is observed to be trapped in periodic oscillations that correspond to the fixed-point bifurcations, which have been widely studied as a branch of the chaos theory. A particularly related study is available in [235]. This behaviour is easier to visualize for a scalar quantity such as the effective multiplication factor, but also the considered 3D fields exhibit this type of oscillations. In

Fig. 6-7, an example is given for the effective multiplication factor. For a given setting ("100-40"), increasing the relaxation factor from 0.6 to 0.7 completely changes the convergence process. For α equals to 0.6, the algorithm clearly converges to a unique solution. With respect to a relaxation factor of 0.7, the solution strictly oscillates between four solutions. Even the 3D fields exactly repeats along these four solutions, with all the precision required for the final solution. Since the four solutions considered in this case are sufficiently far from each others, convergence is not met. It should be noticed that, like in this example, the oscillations may not contain at all the converged multiplication factor: the converged results for the effective multiplication factor all agree on the value of 1.13689, while the oscillations range within 1.14129 $\pm$ 100 pcm (this value just being the arithmetic average of the four).

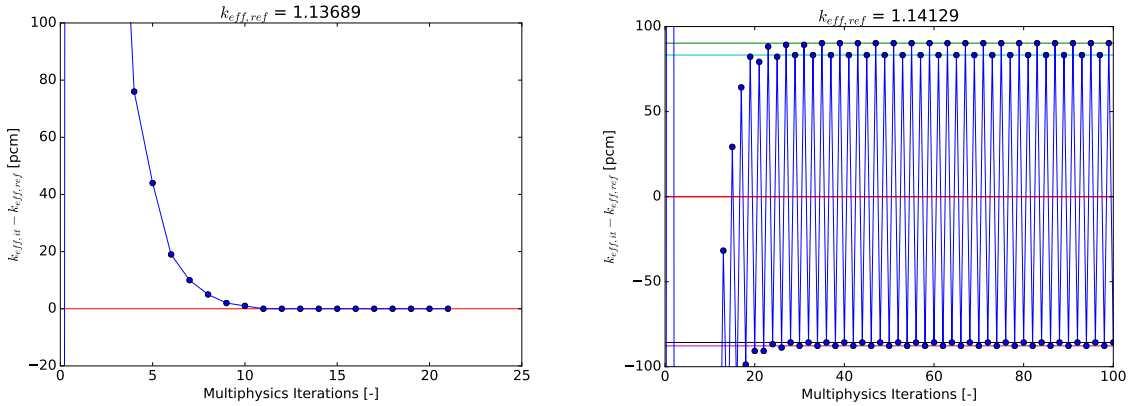

(a) $\alpha = 0.6$ (b) $\alpha = 0.7$

Figure 6-7: Different convergence behaviours of the multiplication factor for two values of the relaxation parameter, here the "100-40" setting is considered. On the left-hand side, monotonous convergence is observed, while for slightly larger relaxation-factor, the previous mentioned non-converging oscillations of period four are reported.

Very often, the solution is trapped in these oscillations after a rather small number of iterations. Therefore, an adaptive algorithm could be implemented. The residual could be tested to detect potential bifurcations and the damping factor could be reduced in case their presence is suspected.

6.3 Assessment of the Performance of the Anderson Algorithm

The Anderson acceleration method has been introduced in sub-section 2.2.2 and the reasons that motivate its deployment in the considered coupling scheme are discussed in sub-section 2.2.4. Among the strong points of the Anderson algorithm it is important to repeat that, with low additional complexity it provides a low order secant method (finite different approximation of the Newton algorithm) that, most of the times, performs better than the fixed-point [139, 236]. Moreover,

as reported in sub-section 2.2.2, [149] has underlined that this method offers a greater tolerance to numerical noise than higher order Newton algorithms, which might be crucial when combining multiple solvers with different precisions. In this section, the Anderson algorithm is compared to the generalised fixed-point with partial convergences.

6.3.1 Implementation Details

For this work, the Anderson algorithm is imported from the Scipy-Optimize library [237]. This version of the algorithm offers more than the "simple" Anderson iterative scheme. Two main extensions are available, the possibility to apply a regularization parameter and the line-search. The regularization parameter reduces the ill-conditioning problem in change of a minor deceleration of the iteration process. Hence, it could be used to select higher M parameter with a small loss of accuracy in the weights determination. The second extension allows to dynamically determine the weight used to combine the results at the previous and the current iterations in order to meet a criterion that links the descent slope and the equivalent step's size to be chosen. The criterion is given either by Wolfe's [238, 239] or by Armijo's [240] rules. Both the techniques may require several function evaluations before the condition is met. Due to the associated computation costs and as anticipated by [149], the line search might not be particularly effective for problems like the considered one. Anyway, it is still tested for a preliminary study to measure its impact on the robustness of the scheme.

Even if the relaxation technique is not totally overlapping with the line-search, in every application presented here, the Anderson algorithm is used without relaxation. In fact, even Anderson suggested not to apply relaxation unless empirical experience is available [139]. In order to use this library, it is only necessary to systematically convert the MED fields into the Scipy standard and vice-versa and to switch to the residual formalism, which is given in Eq. (6.8). For this purpose, the new non-dimensionalised variables and operators are defined in Eq. (6.6) and (6.7).

$$\hat{\boldsymbol{x}} := [\boldsymbol{q_w} * 1/c_{\boldsymbol{q_w}}, ..., \boldsymbol{\rho_w} * 1/c_{\boldsymbol{\rho_w}}, ...] = [\hat{\boldsymbol{q}}_{\boldsymbol{w}}, ..., \hat{\boldsymbol{\rho}}_{\boldsymbol{w}}, ...] \tag{6.6}$$

$$\hat{TH}(\hat{\boldsymbol{q_w}}, \hat{\boldsymbol{q_f}}) := ([TH(\boldsymbol{q_w}, \boldsymbol{q_f})]_{\boldsymbol{\rho_w}} * 1/c_{\boldsymbol{\rho_w}}, [TH(\boldsymbol{q_w}, \boldsymbol{q_f})]_{\boldsymbol{T_f}} * 1/c_{\boldsymbol{T_f}}) \tag{6.7}$$

$$\hat{\boldsymbol{F}}(\hat{\boldsymbol{x}}^k) = \begin{bmatrix} \hat{TH}(\hat{\boldsymbol{q}}_{\boldsymbol{w}}^k, \hat{\boldsymbol{q}}_{\boldsymbol{f}}^k) - (\hat{\boldsymbol{\rho}}_{\boldsymbol{w}}^k, \hat{\boldsymbol{T}}_{\boldsymbol{f}}^k) \\ \hat{N}(\hat{\boldsymbol{\rho}}_{\boldsymbol{w}}^{k+1}, \hat{\boldsymbol{T}}_{\boldsymbol{f}}^{k+1}, \hat{\boldsymbol{C}}_{\boldsymbol{FP}}^k) - (\hat{\boldsymbol{\tau}}^k, \hat{\boldsymbol{q}}_{\boldsymbol{w}}^k, \hat{\boldsymbol{q}}_{\boldsymbol{f}}^k) \\ \hat{FP}(\hat{\boldsymbol{\tau}}^{k+1}) - \hat{\boldsymbol{C}}_{\boldsymbol{FP}}^k \end{bmatrix} \tag{6.8}$$

As introduced in sub-section 2.2.2, this notation change is justified by the willing to have an unknown vector containing quantities approximately of the same order of magnitude in order to avoid a decoupling of the algorithm. The physical operators are then modified in order to accept

and return the normalized quantities, in this case a circumflex accent is present on the operator. The scaling factors are the individual convergence criteria (c_i) previously defined for each variable and expressed in its units of measure. After this nondimensionalization, at least close to convergence, the L2-norm of each variable should be at the same order of magnitude. Also in this case, the convergence is tested on the L2-norm of the absolute difference of the variable between two consecutive iterations.

Without further implementations a wide list of algorithms, including the JFNK is ready to be used. Since only minor tests have been performed during the PhD work on the application of JFNK to the considered problems, they are not reported in this thesis.

6.3.2 Comparison to the generalised Fixed-Point with Partial-Convergences

The benefits of the Anderson acceleration in comparison to the standard damped fixed-point are expected both in terms of stability and of convergence rate. The first comparison deals with the fixed-point and the Anderson method, both with full convergence and both using the iteration function defined by Eq. (6.8). In every case, the relaxation factor is imposed equal to one (no relaxation). Different values of the M parameter are explored for the extended Anderson algorithm, Armijo's criterion is imposed. The results are reported in Fig. 6-8a, in terms of convergence of the power integrated in the water.

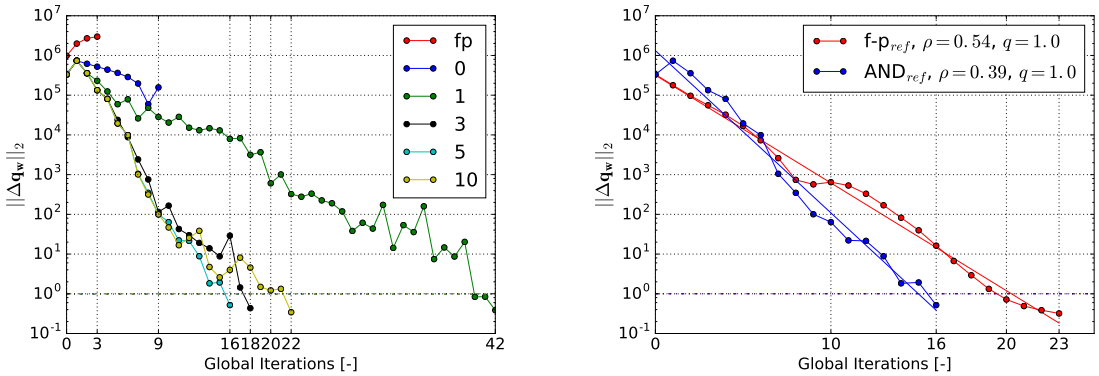

(a) Robustness comparison

(b) Rate of convergence comparison

Figure 6-8: Convergence slopes of the residual of the power vector for different methods. On the left, the fixed-point is compared to the Anderson method for different M values (appearing in the legend). In every case, full convergence is imposed and the relaxation is not applied. On the right, the Anderson method with M=5 is compared to the best performing fixed-point algorithm with partial convergences ($\alpha = 0.6, N_N = 20, N_{TH} = 40$); ρ is the average factor by which the residual decreases and q represents the order of convergence.

As expected, especially after the analysis reported in Fig. 6-1, also this fixed-point function diverges after few iterations. Anderson with M equals zero strictly corresponds to the fixed-point plus line-search. This extension makes the algorithm slightly more stable, but also in this case

after some more iterations the algorithm diverges. On the contrary, for any tested value of M larger than zero, the convergence is reached, showing the greater robustness of the method. For the current application, the Anderson algorithm allows to strongly reduce the importance of the choice of the relaxation parameter, which becomes not crucial for the stability of the method. Even if the results presented are obtained by the algorithm including the line-search, it has been found that even without this feature the algorithm converges for any M larger than zero.

In Fig. 6-8b, the convergence slope of the best generalised fixed-point with partial-convergences ($\alpha = 0.6, N_N = 20, N_{TH} = 40$) is compared to the Anderson method with M equals five and no limitation on the internal iterations. In the x-axis, the global iterations are reported, they differ from the multiphysic ones only because they do not account for the extra-evaluations eventually performed for the line-search. For this reason, this could be considered as the best rate of convergence that is possible to obtain with the Anderson algorithm, as it does not penalize the extra function evaluations performed for the line-search. Both the methods exhibit a linear convergence. In the labels, it also appears an estimate of the rate of convergence (ρ), whose definition is recalled in Eq. (6.9) (where it appears as $\mu \in]0, 1[$). Its estimation is based on the linear fitting of the logarithm of the residual as a function of the global iteration number, which is represented by the solid line (e.g. ρ =0.39 means that the residual is on average multiplied by this quantity at each global iteration).

$$\mu := \lim_{k \to \infty} \frac{\|\boldsymbol{x}^{k+1} - \boldsymbol{x}^*\|}{\|\boldsymbol{x}^k - \boldsymbol{x}^*\|} \tag{6.9}$$

Exploiting Eq. (2.2), it is possible to derive that, for the fixed-point, the estimation of the rate of convergence also corresponds to that of the spectral radius of $\mathbf{G}_\alpha$. Anderson convergence rate is better, it needs less global iterations and less multiphysic ones as well. However, as highlighted in the previous sections, this does not necessarily imply a lower computing time. Indeed, considering the same high data manipulation time of the previous section (200 s), this Anderson algorithm is 8.5 times slower than the best fixed-point with partial convergence and only 5 % faster than the best fixed-point with full convergence. It should be noticed that, in this way, the increase of the data manipulation and exchange time linked to the Anderson algorithm and specifically to the choice of the M parameter is totally neglected. However, the tests made confirm that the variations of this time are in the order of few percent, hence, do not change the final results. A further improvement can be obtained by switching off the two previously mentioned Scipy extensions (regularization parameter and line search), obtaining a relative equivalent calculation time of 7.2. To sum it up, the Anderson method has proven the expected superior performance in terms of robustness, convergence rate and equivalent calculation time on the standard fixed-point algorithms. As compared to the generalised fixed-point, Anderson's method also provides better robustness and convergence rate. Nevertheless, if it is compared to most of the partial-convergence fixed-point schemes, its equivalent calculation time is not competitive as the full-convergence multiphysic evaluations are much more

expensive.

6.4 Customization of the Anderson Algorithm with Partial-Convergences

Since the generalised fixed-point with partial-convergences has shown such an outstanding performance in terms of equivalent calculation time, in this section, it is tested to customize the Anderson algorithm following the principles of partial-convergences. The objective is to obtain an even higher performance or at least a better trade-off between the equivalent calculation time and the robustness of the method. Two attempts are reported, the first one is based on the control of the number of single-solver iterations and the second on an increasing refinement of the internal convergence criteria of the solvers. The results of preliminary tests are described for both the implemented generalised Anderson algorithms.

6.4.1 Strategy Based on the Single-Solver Iterations

In this sub-section, it is tested to control the convergence of the specialised operators via the limitation on the number of single-physics iterations. This strategy could be seen as a simple extension of what has been done for the fixed-point. As introduced in Section 6.2, the iteration function of the generalised fixed-point with partial-convergences evolves along the multiphysic iterations ($\boldsymbol{G}$ becomes $\boldsymbol{G}^k$). While for the fixed-point no extrapolation is performed, a constant relaxation factor is used along all the process, the Anderson acceleration determines the weight to assign to each iteration by minimizing the squared residuals. For this reasons Eq. (2.9) becomes Eq. (6.10) and the residual (definition recalled in Eq. (6.11)) is minimized for the set of M iteration functions $\hat{\boldsymbol{F}}^{k-j}$ for $j \in [0, M_k]$, instead of a single one.

$$\hat{\bar{\boldsymbol{F}}}^k := \hat{\boldsymbol{F}}^k(\hat{\boldsymbol{x}}^k) + \sum_{j=1}^{M_k} \theta_j^k * (\hat{\boldsymbol{F}}^{k-j}(\hat{\boldsymbol{x}}^{k-j}) - \hat{\boldsymbol{F}}^k(\hat{\boldsymbol{x}}^k)) \tag{6.10}$$

$$R^k = \frac{1}{2}(\hat{\bar{\boldsymbol{F}}}^k)^T \cdot \hat{\bar{\boldsymbol{F}}}^k \tag{6.11}$$

It should be noticed that, in this way, the difference between two evaluations of the iteration function is not bounded by any value. For this reason, if $\boldsymbol{G}^k$ varies too much, the effectiveness of the extrapolation should be compromised. Therefore, low values of the M parameter are tested. The guess is that the solvers initializations do not vary too much over few consecutive iterations. This is a very complex trade-off that should be facilitated by the higher tolerance offered by the lower order approximations of the inverse of the Jacobian.

This approach is tested for some of the iterations limits of the previous section and for different values of the M parameter. In all the cases, the extensions are not activated and the relaxation is not applied. In fact, the line-search is expected not to work properly with the partial-convergences. The results for the "20-40" and the "100-150" are available in Fig. 6-9.

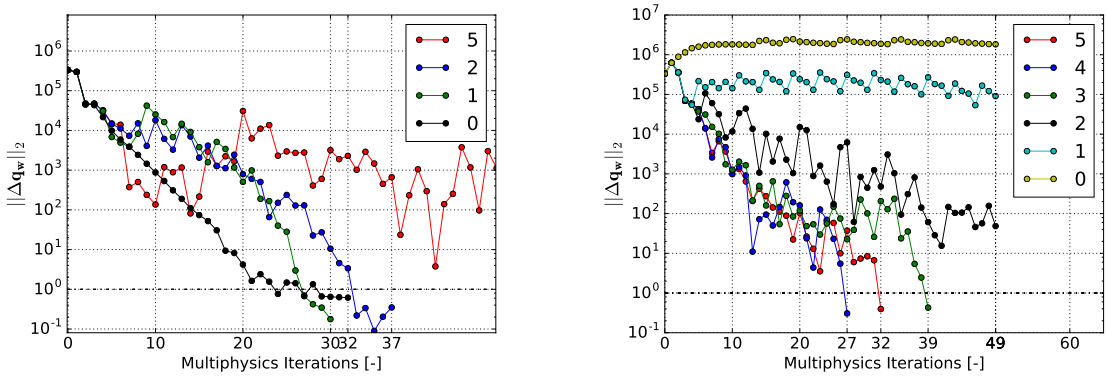

(a) "20-40"

(b) "100-150"

Figure 6-9: Convergence of the residual of the total power in the water using the generalised Anderson with the two tuples of iterations limits per solver call and for different M parameters appearing in the legend. No line-search, no regularization parameter and no relaxation are applied.

The "20-40" seems to confirm the idea that an M parameter of 1 or 2 could be combined with the considered iterations limits, while higher values of M would lead to an unstable algorithm. In respect of "100-150", a different behaviour is observed: it converges only for M>1 and the convergence rate improves up to M=4. In addition, the module of the residual oscillates severely even when the scheme converges. An interpretation to that could be found in the narrower range of acceptable relaxation factors, which is linked to the tolerance on the approximation of the inverse Jacobian.

Another attempt is made with the "1-1" setting, as within this approach, the initialisation of the solver should not evolve so much at each multiphysic iteration. However, in this case, the algorithm does not converge for any value of the M parameter. It has been tested also to combine the fixed-point iterations with partial-convergences followed by Anderson iterations with full-convergence to improve the rate of convergence of the final part. However, preliminary results have shown that the performance is not significantly improved by this approach either.

Overall, this approach does not bring to satisfactory results, the time performance is similar to that obtained with the generalised fixed-point with partial-convergences with the same iteration limits, but, a loss of stability of the method is observed. In terms of equivalent calculation time, both "20-40" with M=1 and "100-150" with M=4 are around 20 to 30 % more expensive than the generalised fixed-point with equal settings and optimised relaxation factor. Low values of the M parameter are not always increasing the stability of the method, hence it would be complicated to select a good combination of the parameters without making several tests.

6.4.2 Strategy Based on the Progressive Refinement of the Internal Convergence Criteria

This strategy deals with the control of the internal convergence criteria of each specialised solver. Through these parameters, it is easier to bound the level of inconsistency that may arise between two iterations. Moreover, by controlling these parameters, the dependency on the particular solvers initialisations is significantly reduced.

More into details in the proposed algorithm, the convergence process is divided into a sequence of Anderson calculation blocks at constant internal precisions. A switching criterion is defined in order to move from one block to another. In the final block, the same multiphysic and internal convergence criteria used in the other algorithms are imposed to guarantee the same level of precision. This global scheme is represented in Fig. 6-10. A simple and empiric switching criterion is defined: when the number of neutronic iterations becomes smaller than ten, arbitrary choice, the algorithm moves to the next tuple. This choice derives from the fact that this quantity is a sort of measure of the distance between to consecutive solver calls. Hence, it is used to avoid to push too far the multiphysic convergence for the degraded internal criteria. Analogously, for very unstable problems, a criterion could be implemented to reduce the demanded precision to intermediate values in case of unstable algorithm after switching block.

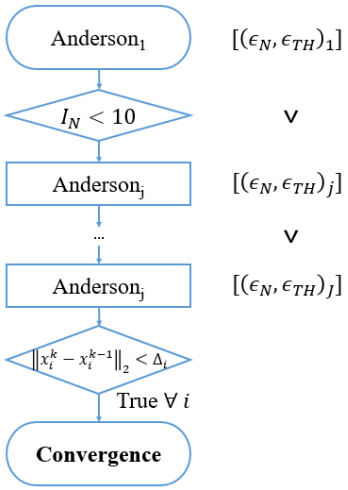

Figure 6-10: Anderson with partial-convergences controlled by the internal precision. A sequence of Anderson calculation blocks characterized by an increasingly finer convergence criterion for both the thermal-hydraulics and the neutronics. In this example, the algorithm switches to the next block when the number of neutronic power iterations to convergence is lower than ten. In the final block, all the convergence criteria used for the other methods apply here.

An application of this method is reported here. The Scipy extensions are deactivated and there is no relaxation. A sequence of four tuples of internal precisions is chosen, the values are simply constantly reduced by a factor ten at each step but the first, in which it is divided by a factor fifty,

as reported in Table 6.1. It should be noticed that for the neutronics the test on the precision is performed only on the last two iterations, while for the thermal-hydraulics this check is set so that it has to be satisfied five consecutive times.

Table 6.1: Sequence defining the progressive refinement of the precision on neutronic and thermal-hydraulic variables. ε_N and ε_{TH} respectively refer to the neutron flux and the moderator density convergence criteria.

Block number:	ε_N	ε_{TH}
1	5E-2	5E-3
2	1E-3	1E-4
3	1E-4	1E-5
4	1E-5	1E-6

This larger reduction in the first block simply is motivated by the willing to reduce even more the single-solver iterations at the beginning of the process. The convergence slopes are available in Fig. 6-11 for a range of M parameters.

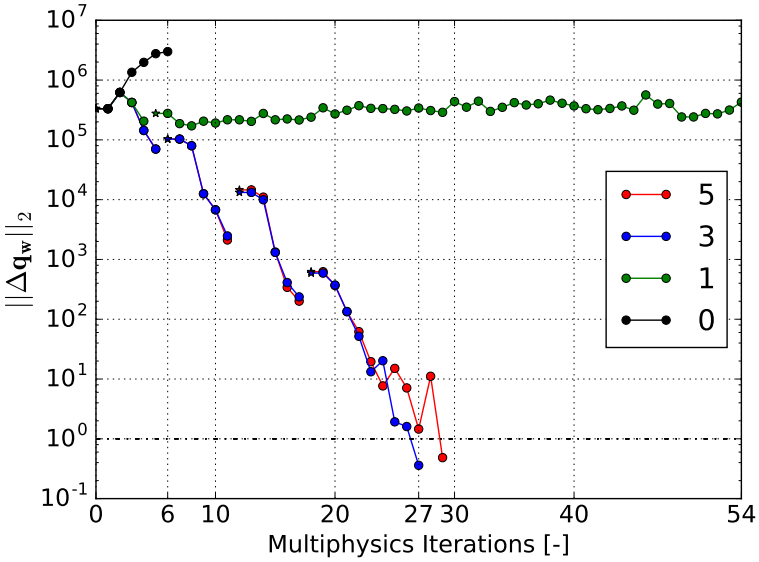

Figure 6-11: Anderson with partial-convergences controlled by the internal precision. The method is tested for a range of M parameters appearing in the label. The star-markers correspond to the first fixed-point iteration of every Anderson block, to which no calculation of the residual is associated.

The fixed-point iterations, which correspond to M=0, are diverging. It is expected that with an even coarser first tuple of convergence criteria it would be possible to obtain a converging algorithm. For M=1, the method is diverging very slowly in the second Anderson block. As proposed before, after testing few iterations, an intermediate tuple of internal precisions could be asked. For larger values of M, almost no oscillations are observed in the convergence of the residuals and the rate of convergence is rather satisfactory. In terms of equivalent calculation time, this simulation is 1.5 times faster than the best Anderson with full convergences, which on the other hand means

that it is 4.8 times slower than the best fixed-point with partial convergences. Even if in terms of equivalent calculation time its performance is still significantly lower than the best fixed-point, it should be noticed that the fixed-point settings are issued by an empirical optimization, while the switching criterion and the demanded internal precisions are just a first trial. Moreover, the number of iterations strongly depends on the analysed core size and on the operating conditions. Therefore, further studies should be carried on the definition of the internal precision sequence and of the switching criterion. Finally, the two methods should be compared for a range of core configurations and operating conditions.

6.5 Chapter Conclusion

To conclude, the damped fixed-point is considered as not very suitable for applications similar to the given case study. Its generalised version based on the partial-convergences offers the best performing algorithm in terms of equivalent calculation time. However, its robustness should be tested on different case studies and its effectiveness might vary if using different solvers. The standard Anderson algorithm is the most robust solution, but it is slower than most of the considered generalised fixed-point with partial convergences. The first attempt to customize the Anderson algorithm by controlling the level of convergence via the limits on the single-physics iterations requires more work. The second strategy is based on the progressive refinement of the convergence criteria of the specialised solvers. Preliminary tests on this new algorithm show promising results that collocate it in between the standard Anderson and the generalised fixed-point with partial-convergences in terms of equivalent calculation time and robustness of the performance.

Part of the results contained in this chapter have been partly published in [241] and others are under review in [242].

Until this point, the coupling scheme has addressed only the steady-state problem for burnup independent thermodynamic properties. In the following chapter, a model to integrate the evolution of the fuel conductivity and the gap heat transfer coefficient is included in the scheme, its impact is studied and a simple depletion calculation scheme is implemented.

Chapter 7

Evolution Calculation

In the previous chapter, the coupling scheme for steady-state calculations of neutronics, thermal-hydraulics and research of the equilibrium concentration of fission products is optimized from the numerical point of view. In particular, for all the following analyses the generalised fixed-point with partial-convergences is adopted (α =0.6, N_N =20, N_{TH} =40). In this chapter, the coupling scheme is extended to perform depletion calculations. More into details, the modelling of the evolution of the fuel's thermodynamic properties is included. After that, a common algorithm for the research of the critical boron concentration is adapted in order to be compatible with the partial-convergences. Finally, the depletion calculation scheme is implemented and it is tested on a simple irradiation scenario.

7.1 Integration of Burnup Dependent Thermodynamic Variables

As introduced in sub-section 1.1.2, the fuel thermodynamic properties vary along irradiation and this can have a strong impact on the neutronics. The available models for fuel performance are described in Section 3.4. Among them, a model is selected and implemented. Finally, its impact on the calculation scheme is assessed.

7.1.1 Fuel Conductivity Law

Various semi-empirical correlations are available for the modelling of the evolution of the thermodynamic properties. One of the reference documents for the modelling of the thermal-mechanic properties of the nuclear fuel is [243], published by the International Atomic Energy Agency (IAEA). The most important parameter on which the fuel conductivity of the solid uranium dioxide depends is the local temperature. Many widespread correlations only include this parameter. Until this point

of the thesis, the conductivity law used for the fuel is the Ronchi one, which is reported in Eq. (7.1), recommended by [243], page 89. In this equation t is the normalised fuel temperature ($t := T_f/1000$, T_f [K]). As mentioned in the reference, the associated uncertainty is 10 % in the temperature range from 298 to 2000 K and around 20 % between 2000 to 3120 K.

$$\lambda(t) = \frac{100}{7.5408 + 17.692t + 3.6142t^2} + \frac{6400}{t^{\frac{5}{2}}} * exp\left(\frac{-16.35}{t}\right) \tag{7.1}$$

Eventually, a correction can be applied to account for the formation of porosity. In this way, it would be possible to account for a part of the burnup effect. However, it is difficult to predict the variation of porosity in the fuel without the deployment of a fuel performance code. Therefore, for the following studies the Halden correlation, recommended by [243], page 144 and reported in Eq. (7.2), is chosen. This relation directly accounts for the burnup dependency. In this case, T_f is expressed in °C and BU in MWd/kg.

$$\lambda(T_f, BU) = \frac{1}{0.1148 + 0.0035BU + 2.47510^{-4}(1 - 0.00333BU)T_f} + 0.0132 * exp(0.00188T_f) \tag{7.2}$$

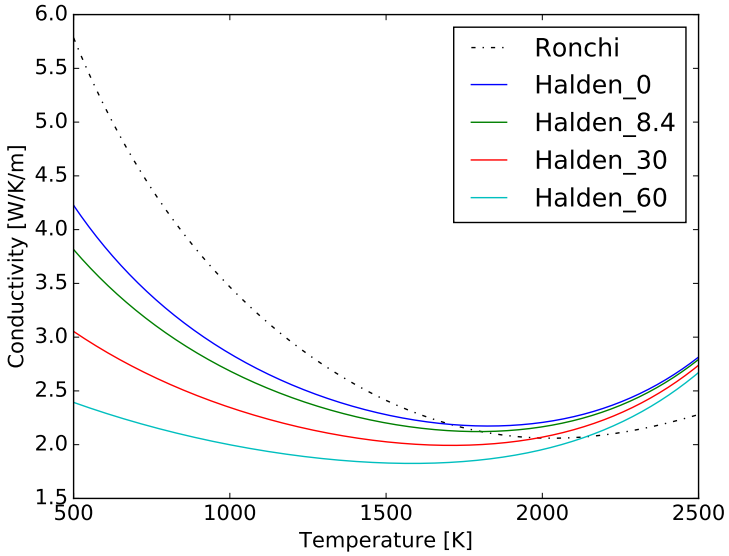

Figure 7-1: The conductivity laws for solid UO_2 from Ronchi et al. (burnup independent) and from the Halden project are compared over a large range of temperatures. The Halden conductivity is plotted for four burnup values expressed in MWd/kg ranging from fresh fuel to end of cycle. The value 8.4 MWd/kg corresponds to the average burnup of the loading plan considered for the case study.

In Fig. 7-1, the two laws are compared for a set of typical burnup values. It is possible to observe a significant degradation of the conductivity along irradiation, which is manly linked to the increase

in fuel structural defects. The Halden conductivity law is directly implemented in FLICA4, which receives the burnup distribution from APOLLO3® under the MED format.

7.1.2 Fuel Gap Heat Transfer Coefficient

As presented in Section 3.4, two main options are available for the modelling of the fuel gap heat transfer coefficient: ALCYONE fuel performance code and a simplified model derived from it. In the context of CORPUS, ALCYONE has been included in several coupling schemes [244, 216] and its integration in the coupling scheme realised during this work is not expected to be too complicated. However, in pin-by-pin simulations, the number of parallel computations becomes important and eventually prohibitive for a single computer like the considered one. For this reason, it is decided rather to test the simplified model. Therefore, a qualitative reproduction of the evolution of the fuel-clad gap is sufficient for the scope of the study. The variation of the fuel gap heat transfer coefficient along irradiation, as predicted by this simplified model, is reported in Fig. 7-2, for three linear powers (100, 160 and 300 W/cm), average coolant bulk temperature (300 °C) and gap's closure at 10 MWd/kg.

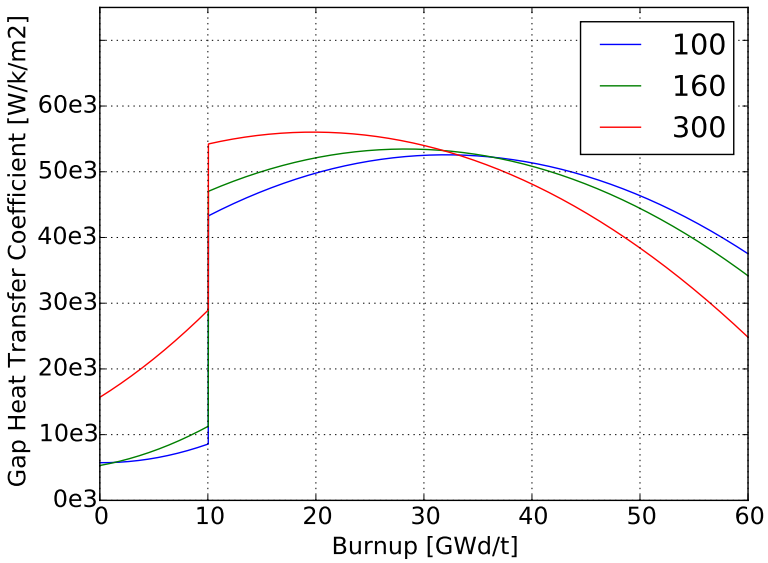

Figure 7-2: Representation of the prediction of the simplified model for the fuel gap heat transfer coefficient along irradiation for three linear powers reported in the legend (100, 160 and 300 W/cm), average coolant bulk temperature (300 °C) and gap's closure at 10 MWd/kg.

In terms of implementation details, this model is treated just as the other operators, while from the point of view of numerics, it is incorporated in the thermal-hydraulic one. The gap heat transfer coefficient is treated as an internal variable, hence its convergence over multiphysic iterations is not directly tested. As introduced, this model reproduces the fuel gap heat transfer coefficient as a function of local burnup, linear power and moderator bulk temperature. Those quantities are

directly received from the other models under the MED format. For each fuel rod slice, four gap heat transfer coefficients are defined corresponding to the four water bulk temperatures as described by Fig. 7-3. One unique heat conduction calculation is performed using the H_{gap} and wall temperature resulting from the average of the four values.

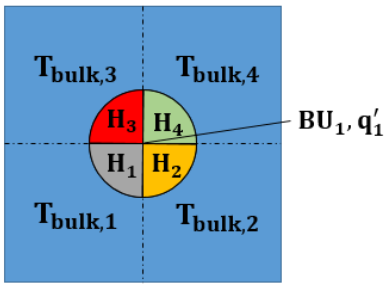

Figure 7-3: Gap heat transfer coefficients associated to each fuel rod depending on the fuel burnup and linear power and the bulk temperature of the corresponding thermal-hydraulic channel.

The gap heat transfer coefficients MED field (for simplicity called H_{gap}) is then transferred to FLICA4, which exploits it during the following heat conduction computation.

7.1.3 Impact on the Steady-State Calculation

In this sub-section it is assessed the impact of the integration of the H_{gap} model and the Halden conductivity law. The focus is mainly on how this affects the numerical convergence. However, the discrepancies in the solution among the different models are described before, as they give an insight on how much each model weights on the rest of the coupling scheme.

Discrepancies Among the Models

The full coupling scheme including also the burnup dependent thermodynamic variables is solved using the generalised fixed-point with partial-convergences. In particular, the optimal settings found in the previous chapter are adopted ($\alpha = 0.6, N_N = 20, N_{TH} = 40$). The converged results are compared with those obtained with constant H_{gap} equals to 5'000 W/m^{2}K and burnup independent conductivity law. The field of gap heat transfer coefficient is reported in Fig. 7-4 (2D radial section) and in Fig. 7-5a (3D visualization).

It is possible to notice the impact of the loading plan. According to the model, the high-burnup assemblies have a significantly higher H_{gap} thanks to the closure of the gap. The dependency on the linear power is less visible, but still recognizable, especially in terms of power axial profile in the $\boldsymbol{H}_{gap}$ field. The radial effect of the linear power is hidden by the impact of the loading plan. In fact, the fuel thermal expansion is strongly affected by the local linear power. This phenomenon makes the fuel's outer radius grow instantaneously and contributes to the gap closure. In respect of the

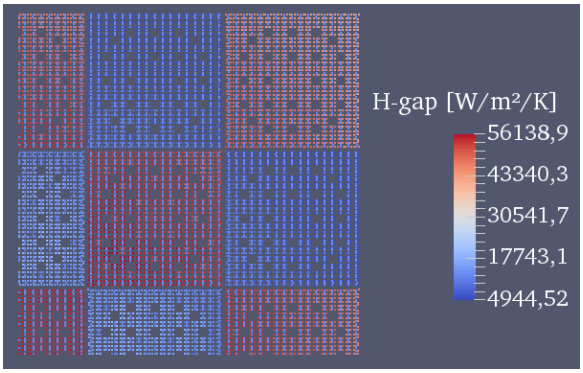

Figure 7-4: Radial section at half of the core height of gap heat transfer coefficients as predicted by the simplified model for the initial steady-state conditions (north east quarter symmetry is used).

fuel temperature, the field obtained with the complete scheme is given in Fig. 7-5c and it should be compared to the previous result, which appears in Fig. 7-5b. Since the heat transfer is significantly improved where the power is higher, the fuel temperature picks are strongly reduced.

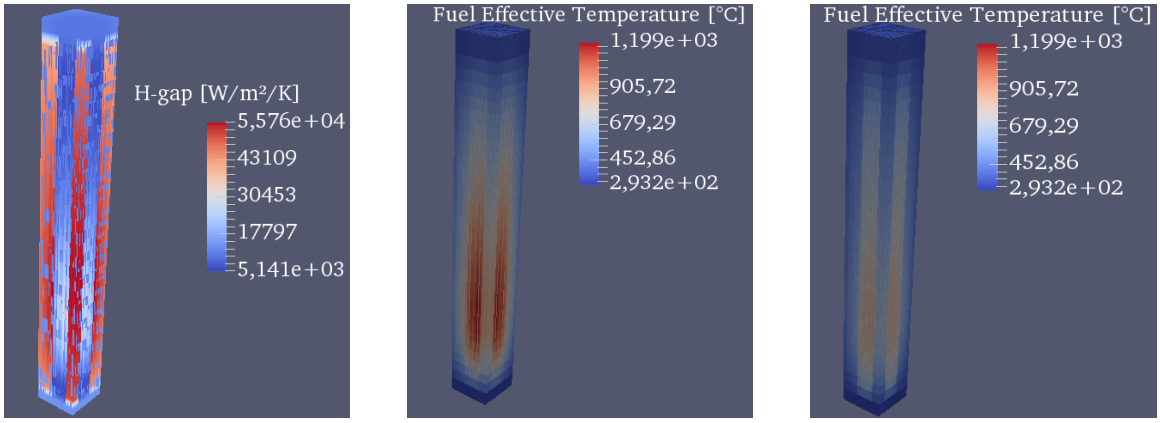

(a) $\boldsymbol{H_{gap}}$ (b) $\boldsymbol{T_f}$, $H_{gap} = const$ and λ_{Ron} (c) $\boldsymbol{T_f}$, H_{gap} and λ_{Hal}

Figure 7-5: Results concerning the integration of a model for the prediction of the fuel gap heat transfer coefficients (H_{gap} appearing on the left). The other two plots concern the comparison of the new estimation of the fuel temperature ($\boldsymbol{T_f}$, H_{gap} and λ_{Hal}) against the precedent one ($\boldsymbol{T_f}$, $H_{gap} = const$ and λ_{Ron}). The results are displayed for the north-east quarter of the mini-core (radial reflector excluded).

The enhancement of the H_{gap} corresponds to a reduction of the fuel effective temperature, especially where the power is high. Therefore, as expected, the power peaking factor increases, the peak of linear power growths from 370.0 to 385.5 W/cm. The current estimation of the power profile is available in Fig. 7-6a and the absolute discrepancies with the simpler model ($H_{gap} = const$ and λ_{Ron}) are reported in Fig. 7-6b. The overall effect on the power distribution is milder than the one on the fuel temperature field, but it is clear that the power moves even more towards the bottom of the reactor.

As already introduced, in steady-state conditions, no power is accumulated in the fuel, for this

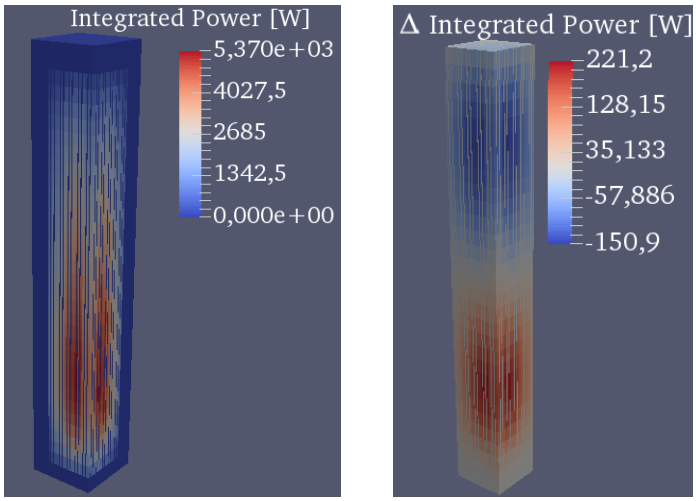

(a) $\boldsymbol{q_f}$, H_{gap} and λ_{Hal} (b) $\Delta\boldsymbol{q_f}$

Figure 7-6: The results are displayed on the north-east quarter of the mini-core. On the left, the prediction of the power including the burnup dependent models for the thermodynamic properties of the fuel (radial reflector included). On the right, the absolute discrepancies with the scheme with burnup independent thermodynamic properties (radial reflector excluded). An additional shift of the power towards the bottom of the reactor is observed.

reason the thermal-hydraulics is independent from the heat conduction: in this case, density variations are only caused by changes in the power distribution. For this reason, the impact on the moderator density is expected to be even lower. A more quantitative assessment of the impact on the fuel effective temperature, on the moderator density and on the power integrated in the fuel is available in Table 7.1.

Table 7.1: Assessment of the discrepancies that raise among the different models for the evolution of the thermodynamic properties.

RMS(Δ_{rel})/MAX(ABS(Δ_{rel})) [%]	$\boldsymbol{T_f}$	$\boldsymbol{\rho_w}$	$\boldsymbol{q_f}$
Simple	-	-	-
H_{gap}	15.65/-27.63	0.13/-0.72	3.76/-8.10
$H_{gap} + \lambda_{Hal}$	15.52/-27.60	0.13/-0.73	3.79/-8.11

The results refer to three models: burnup independent thermodynamic variables ($\bar{H}_{gap}$ =5000 W/m^{2}K), H_{gap} model ($\bar{H}_{gap}$ =26600 W/m^{2}K) and H_{gap} model combined with Halden conductivity ($\bar{H}_{gap}$ =27500 W/m^{2}K). It appears that the impact of the different conductivity laws is rather minor. On the contrary, this simple H_{gap} model shows that taking into account the variation of the fuel gap heat transfer coefficient can lead to significantly different solutions. However, it should be noticed that the constant value chosen for the constant H_{gap} is not even close to the average heat transfer coefficient predicted by the other models, therefore, a more accurate choice would have probably lead to significantly lower discrepancies.

Impact on the Numerical Convergence

The convergence curves corresponding to the three different models for the evolution of the thermodynamic properties are reported in Fig. 7-7. In every case, the generalised fixed-point with partial -convergences is used ($\alpha = 0.6, N_N = 20, N_{TH} = 40$). As expected, the considered H_{gap} model leads to a minor destabilization, while the conductivity law has almost no impact on the convergence slope.

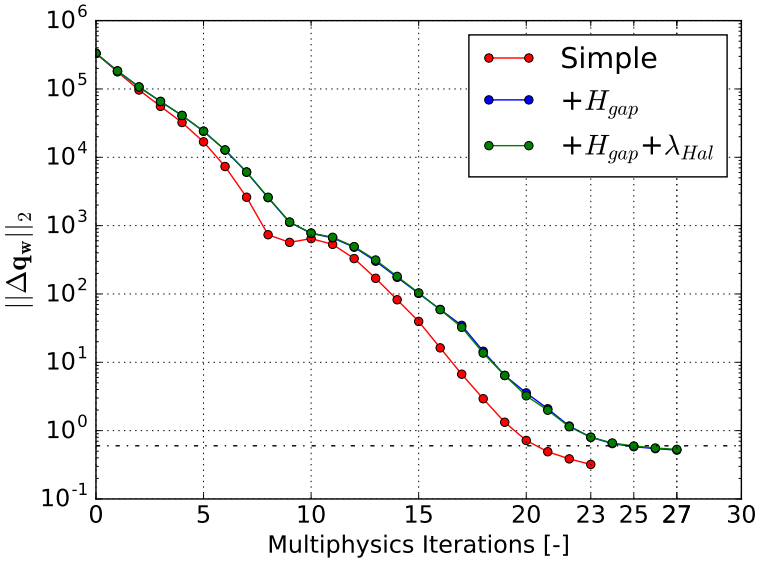

Figure 7-7: Comparison of the convergence process for the three models for the evolution of the thermodynamic properties. Simple refers to constant gap heat transfer coefficient and Ronchi conductivity law. The coupling schemes including the H_{gap} model take four additional multiphysics iterations.

The small destabilization is interpreted as the sum of two factors. From an asymptotic reasoning, the larger the gap heat transfer coefficient the more stable the scheme becomes due to the consequent decoupling of neutronics and heat conduction. In this sense, the increase of the average gap heat transfer coefficient ($\bar{H}_{gap}$) from 5000 to about 27000 W/m^{2}K is expected to have a globally stabilizing effect. On the other hand, from the dynamic point of view the effect is the opposite.

Since the burnup is constant during the calculation and the water bulk temperature has a minor impact on the H_{gap} model, it is possible to focus on the power integrated in the fuel. The model almost behaves like a positive power feedback. By positive power feedback, it is meant that a local power increase would lead to an augmentation of the H_{gap} and vice-versa. The "almost" corresponds to the fact that an increase of the H_{gap}, following a power augmentation, may not cause a decrease of the fuel temperature, as not enough to counterbalance the power increase. Hence, the power may not increase. Anyway, the effect is destabilizing as it hinders the Doppler effect by lowering the sensitivity of the fuel temperature on the local power, but since it interacts with the neutronics only

through the heat conduction operator, strictly speaking it is not a positive power feedback. The destabilizing effect is confirmed by the larger power peaking factor, which is representative of the lower weight of the Doppler effect. In addition, this destabilizing effect decreases in magnitude for high values of the fuel gap heat transfer coefficient as expressed by Eq. (7.3).

$$\Delta T_{gap} := T_{f,out} - T_{c,in} = \frac{q'}{2\pi r_{f,out} H_{gap}} \tag{7.3}$$

Simply by plotting this relation for the considered fuel radius and for a set of fuel linear power, it is possible to visualize that the effect of the H_{gap} on the temperature raise in the gap becomes marginal at high values. The plot is reported in Fig. 7-8. It should be noticed that when the gap heat transfer coefficient never tends to zero. When the heat conduction is very poor (large gap thickness), the radiation heat transfer mechanism is no longer negligible ensuring a minimum value of the heat transfer coefficient.

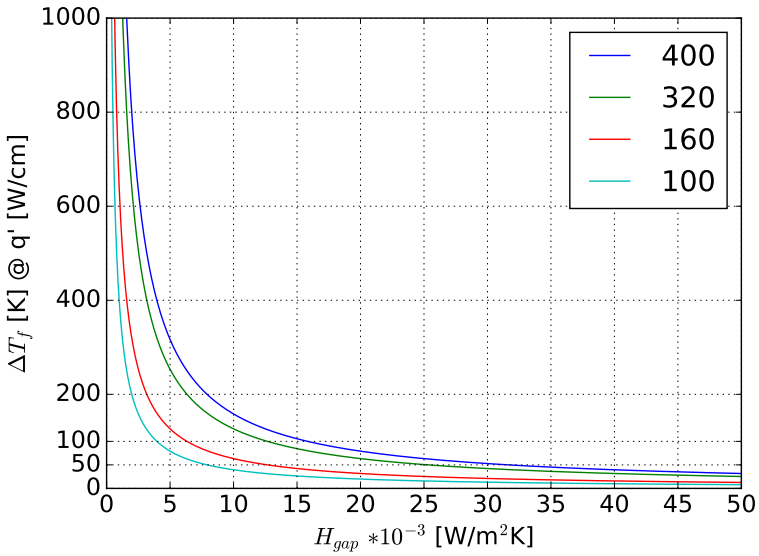

Figure 7-8: Vanishing impact of the fuel gap heat transfer coefficient on the temperature raise in the gap for high values of the coefficient. The plot is repeated for a wide set of linear power.

To summarise, the schemes representing the dynamic behaviour of each operator and in particular of the H_{gap} model is given in Fig. 7-9.

To conclude, the robustness of the algorithm is not compromised by the integration of the H_{gap} model and of the Halden conductivity law.

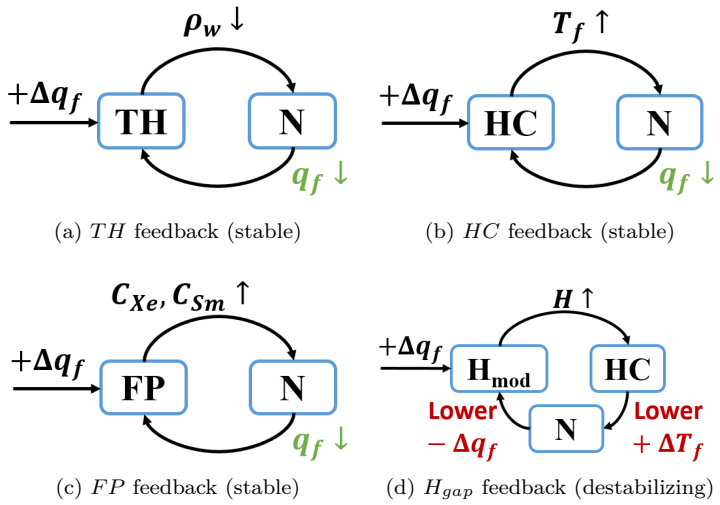

(a) TH feedback (stable)

(b) HC feedback (stable)

(c) FP feedback (stable)

(d) H_{gap} feedback (destabilizing)

Figure 7-9: Dynamic response of the considered operators to a power increase. In particular the H_{gap} model which is included in the heat conduction operator hinders the negative feedback of the latter. Hence, the model adds a destabilizing effect.

7.2 Research of the Target Boron Concentration

As specified in sub-section 1.1.2, during normal operation, the nuclear reactors hardly ever move away from critical conditions. To keep this balance, either the control rods insertion or the boron concentration is managed. For simplicity this work only deals with the modelling of the adjustment of the boron concentration to reach the criticality. For this purpose, simple and effective algorithms are available in literature (e.g. [142]), but no algorithm suitable for a generalised fixed-point with partial-convergences is found. In more general terms, these algorithms may also research the boron concentration that leads to a target reactivity. In this section, an algorithm based on the approximated Newton method is proposed and the impact of this additional problem is analysed.

To include the research of the target boron concentration in the standard Anderson algorithm presented in Section 6.3 would be rather straightforward, but is not investigated in this work.

7.2.1 Definition of the Algorithm

This sub-section is divided in two parts. Firstly, the incompatibility of the standard methods with the generalised fixed-point with partial-convergence are described and after that an alternative is proposed.

Incompatibility of the Standard Methods

Since the boron concentration is assumed homogeneous throughout the entire core, the corresponding research consists just in finding the scalar that leads to a given reactivity (ρ_{target}). Furthermore, the boron efficiency ($b_{eff} := \frac{\partial \rho}{\partial C_B}$ $[pcm/ppm]$) is rather constant, hence, very often

a simple secant method is included in the neutronic operator to find the boron concentration. For instance, Algorithm 4 would become the nested fixed-point presented in Algorithm 6, with $N_B := N(C_B^{k+1}; \boldsymbol{\rho_w}^{k+1}, \boldsymbol{T_f}^{k+1}, \boldsymbol{C_{FP}}^k)$ and with C_B^{k+1} defined as the solution of Algorithm 7. In this example, a secant method is used for the resolution of the problem $f(C_B^*) = \rho(C_B^*) - \rho_{target} = 0$. The derivative of this function ($f(C_B)$) is simply the boron efficiency (b_{eff}), which is approximated by the angular coefficient of the line passing through the last two iterations.

Algorithm 6 Damped fixed-point including the research of the target boron concentration.

Flat power distribution
while $\|\Delta \boldsymbol{x}_i^k\|_2 > \Delta_i * \alpha$, for any i **do**
  $(\boldsymbol{\rho_w}^{k+1}, \boldsymbol{T_f}^{k+1}) = TH(\boldsymbol{q_w}^k, \boldsymbol{q_f}^k)$
  $(\boldsymbol{\tau}^{k+1}, \boldsymbol{q_w}^{k+1}, \boldsymbol{q_f}^{k+1}) = \alpha * N_B(\boldsymbol{\rho_w}^{k+1}, \boldsymbol{T_f}^{k+1}, \boldsymbol{C_{FP}}^k) + (1-\alpha) * (\boldsymbol{\tau}^k, \boldsymbol{q_w}^k, \boldsymbol{q_f}^k)$
  $\boldsymbol{C_{FP}}^{k+1} = FP(\boldsymbol{\tau}^{k+1})$
end while

Algorithm 7 Inner loop based on the secant method for the research of a target boron concentration.

while $j < j_{max}$ **do**
  $k_{eff}^j = N(C_B^j; \boldsymbol{\rho_w}^{k+1}, \boldsymbol{T_f}^{k+1}, \boldsymbol{C_{FP}}^k)$
  if $\Delta\rho_{target}^j = abs(\frac{1}{k_{target}} - \frac{1}{k_{eff}^j}) < \epsilon_\rho$ **then**
    Convergence reached: **break**.
  end if
  $\Delta\rho_{its}^j = \frac{1}{k_{eff}^{j-1}} - \frac{1}{k_{eff}^j}$
  if $j = 0$ **then**
    $b_{eff}^0 = -6\ pcm/ppm$
  else
    $b_{eff}^j = \frac{\Delta\rho^j}{C_B^j - C_B^{j-1}}$
  end if
  $C_B^{j+1} = C_B^j + \frac{\Delta\rho_{target}^j}{b_{eff}^j}$
end while
$C_B^{k+1} = C_B^j$

This method is inherently incompatible with the generalised fixed-point with partial-convergences. In the inner loop, two consecutive estimations of the reactivity are used to find the new boron concentration, for this reason the operator N should not vary too much. As it has been observed in sub-section 6.4.1 for the Anderson method with limited internal iterations, with this strategy it is not simple to bound the variation of the operators. Moreover, a inner loop is expected to affect the balance between the internal convergence of the thermal-hydraulic and neutronic solvers.

Adaptation of the Approximated Newton Method

To solve these incompatibilities, several modifications are implemented. Algorithm 5, presented in Section 6.2, becomes Algorithm 8, in which $N_{B,n_{int.}}^k := N_{n_{int.}}^k(C_B^{k+1}; \boldsymbol{\rho_w}^{k+1}, \boldsymbol{T_f}^{k+1}, \boldsymbol{C_{FP}}^k)$ and C_B^{k+1} is found by Algorithm 9.

Algorithm 8 Damped fixed-point with partial convergences.

Flat power distribution
while $\Delta \boldsymbol{x}_i^k > \Delta_i * \alpha$, for any i **do**
$(\boldsymbol{\rho_w^{k+1}}, \boldsymbol{T_f^{k+1}}) = TH_{m_{int.}}^k(\boldsymbol{q_w^k}, \boldsymbol{q_f^k})$
$(\boldsymbol{\tau}^{k+1}, \boldsymbol{q_w^{k+1}}, \boldsymbol{q_f^{k+1}}) = \alpha * N_{B,n_{int.}}^k(\boldsymbol{\rho_w^{k+1}}, \boldsymbol{T_f^{k+1}}, \boldsymbol{C_{FP}^k}) + (1-\alpha) * (\boldsymbol{\tau}^k, \boldsymbol{q_w^k}, \boldsymbol{q_f^k})$
$\boldsymbol{C_{FP}^{k+1}} = FP(\boldsymbol{\tau}^{k+1})$
end while

In this context, $Bool_{conv,N,k}^k$ is the boolean that verifies the internal convergence of the neutronic solver on the multiplication factor and δ_B is a small perturbation of the boron concentration, which is used to estimate the boron efficiency. The value of δ_B is typically fixed to 1 ppm along the entire process.

Algorithm 9 Additional approximated Newton method for the research of a target boron concentration.

$\Delta^k k_{target} = (\frac{1}{k_{eff}^k} - \frac{1}{k_{target}})$
if $Bool_{conv,N,k}^k$ **and** $abs(\Delta^k k_{target}) < \epsilon_{\rho,target}$ **then**
$\Delta^k k_{MP} = (\frac{1}{k_{eff}^k} - \frac{1}{k_{eff}^{k-1}})$
if $abs(\Delta^k k_{MP}) < \epsilon_{\rho,MP}$ **then**
set neutronic reference state
$C_{B,pert}^k = C_B^k + \delta_B$
$k_{pert}^k = N(C_{B,pert}^k; \boldsymbol{\rho_w^{k+1}}, \boldsymbol{T_f^{k+1}}, \boldsymbol{C_{FP}^k})$
restore neutronic reference state
$b_{eff} = \frac{(1/k_{eff}^k - 1/k_{pert})}{\delta_B}$
$C_B^{k+1} = C_B^k + \frac{\Delta^k k_{target}}{b_{eff}}$
else
$C_B^{k+1} = C_B^k$
end if
else
$C_B^{k+1} = C_B^k$
end if
$k_{eff}^{k+1} = N_{n_{int.}}^k(C_B^{k+1}; \boldsymbol{\rho_w^{k+1}}, \boldsymbol{T_f^{k+1}}, \boldsymbol{C_{FP}^k})$

The main difference is that the critical boron research is not performed at each multiphysic iteration, but only under three conditions. Two requirements are imposed on the previous multiphysic iteration, the internal convergence on the k_{eff} has to be reached and the current reactivity should not be the target one. The third criterion to be met concerns the reactivity difference among the last two multiphysic iterations, its value should be smaller than a given limit. Another important difference lies in the fact that, in this case, the update of the boron concentration is linearly inserted in the algorithm, instead of creating a nested loop. Moreover, to compute the state with the perturbed boron concentration, the full internal convergence on the multiplication factor is imposed to the solver. This calculation does not impact the solver initialisation, as the internal state of the solver is saved before and restored afterwards.

Requiring the internal convergence of the neutronic solver on the k_{eff} and imposing a limit on the variation of the reactivity between the two previous iterations is necessary to eliminate the contribution of the other multiphysic variables to the reactivity change from the last computed neutronic result. In this way, the boron research is partly decoupled from the rest of the problem, but, this is not detrimental because it constitutes a much simpler numerical problem than the rest. Thanks to the almost constant boron efficiency, the target concentration is found in very few Newton extrapolations. Furthermore, the convergence on the effective multiplication factor is normally reached way before than the convergence on the flux or on the other multiphysic variables, hence, the boron research starts early in the process. The alternative would be to release the constraint on the multiphysic reactivity change and to compute the new reactivity before performing the boron research. In order to limit the impact on the partial-convergences the reference state should be set before performing the estimation of the current reactivity. For this reason, even if this alternative would allow to start the boron research earlier in the process, it is expected to perform worse as more neutronic iterations would be computed and rejected due to the set and restore mechanism.

The approximated Newton offers two main advantages. The first is that it allows to estimate the new boron efficiency for the current solution $(C_B^k; \boldsymbol{\rho_w}^{k+1}, \boldsymbol{T_f}^{k+1}, \boldsymbol{C_{FP}}^k)$, instead of using a previous estimation. The second one is that the computation of the perturbed state generally requires very few iterations, as it is expected to be similar to the reference state. The algorithm is tested in the following sub-section.

7.2.2 Impact on the Steady-State Calculation

Even if, for safety reasons, the allowed range of boron concentration used in commercial PWRs is narrower, for numerical simulations a typical constraint on the boron concentration is that the minimum value should be larger than 0.1 ppm and the maximum one should not exceed 2000 ppm. This is also the range of values included in the cross-sections. For the conditions defined in the case study, before starting the irradiation, the reactor is significantly overcritical even with the maximum boron concentration (consequence of the absence of control rods and of the loading plan). Due to this excess of reactivity, it is chosen to compute the reactivity corresponding to 1600 ppm and to set it as the target. The effective multiplication factor corresponding to a boron concentration of 1600 ppm is 1.06903 ($\rho = 6457$ pcm).

As already mentioned, the boron concentration is assumed to be homogeneously distributed in the core, but since it represents the proportion of boric acid in the water, where the moderator is denser the number density of the boron isotopes is larger. For this reason, the impact of the boron concentration on the power distribution depends on the moderator density field. The power integrated in the fuel for the two boron concentrations is reported in Fig. 7-10. The higher boron concentration gives a strong contribution to the axial flattening of the power profile, whose peak

decreases and moves towards the centre.

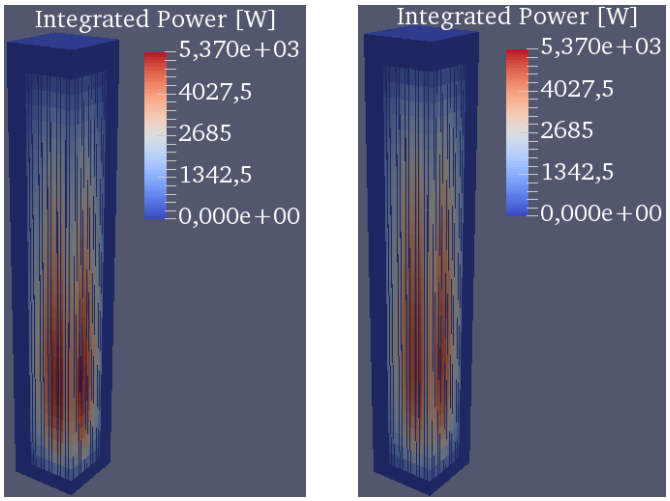

(a) 600*ppm* (b) 1600*ppm*

Figure 7-10: Comparison of the power distribution for two boron concentrations.

The algorithm is tested researching the target boron concentration (known to be 1600 ppm) for the case study, starting from 600 ppm, which corresponds to a rather poor guess that challenges the robustness of the scheme. The results are available in Fig. 7-11.

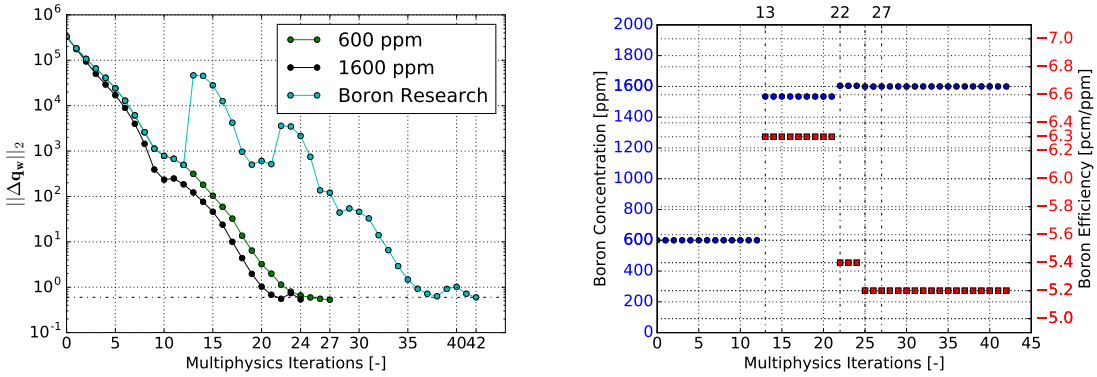

(a) Convergence slope (b) C_B, b_{eff}

Figure 7-11: On the left, comparison of the convergence slope with constant boron concentration and with the research of the target boron concentration. On the right, the boron concentration and the boron efficiency are reported for each multiphysic iteration. The vertical dash-dotted lines point out the iterations in which the research of the target boron concentration is carried out.

In particular, it appears that the global convergence rate is significantly impacted by the research of the target boron concentration. The number of multiphysic iterations required increases from 27 to 42 and the boron research is performed four times (at the iterations 13, 22, 25 and 27). On the other hand, as shown by Fig. 7-11b, the scheme is rather robust as the boron concentration converges

very close to the target value already at the very first iteration. To include the boron research in the Anderson algorithm would probably have a smaller impact on the global performance. However, it is worth noticing that this simulation is still about four times faster than the calculation presented during the previous chapter that uses the optimised standard Anderson method (no H_{gap} nor boron research). Therefore, the efficiency of this algorithm is still satisfactory even for such a challenging choice of the initial boron concentration.

As expected, the boron efficiency is rather constant, even if it decreases for large concentrations. This reduction of efficiency simply corresponds to the effect on the energy spectrum of the neutron flux. Boron-10 is a thermal absorber and large concentrations of this isotope can significantly reduce the thermal neutron flux in the reactor and consequently its efficiency.

Looking at the convergence of the residual, it is clear that after performing the first boron research, the convergence process has to restart almost from the beginning: at iteration thirteen the norm of the residual is comparable to the one previously reached at iteration four. The increase of the norm of the residual is connected to the difference in the boron concentration, such a large gap is observed only at the very first target boron concentration research. Furthermore, along the depletion calculations the typical change in the boron concentration is expected to be much smaller, hence, the algorithm is considered adequate to the task.

7.3 Depletion Calculations

As specified in the introduction, the depletion calculations aim at reproducing the reactor behaviour along irradiation. The approach adopted in this work deals with this problem as a sequence of steady-states characterized by evolving isotopic concentrations and core operating conditions. In this section, a multiphysic time evolution scheme is defined and tested on a simple scenario.

7.3.1 Definition of the Multiphysic Time Evolution Scheme

To understand how the multiphysics affects the time evolution scheme, it is important to review the basic elements of a conventional algorithm. First of all, the depletion problem at a given time (t_i) consists in the research of the number densities of the particularized isotopes after a time step (Δt_i). In fact, it should be recalled that a different treatment is used for a set of isotopes (called particularized) that are separated from the rest (kept as number densities and microscopic cross-sections), which is assembled in a unique macro-isotope as described in sub-section 1.3.1. For what concerns the macro-isotope, the problem simply deals with the computation of the local burnup increase during Δt_i, as the macroscopic cross-sections are obtained by interpolating on this quantity. On the contrary, for what concerns the particularized isotopes, the Bateman equations have to be solved. At the end of sub-section 1.3.1 a time evolution scheme characterized by a combination of

polynomial extrapolation of the neutron flux and reaction rates within a time step and a predictor-corrector method is described. In MPACT, a similar time evolution scheme is implemented, but it uses a constant approximation of the neutron flux and of the reaction rates within the time steps and a different variant of the predictor-corrector. This scheme is outlined here, for the complete description please refer to [12]. In this case, the corrector step is always performed. The predicted number densities fields are produced by the depletion calculation made using the scalar flux and the reaction rates at the beginning of the time-step. After that, these number densities are used to perform a steady-state calculation and obtain new scalar flux and reaction rates. Afterwards, the corrected number density fields are obtained from the depletion calculation made with the newly computed neutronic quantities and the initial isotopic concentrations. Finally, the number densities of the new time step are obtained as the average of the predicted and the corrected ones. In addition, to ensure the convergence, the substep method is applied. The time step is divided into a sufficient number of sub-steps for which no steady-state computations is carried out, but the power is renormalized to account for the variation of the fission cross-sections. This method, firstly introduced by [245] allows to performs larger time steps for a given number of steady-state calculations. A schematic of this predictor-corrector evolution scheme is available in Fig. 7-12.

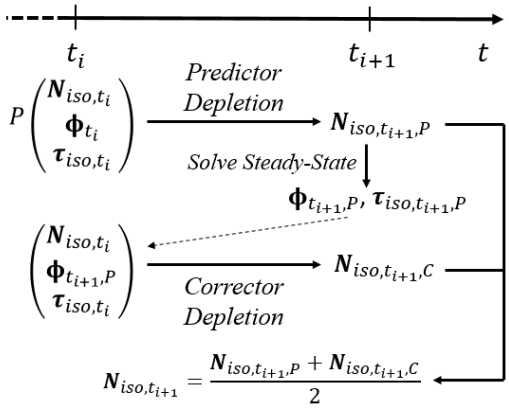

Figure 7-12: The predictor-corrector scheme using a constant neutron flux and reaction rates approximation within each time step described in [12] for MPACT.

It is important to underline that in multiphysic simulations, the resolution of the steady-state does not simply deal with a neutron transport calculation, but rather with calculation schemes like the one described in this work. Moreover, in this context, the reaction rates vary within a time step, because the cross-sections evolve also according to the different temperature and density fields. Due to the lack of flexibility of the considered depletion solver, it is not possible to perform the polynomial interpolation and the predictor-corrector (as described in sub-section 1.3.1) with a generic steady-state calculation scheme like the one considered for this work. What is possible is to perform is a single-step depletion procedure (no polynomial interpolation and no predictor-corrector) and this

fundamental operation can be used to reconstruct similar algorithms outside of the perimeter of the specialised codes.

A simple time evolution scheme is implemented. It deals with the alternation of steady-state computations using the average working conditions along the time step (namely the total power) and a depletion calculation at constant neutronic variables. The time step is divided in two parts, by default equal (half and half), to combine the evolution of the particularized isotopes (referred to as micro-evolution) with that of the macro-isotope (called macro-evolution). The micro-evolution is performed for the first portion of time, then the macroscopic cross-sections are interpolated for the burnup corresponding to the end of the entire time step and finally the depletion of the particularized isotope is completed for the remainder of time step. A constant time step size is considered and no control test is done.

7.3.2 Application to a Constant Power Irradiation Scenario

The irradiation scenario corresponds to constant operating conditions, as defined in the case study, for a period of 365 days. The first steady-state calculation is also used to set the equilibrium fission products concentrations. For the following steps, the research of the equilibrium concentration is completely switched off as their evolution is computed for the considered time steps.

For the first test, a large time step is chosen in order to challenge the boron research algorithm with large variations of the boron concentration. Due to the absence of convergence check on the time step size, it should be seen just as a numerical test. The irradiation period is divided into ten points, corresponding to nine time steps of about 40.6 days and 1.4 MWd/kg each. To assess the impact of the boron research on the convergence process, the steady-state scheme including all the models is compared to that obtained by switching off the boron research. The results appear in Fig. 7-13a, while the boron concentration at each step is reported in Fig. 7-13b. For simplicity, in this case, the initial boron concentration is directly set to 1600 ppm.

Even if a large time step is considered and a wide range of boron concentrations is explored, the boron research always reaches the convergence reassuring about the robustness of the method. On average, the scheme with the research of the target boron concentration requires about 13.6 additional multiphysic iterations per each steady-state corresponding to 17 % of the total. Therefore, also in terms of efficiency, the performance of this algorithm is judged as satisfactory. The convergence slopes show that an increasing number of multiphysic iterations is required to solve each steady-state, this aspect is analysed in the following paragraph.

In order to find a small enough time step size for convergence, three time discretization are tested (10, 50 and 100 time steps), the results are available in Fig. 7-14. Four variables are considered (C_B, q'_{max}, $T_{f,max}$ and $H_{gap,max}$) along the irradiation period.

Comparing the coarse meshing with the intermediate one confirms that this time step is too

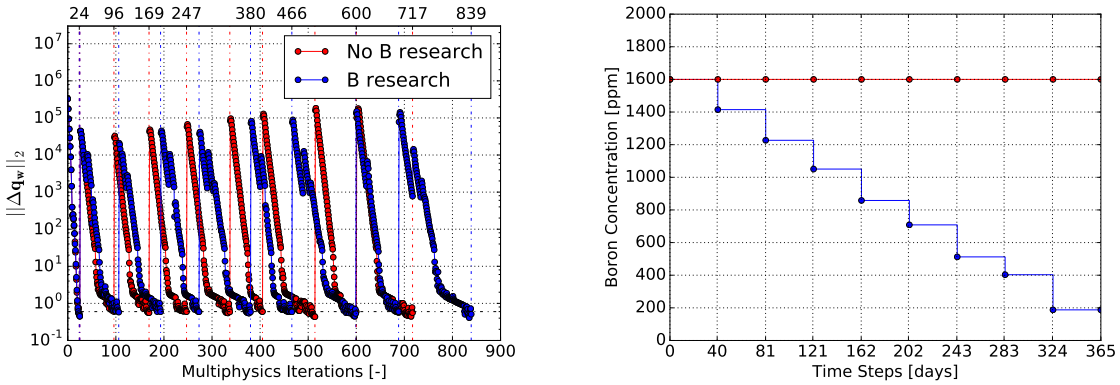

(a) Convergence slopes

(b) $C_B(t_i)$

Figure 7-13: Assessment of the impact of the research of the target boron concentration on the convergence of the depletion calculation. A coarse time step (40.6 days) is considered. The vertical dash-dotted lines are used to underline the multiphysic iteration at which the steady-state scheme converges.

large for this depletion calculation. The significant discrepancies found at the end of the cycle underline the importance of ensuring the convergence of the time discretization. The scheme using the intermediate number of time steps is found to be consistent with the most refined computation. As expected, the maximum linear power decreases along irradiation due to the larger burnup increase in the regions where the power is higher. The maximum fuel effective temperature also decreases significantly as it is largely related to the linear power. With respect to the maximum fuel gap heat transfer, the discontinuity in the derivative corresponds to a change of the location of the peak value. Initially, the maximum H_{gap} is located in the fuel rods that are loaded at high burnup. However, after the gap closure, the heat transfer coefficient degrades due to the presence of gaseous fission products with lower conductivity. This appears in Fig. 7-14d approximately during the first 200 days. Afterwards, the peak moves to a fuel rod with lower burnup, whose gap heat transfer coefficient still benefits from the burnup increase.

In Fig. 7-13a, it is possible to notice also that the number of multiphysic iterations required to compute each time step is significantly larger than those required for the first steady-state and that this number increases along irradiation. It seems that the steady-states are characterized by an increasingly different isotopic concentration, hence starting from the last computed solution does not improve much the efficiency of the scheme. To explore this aspect, the convergence of the three depletion calculations is analysed. In Fig. 7-15, the equivalent computing time per each complete steady-state calculation is reported. In Fig. B-6, in the appendix, the same plot is produced for the number of multiphysic iterations. Since, the same limits on the single-physic iterations are imposed, this two figures are very similar.

From the results it emerges that only for the coarse time discretization, the equivalent computing

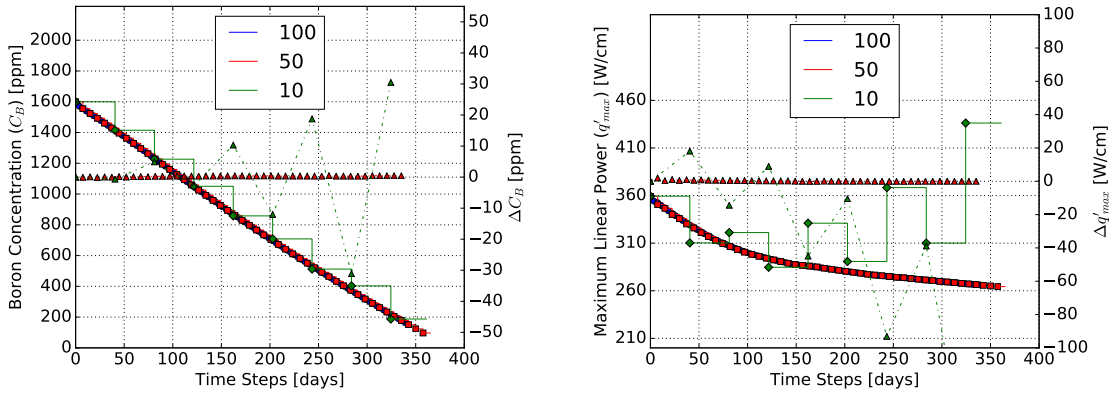

(a) C_B

(b) q'_{max}

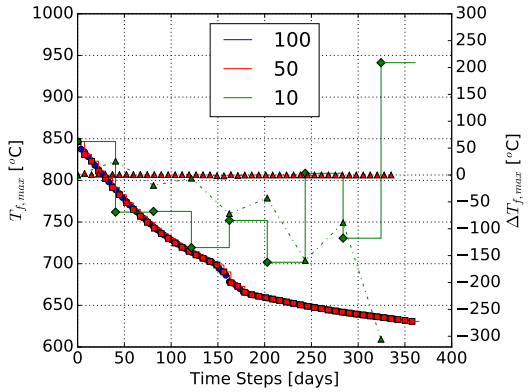

(c) $T_{f,max}$

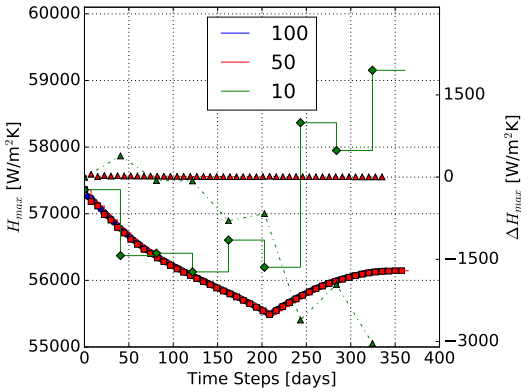

(d) $H_{gap,max}$

Figure 7-14: Convergence analysis of the full depletion calculation scheme on the boron concentration, the maximum linear power, the maximum fuel effective temperature and the maximum value of the fuel gap heat transfer coefficient. Three time discretization are tested, by dividing the irradiation period in 10, 50 and 100 equal time steps. Triangular markers are used to show the discrepancy of the considered discretization (indicated by the color) with respect to the finer one, their values appear on the y-axis on the right. The intermediate level of refinement is judged as satisfactory.

time per steady-state (or equivalently in the number of multiphysic iterations) increases significantly along the irradiation period. Therefore, it is supposed that this trend is caused by the too coarse time discretization and the consequent divergent behaviour. Comparing the average equivalent computing time per steady-state of the three different time discretizations, it decreases with more refined time meshes. However, the equivalent calculation time of the entire depletion calculation follows the opposite trend as the reduction in unit time is insufficiently large. This trade-off is analysed more into details in Fig. B-7, in the appendix. This rather predictable result confirms the interest of using an efficient depletion scheme, which can allow to reduce the number of steady-states to be computed for the depletion calculations over a given irradiation period.

While, ten time steps corresponds to the lowest computing time, this time refinement is not suf-

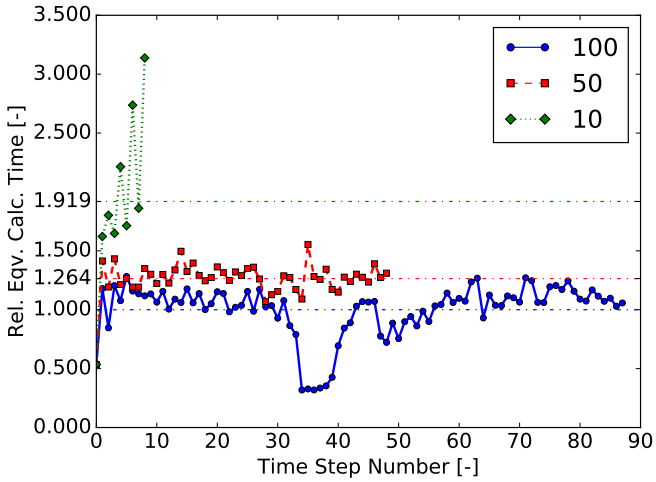

Figure 7-15: Relative equivalent calculation time required for each time step for the three considered time discretizations (10, 50 and 100 equal time steps). Every equivalent calculation time is divided by the minimum average value.

ficient. The full depletion calculation scheme, with a sufficiently small time step, allows to compute a large range of local variables along the considered irradiation period. For instance, in Fig. 7-16, the evolution of the power distribution is reported for 0, 200 and 365 days from the beginning of irradiation.

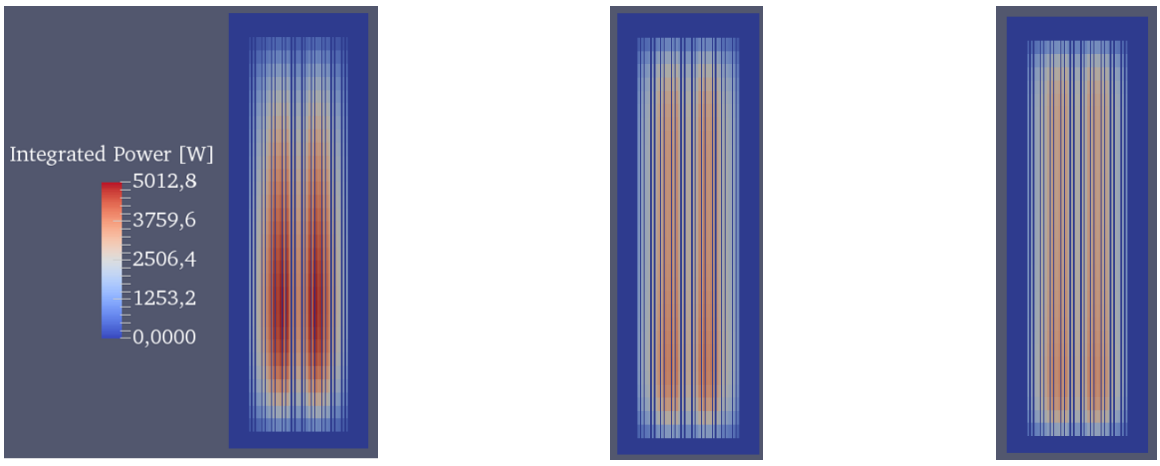

(a) 0 days (b) 200 days (c) 365 days

Figure 7-16: Evolution of the power distribution along irradiation. Three time steps are considered after 0, 200 and 365 days.

From these axial sections of the power, it is even more visible the flattening effect of the fuel depletion. The radial sections are available in the appendix, in Fig. B-8. To measure the impact of the fuel gap heat transfer coefficient model on the power distribution, the discrepancies with the full calculation scheme without H_{gap} model are computed for the same irradiation times. The results

are reported in Fig. 7-17. It should be noticed that the comparison reported in Fig. 7-17a differs from that of Fig. 7-6b because in this case the boron research is also included.

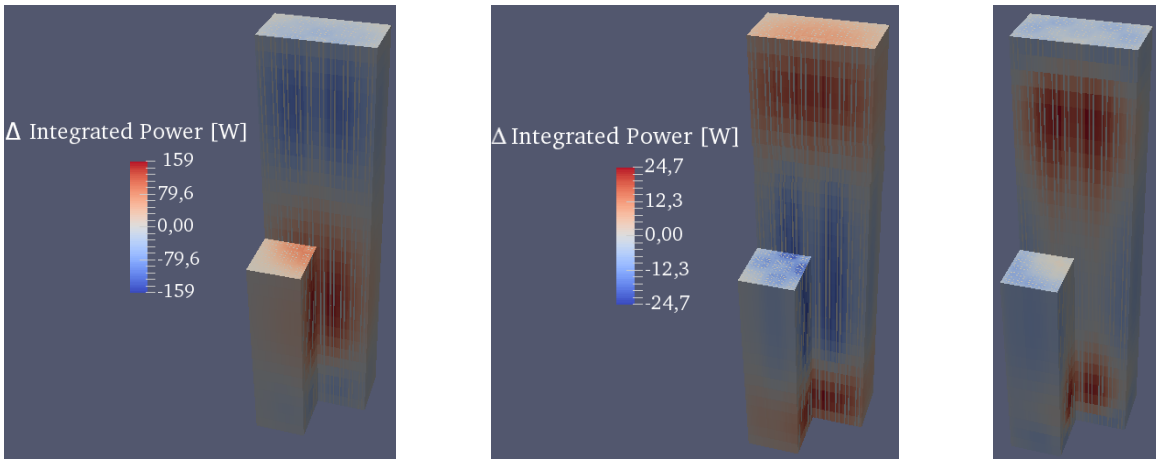

(a) 0 days (b) 200 days (c) 365 days

Figure 7-17: Discrepancies on the 3D power distribution between the coupling scheme with and without H_{gap} model for three different irradiation times. Fig. 7-17b and 7-17c share the same color scale different from that of Fig. 7-17a.

It appears that the discrepancies between these two modelling choices tend to decrease significantly along irradiation. In relative terms, the maximum error at BOC is -6.3 %, while at the EOC it is 1.2 %. Interpreting Fig. 7-17, this could be explained simply by the faster depletion occurring at the bottom of the core when including the H_{gap} model.

The preliminary tests on this simple irradiation scenario are satisfactory. For the future improvements, the priority is to implement a convergence check to ensure that the time step is sufficiently small. In addition, without a lot of effort, the substep method could be included to reduce the number of required time steps. Finally, the complete algorithm could be tested on a more complex irradiation scenario like the one presented in the BEAVRS benchmark [26].

7.4 Chapter Conclusion

In this chapter, the coupling scheme is extended to add the possibility of using burnup dependent thermodynamic properties (conductivity law and fuel gap heat transfer coefficient simplified model). The update of the conductivity law has shown to have a minor impact on the considered variables. On the contrary, the fuel gap heat transfer coefficient simplified model strongly affects the predicted temperature and power fields, underlining the importance of correctly modelling this coefficient. On the other hand, the impact on the numerical scheme corresponds to a minor destabilization. Afterwards, an algorithm for the research of a target boron concentration suitable for the generalised fixed-point with partial-convergences is proposed. The robustness and the efficiency of this scheme is

tested on the steady-state case study producing satisfactory results. Finally, a simple time evolution scheme including all the previously mentioned models is implemented and successfully tested on a constant power irradiation scenario.

Chapter 8

Conclusions

8.1 Research Problem

This thesis deals with the development of a multiphysic depletion calculation scheme for the prediction of local (fuel pin cell resolution) design parameters of PWRs. The multiphysic problem is modelled by combining a set of pre-existing specialised codes of neutronics, thermal-hydraulics, heat conduction and isotopic depletion. Within this context, some of the fundamental questions to be answered concern the choice of the most appropriate combination of models. Among the key elements to be considered, there are the modelling scales, the target accuracy for each variable and the consequent computing time. Depending on the sensitivity of a target variable on the others, different degrees of simplification could be introduced to increase the efficiency of the scheme. Another important aspect concerns the definition of how the selected models are combined together (i.e. the coupling scheme). Ultimately, these elements defines the global robustness and efficiency of the calculation scheme.

8.2 Main Results

The depletion of the core is modelled as a sequence of steady-state calculations interconnected by the evolving isotopic concentrations and operating conditions. For this reason, the development of the steady-state calculation scheme is a major step of the thesis. Initially the focus is set on the neutronic, thermal-hydraulic and heat conduction models. Basing on the analysis of the state of the art (see Section 2.1) and on the tests performed on a simplified case study (refer to Chapter 5 and in particular to Table 5.4), it is decide to use a two-step neutronic model with pin-cell homogenization together with subchannel thermal-hydraulics and heat conduction for all the fuel rods. More into details, the neutronic model is derived from APOLLO3® code. The MOC solver (TDT) is used for

the lattice calculations, the SP_3 (MINOS) with 8 energy groups for the core calculations and the SPH algorithm as equivalence technique. The 3D, four equations and single-field solver of FLICA4 is used for the thermal-hydraulics. The same code is also used to model the 1D-radial heat conduction in each fuel rod axial slice.

For what concerns the numerical method for the resolution of the steady-state problem of neutronics, thermal-hydraulics, heat conduction and research of the equilibrium fission products, the damped fixed-point and the Anderson algorithm are tested. The results confirm the higher robustness and efficiency of the second method (see sub-section 6.3.2 and in particular Fig. 6-8a). A variant of the fixed-point based on the partial-convergences is deeply analysed for the specific coupling scheme considered so far (see section 6.2 and in particular Fig. 6-2). This method has proven to overcome the major robustness problem presented by the standard damped fixed-point and, for an appropriate choice of parameters, to be significantly more efficient than the Anderson algorithm. Therefore, a generalization of the Anderson method based on partial-convergences is proposed. Preliminary results confirm the interest on this new variant (refer to sub-section 6.4.2). In terms of efficiency, the first tests place this new algorithm in between the standard Anderson method and the generalised fixed-point with partial-convergences. On the other hand, in terms of robustness and sensitivity to the input parameters, it is expected to perform better than the generalised fixed-point with partial-convergences. For the rest of this work the generalised fixed-point with partial-convergences is kept (α =0.6, N_N =20, N_{TH} =40).

To account for the evolution of the fuel thermal-mechanical properties along irradiation, a simplified gap heat transfer model is included in the coupling scheme. For the considered case study, including this model has a large impact on the target variables (refer to Table 7.1), which reinforces the importance of accounting for this phenomenon in such a multiphysic coupling scheme. As required by the depletion calculation scheme, the algorithm for the research of the target boron concentration is implemented. To obtain a method compatible with the generalised fixed-point with partial-convergences, a variant of the approximated Newton algorithm is proposed. Basing on two simple tests (see Fig. 7-11 and 7-13), this algorithm is judged as satisfactory both in terms of robustness and efficiency. Finally, a simple time evolution scheme is implemented. Its application on a constant power irradiation scenario has allowed to successfully test the combination of all the models mentioned so far in a unique multiphysic depletion calculation scheme (refer to Fig. 7-14).

8.3 Discussion

The discussion section is divided into three parts respectively dealing with the selection of the models for the steady-state simulations, the numerical optimization of the steady-state scheme and the choice of the models for the depletion simulations.

8.3.1 Models Selection for Steady-State Simulations

Interpretation

Both the choice of solving the multiphysic problem through the combination of specialised codes and that of treating the depletion calculations as a sequence of interconnected steady-states represent the most common solution found in literature (e.g. [49, 50] and [36, 38, 51]).

With respect to the selection of the neutronic, thermal-hydraulic and heat conduction models, the interest of testing this combination of modelling scales emerges mainly from the literature review. In fact, this approach is meant to fill the space between the faster running schemes based on the pin-power-reconstruction [36, 37], which rely on a larger number of hypothesis and the *high-fidelity* ones based on the direct neutronic simulations with massive parallelization [38, 39], which require a larger computing power. More into details, the good performance of the SP_N model was somehow predictable as the homogenization phase significantly reduces the anisotropy of the problem, hence, it limits the benefits of resorting to more complex core solvers. In respect of the choice of subchannel thermal-hydraulics and heat conduction for all the fuel rods, it is totally in line with the literature. Indeed, the selection of these modelling scales is shared by the vast majority of the coupling schemes found in literature (as it appears in sub-sections 2.1.2 and 2.1.3).

Recommendations

During the considered analyses, the combination of specialised codes has not hindered the stability of the calculation scheme. In the current coupling scheme, without a large effort, it is possible to switch the specialised models, by selecting another solver or even another computing code. For these reasons, at least for similar applications, it is just simpler to rely on pre-existing specialised solvers. For what concerns the two-steps neutronic modelling, due to lack of comparisons with the alternatives, it is difficult to give recommendations. Nevertheless, the cross-section homogenization for a set of parameters allows to significantly simplify the neutronic calculations during a multiphysic iteration. Therefore, the deployment of two-steps neutronic models is especially suitable in the context of systematic studies requiring repeated simulations of a reactor core.

8.3.2 Numerical Optimization of the Steady-State Scheme

Interpretation

As introduced in the second chapter, the damped fixed-point and the Anderson methods are two of the most widespread algorithms used for the resolution of this type of coupled problems. The higher robustness and efficiency of the Anderson method as compared to the fixed-point is rather predictable due to the nature of these algorithms. Furthermore, similar results are in agreement with what found in [141]. For what concerns the generalised fixed-point with partial-convergences, this

method is rather widespread in the industry, but not so popular in literature. Studies concerning this algorithm are hard to find in literature, the closest one, dealing just with the control on the limits of neutronic iterations within a small range of values, is given by [125]. Therefore, even if the presented results are definitely solvers dependent, they are helpful to better understand the dynamics of partial-convergences and the range of applicability of this method. It was rather unexpected that this method could reach such a high efficiency: up to 15 times faster than the standard fixed-point with optimal damping and 7 times faster than the optimal standard Anderson algorithm. The robustness of the results is even reinforced by the large number of tests, which in case of convergence are in good agreement among each others. In respect of the proposed variant of the Anderson method based on partial-convergences, the fact that even with unoptimised settings it allows to achieve the result in 1.5 times shorter time than the best standard Anderson method is rather promising. Moreover, this result gives positive expectations about the sensitivity of this method on the choice of the new parameters (sequence of internal precisions and switching criteria).

Recommendations

Basing on the results observed so far, the generalised fixed-point with partial-convergences represents the most recommended algorithm for this solver combination and for case studies similar to the considered one. The suggested setting is to limit the neutronic and thermal-hydraulic iterations to few tens and to apply a damping factor about 0.6. In case of very large time cost required for the data manipulation and exchange during each multiphysic iteration, it should be considered to set larger limits on the single-physic iterations. In case robustness is strongly preferred over efficiency, the recommended method is the standard Anderson method. In this case, it is suggested to use a M parameter around 3, no damping and to not apply the optional extension provided by Scipy. This is somehow coherent with the recommendation of Anderson himself for a general application [139]. The normalisation of the components of the unknown vector is a necessary step for the efficiency and stability of the method. Although very promising, the proposed Anderson with partial-convergences needs further exploration to compete with the other more consolidated alternatives.

8.3.3 Models Selection for Depletion Simulations

Interpretation

With respect to the integration of the fuel gap heat transfer coefficient simplified model, such a large impact on the prediction of the power distribution was somehow unexpected for the author. *High-fidelity* simulations adopting a constant value for this coefficient do not exhibit so large discrepancies against the measured power distribution (e.g. [127, 134]). On the other hand, this might correspond to a more adequate choice of the constant fuel gap heat transfer coefficient. Another explanation

is linked to the case study, the impact of this model on the power distribution is expected to be larger in case of smaller reactors. In fact, higher power peaking factors contribute to increase the discrepancies in the value of this coefficient, which in turn contrasts the flattening of the power shape due to the Doppler effect. Moreover, these discrepancies have shown to attenuate along irradiation. Ultimately, the results are rather in line with the sensitivity analysis given by [10].

For what concerns the research of the target boron concentration, the tests on its efficiency and robustness lack of a comparison with conventional alternatives. For instance, to research the target boron concentration with the Anderson method would be rather straightforward and potentially efficient. Nevertheless, the proposed algorithm is not expected to significantly undermine the robustness of the scheme and its global efficiency is satisfactory. In fact, the computation of the full steady-state problem (including the gap heat transfer model and the boron research) with the generalised fixed-point with partial-convergences is about four times faster than the resolution of the simple steady-state (without these extensions) with the optimized standard Anderson algorithm.

The implemented time evolution scheme is rather basic, but with little effort it could be refined. The individuated developments are widespread and relatively straightforward to implement. Overall, the global scheme successfully and efficiently combines a set of advanced models and it constitutes a powerful tool in support of the fine-scale design and safety analyses of PWRs along irradiation.

Recommendations

Including the fuel gap heat transfer model has demonstrated to have a large impact on the power distribution. For this reason, it is highly recommended to account for the evolution of this coefficient in a multiphysic depletion calculation scheme. It is expected to be particularly important in case of fuel pin cell calculations, where each fuel rod slice is characterised by its own conditions (e.g. linear power, burnup and coolant temperature). The use of simplified models calibrated on the results of specialised solvers, like the one adopted in this thesis, seems promising. Methodologies providing also the uncertainties associated to the calibration are also very recommended (e.g. [209]). In any case, the validation against experiments and reference simulations is a necessary step to reinforce their credibility.

For what concerns the algorithm for the research of the target boron concentration, its overall performance is rather satisfactory, hence, it is a suitable method to combine with the generalised fixed-point with partial-convergences. Finally, as expected and as confirmed by Fig. 7-15, it is very important to reduce as much as possible the number of time steps to compute in a depletion calculation. Therefore, methods that can allow to perform larger time steps with a marginal cost, like the substep [245], are strongly recommended to increase the efficiency of the depletion algorithm.

8.4 Perspectives

From the point of view of the author, this research has led to a large number of open questions and different perspectives. The highest priority is given to the implementation of a predictor-corrector method to ensure the convergence of the depletion calculation. Alongside with that the substep method appears as a simple and effective solution, hence, it should be included in the time evolution scheme. Afterwards, it would be extremely important to strengthen the calculation scheme by testing it on an international benchmark like the BEAVRS [26]. Alternatively, a simpler test would be to include a fuel performance code in the coupling scheme to measure the discrepancies and the time saving introduced by the simplified fuel gap heat transfer model.

For what concerns the numerical optimization, it would be particularly interesting to test the proposed Anderson algorithm with partial-convergences for different settings and a range of case studies (mainly varying the size of the domain and the operating conditions). In a similar way, also the generalised fixed-point with partial-convergences should be tested to analyse its performance on different case studies. Moreover, the dependency on the limits on the single-solver iterations could be further analysed to question whether it is possible to somehow predict the optimal settings or at least to better understand the numerics behind this problem.

Appendix A

Tables

Table A.1: Performance assessment under isothermal conditions of the neutronic models in terms of multiplication factor, reactivity difference and computing times ratio. Both *S8* calculations are performed with twenty processors, whilst the others with only one.

	S8-30g	*S8-20g*	*SP3-8g*	*Diff.-2g*	*Diff.-2g (quarter)*
k_{eff} [-]	1.18672	1.18596	1.18589	1.18172	1.18149
$\Delta\rho$ [pcm]	-	-54	-59	-357	-373
t_i/t_{ref} [%]	100	63	3.7	0.15	0.02

Table A.2: Performance assessment of the neutronic models in the coupling scheme in terms of multiplication factor, reactivity difference and computing times ratio. Both *S8* calculations are performed with twenty processors, whilst the others with only one.

	S8-30g	*S8-20g*	*SP3-8g*	*Diff.-2g*	*Diff.-2g (quarter)*
k_{eff} [-]	1.17768	1.17689	1.1768	1.17250	1.17223
$\Delta\rho$ [pcm]	-	-57	-63	-375	-395
t_i/t_{ref} [%]	100	47	1.5	1.1	0.08

Appendix B

Figures

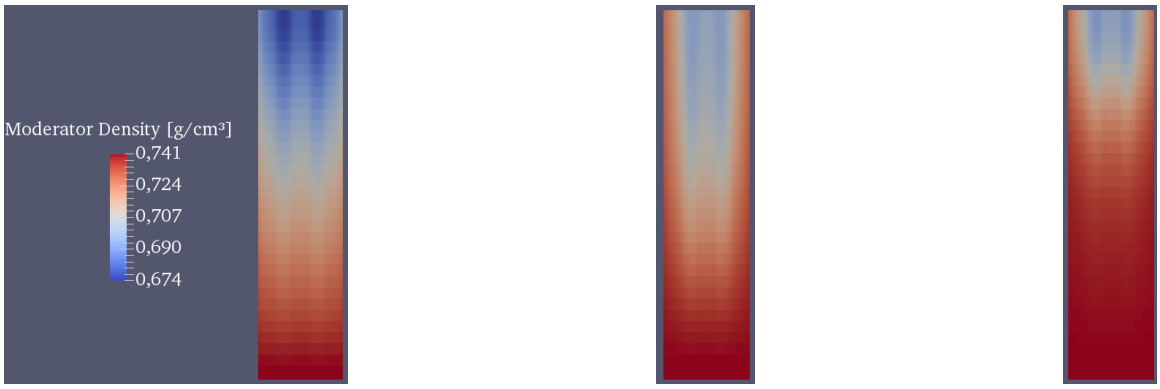

(a) Iteration 0 (b) It. 1 (c) It. 2

Figure B-1: Divergent oscillations of the moderator density field (axial slice at the centre) occurring along the multiphysic iterations when using the standard fixed-point without relaxation.

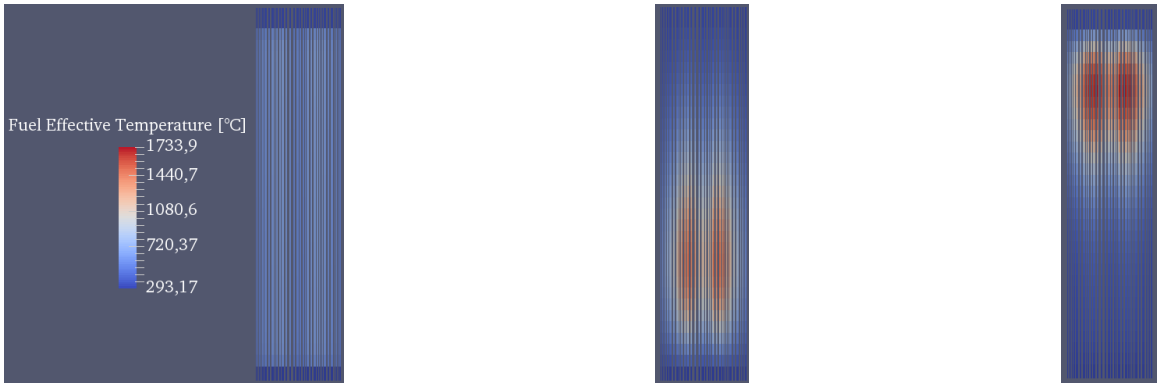

(a) Iteration 0 (b) It. 1 (c) It. 2

Figure B-2: Divergent oscillations of the effective fuel temperature (axial slice at the centre) occurring along the multiphysic iterations when using the standard fixed-point without relaxation.

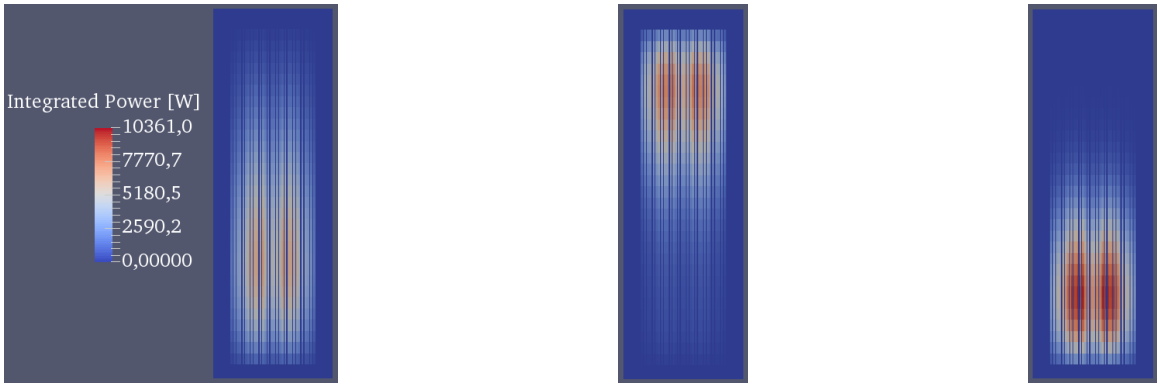

(a) Iteration 0 (b) It. 1 (c) It. 2

Figure B-3: Divergent oscillations of the integrated power in the fuel field (axial slice at the centre) occurring along the multiphysic iterations when using the standard fixed-point without relaxation.

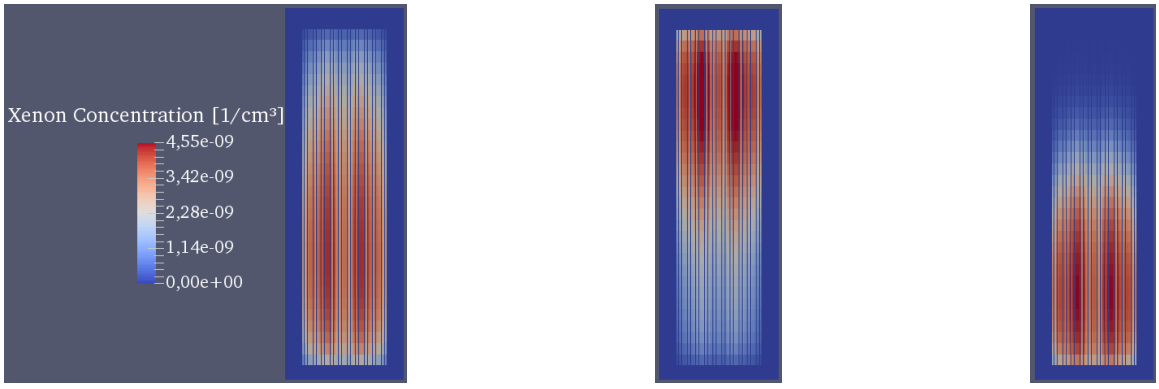

(a) Iteration 0 (b) It. 1 (c) It. 2

Figure B-4: Divergent oscillations of the xenon concentration field (axial slice at the centre) occurring along the multiphysic iterations when using the standard fixed-point without relaxation.

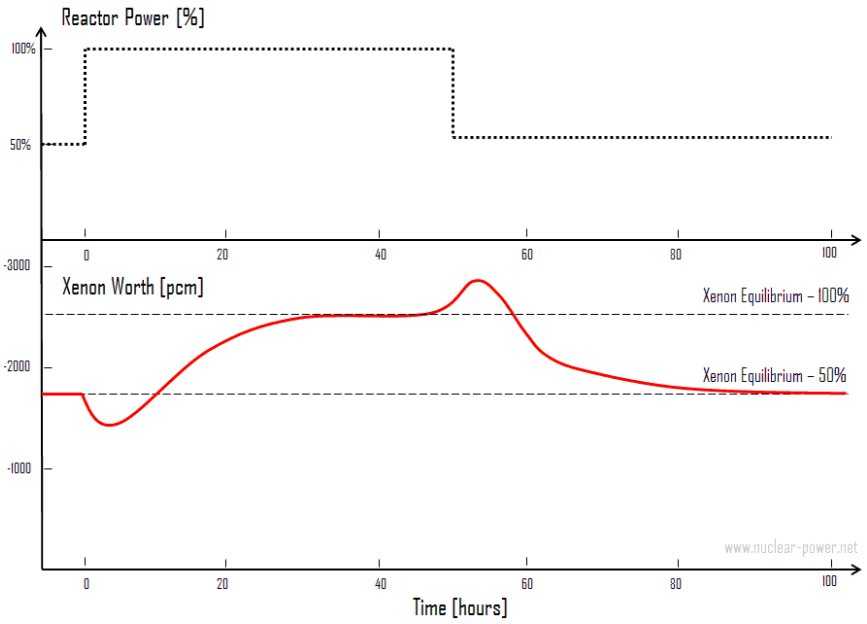

(a) Xenon-135

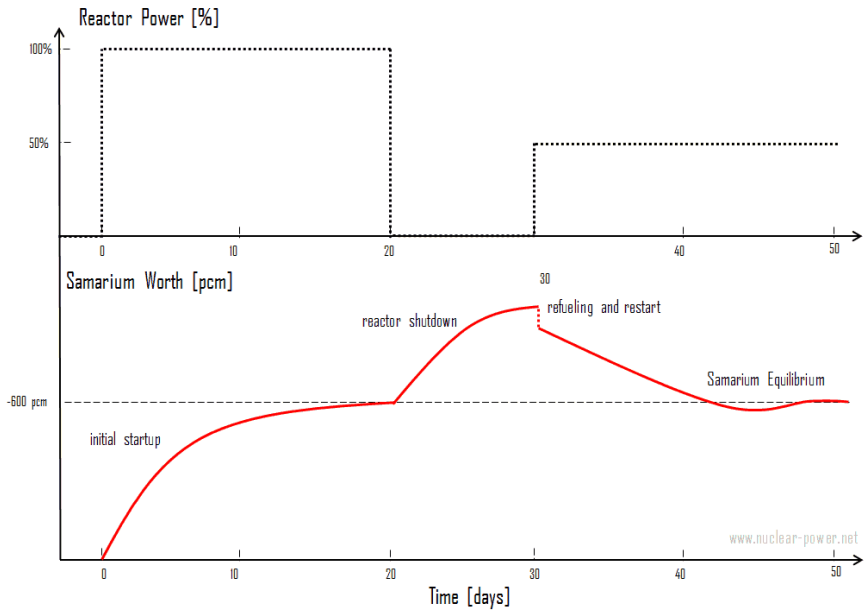

(b) Samarium-149

Figure B-5: Comparisons of the evolution of the fission product concentrations after a power change. The convergence of xenon presents large and not monotonous variations before reaching the asymptotic value. Courtesy of [13] and [14].

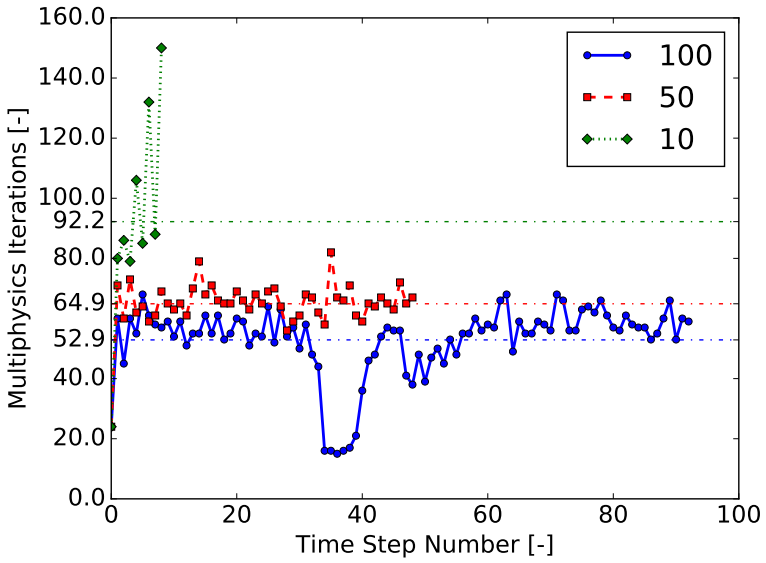

Figure B-6: Number of multiphysics iterations required per each time step for the three considered time discretizations. Referring to the full scheme presented in sub-section 7.3.2.

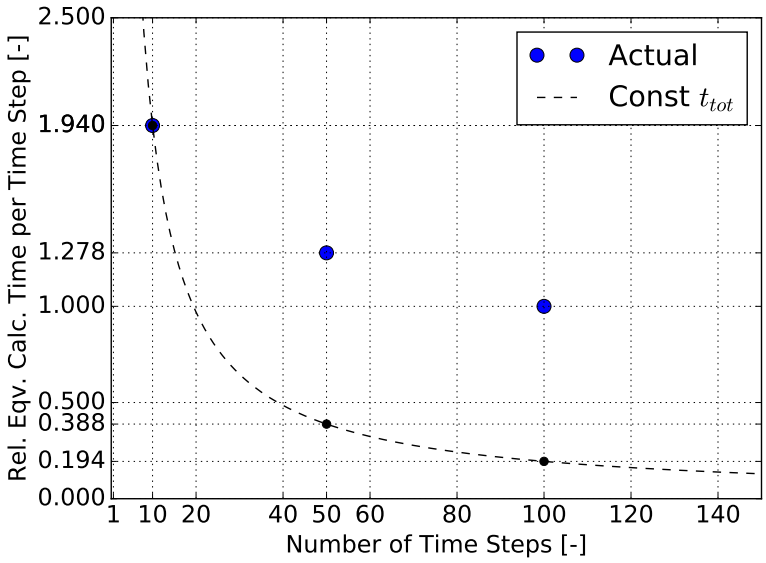

Figure B-7: The black dashed line represents how the relative equivalent computing time per steady-state should decrease in order to keep constant the time associated to the entire depletion calculation. The three blue dots are the values found when dividing the total irradiation time in 10, 50 and 100 time steps. Predictably, the unitary computational cost does not decrease enough (1.278>0.388 and 1>0.194) to reduce the total equivalent computing time, which is respectively 3.3 and 5.2 times larger than for ten steps.

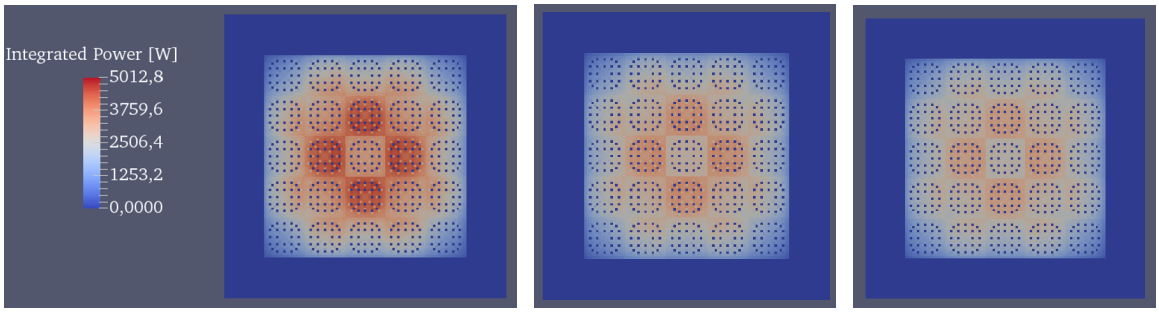

(a) 0 days (b) 194 days (c) 365 days

Figure B-8: Evolution of the power distribution along irradiation. Three time steps are considered after 0, 194 and 365 days.

Bibliography

[1] Nicolas Soppera, Manuel Bossant, Oscar Cabellos, Emmeric Dupont, and Carlos J Díez. JANIS: NEA JAva-based Nuclear Data Information System. In *EPJ Web of Conferences*, volume 146, page 07006. EDP Sciences, 2017.

[2] Paul Reuss. *Précis de neutronique*. EDP sciences, 2012.

[3] Jean-Luc Guillet and Yannick Guérin. *Nuclear fuels*. CEA Saclay and Groupe Moniteur (Éditions du Moniteur), 2009.

[4] Henryk Anglart. Thermal-Hydraulics in Nuclear Systems. 2015.

[5] Wolfgang Wiesenack. Introduction to Fuel Behaviour Modelling. In *Joint ICTP-IAEA Advanced Workshop on Multi-Scale Modelling for Characterization and Basic Understanding of Radiation Damage Mechanisms in Materials Trieste, April 12-23, 2010*. Accessed: 08-06-2020.

[6] John R. Lamarsh and Anthony John Baratta. *Introduction to nuclear engineering*, volume 3. Prentice hall Upper Saddle River, NJ, 2001.

[7] Alexandre Targa. *Development of multi-physics and multi-scale Best Effort Modelling of pressurized water reactor under accidental situations*. PhD thesis, 2017.

[8] A. Godfrey. Vera core physics benchmark progression problem specifications, revision 4. *CASL, CASL-U-2012-0131*, 4:1–173, 2014.

[9] Updated Final Safety Analysis Report for Turkey Point Units 3 and 4. Chapter 3: Reactor Core. Technical report, Florida Power and Light Company, 2010.

[10] Andrew Scott Bielen. *Sensitivity and Uncertainty Analysis of Multiphysics Nuclear Reactor Core Depletion*. PhD thesis, 2015.

[11] Paolo Cattaneo, Frédéric Damian, Jean-Charles Le Pallec, Elsa Merle, and Didier Schneider. Development of a Multiphysics Best-Estimate Approach for LWR Reference Calculation. In *Proceedings of the International Congress on Advances in Nuclear Power Plants (ICAPP)*, Juan les Pins, France, 2019.

[12] Ang Zhu, Benjamin Collins, Brendan Kochunas, and Thomas Downar. Assessment of the Depletion Capability in MPACT. *Proc. PHYSOR 2014*, 2014.

[13] Xenon 135. `https://www.nuclear-power.net/nuclear-power/reactor-physics/reactor-operation/xenon-135/`. Accessed: 26-06-2020.

[14] Samarium 149. `https://www.nuclear-power.net/nuclear-power/reactor-physics/reactor-operation/samarium-149/`. Accessed: 26-06-2020.

[15] W. Yang, S. Mo, D. Lianga, and F. Zhen. Numerical Study of Overheat Fault in Copper Wire Caused by Bad Contact Base on Multi-physics Coupling. In *2014 7th International Conference on Intelligent Computation Technology and Automation*, pages 400–405, 2014.

[16] Simon Dubitsky, George Greshnyakov, and Nikolay Korovkin. Refinement of underground power cable ampacity by multiphysics FEA simulation. *International Journal of Energy*, 9:12–19, 2015.

[17] M. Errera, A. Dugeai, Ph. Girodroux-Lavigne, J. D. Garaud, M. Poinot, S. Cerqueira, and G. Chaineray. Multi-Physics Coupling Approaches for Aerospace Numerical Simulations. 2011.

[18] Alfio Quarteroni, Toni Lassila, Simone Rossi, and Ricardo Ruiz-Baier. Integrated Heart—Coupling multiscale and multiphysics models for the simulation of the cardiac function. *Computer Methods in Applied Mechanics and Engineering*, 314:345 – 407, 2017. Special Issue on Biological Systems Dedicated to William S. Klug.

[19] Radomir Chabiniok, Vicky Y. Wang, Myrianthi Hadjicharalambous, Liya Asner, Jack Lee, Maxime Sermesant, Ellen Kuhl, Alistair A. Young, Philippe Moireau, Martyn P. Nash, et al. Multiphysics and multiscale modelling, data–model fusion and integration of organ physiology in the clinic: ventricular cardiac mechanics. *Interface focus*, 6(2):20150083, 2016.

[20] Nuclear Power Reactors in the World. Technical report, International Atomic Energy Agency (IAEA), 2017.

[21] Nuclear Power in a Clean Energy System. Technical report, International Energy Agency (IEA), 2019.

[22] International Hydropower Association et al. Hydropower status report. *International Hydropower Association: London, UK*, 2018.

[23] Data and statistics. Technical report, International Energy Agency (IEA), 2019.

[24] Nuclear Power in France. Technical report, World Nuclear Association, 2020.

[25] J. Strumpell, S. Cole, and P. Mollard. Fuelling innovation. `https://www.neimagazine.com/features/featurefuelling-innovation-4899801/ /featurefuelling-innovation-4899801-477573.html`, 2016.

[26] Nicholas Horelik, Bryan Herman, Benoit Forget, and Kord Smith. Benchmark for evaluation and validation of reactor simulations (BEAVRS), v1. 0.1. In *Proc. Int. Conf. Mathematics and Computational Methods Applied to Nuc. Sci. & Eng*, pages 5–9, 2013.

[27] Nuclear Regulatory Commission. Nuclear Fuel Pellets. `https://www.flickr.com/photos/nrcgov/14492225000/`, 2014. Accessed: 23/04/2020.

[28] B. J. Yun, A. Splawski, S. Lo, and C. H. Song. Prediction of a subcooled boiling flow with mechanistic wall boiling and bubble size models. *Proc. CFD4NRS-3, Washington DC, USA*, pages 14–16, 2010.

[29] Shiro Nukiyama. The maximum and minimum values of the heat q transmitted from metal to boiling water under atmospheric pressure. *International Journal of Heat and Mass Transfer*, 9(12):1419 – 1433, 1966.

[30] Richard L. Williamson, J. D. Hales, S. R. Novascone, M. R. Tonks, D. R. Gaston, C. J. Permann, D. Andrs, and R. C. Martineau. Multidimensional multiphysics simulation of nuclear fuel behavior. *Journal of Nuclear Materials*, 423(1-3):149–163, 2012.

[31] Mireille Coste-Delclaux, Cheikh M'Backé Diop, Fausto Malvagi, and Anne Nicolas. *Neutronics*. CEA Saclay and Groupe Moniteur (Éditions du Moniteur), 2015.

[32] Hansjoachim Matzke and Gustav Schumacher. *Nuclear materials for fission reactors*. Elsevier, 2012.

[33] Charles L. Fefferman. Existence and smoothness of the Navier-Stokes equation. *The millennium prize problems*, 57:67, 2006.

[34] Derek Gaston, Chris Newman, Glen Hansen, and Damien Lebrun-Grandié. MOOSE: A parallel computational framework for coupled systems of nonlinear equations. *Nuclear Engineering and Design*, 239(10):1768 – 1778, 2009.

[35] Harry Bateman. The solution of a system of differential equations occurring in the theory of radio-active transformations. *Proc. Cambridge Phil. Soc., 1908*, 15:423–427, 1908.

[36] Tamer Bahadir, Sten-Örjan Lindahl, and Studsvik Scandpower Ab. STUDSVIK'S NEXT GENERATION NODAL CODE SIMULATE-5. 2009.

[37] Yann Périn and Kiril Velkov. CTF/DYN3D multi-scale coupled simulation of a rod ejection transient on the NURESIM platform. *Nuclear Engineering and Technology*, 49(6):1339 – 1345, 2017. Special Issue on International Conference on Mathematics and Computational Methods Applied to Nuclear Science and Engineering 2017 (M&C 2017).

[38] Brendan Kochunas, Benjamin S. Collins, Daniel Jabaay, Kang Seog Kim, Aaron Graham, Shane Stimpson, William A Wieselquist, Kevin T Clarno, Scott Palmtag, Thomas Downar, and Jess C Gehin. VERA Core Simulator Methodology for PWR Cycle Depletion. Technical report, 2015.

[39] Yeon Sang Jung and Han Gyu Joo. Decoupled planar MOC solution for dynamic group constant generation in direct three-dimensional core calculations. *Proc. M&C*, pages 3–7, 2009.

[40] Glenn O. Brown. The history of the Darcy-Weisbach equation for pipe flow resistance. In *Environmental and Water Resources History*, pages 34–43. 2003.

[41] Brian Edward Launder and Dudley Brian Spalding. The numerical computation of turbulent flows. In *Numerical prediction of flow, heat transfer, turbulence and combustion*, pages 96–116. Elsevier, 1983.

[42] K. J. Geelhood, Walter G. Luscher, C. E. Beyer, and M. E. Flanagan. *FRAPCON-3.4: a computer code for the calculation of steady state thermal-mechanical behavior of oxide fuel rods for high burnup*. US Nuclear Regulatory Commission, Office of Nuclear Regulatory Research, 2011.

[43] K. J. Geelhood, W. G. Luscher, C. E. Beyer, and J. M. Cuta. FRAPTRAN 1.4: a computer code for the transient analysis of oxide fuel rods. *US Nuclear Regulatory Commission, Office of Nuclear Regulatory Research, NUREG/CR-7023*, 1, 2011.

[44] Coline Brosselard et al. COCAGNE: EDF new neutronic core code for ANDROMÈDE calculation chain. In *International Conference on Mathematics and Computational Methods Applied to Nuclear Science and Engineering 2017 (M&C 2017)*, Jeju, South Korea, 2017.

[45] Emiliano Masiello, Richard Sanchez, and Igor Zmijarevic. New Numerical Solution with the Method of Short Characteristics for 2-D Heterogeneous Cartesian Cells in the APOLLO2 Code: Numerical Analysis and Tests. *Nuclear Science and Engineering*, 161(3):257–278, 2009.

[46] David E. Keyes, Lois C. McInnes, Carol Woodward, William Gropp, Eric Myra, Michael Pernice, John Bell, Jed Brown, Alain Clo, Jeffrey Connors, et al. Multiphysics simulations: Challenges and opportunities. *The International Journal of High Performance Computing Applications*, 27(1):4–83, 2013.

[47] Han Zhang, Jiong Guo, Jianan Lu, Jinlin Niu, Fu Li, and Yunlin Xu. The comparison between nonlinear and linear preconditioning JFNK method for transient neutronics/thermal-hydraulics coupling problem. *Annals of Nuclear Energy*, 132:357–368, 2019.

[48] C. Patricot, G. Allaire, and O. Fandeur. A First Finite Element Solver Shared By Neutron Diffusion, Heat Transfer And Mechanics. In *M&C - 2017 International Conference on Mathematics and Computational Methods Applied to Nuclear Science and Engineering*, Jeju, South Korea, April 2017.

[49] Bruno Chanaron, Carol Ahnert, Nicolas Crouzet, Victor Sanchez, Nikola Kolev, Olivier Marchand, Soeren Kliem, and Angel Papukchiev. Advanced multi-physics simulation for reactor safety in the framework of the NURESAFE project. *Annals of Nuclear Energy*, 84:166–177, 2015.

[50] John A. Turner, Kevin Clarno, Matt Sieger, Roscoe Bartlett, Benjamin Collins, Roger Pawlowski, Rodney Schmidt, and Randall Summers. The virtual environment for reactor applications (VERA): design and architecture. *Journal of Computational Physics*, 326:544–568, 2016.

[51] Yeon Sang Jung, Cheon Bo Shim, Chang Hyun Lim, and Han Gyu Joo. Practical numerical reactor employing direct whole core neutron transport and subchannel thermal/hydraulic solvers. *Annals of Nuclear Energy*, 62:357 – 374, 2013.

[52] Carlo Fiorina, Ivor Clifford, Manuele Aufiero, and Konstantin Mikityuk. GeN-Foam: a novel OpenFOAM® based multi-physics solver for 2D/3D transient analysis of nuclear reactors. *Nuclear Engineering and Design*, 294:24–37, 2015.

[53] Mark DeHart, Frederick Gleicher, Javier Ortensi, Anthony Alberti, and Todd Palmer. Multiphysics simulation of TREAT kinetics using MAMMOTH. Technical report, Idaho National Lab.(INL), Idaho Falls, ID (United States), 2015.

[54] Jaakko Leppänen, Ville Hovi, Timo Ikonen, Joona Kurki, Maria Pusa, Ville Valtavirta, and Tuomas Viitanen. The numerical multi-physics project (numps) at vtt technical research centre of finland. *Annals of Nuclear Energy*, 84:55 – 62, 2015. Multi-Physics Modelling of LWR Static and Transient Behaviour.

[55] Y. Q. Yu, E. R. Shemon, J. W. Thomas, Vijay S. Mahadevan, Ronald O. Rahaman, and Jerome Solberg. SHARP user manual. Technical report, Argonne National Lab.(ANL), Argonne, IL (United States), 2016.

[56] Charlotte Sandrin, Richard Sanchez, and Florence Dolci. An analysis of reflector homogenization techniques for full core diffusion calculations. *Nuclear science and engineering*, 168(1):59–72, 2011.

[57] R. D. Lawrence. Progress in nodal methods for the solution of the neutron diffusion and transport equations. *Progress in Nuclear Energy*, 17(3):271 – 301, 1986.

[58] Joaquim Peiró and Spencer Sherwin. Finite difference, finite element and finite volume methods for partial differential equations. In *Handbook of materials modeling*, pages 2415–2446. Springer, 2005.

[59] J.-J. Lautard, S. Loubière, and C. Fedon-Magnaud. CRONOS: a modular computational system for neutronic core calculations. 1992.

[60] A. Kavenoky and J.-J. Lautard. The neutron kinetics and thermal-hydraulic transient computational module of the neptune system: CRONOS. 1982.

[61] Greg Hobson, Stephan Merk, Hans-Wilhelm Bolloni, Karl-Albert Breith, Florin Curca-Tivig, Rene Van Geemert, Jochen Heinecke, Bettina Hartmann, Dieter Porsch, Viatcheslav Tiles, et al. ARTEMIS: The core simulator of AREVA NP's next generation coupled neutronics/thermal-hydraulics code system ARCADIA. *PHYSOR 2008 Proceedings*, pages 14–19, 2008.

[62] Andre Ribes and Christian Caremoli. Salome platform component model for numerical simulation. In *31st Annual International Computer Software and Applications Conference (COMPSAC 2007)*, volume 2, pages 553–564. IEEE, 2007.

[63] Mike Folk, Gerd Heber, Quincey Koziol, Elena Pourmal, and Dana Robinson. An overview of the HDF5 technology suite and its applications. In *Proceedings of the EDBT/ICDT 2011 Workshop on Array Databases*, pages 36–47, 2011.

[64] C. Demazière, V. H. Sanchez-Espinoza, and B. Chanaron. Advanced numerical simulation and modelling for reactor safety–contributions from the CORTEX, HPMC, MCSAFE and NURESAFE projects. In *FISA 2019*. FISA 2019, 2019.

[65] KRAL Pavel. Latest activities of nugenia in the field of deterministic and probabilistic assessment.

[66] Fabrice Gaudier. URANIE: the CEA/DEN uncertainty and sensitivity platform. *Procedia-Social and Behavioral Sciences*, 2(6):7660–7661, 2010.

[67] K. R. Rempe, K. S. Smith, and A. F. Henry. SIMULATE-3 pin power reconstruction: methodology and benchmarking. *Nuclear Science and Engineering*, 103(4):334–342, 1989.

[68] Klaus Koebke and Manfred R. Wagner. The determination of the pin power distribution in a reactor core on the basis of nodal coarse mesh calculations. *Atomkernenergie*, 30(2):136–142, 1977.

[69] Armando Miguel Gomez-Torres, Victor Hugo Sanchez-Espinoza, Sören Kliem, and Andre Gommlich. Implementation of a fast running full core pin power reconstruction method in DYN3D. *Nuclear Engineering and Design*, 274:44–55, 2014.

[70] Ulrich Grundmann, Ulrich Rohde, Siegfried Mittag, and Sören Kliem. DYN3D version 3.2-code for calculation of transients in light water reactors (LWR) with hexagonal or quadratic fuel elements-description of models and methods. 2005.

[71] Maria N. Avramova and Robert K. Salko. CTF theory manual. Technical report, Oak Ridge National Laboratory (ORNL), 2016.

[72] Tomasz Kozlowski and Thomas J. Downar. PWR MOX/UO2 Core Transient Benchmark Final Report. *NEA/NSC/DOC*, page 20, 2006.

[73] Armando Miguel Gomez-Torres, Victor Hugo Sanchez-Espinoza, Kostadin Ivanov, and Rafael Macian-Juan. DYNSUB: A high fidelity coupled code system for the evaluation of local safety parameters–Part I: Development, implementation and verification. *Annals of nuclear energy*, 48:108–122, 2012.

[74] Armando Miguel Gomez-Torres, Victor Hugo Sanchez-Espinoza, Kostadin Ivanov, and Rafael Macian-Juan. DYNSUB: A high fidelity coupled code system for the evaluation of local safety parameters–Part II: Comparison of different temporal schemes. *Annals of nuclear energy*, 48:123–129, 2012.

[75] Miriam Knebel, Luigi Mercatali, Victor Sanchez, Robert Stieglitz, and Rafael Macian-Juan. Validation of the Serpent 2-DYNSUB code sequence using the Special Power Excursion Reactor Test III (SPERT III). *Annals of Nuclear Energy*, 91:79 – 91, 2016.

[76] J. Dugone. SPERT III reactor facility: E-core revision. Technical report, Phillips Petroleum Co., Idaho Falls, Idaho. Atomic Energy Div., 1965.

[77] R. K. McCardell, D. I. Herborn, and J. E. Houghtaling. Reactivity accident test results and analyses for the SPERT III E-core: a small, oxide-fuelled, Pressurized-Water Reactor. Technical report, Phillips Petroleum Co., Idaho Falls, Idaho. Atomic Energy Div., 1969.

[78] Javier Jiménez Escalante, José Javier Herrero Carrascosa, Diana Cuervo Gómez, and José María Aragonés Beltrán. Whole Core Pin-by-Pin Coupled Neutronic-Thermal-hydraulic Steady state and Transient Calculations using COBAYA3 code. In *Proceedings of the 17th Pacific Basin Nuclear Conference 2010, PBNC-2010*, Puerto Vallarta, Mexico, 2010. SNM, Sociedad Nuclear Mexicana.

[79] Trost, Nico, Jiménez, Javier, Lukarski, Dimitar, and Sanchez, Victor. Accelerating COBAYA3 on multi-core CPU and GPU systems using PARALUTION. In Array, editor, *SNA + MC 2013 - Joint International Conference on Supercomputing in Nuclear Applications + Monte Carlo*, page 04108, 2014.

[80] Juan-Andrés Lozano, Nuria García-Herranz, Carol Ahnert, and José-María Aragonés. The analytic nodal diffusion solver ANDES in multigroups for 3D rectangular geometry: Development and performance analysis. *Annals of Nuclear Energy*, 35(12):2365 – 2374, 2008.

[81] Manuel Calleja, J. Jimenez, U. Imke, V. Sanchez, R. Stieglitz, José J. Herrero, and R. Macián. Implementation of hybrid simulation schemes in COBAYA3/SUBCHANFLOW coupled codes for the efficient direct prediction of local safety parameters. *Annals of Nuclear Energy*, 70:216–229, 2014.

[82] V. Sanchez, U. Imke, A. Ivanov, and R. Gomez. SUBCHANFLOW: a thermal hydraulic sub-channel program to analyse fuel rod bundles and reactor cores. 2010.

[83] Uwe Imke and Victor Hugo Sanchez. Validation of the subchannel code SUBCHANFLOW using the NUPEC PWR tests (PSBT). *Science and Technology of Nuclear Installations*, 2012, 2012.

[84] Omar Zerkak, Ivan Gajev, Annalisa Manera, Tomasz Kozlowski, Andre Gommlich, Stéphanie Zimmer, Sören Kliem, Nicolas Crouzet, and Martin A Zimmermann. Revisiting Temporal Accuracy in Neutronics/TH Code Coupling Using the NURESIM LWR Simulation Platform. In *NURETH-14, The 14 th International Topical Meeting on Nuclear Reactor Thermal hydraulic, September 25th-30th, 2011, Toronto, Ontario, Canada*, 2011.

[85] E. Federici, F. Lamare, V. Bessiron, and J. Papin. The SCANAIR code version 3.2: Main features and status of qualification. *Fuel behaviour under transient and LOCA conditions*, page 88, 2002.

[86] S. Bascou, O. De Luze, S. Ederli, and G. Guillard. Development and validation of the multiphysics DRACCAR code. *Annals of Nuclear Energy*, 84:1–18, 2015.

[87] André Fargette. Simulation of REBEKA 6 with DRACCAR v2. 1. *Nuclear Engineering and Design*, 321:244–257, 2017.

[88] J. Papin, B. Cazalis, J.-M. Frizonnet, J. Desquines, F. Lemoine, V. Georgenthum, F. Lamare, and M. Petit. Summary and interpretation of the CABRI REP-Na program. *Nuclear technology*, 157(3):230–250, 2007.

[89] Motoe Suzuki, Hiroaki Saitou, and Toyosi Fuketa. Analysis on split failure of cladding of high burnup BWR rods in reactivity-initiated accident conditions by RANNS code. *Nuclear Engineering and Design*, 236(2):128–139, 2006.

[90] I. Toumi, A. Bergeron, D. Gallo, E. Royer, and D. Caruge. FLICA-4: a three-dimensional two-phase flow computer code with advanced numerical methods for nuclear applications. *Nuclear Engineering and Design*, 200(1-2):139–155, 2000.

[91] G. Geffraye, O. Antoni, M. Farvacque, D. Kadri, G. Lavialle, B. Rameau, and A. Ruby. CATHARE 2 v2. 5_2: a single version for various applications. *Nuclear Engineering and Design*, 241(11):4456–4463, 2011.

[92] Alain Moal, Vincent Georgenthum, and Olivier Marchand. SCANAIR: A transient fuel performance code: Part one: General modelling description. *Nuclear Engineering and Design*, 280:150–171, 2014.

[93] Vincent Georgenthum, Alain Moal, and Olivier Marchand. SCANAIR a transient fuel performance code Part two: Assessment of modelling capabilities. *Nuclear Engineering and Design*, 280:172–180, 2014.

[94] T. Glantz, T. Taurines, O. [De Luze], S. Belon, G. Guillard, and F. Jacq. DRACCAR: A multiphysics code for computational analysis of multi-rod ballooning, coolability and fuel relocation during LOCA transients Part one: General modeling description. *Nuclear Engineering and Design*, 339:269 – 285, 2018.

[95] Pierre Ruyer, N. Seiler, B. Biton, F. Lelong, F. Secondi, D. Baalbaki, and Michel Gradeck. Two-phase flow across a partially damaged core during the reflood phase of a loca. *Nuclear Engineering and Design*, 264:187–194, 2013.

[96] K. Lassmann. Transuranus: a fuel rod analysis code ready for use. *Journal of Nuclear Materials*, 188:295 – 302, 1992.

[97] L. Holt, U. Rohde, M. Seidl, A. Schubert, P. Van Uffelen, and R. Macián-Juan. Development of a general coupling interface for the fuel performance code TRANSURANUS–Tested with the reactor dynamics code DYN3D. *Annals of Nuclear Energy*, 84:73–85, 2015.

[98] L. Holt, U. Rohde, S. Kliem, S. Baier, M. Seidl, P. Van Uffelen, and R. Macián-Juan. Investigation of feedback on neutron kinetics and thermal hydraulics from detailed online fuel behavior modeling during a boron dilution transient in a PWR with the two-way coupled code system DYN3D-TRANSURANUS. *Nuclear Engineering and Design*, 297:32–43, 2016.

[99] X MCNP. Monte Carlo Team, MCNP–A General Purpose Monte Carlo N-Particle Transport Code, Version 5. Technical report, LA-UR-03 1987, Los Alamos National Laboratory, April 2003, The MCNP5 code can be obtained from the Radiation Safety Information Computational Center (RSICC), PO Box 2008, Oak Ridge, TN, 37831-6362, 5., 5.

[100] V. S. W. Sherriffs. MONK-a general purpose Monte Carlo neutronics program. Technical report, UKAEA Safety and Reliability Directorate, 1978.

[101] Jaakko Leppänen, Maria Pusa, Tuomas Viitanen, Ville Valtavirta, and Toni Kaltiaisenaho. The Serpent Monte Carlo code: Status, development and applications in 2013. In *SNA+ MC 2013-Joint International Conference on Supercomputing in Nuclear Applications+ Monte Carlo*, page 06021. EDP Sciences, 2014.

[102] E. Brun, F. Damian, C. M. Diop, E. Dumonteil, F.-X. Hugot, C. Jouanne, Y. K. Lee, F. Malvagi, A. Mazzolo, O. Petit, et al. Tripoli-4®, CEA, EDF and AREVA reference Monte Carlo code. In *SNA+ MC 2013-Joint International Conference on Supercomputing in Nuclear Applications+ Monte Carlo*, page 06023. EDP Sciences, 2014.

[103] J. Eduard Hoogenboom, Aleksandar Ivanov, Victor Sanchez, and Cheikh M. Diop. A flexible coupling scheme for Monte Carlo and thermal-hydraulics codes. 2011.

[104] Diego Ferraro, Manuel Garcia, Uwe Imke, Ville Valtavirta, Jaakko Leppänen, and Victor Sanchez-Espinoza. Serpent/scf pin-level multiphysics solutions for the vera fuel assembly benchmark. *Annals of Nuclear Energy*, 128:102 – 114, 2019.

[105] Manuel García, Diego Ferraro, Ville Valtavirta, Riku Tuominen, Uwe Imke, Jaakko Leppänen, and Victor Sanchez-Espinoza. Serpent2-subchanflow pin-by-pin modelling capabilities for vver geometries. *Annals of Nuclear Energy*, 135:106955, 2020.

[106] Margaux Faucher. *Coupling between Monte Carlo neutron transport and thermal-hydraulics for the simulation of transients due to reactivity insertions*. PhD thesis, Université Paris-Saclay, 2019.

[107] Heikki Suikkanen, Ville Rintala, Arndt Schubert, and Paul [Van Uffelen]. Development of coupled neutronics and fuel performance analysis capabilities between Serpent and TRANSURANUS. *Nuclear Engineering and Design*, 359:110450, 2020.

[108] J. A. Turnbull. IFPE/GAIN, Gadolinia Doped UO 2 Fuel Behaviour Experiment. 2002.

[109] Maria Pusa and Jaakko Leppänen. Solving linear systems with sparse gaussian elimination in the chebyshev rational approximation method. *Nuclear Science and Engineering*, 175(3):250–258, 2013.

[110] Nathan Greiner. *Prise en compte d'un couplage fin neutronique-thermique dans les calculs d'assemblage pour les réacteurs à eau pressurisée*. PhD thesis, École Polytechnique de Montréal, 2015.

[111] Daniele Tomatis, Igor Zmijarevic, and Paolo Cattaneo. A simple multiphysics coupling for high-fidelity neutronic modelling in fuel performance codes. In *Proceedings of the International Conference on PHYSics Of Reactors (PHYSOR 2018-Reactor Physics Paving The Way Towards More Efficient Systems)*, 2018.

[112] V. Bykov, A. Vasiliev, H. Ferroukhi, and A. Pautz. Solution of the BEAVRS benchmark using CASMO-5/SIMULATE-5 Code sequence. *Physics of Reactors*, pages 1–5, 2016.

[113] Maria Pusa and Aarno Isotalo. Uncertainty analysis of assembly and core-level calculations with application to CASMO-4E and SIMULATE-3. *Annals of Nuclear Energy*, 104:124 – 131, 2017.

[114] Ronaldo Szilard, Hongbin Zhang, Doug Kothe, and Paul Turinsky. The Consortium for Advanced Simulation of Light Water Reactors. Technical report, Idaho National Laboratory (INL), 2011.

[115] Brendan Kochunas, Benjamin Collins, Shane Stimpson, Robert Salko, Daniel Jabaay, Aaron Graham, Yuxuan Liu, Kang Seog Kim, William Wieselquist, Andrew Godfrey, Kevin Clarno, Scott Palmtag, Thomas Downar, and Jess Gehin. VERA Core Simulator Methodology for Pressurized Water Reactor Cycle Depletion. *Nuclear Science and Engineering*, 185(1):217–231, 2017.

[116] C. S. Brown and Hongbin Zhang. Uncertainty quantification and sensitivity analysis with CASL Core Simulator VERA-CS. *Annals of Nuclear Energy*, 95:188 – 201, 2016.

[117] M. P. Short, D. Hussey, B. K. Kendrick, T. M. Besmann, C. R. Stanek, and S. Yip. Multiphysics modeling of porous CRUD deposits in nuclear reactors. *Journal of nuclear materials*, 443(1-3):579–587, 2013.

[118] Robert Salko, Stuart Slattery, Travis Lange, Marc-Oliver Delchini, William Gurecky, Emre Tatli, and Benjamin Collins. Development of Preliminary VERA-CS Crud Induced Localized Corrosion Modeling Capability. Technical report, Oak Ridge National Lab.(ORNL), Oak Ridge, TN (United States), 2018.

[119] MPACT TEAM et al. MPACT Theory Manual v2. 1.0. Technical report, Consortium for Advanced Simulation of Light Water Reactors, CASL-U-2015-0078-000, Oak Ridge, NT, USA, 2015.

[120] O. W. Hermann and R. M. Westfall. ORIGEN-S: SCALE system module to calculate fuel depletion, actinide transmutation, fission product buildup and decay, and associated radiation source terms. *Vol. II, Sect. F7 of SCALE: A Modular Code System for Performing Standardized Computer Analyses for Licensing Evaluation, NUREG/CR-0200, Rev*, 6, 1998.

[121] Benjamin Collins, Shane Stimpson, Blake W. Kelley, Mitchell T. H. Young, Brendan Kochunas, Aaron Graham, Edward W. Larsen, Thomas Downar, and Andrew Godfrey. Stability and accuracy of 3D neutron transport simulations using the 2D/1D method in MPACT. *Journal of Computational Physics*, 326:612 – 628, 2016.

[122] Han Gyu Joo, Jin Young Cho, Kang Seog Kim, Chung Chan Lee, and Sung Quun Zee. Methods and performance of a three-dimensional whole-core transport code DeCART. 2004.

[123] N. Z. Cho, Gil Lee, and Chang Park. Fusion method of characteristics and nodal method for 3D whole core transport calculation. *Trans. Am. Nucl. Soc.*, 86:322–324, 01 2002.

[124] R. L. Williamson, K. A. Gamble, D. M. Perez, S. R. Novascone, G. Pastore, R. J. Gardner, J. D. Hales, W. Liu, and A. Mai. Validating the BISON fuel performance code to integral LWR experiments. *Nuclear Engineering and Design*, 301:232–244, 2016.

[125] Kevin T. Clarno, R. P. Pawlowski, Thomas M. Evans, B. Kochunas, and J. Turner. High fidelity modeling of pellet-clad interaction using the CASL virtual environment for reactor applications. In *Proceedings of the ANS Joint International Conference on Mathematics and Computation (M&C 2015), Supercomputing in Nuclear Applications (SNA) and the Monte Carlo (MC) Method*, pages 2345–2360, 2015.

[126] Lester M. Petrie and Nancy F. Landers. KENO Va: an improved Monte Carlo criticality program with supergrouping. Technical report, 1984.

[127] Benjamin Collins and Andrew Godfrey. Analysis of the BEAVRS Benchmark using VERA-CS. In *ANS MC2015–Joint International Conference on Mathematics and Computation (M&C), Supercomputing in Nuclear Applications (SNA) and the Monte Carlo (MC) Method*, 2015.

[128] Steven P. Hamilton, Thomas M. Evans, Gregory G. Davidson, Seth R. Johnson, Tara M. Pandya, and Andrew T. Godfrey. Hot zero power reactor calculations using the insilico code. *Journal of Computational Physics*, 314:700 – 711, 2016.

[129] Thomas M. Evans, Alissa S. Stafford, Rachel N. Slaybaugh, and Kevin T. Clarno. Denovo: A new three-dimensional parallel discrete ordinates code in SCALE. *Nuclear technology*, 171(2):171–200, 2010.

[130] Tara M. Pandya, Seth R. Johnson, Gregory G. Davidson, Thomas M. Evans, and Steven P. Hamilton. Shift: a massively parallel monte carlo radiation transport package. *Proc. Mathematics and Computational Methods (M&C 2015)*, pages 19–23, 2015.

[131] Mark A. Christon, Jozsef Bakosi, Balasubramanya T. Nadiga, Markus Berndt, Marianne M. Francois, Alan K. Stagg, Yidong Xia, and Hong Luo. A hybrid incremental projection method for thermal-hydraulics applications. *Journal of Computational Physics*, 317:382–404, 2016.

[132] B. Kendrick, V. Petrov, D. Walter, A. Manera, B. Collins, T. Downar, J. Secker, and K. Belcourt. CASL multiphysics modeling of crud deposition in PWRs. *Proc. LWR Fuel Performance Mtg. TopFuel 2013*, pages 15–19, 2013.

[133] Dae Hyun Hwang, Kyung Won Seo, and Hyouk Kwon. Validation of a Subchannel Analysis Code MATRA Version 1.0. Technical report, Korea Atomic Energy Research Institute, 2008.

[134] Min Ryu, Yeon Sang Jung, Hyun Ho Cho, and Han Gyu Joo. Solution of the BEAVRS benchmark using the nTRACER direct whole core calculation code. *Journal of Nuclear Science and Technology*, 52(7-8):961–969, 2015.

[135] Grzegorz Kępisty, Cyril Patricot, Daniel Broc, and Guillaume Campioni. SFR mechanical scenarios and neutron transport transients with CAST3M code. *Annals of Nuclear Energy*, 101:226 – 236, 2017.

[136] Richard P. Brent. *Algorithms for minimization without derivatives*. Courier Corporation, 2013.

[137] Rodney C. Schmidt, Kenneth Belcourt, Kevin T. Clarno, Russell Hooper, Larry L. Humphries, Alfred L. Lorber, Richard J. Pryor, and William F. Spotz. Foundational development of an advanced nuclear reactor integrated safety code. *Sandia Report SAND2010-0878, Sandia National Laboratories*, 2010.

[138] Han Zhang, Jiong Guo, Jianan Lu, Fu Li, Yunlin Xu, and T. J. Downar. The improvement of coupling method in TINTE by fully implicit scheme. *Nuclear Science and Engineering*, 190(2):156–175, 2018.

[139] Donald G. Anderson. Iterative procedures for nonlinear integral equations. *Journal of the ACM (JACM)*, 12(4):547–560, 1965.

[140] Peter N. Brown and Youcef Saad. Hybrid Krylov methods for nonlinear systems of equations. *SIAM Journal on Scientific and Statistical Computing*, 11(3):450–481, 1990.

[141] Alexander Toth, C. T. Kelley, Stuart Slattery, Steven Hamilton, Kevin Clarno, and R. Pawlowski. Analysis of Anderson acceleration on a simplified neutronics/thermal hydraulics system. In *Joint International Conference on Mathematics and Computation (M&C), Supercomputing in Nuclear Applications (SNA), and the Monte Carlo (MC) Method*, page 34, 2015.

[142] Steven Hamilton, Mark Berrill, Kevin Clarno, Roger Pawlowski, Alex Toth, C. T. Kelley, Thomas Evans, and Bobby Philip. An assessment of coupling algorithms for nuclear reactor core physics simulations. *Journal of Computational Physics*, 311:241–257, 2016.

[143] Bobby Philip, Mark A. Berrill, Srikanth Allu, Steven P. Hamilton, Rahul S. Sampath, Kevin T. Clarno, and Gary A. Dilts. A parallel multi-domain solution methodology applied to nonlinear thermal transport problems in nuclear fuel pins. *Journal of Computational Physics*, 286:143 – 171, 2015.

[144] Josef Stoer and Roland Bulirsch. *Introduction to numerical analysis*, volume 12. Springer Science & Business Media, 2013.

[145] Jean C. Ragusa and Vijay S. Mahadevan. Consistent and accurate schemes for coupled neutronics thermal-hydraulics reactor analysis. *Nuclear Engineering and Design*, 239(3):566–579, 2009.

[146] Alfio Quarteroni, Riccardo Sacco, and Fausto Saleri. *Numerical mathematics*, volume 37. Springer Science & Business Media, 2010.

[147] Cyril Patricot. *Multi-physics couplings: methodology impact evaluation for neutron transport /heat transfer /mechanics coupling simulations.* Theses, Université Paris-Saclay, March 2016.

[148] V. Eyert. A comparative study on methods for convergence acceleration of iterative vector sequences. *Journal of Computational Physics*, 124(2):271–285, 1996.

[149] Haw-ren Fang and Yousef Saad. Two classes of multisecant methods for nonlinear acceleration. *Numerical Linear Algebra with Applications*, 16(3):197–221, 2009.

[150] Dana A. Knoll and David E. Keyes. Jacobian-free Newton–Krylov methods: a survey of approaches and applications. *Journal of Computational Physics*, 193(2):357–397, 2004.

[151] Vijay S. Mahadevan, Jean C. Ragusa, and Vincent A. Mousseau. A verification exercise in multiphysics simulations for coupled reactor physics calculations. *Progress in Nuclear energy*, 55:12–32, 2012.

[152] Erik D. Walker, Benjamin Collins, and Jess C. Gehin. Jacobian-Free Newton-Krylov Coupling Methods for Nuclear Reactors. In *International Conference on Mathematics and Computational Methods Applied to Nuclear Science and Engineering, Jeju, Korea*, 2017.

[153] Qingming He, Yijun Zhang, Zhouyu Liu, Liangzhi Cao, and Hongchun Wu. The JFNK method for the PWR's transient simulation considering neutronics, thermal hydraulics and mechanics. *Nuclear Engineering and Technology*, 52(2):258–270, 2020.

[154] Yousef Saad. *Iterative methods for sparse linear systems*, volume 82. siam, 2003.

[155] Henk A. Van der Vorst. Bi-CGSTAB: A fast and smoothly converging variant of Bi-CG for the solution of nonsymmetric linear systems. *SIAM Journal on scientific and Statistical Computing*, 13(2):631–644, 1992.

[156] Roland W. Freund. A transpose-free quasi-minimal residual algorithm for non-Hermitian linear systems. *SIAM journal on scientific computing*, 14(2):470–482, 1993.

[157] Erik D. Walker, Benjamin Collins, and Jess C. Gehin. Low-order multiphysics coupling techniques for nuclear reactor applications. *Annals of Nuclear Energy*, 132:327–338, 2019.

[158] L. Martin-Deidier, A. Santamarina, S. Cathalau, J.-M. Gomit, and J.-P. Chauvin. Undermoderated PWR neutronic qualification through the Erasme experiments. In *Advances in Reactor Physics, Mathematics and Computation. Volume 1*. 1987.

[159] Richard Sanchez, Jacques Mondot, Žarko Stankovski, Antoine Cossic, and Igor Zmijarevic. APOLLO II: A User-Oriented, Portable, Modular Code for Multigroup Transport Assembly Calculations. *Nuclear Science and Engineering*, 100(3):352–362, 1988.

[160] Richard Sanchez, Igor Zmijarevi, Mireille Coste-Delclaux, Emiliano Masiello, Simone Santandrea, Emanuele Martinolli, Laurence Villate, Nadine Schwartz, and Nathalie Guler. Apollo2 year 2010. *Nuclear engineering and technology*, 42(5):474–499, 2010.

[161] D. Schneider, F. Dolci, F. Gabriel, J.-M. Palau, M. Guillo, B. Pothet, P. Archier, K. Ammar, F. Auffret, R. Baron, et al. APOLLO3: CEA/DEN deterministic multi-purpose code for reactor physics analysis. *Proc. PHYSOR 2016*, pages 1–5, 2016.

[162] A. Ivanov, V. Sanchez, and J. E. Hoogenboom. Single pin BWR benchmark problem for coupled Monte Carlo-Thermal hydraulics analysis. *Proceedings of PHYSOR 2012*, 2012.

[163] E. Dumonteil and C. M. Diop. Biases and statistical errors in Monte Carlo burnup calculations: An unbiased stochastic scheme to solve Boltzmann/Bateman coupled equations. *Nuclear Science and Engineering*, 167(2):165–170, 2011.

[164] F. Damian and E. Brun. ORPHEE research reactor: 3D core depletion calculation using Monte-Carlo code TRIPOLI-4®. *Annals of Nuclear Energy*, 82:203 – 216, 2015. Joint International Conference on Supercomputing in Nuclear Applications and Monte Carlo 2013, SNA + MC 2013. Pluri- and Trans-disciplinarity, Towards New Modeling and Numerical Simulation Paradigms.

[165] Gérald Rimpault. Algorithmic features of the ECCO cell code for treating heterogeneous fast reactor subassemblies. In *Proceedings of the international conference on mathematics and computations, reactor physics, and environmental analyses. Volume 1 and 2*, 1995.

[166] Gérald Rimpault, Danièle Plisson, J. Tommasi, R. Jacqmin, and Jean-Marie Rieunier. The ERANOS Code and Data System for Fast Reactor Neutronic Analyses. 11 2002.

[167] Li Lei-Mao. *Modèles d'autoprotection d'APOLLO3: analyse et orientation technique.* CEA/DANS/DM2S/SERMA/LTSD, dec 2007.

[168] F. Jeanpierre and M. Livolant. Autoprotection des résonances dans les réacteurs nucléaires. *Rapport CEA R-4533*, 1974.

[169] Mireille Coste-Delclaux. *Modélisation du phénomène d'autoprotection dans le code de transport multigroupe APOLLO2.* PhD thesis, Paris, CNAM, 2006.

[170] Elmer Eugene Lewis and Warren F. Miller. Computational methods of neutron transport. 1984.

[171] Simone Santandrea, Laurent Graziano, and Daniele Sciannandrone. Accelerated polynomial axial expansions for full 3D neutron transport MOC in the APOLLO3® code system as applied to the ASTRID fast breeder reactor. *Annals of Nuclear Energy*, 113:194–236, 2018.

[172] L. Mao, R. Sanchez, and I. Zmijarevic. Considering the upscattering in resonance interference treatment in APOLLO3. *Proceedings of Mathematics and Computational Methods Applied to Nuclear Science & Engineering (M&C)*, pages 19–23, 2015.

[173] Igor Zmijarevic. IDT solution to the 3D transport benchmark over a range in parameter space. 2008.

[174] R. Lenain, E. Masiello, F. Damian, and R. Sanchez. Domain decomposition method for 2D and 3D transport calculations using hybrid MPI/OPENMP parallelism. In *ANS MC2015-Joint International Conference on Mathematics and Computation (M&C), Supercomputing in Nuclear Applications (SNA) and the Monte Carlo (MC) Method*, 2015.

[175] S. Santandrea and P. Mosca. Linear surface characteristic scheme for the neutron transport equation in unstructured geometries. *Proceeding of Physor2006*, pages 10–14, 2006.

[176] D. Sciannandrone, S. Santandrea, R. Sanchez, L. Lei-Mao, J. Vidal, J. Palau, and P. Archier. Coupled Fine-Group Three-Dimensional Flux Calculation and Subgroups Method for a FBR Hexagonal Assembly with the APOLLO3® Core Physics Analysis Code. *Proc. M&C+ SNA+ MC 2015*, pages 19–23, 2015.

[177] Young Suk Ban, Emiliano Masiello, Roland Lenain, Han Gyu Joo, and Richard Sanchez. Code-to-code comparisons on spatial solution capabilities and performances between nTRACER and the standalone IDT solver of APOLLO3®. *Annals of Nuclear Energy*, 115:573 – 594, 2018.

[178] P. Archier, J.-M. Palau, J.-F. Vidal, S. Santandrea, and D. Sciannandrone. Validation of the Newly Implemented 3D TDT-MOC Solver of APOLLO3 Code on a Whole 3D SFR Heterogeneous Assembly. In *PHYSOR 2016-Unifying Theory and Experiments in the 21st Century*, 2016.

[179] A. Kavenoky. Assembly homogenization techniques for light water reactor analysis. Technical report, IAEA-TECDOC-231, Lugano, Switzerland, 1978.

[180] Anne-Marie Baudron and Jean-Jacques Lautard. MINOS: a simplified PN solver for core calculation. *Nuclear Science and Engineering*, 155(2):250–263, 2007.

[181] Jean-Jacques Lautard and Jean-Yves Moller. MINARET, a deterministic neutron transport solver for nuclear core calculations. In *International Conference on Mathematics and Computational Methods Applied to Nuclear Science and Engineering (M& C 2011)*.

[182] A.-M. Baudron, J.-J. Lautard, Y. Maday, and O. Mula. MINARET: Towards a time-dependent neutron transport parallel solver. In *SNA+ MC 2013-Joint International Conference on Supercomputing in Nuclear Applications+ Monte Carlo*, page 04103. EDP Sciences, 2014.

[183] Pierre-Arnaud Raviart and Jean-Marie Thomas. A mixed finite element method for 2-nd order elliptic problems. In *Mathematical aspects of finite element methods*, pages 292–315. Springer, 1977.

[184] Jean-Claude Nédélec. Mixed finite elements in R 3. *Numerische Mathematik*, 35(3):315–341, 1980.

[185] Jean-Claude Nédélec. A new family of mixed finite elements in R 3. *Numerische Mathematik*, 50(1):57–81, 1986.

[186] Marvin L. Adams and William R. Martin. Diffusion synthetic acceleration of discontinuous finite element transport iterations. *Nuclear science and engineering*, 111(2):145–167, 1992.

[187] Yaqi Wang. *Adaptive mesh refinement solution techniques for the multigroup SN transport equation using a higher-order discontinuous finite element method*. PhD thesis, 2009.

[188] Alain Hebert. A consistent technique for the pin-by-pin homogenization of a pressurized water reactor assembly. *Nuclear Science and Engineering*, 113(3):227–238, 1993.

[189] Akio Yamamoto, Masahiro Tatsumi, Yasunori Kitamura, and Yoshihiro Yamane. Improvement of the SPH method for pin-by-pin core calculations. *Journal of nuclear science and technology*, 41(12):1155–1165, 2004.

[190] B. Roque, A. Rizzo, V. Pascal, and P. Archier. Experimental validation of the new code package APOLLO3-SFR against ZPPR-10A experiment for critical and voided configurations. In *PHYSOR 2016-International Conference on the Advances in Reactor Physics Unifying Theory and Experiments in the 21st Century*, 2016.

[191] Ely M. Gelbard. Simplified spherical harmonics equations and their use in shielding problems. Technical report, Westinghouse Electric Corp. Bettis Atomic Power Lab., Pittsburgh, 1961.

[192] Gerald C. Pomraning. Asymptotic and variational derivations of the simplified PN equations. *Annals of Nuclear Energy*, 20(9):623–637, 1993.

[193] Edward W. Larsen, Jim E. Morel, and John M. McGhee. Asymptotic derivation of the simplified PN equations. In *Proceedings of the Joint International Conference on Mathematical Methods and Supercomputing in Nuclear Applications*, volume 1, page 718, 1993.

[194] P. S. Brantley and E. W. Larsen. Variational Derivation of the Simplified P3 Approximation. In *Proceedings of ANS Topcial Meeting on Mathematical Models and Supercomputing for Nuclear Applications*. Saratoga Springs New York, 1997.

[195] Anne-Marie Baudron and Jean-Jacques Lautard. Simplified P_N transport core calculations in the APOLLO3® system. 2011.

[196] P. Emonot, A. Souyri, J. L. Gandrille, and F. Barré. CATHARE-3: A new system code for thermal-hydraulics in the context of the NEPTUNE project. *Nuclear Engineering and Design*, 241(11):4476 – 4481, 2011. 13th International Topical Meeting on Nuclear Reactor Thermal Hydraulics (NURETH-13).

[197] C. Patricot. THEDI: a multi-1D two-phase flow solver for neutronic codes. In *Proceedings of the International Congress on Advances in Nuclear Power Plants (ICAPP)*, 2019.

[198] Pierre-Emmanuel Angeli, Ulrich Bieder, and Gauthier Fauchet. Overview of the TrioCFD code: main features, V&V procedures and typical applications to nuclear engineering. In *Proceedings of 16th International Topical Meeting on Nuclear Reactor Thermal Hydraulics (NURETH-16)*, 2015.

[199] Sylvie Aniel, André Bergeron, Philippe Fillion, Danielle Gallo, Fabrice Gaudier, Olivier Grégoire, Matthieu Martin, Edwige Richebois, Eric Royer, Patricia Salvatore, et al. FLICA4: Status of numerical and physical models and overview of applications. In *Proc. 11th Int. Top. Meeting on Nuclear Thermo-Hydraulics (NURETH-11)*, pages 2–6, 2005.

[200] N. Zuber and J. A. Findlay. Average Volumetric Concentration in Two-Phase Flow Systems. *Journal of Heat Transfer*, 87(4):453–468, 11 1965.

[201] Mamoru Ishii. One-dimensional drift-flux model and constitutive equations for relative motion between phases in various two-phase flow regimes. Technical report, Argonne National Lab., Ill.(USA), 1977.

[202] A. Tsilanizara, C. M. Diop, B. Nimal, M. Detoc, L. Luneville, M. Chiron, T. D. Huynh, I. Bresard, M. Eid, J.-C. Klein, et al. DARWIN: an evolution code system for a large range of applications. *Journal of Nuclear Science and Technology*, 37(sup1):845–849, 2000.

[203] S. Lahaye, P. Bellier, H. Mao, A. Tsilanizara, and Y. Kawamoto. First verification and validation steps of MENDEL release 1.0 cycle code system. In *Proc. Int. Conf. PHYSOR2014, Kyoto, Japan*, 2014.

[204] Vincent Marelle, Patrick Goldbronn, Stéphane Bernaud, Étienne Castelier, Jérôme Julien, Katherine Nkonga, Laurence Noirot, and Isabelle Ramière. New developments in ALCYONE 2.0 fuel performance code. In *Top Fuel 2016-Light Water Reactor (LWR) Fuel Performance Meeting*, 2016.

[205] P. Verpeaux, T. Charras, and A. Millard. Castem 2000: une approche moderne du calcul des structures. *Calcul des structures et intelligence artificielle*, 2:261–271, 1988.

[206] Emmanuelle Le Fichoux. Présentation et utilisation de cast3m. *ENSTA-LME (http://wwwcast3m. cea. fr)*, 2011.

[207] D. Plancq. PLEIADES: a unified environment for multidimensional fuel performance modeling. In *Proc. Int. Meeting on LWR Fuel Performance, Orlando, Florida USA, 2004*, 2004.

[208] Bruno Michel, Chrystelle Nonon, Jerome Sercombe, Frederic Michel, and Vincent Marelle. Simulation of pellet-cladding interaction with the PLEIADES fuel performance software environment. *Nuclear Technology*, 182(2):124–137, 2013.

[209] Gregory Delipei. *Development of an Uncertainty Quantification methodology for Multi-Physics Best Estimate analysis and application to the Rod Ejection Accident in a Pressurized Water Reactor*. PhD thesis, 2019.

[210] J.-C. Le Pallec, K. Mer-Nkonga, and N. Crouzet. Neutronics/Fuel Thermomechanics coupling in the framework of a REA (Rod Ejection Accident) Transient Scenario Calculation. In *PHYSOR 2016 Conference: Unifying Theory and Experiments in the 21st Century, Sun Valley, Idaho, USA*, 2016.

[211] M. Clergeau, F. Dubois, B. Normand, and A. Sargeni. HEMERA: A 3D Computational Tool for Analysis of Accidental Transients. In *PHYSOR 2010 Conference, Pittsburgh, PA*, 2010.

[212] J.-C. Le Pallec, C. Poinot-Salanon, N. Crouzet, and S. Zimmer. HEMERA V2: An evolutionary tool for PWR multi-physics analysis in salome platform. In *Proceedings of ICAPP*, page 2851, 2011.

[213] A. Targa, J.-C. Le Pallec, P. Le Tallec, K. Nkonga, N. Crouzet, and S. Chemin. Thermohydraulics-Thermomechanics Best Estimate coupled approach in a Rod Ejection Accident core calculation. *ICAPP2016, San Francisco, CA,(USA)*, 2016.

[214] A. Targa, P. Le Tallec, and J.-C. Le Pallec. Multiscale and multisolver pin power reconstruction approach in a reactor core calculation. In *ICAPP 2015-International Congress on Advances in Nuclear Power Plants*, 2015.

[215] G. K. Delipei, J. Garnier, J.-C. Le Pallec, and B. Normand. Uncertainty analysis methodology for multi-physics coupled rod ejection accident.

[216] G. Delipei, J. Garnier, J.-C. Le Pallec, and B. Normand. Multi-physics uncertainties propagation in a PWR rod ejection accident modeling-Analysis methodology and first results. ANS Best Estimate Plus Uncertainty International Conference (BEPU 2018), 2018.

[217] D. Caron, A. Calloo, J.-C. Lepallec, and C. Patricot. Analysis of methodologies for the coupling of multi-physics phenomena in the quasi-static approach to nuclear reactor dynamics. In *International Conference on Mathematics and Computational Methods applied to Nuclear Science and Engineering (MandC 2019)*, 2018.

[218] M.F. James. Energy released in fission. *Journal of Nuclear Energy*, 23(9):517 – 536, 1969.

[219] Joel Rhodes, Kord Smith, and Deokjung Lee. CASMO-5 development and applications. In *Proceedings of the PHYSOR-2006 conference, ANS Topical Meeting on Reactor Physics (Vancouver, BC, Canada, 2006) B*, volume 144, 2006.

[220] Clément Liegeard, Ansar Callo, Guy Marleau, and Enrico Girardi. Impact of photon transport on power distribution. In *International Conference on Mathematics and Computational Methods applied to Nuclear Science and Engineering (MandC 2017)*, 2017.

[221] M. Fliscounakis, E. Girardi, T. Courau, and D. Couyras. Potential of pin-by-pin SPN calculations as an industrial reference. In *Proceedings of the 2012 International Congress on Advances in Nuclear Power Plants-ICAPP'12*, 2012.

[222] Boris Grigorievich Korenev. *Bessel functions and their applications*. CRC Press, 2002.

[223] A. Bouloré, C. Struzik, and F. Gaudier. Uncertainty and sensitivity analysis of the nuclear fuel thermal behavior. *Nuclear Engineering and Design*, 253:200 – 210, 2012. SI : CFD4NRS-3.

[224] G. Rowlands. *Resonance absorption and non-uniform temperature distributions*. United Kingdom Atomic Energy Authority, 1961.

[225] A. Meister and A. Santamarina. The effective temperature for Doppler broadening of neutron resonances in UO2. In *Proc. Int. Conf. on the Physics of Nuclear Science and Technology, PHYSOR-98, Long Island, NY, USA, Oct. 5-8, 1998*, 1998.

[226] Interpolation presentation. `https://docs.salome-platform.org/7/dev/MEDCoupling/intro-interp.html`. Accessed: 03-06-2020.

[227] Fausto Franceschini, Marjan Kromar, Dušan Ćalić, A Godfrey, Benjamin S Collins, Thomas M Evans, and Jess C Gehin. Simulation of the NPP KRSKO startup core with CASL core simulator, VERA-CS. In *Proceedings of the International Conference Nuclear Energy for New Europe (NENE), Portoroz, Slovenia*, 2014.

[228] N. Z. Cho. KAIST Nuclear Reactor Analysis and Particle Transport Laboratory, Benchmark Problem 1A. *KAIST Nuclear Reactor Analysis and Particle Transport Laboratory, March*, 2013.

[229] M. Schlieck, H.-D. Berger, and A. Neufert. Optimized gadolinia concepts for advanced in-core fuel management in pwrs. *Nuclear Engineering and Design*, 205(1):191 – 198, 2001.

[230] Dan Kotlyar. *Development of Advanced Burnup-thermal Hydraulic Coupling Methods for Monte Carlo Codes*. PhD thesis, Ben-Gurion University of the Negev, 2013.

[231] Serge Marguet. *The physics of nuclear reactors*. Springer, 2018.

[232] Alex Toth, J. Austin Ellis, Tom Evans, Steven Hamilton, C.T. Kelley, Roger Pawlowski, and Stuart Slattery. Local improvement results for Anderson acceleration with inaccurate function evaluations. *SIAM Journal on Scientific Computing*, 39(5):S47–S65, 2017.

[233] Alexandre Ern and Martin Vohralík. Adaptive inexact newton methods with a posteriori stopping criteria for nonlinear diffusion pdes. *SIAM Journal on Scientific Computing*, 35(4):A1761–A1791, 2013.

[234] Youcef Saad. Chebyshev acceleration techniques for solving nonsymmetric eigenvalue problems. *Mathematics of Computation*, 42(166):567–588, 1984.

[235] Yuri A. Kuznetsov. Elements of applied bifurcation theory. *Applied mathematical sciences*, 112:591, 1998.

[236] Claire Evans, Sara Pollock, Leo G. Rebholz, and Mengying Xiao. A proof that anderson acceleration improves the convergence rate in linearly converging fixed-point methods (but not in those converging quadratically). *SIAM Journal on Numerical Analysis*, 58(1):788–810, 2020.

[237] E. Jones, E. Oliphant, and P. Peterson. SciPy: Open Source Scientific Tools for Python (SciPy Developers, 2001), 2019.

[238] Philip Wolfe. Convergence conditions for ascent methods. *SIAM Review*, 11(2):226–235, 1969.

[239] Philip Wolfe. Convergence conditions for ascent methods. ii: Some corrections. *SIAM Review*, 13(2):185–188, 1971.

[240] Larry Armijo. Minimization of functions having lipschitz continuous first partial derivatives. *Pacific Journal of mathematics*, 16(1):1–3, 1966.

[241] P. Cattaneo, R. Lenain, E. Merle, C. Patricot, and D. Schneider. Numerical optimization of a multiphysics calculation scheme. In *Proceedings of the International Conference on PHYSics Of Reactors (PHYSOR 2020–Transition to a Scalable Nuclear Future)*, Cambridge, United Kingdom.

[242] P. Cattaneo, R. Lenain, E. Merle, C. Patricot, and D. Schneider. Numerical optimization of a multiphysics calculation scheme based on partial convergence. *Annals of Nuclear Energy*, Submitted in March 2020.

[243] International Atomic Energy Agency. *Thermophysical Properties Database of Materials for Light Water Reactors and Heavy Water Reactors. IAEA TECDOC Series No. 1496*. International Atomic Energy Agency, 2006.

[244] K. Mer-Nkonga, N. Crouzet, J.-C. Le Pallec, B. Michel, D. Schneider, and A. Targa. Coupling of fuel performance and neutronic codes for pwr. In *11th World Congr. Comput. Mech. WCCM XI 5th Eur. Conf. Comput. Mech. ECCM*, volume 6, 2014.

[245] A.E. Isotalo and P.A. Aarnio. Substep methods for burnup calculations with bateman solutions. *Annals of Nuclear Energy*, 38(11):2509 – 2514, 2011.